Two study of collective properties in quantum systems : nuclear spin squeezing in helium-3 via quantum non-demolition measurement and phonons damping in a 2D superfluid

Alan Serafin

SORBONNE UNIVERSITÉ

Thèse de doctorat de Sorbonne Université

Spécialité : Physique

Ecole doctorale n°564 : Physique en Île-de-France

réalisée sous la direction de Alice SINATRA
et co-dirigée avec Yvan CASTIN

au Laboratoire Kastler Brossel

Laboratoire Kastler Brossel
Physique quantique et applications

présentée par

Alan SERAFIN

Sujet de la thèse :

Deux études de propriétés collectives de systèmes quantiques

Soutenue le 5 décembre 2022

devant le jury composé de :

M. Jean-Francois Roch	Professeur	ENS Paris-Saclay	Président
Mme. Isabelle Bouchoule	Directrice de recherche	Lab. Charles-Fabry	Rapporteuse
M. Tommaso Roscilde	Maître de Conférence	ENS Lyon	Rapporteur
M. Jean-Noël Fuchs	Directeur de recherche	LPTMC	Examinateur
M. Yvan Castin	Directeur de recherche	LKB	Co-encadrant
Mme. Alice Sinatra	Professeure	LKB	Directrice de thèse

Contents

List of Figures

Remerciements

Le travail présenté dans ce manuscrit est le fruit de trois années de recherche effectuée au sein du laboratoire Kastler Brossel entre mai 2019 et décembre 2022. Je souhaite remercier l'ensemble de ses membres pour l'accueil chaleureux qu'ils m'ont offert. Je remercie en particulier son personnel administratif, toujours sympathique et disponible.

Je voudrais remercier tout particulièrement Alice Sinatra et Yvan Castin pour avoir dirigé cette thèse avec tant de bienveillance. Merci Alice pour ta confiance lorsque tu m'as pris comme doctorant et durant tout le reste de la thèse et merci Yvan pour ces discussions animées et amicales. Votre bonne humeur et votre attention ont permis un environnement de travail enrichissant tout au long de la thèse. Nos discussions hebdomadaires de physique furent des enseignements précieux et le travail commun, toujours méthodique et rigoureux, fut une formation scientifique profonde dont je vous suis reconnaissant. Ces discussions de travail furent aussi simplement des moments dont j'ai toujours pris du plaisir à participer, souvent amusante et où l'on riait beaucoup. Je vous remercie encore tous deux pour toutes ces raisons.

Merci aussi aux membres de l'équipe microcircuit à atomes et tous les doctorants qui y sont passés ces trois dernières années. Je remercie en particulier Jean Hare pour toutes les conversations de fin d'après-midi. Je voudrais aussi remercier Jules Grucker, pour son parrainage pris au sérieux, et Félix Werner pour m'avoir introduit aux calculs sur clusters.

Je remercie les membres du jury, Jean-François Roch, Jean-Noël Fuchs ainsi que Isabelle Bouchoule et Tommaso Roscilde dont je suis reconnaissant d'avoir accepté d'être les rapporteurs de la thèse.

Enfin, j'aimerais remercier mes parents et mes soeurs pour leur soutien continu, et mes ami-es de la diaspora caennaise et d'ailleurs. Merci aussi à toi Léa, pour les relectures du manuscrit et pour tout le reste.

This manuscript was originally written in french before being translated to english. The translation was done via the DeepL software followed by a careful proofreading.

Part I

Nuclear Spin Squeezing via Continuous Non-Demolition Measurements

Chapter 1

Introduction

Foreword

The nuclear spin of helium-3 atoms in a gas at room temperature is a very well isolated quantum system with record coherence times of up to several days [1]. It is now used in many applications, such as magnetometry [2], gyroscopes for navigation [3], as a target in particle physics experiments [1], and even in medicine for magnetic resonance imaging of the human respiratory system [4, 5]. In addition, helium-3 filled cells are used for precision measurements in fundamental physics, i.e. in the search for anomalous forces [6] or violations of fundamental symmetries in nature [7].

While the exceptional isolation of helium-3 nuclear spins is essential to obtain long coherence times, it makes its measurement and control difficult. Remarkably, nuclear spins in noble gases can be optically pumped polarized via metastability exchange collisions or alternatively via spin exchange collisions, exploiting collisions between atoms in different states or of different species that transfer optically induced electron polarization to nuclei [1, 8]. However, the role of quantum coherence, quantum noise, and quantum many-body correlations in this process is only beginning to be studied [9, 10, 11]. Optical quantum control of rare gas nuclear spin ensembles is still in its infancy, and key concepts in quantum technology, such as the generation of nonclassical states for quantum metrology [12] or the storage of quantum states of light [13], have not yet been demonstrated.

In this work, we propose a technique for the optical manipulation of helium-3 nuclear spins in the quantum regime. Since the nuclear spin state cannot be manipulated directly with light, our approach uses metastability exchange collisions to establish an effective coupling between light and nuclear spin. Contrary to some ideas previously proposed [9, 10] at the Laboratoire Kastler Brossel, where the theoretical work presented in this thesis was carried out, the scheme considered here realizes a Faraday interaction [14] coupling the fluctuations of light and nuclear spin. This interaction is nowadays commonly used as a powerful and versatile spin-light quantum interface in experiments with alkali vapors [14, 15]. Because our scheme does not require other atomic species as a mediator [11] and the metastability exchange collision rates are comparatively high [1], it can operate at room temperature and millibar pressures, as is the case in experiments with helium-3. Furthermore, the interaction can be switched on and off, switching the weak electric discharge that populates the metastable state, allowing for effective coupling between nuclear spin and light. Our scheme

will enable the development of quantum-enhanced technologies with helium-3, such as measurement devices with sensitivity beyond the standard quantum limit [12]. This work gives a detailed theoretical presentation of the squeezing mechanism and its limits as well as a feasibility study taking into account experimentally accessible values of the parameters. Very recently, similar ideas have been put forward in a different physical system, the alkali rare gas mixture [11, 16].

This chapter introduces the main concepts and proposals on which the first part of this thesis is based. The first section discusses the helium-3 atom and its nuclear spin at the exceptional coherence time, it also addresses the question of optical pumping of an ensemble of helium-3 atoms. This question is not unrelated to our work: on the one hand, the experiment we plan requires that the atoms be initially polarized, on the other hand, our proposal is a conversion of the optical pumping techniques in helium-3. Moreover, the equations that were developed to describe the optical pumping of helium form the starting point of our analytical study. In the following section, we present spin-squeezed states as well as a metric for them with each other based on their metrological utility. Section 1.3 presents the experimental scheme as we envision it. Finally, we end this introductory chapter with a discussion around nondestructive quantum measurement, the technique by which we create quantum correlations in the nuclear spin ensemble.

1.1 Helium-3: Physical Properties and Optical Pumping

Helium-3 is the second stable isotope of helium in terms of abundance. Its nucleus is composed of two protons and one neutron, which gives it a non-zero nuclear spin $I = 1/2$. Moreover, as a noble gas, the electronic layers of the atom are all complete in the ground state and its electronic spin is then zero. Which makes a remarkable property: the total spin of helium-3 is therefore purely nuclear in its ground state. As a consequence, these spins can have very large coherence times in the cell. Thus, a coherence time T_2^* higher than 60 hours has been measured in ultra-precise magnetometry devices [17], and seems to be limited only by the longitudinal decay time T_1 due to collisions with the walls. [1] These values make the macroscopic nuclear spin of a gas at room temperature an ideal system for the production, the study and the use of entangled states, and thus a competitor of cold atomic gases and Bose-Einstein condensates in metrology and quantum information processing [12].

Optical pumping in helium and metastability exchange collisions By a well-controlled indirect nuclear polarization technique of helium-3, one can routinely prepare a giant collective nuclear spin, reaching a rate of 90%, with an extremely long lifetime. This old technique is now called "metastability exchange collision". Historically, the standard direct optical pumping for polarization could not be applied on ^{3}He gases because no transition was accessible to the atomic lamps of that time. Let us recall that the principle of optical pumping consists in creating a situation of asymmetry between an excitation process (or processes) of the atom on the one hand and a de-excitation process (such as spontaneous emission) on the other hand in order to bring as many atoms as possible into a given Zeeman sub-level. This requires the ability to interact optically with the excited states of the atom. For the helium-3 atom, the first excited state is far away in the ultraviolet, around 20 eV

[1] Times T_1 of several hundred hours can even be obtained [1].

from the ground state, and even to this day, lasers accessing such transitions in experiments are not standards. This problem of nuclear polarization of the helium atom was of great importance in the post-war years because there was a large demand for polarized targets in nuclear physics experiments [18]. The impossibility of creating such targets gave rise to many alternative proposals, for example via polarization effects in solids such as the "Overhauser" effect or in helium-3 liquids, but these methods proved insufficient. In 1960, the optical method made a comeback with an article by Bouchiat, Carver and Varnum [19]. It consists in an indirect optical pumping by considering a mixture of helium-3 and rubidium where the transfer mechanism is a dipolar interaction. The authors reach only 0.01% polarization, which is still insufficient for nuclear collision experiments. At the same time, the technique of optical pumping of helium-3 atoms in a metastable state was being perfected [20]. The most efficient polarization method was introduced in 1962 by Walters, Colegrove and Schearer [21] with a polarization of a few percent and rapidly improved to 40% polarization in 1963 [22]. It is based (i) on the use of the first excited state of the atom 2^3S_1 that is called "metastable" because its lifetime is of the order of 10^3 seconds [23] and (ii) on the collisions between the atoms of the ground state and those in the metastable state. These collisions have the astonishing property of being able to transfer the polarization from one atom to another, i.e. the states of the electronic clouds are exchanged from one nucleus to another. They were already known but it was not obvious to consider them as a mechanism capable of transferring polarization[2] because the ratio between the two populations, fundamental and metastable, is extremely large so that atoms in the fundamental state do not often collide with a metastable. However, as Walters, Colegrove and Schearer pointed out (i) metastables collide with a ground state very quickly and even more quickly than they absorb photons so the transfer rate is not marginal and (ii) it is sufficient that the relaxation rate of the nuclear spin is lower than this transfer rate for nuclear polarization to occur. However, the nuclear spin is naturally protected against optical relaxations. This opened the way to large polarizations in noble gases which were explored in the following years. Among the remarkable developments of which our work is a continuation, we can mention the articles of J. Dupont-Roc, M. Leduc and F. Laloë [24] in the first half of the 1970's where the equations governing the dynamics of the spin variables of a helium mixture in the ground state and in the metastable state in the presence of these metastability exchange collisions are formally established. These equations are the starting point of our formalism.

1.2 Spin squeezing: concept and issue

By analogy with the squeezed states of light in quantum optics, a spin (here collective) $\vec{I}$ is said to be in a squeezed state if, in a direction Oz orthogonal to that Ox of the mean spin, it admits reduced fluctuations with respect to the standard quantum limit. The standard quantum noise (or limit) corresponds to standard deviations $\Delta I_y^{\rm st} = \Delta I_z^{\rm st} = (|\langle I_x\rangle|/2)^{1/2}$ i.e. to the case of equality with rotational symmetry of the fluctuations around the mean spin in the Heisenberg inequality $\Delta I_y \Delta I_z \geq |\langle I_x\rangle|/2$, our spins being dimensionless here. These squeezed spin states are of great use in the context of quantum metrology. Indeed, high

[2] We can take as an example Colegrove and Franken (1960) [20] which we have already quoted, where collisions are considered as an incoherent process that would destroy the electron spin "memory" of the metastable atom.

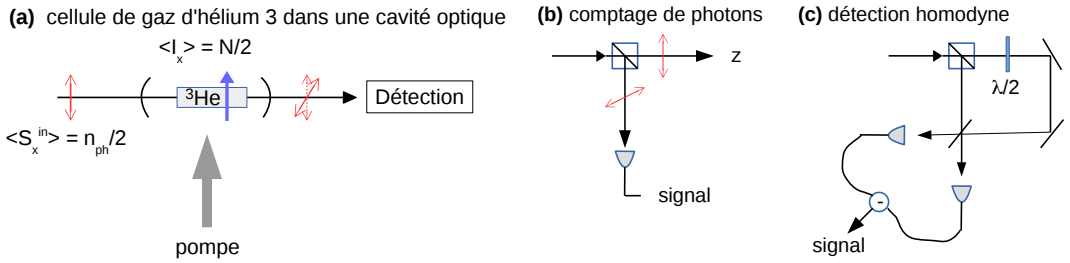

Figure 1.1: Overview of the set-up. (a) Centimeter glass cell filled with helium-3 gas at room temperature and placed in an optical cavity of axis Oz (horizontal axis on the figure). The Stokes spin of the light and the atomic spins (nuclear and metastable) are linearly polarized along Ox (vertical axis on the figure). The Oy polarized cavity field mode, initially empty, is populated by the Faraday effect due to the quantum fluctuations of the spin of the metastables along Oz during its propagation in the gas. It is measured continuously outside the cavity by one of the two following methods: (a) the photons leaving the cavity polarized along Oy are separated from those polarized along Ox by a polarizer cube and then detected in the photon counting regime; (b) a homodyne detection of a quadrature of the Oy polarized outgoing field is performed, using the Ox polarized outgoing field as a local oscillator (whose polarization has been rotated with a half-wave plate beforehand to bring it along Oy).

precision measurements for physical quantities such as the strength or direction of a field or a time interval translate into a phase accumulated in the spin of an atomic ensemble. If one imagines such a fully polarized spin, rotating on the Bloch sphere, then the initial variance of the spin component in the direction of rotation, crucial for any estimate of the accumulated phase, is equal to $\frac{N}{4}$ with N the number of atoms in the ensemble. When discussing squeezed states, it is therefore interesting to compare them with this "classical" state. In the remainder of this section, when we consider the squeezed nuclear spin, we will discuss the ratio of the variance of this state to that of the coherent state, which we will express in decibels ($10\log_{10}(r)$ with r the ratio of variances and $\log_{10}$ the logarithm function in the base 10). Further discussion shows that, in the considered scheme, the noise-to-signal ratio in a precession frequency measurement is in fact proportional to $\xi = (2I)^{1/2}\Delta I_z/|\langle I_x\rangle|$ (this naturally brings out the fluctuations of the angle that gives the spin direction in the xOz plane) rather than to the naively expected $\Delta I_z/\Delta I_z^{\rm st}$ ratio [25]. We will then also use this metric to gauge the interest of a spin squeezed state in the rest of this part.

1.3 Schematic diagram for the experimental set-up

The physical system considered is shown in figure 1.1. A cell filled with a polarized pure gas of helium-3 atoms at a pressure of a few mbar is placed inside an optical cavity whose axis is noted Oz. While the majority of the atoms remain in the fundamental singlet state 1^1S of helium, a weak discharge carries a tiny fraction of the atoms, usually $\simeq 10^{-6}$, into the metastable triplet state 2^3S. We represent on figure 1.2 the useful energy levels of the helium-3 atom. We note $\vec{I}$ the spin associated to the ground state, which is a singlet state. The metastable spin is a triplet state and we note $\vec{K}$ and $\vec{J}$ the spins associated

to the hyperfine multiplicity $F = 1/2$ and $F = 3/2$ respectively. Using the polarization techniques we previously introduced, we polarize the atomic sample in the Ox direction by optical pumping. The coupling between these three subsystems, the total spin of the

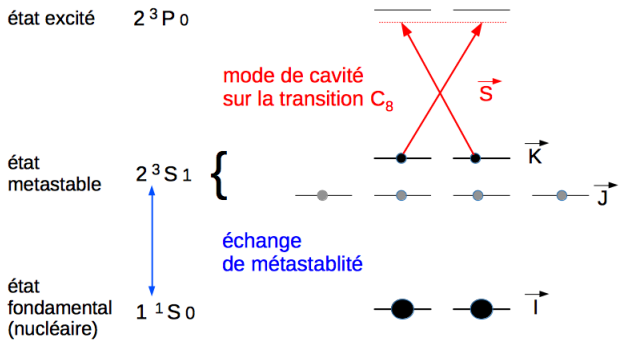

Figure 1.2: Useful energy levels of the ^{3}He atom (the Zeeman sublevels correspond to the choice of Oz as the quantization axis, the atoms being polarized along Ox). The six sublevels of the 2^3S_1 metastable state are coupled to the two (purely nuclear) sublevels of the 1^1S_0 ground state by the metastability exchange collisions.

atoms in the ground state, the total spin of the atoms in the metastable state and the light mode of the cavity is done two by two. On the one hand, a laser beam propagating along the cavity axis Oz and linearly polarized along the direction Ox is injected into the cavity to excite the transition C_8 between the $F = 1/2$ level of the metastable state 2^3S_1 and the highest energy level $F = 1/2$ of the excited state 2^3P, with a negative frequency detuning much larger in absolute value than the Doppler half-width of the excited state (of the order of 1 GHz), so that the resonant velocity class with the laser is almost empty, but much weaker than the 6.74 GHz hyperfine cleavage in the metastable state (and a fortiori than the 29.6 GHz $2^3P_1 - 2^3P_0$ fine cleavage in the excited state), so that the $F = 3/2$ metastable level is very little affected by the laser. [3] An effective Faraday-like coupling between the optical cavity mode and the total spin of the metastable state is then obtained. On the other hand, atoms in the metastable state 2^3S (of hyperfine electronic and nuclear spin) are coupled to atoms in the ground state (of purely nuclear spin) by metastability exchange collisions; remarkably, although each exchange collision is individually incoherent, this leads to a well-defined macroscopic coupling between the corresponding collective spins [24, 27]. As the Faraday interaction with the metastable atoms slightly rotates around the Oz axis the polarization of the light initially directed along Ox, by an angle proportional to the collective spin component of the metastables along Oz as we shall see, a continuous destructive measurement of the polarization component according to Oy of the field leaving the cavity (i) by photon counting as shown in figure 1.1(b) or (ii) by homodyne detection as in figure 1.1(c), realizes in fine a continuous quantum nondemolition (QND) measurement

[3] The frequency spacing does not allow to largely satisfy these two constraints, and one cannot exclude that the coupling of $F = 3/2$ to the field has a small effect on the squeezing dynamics; we neglect it here but it could be taken into account with a more complete Hamiltonian than our minimal model (3.2), such as that of reference [26]. We have furthermore verified, using this reference, that there is no "magic" laser frequency, far from resonance that would cancel the contribution of the $F = 3/2$ level alignment tensor to the light shift operator.

of the collective nuclear spin according to Oz of the helium-3 atoms in the ground state. This quantum nondemolition measurement, which we present in the next section, reduces the quantum fluctuations associated with the measured observables and thus prepares a spin squeezed state. We summarize by the following diagram the set of steps for the case of a homodyne detection.

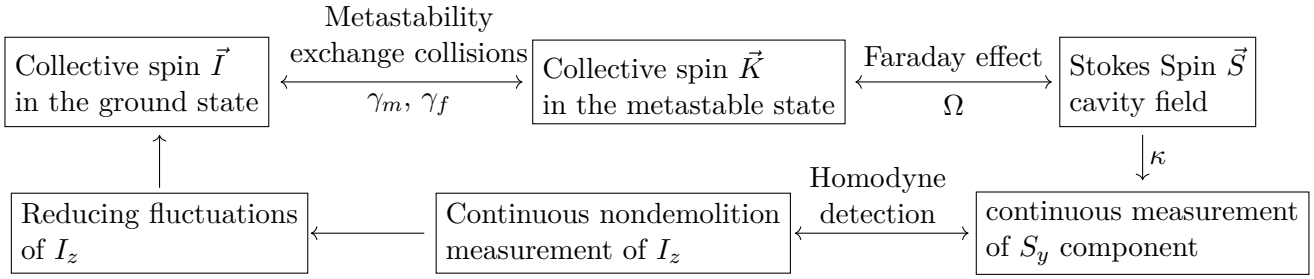

1.4 Quantum nondemolition measurements

In quantum mechanics, we formalize the effect of a measurement on a system as the projection of the state vector onto a certain subspace of the Hilbert space that corresponds to an eigenvalue of the measured quantity. In the case of a perfect measurement, if we note $|\psi\rangle$ the state vector, $\hat{A}$ the measured observable and a the value obtained by the measurement, eigenvalue of $\hat{A}$; then the state of the system just after the measurement is $|a\rangle$, the eigenvector of $\hat{A}$ associated to the eigenvalue a, in the non-degenerate case. Note that the variance of $\hat{A}$ in the state just after the measurement is zero: the measurement has squeezed (infinitely) the state of the system with respect to $\hat{A}$. As expected, the variance in the conjugate operator is infinite (in order to respect the Heisenberg's uncertainty principle between the two operators). This is a situation well known from quantum physics textbooks: when the projective measurement of the position of a particle gives the result $\bar{x}$, the wave function in the position space is the Dirac distribution $\delta(x - \bar{x})$, of zero variance, the wave packet in the momentum space is then uniform over the whole space. In an imperfect measurement, a measurement whose result is compatible with several eigenvalues of the observable, the state vector immediately after a measurement is not an eigenvector of the observable, but we should expect the variance of $\hat{A}$ in this superposition to be less than the initial one if during the measurement we have indeed gained information on the state of the system. As an example, let us consider the case of a particle of mass m in free space, whose motion is governed by the Hamiltonian $\hat{H} = \frac{1}{2m}\hat{P}^2$, with $\hat{P}$ the momentum observable of the particle, conjugated to the observable $\hat{X}$ its position. At an instant t, we measure $\hat{X}$ and we obtain the value $\bar{x}$. This is the same situation as before, except that in the case of an imperfect measurement, we expect a wave function centered on $\bar{x}$ and of non-zero width. Of course, in the case of the free particle, the evolution induced by $\hat{H}$ will quickly destroy any correlations thus created by the measurement. Moreover, the Heisenberg's uncertainty principle between the position and the momentum implies a very large variance in the momentum to compensate for the squeezing in position. Therefore, the wave function will spread rapidly in space after the measurement. Let us now consider the case of a measurement of the $\hat{P}$ momentum at time t, still on our free particle. From then on, it is in the momentum space where the wave function immediately after t is centered and narrow but, unlike the measurement of the position, this

observable is a constant of the motion! Indeed, $[\hat{H}, \hat{P}] = 0$. So not only is the mean of the observable $\hat{P}$ a constant of motion, but so is its variance! Therefore, the measurement of the momentum of a free particle creates lasting correlations in the wave function. To our knowledge, there is no such measurement of the momentum of a free particle but the idea presented here is generic enough to be applied to any kind of quantum system. These nondemolition measurements, due to the commutation of the measured observable with the Hamiltonian are known and discussed since the dawn of quantum mechanics but it is only in the course of the decade 1970 that V. B. Braginskii and Yu. I. Vorontsov proposed for the first time a method based on this property to measure the number of excitations in a resonant electromagnetic cavity without disturbing its energy [28, 29, 30]. At that time, physical measurements became so precise that the quantum formalism was necessary to describe the system and the measuring apparatus. In astrophysics, for example, it became crucial for the then emerging field of gravitational waves detection to be able to measure the number of excitations of a mechanical or electromagnetic oscillator in the quantum regime without disturbing this number of excitations.[4] Later, these techniques diffused into quantum optics when the manipulation of the states of the field in a cavity or of the internal variables of atoms in a cavity took off. In particular, the emergence of the production of "quantum noise" states, i.e. states that saturate the Heisenberg's uncertainty principle for two conjugate variables (one can think of a coherent state of a light mode where $\Delta X = \Delta P = \hbar/2$), transformed this fundamental limit into a technological obstacle to overcome.

As we have already discussed in section 1.2, one can define a "standard quantum limit" for a certain quantity, which corresponds to the value of the variance of this quantity in a coherent state that saturates the Heisenberg principle. A state whose variance on the quantity of interest is lower than this limit is said to be squeezed. In the case of the collective spin of a gas consisting of N atoms polarized along a direction $\langle S_x \rangle = \frac{N}{2}$, i.e. $\Delta S_y \Delta S_z \geq N/4$, the standard quantum limit on one of the directions perpendicular to the average spin is thus equal to $N/4$.

[4] The ideas of V. B. Braginskii and Yu. I. Vorontsov had a bright future since their influence can be found until today in the spectacular first direct observation of a gravitational wave by the LIGO/VIRGO collaboration in 2015 [31], of which Braginskii is a member.

Chapter 2

Metastability Exchange Collisions

Foreword

In this chapter, we will study the equations describing metastability exchange collisions in helium-3 gases and show in particular that they can transfer quantum correlations from the metastable state to the ground state. Known since the 1950s, these collisions exchange the state of the electron cloud between the two atoms and profoundly affect the dynamics of the internal variables of the gas, i.e. its different spin moments. They were first used in 1962 in the context of optical pumping of the nuclear spin of helium-3, but a complete study of the evolution of the one-body density matrix and the observables of the gas was not developed until the early 1970s. These equations form the basis of the quantum description of our system.

This chapter will therefore start with a review of the physical origin of these collisions followed by a description of the effects they have on the internal variables of a gas under the conditions of our study. This will lead us to recall the equations for the evolution of the means of the observables of the system developed by J. Dupont-Roc, M. Leduc and F. Laloë in 1973 [24]. These equations concern average values of atomic observables. In order to study the effect of exchange on quantum correlations, we introduce a description in terms of a master equation of the Lindblad form which we will use in the next chapters. Finally, we close the chapter with a simplified model of the ground-state and metastable helium-3 atom, to illustrate how these collisions can transfer quantum correlations. The mathematical developments necessary for this illustration will form an introduction to those we will present in chapter 3.

2.1 Physical origins of metastability exchange collisions

Among the elastic collisions between two atoms of the same species, the case where one of the two atoms is initially in a metastable excited state has given rise to a rich scientific literature very early on. This history can be linked to the presence of this type of collision in many energy transport phenomena in flames, explosions, or photochemistry [32]. These collisions can be separated into two channels : one can speak of simple scattering when $X + X^* \rightarrow X + X^*$ and exchange or transfer collision for the $X + X^* \rightarrow X^* + X$ process where the electronic excitation of one is transferred to the other. For a given species with

a given excited state, these exchange processes quickly become complicated to analyse. To obtain total or differential cross sections, for example, the interaction potential of the $X - X^*$ dimer must be studied, the N-body Hamiltonian is then characterised by a multitude of energy scales (Van der Walls, fine and hyper-fine interaction) and distance scales (nucleus 1 - nucleus 2, electron cloud 1 - nucleus 1, electron cloud 2 - nucleus 1, etc). Among all the situations in which such processes appear, the case of helium stands out for its a priori unique properties. Firstly, the $He - He^* \rightarrow He^* - He$ process, which is then called metastability exchange collision, plays an important role in the dynamics of a ground-state/metastable mixture and dominates the decoherence processes, even at room temperature. The collision has important effects on the internal variables, since the state of the electron cloud can be considered to be exchanged at the time of the collision. If the subsequent hyperfine interaction is taken into account, then the nuclear spin of the metastable is polarised with the electron spin. Thus, the electron spin of the metastable before the collision has been transferred to the nuclear spin of the ground-state atom following the collision! It is possible to observe these metastable exchange collisions in the case of other noble gases, such as neon or xenon [33, 34], but they are accompanied by other depolarising collision channels that dominate them[1]. Thus only helium seems to have a dynamic strongly driven by exchange collisions. It would be tricky to give a full justification here but its full electronic layer which protects against electronic recombination, even in the case where an electron is excited combined with the low binding energy of the helium dimer (of the order of mK) as well as an internuclear distance of the order of 60Å [37] are atomic properties which seem to favour the exchange process [38].

From a theoretical point of view, some aspects of metastability exchange collisions in helium are relatively simple to analyse. As J. Dupont-Roc points out in his thesis [27], it is possible to treat independently the energetic aspect of the collision, i.e. the calculation of the effective cross sections, and the internal aspect, i.e. the evolution of the spins of the atoms under the effect of the collision. It is indeed possible to obtain the equations for the evolution of the Zeeman sublevel and density matrix populations without ever having to specify the form of the interaction potential. Only needed are considerations of symmetry, conservation and selection rules during the collision. We will not reproduce these developments here, but they can be found in the above mentioned thesis [27] and in reference [24]. In the following section, we will present the internal variables of the atoms and the equations that govern the evolution of the collective variables of a macroscopic mixture of atoms in the ground and metastable states.

2.2 Evolution equations for the observables

In this section, we now consider a helium-3 gas and its collective observables. The situation is similar to that of the diagram in figure 1.1(a) with respect to the cell and the atoms, putting aside any reference to the optical cavity and to light : in the cell, the gas is at room temperature and at a pressure of a few mbar. There are N_{cell} atoms in their ground state to which a low intensity electric discharge is applied, which brings a small fraction of the atoms into the

[1] Let us also mention reference [35], where they try to polarise the nuclear spin of a xenon-129 via the metastable state as for helium, without success. The authors mention possible additional decoherence channels for ground state atoms. A nuclear polarization of a xenon-131 gas was nevertheless realized via metastable exchange collisions in 1967 [36], but within an electron beam.

metastable 2^3S_1 state (and whose lifetime is finite because the atom de-excites by collision with the cell walls). The discharge is maintained continuously during the experiment, which allows us to consider the number of metastable n_{cell} fixed. Metastability exchange collisions are then the only processes affecting the atomic variables. In the remainder of this section, after defining these variables, we discuss their evolution during a collision and then their evolution at the macroscopic level, first by means of density matrices and then by collective averages.

Definitions of observables The ground state of helium-3 is of configuration 1^1S_0. In this configuration, an atom has a nuclear spin of quantum number $I = 1/2$ while the spin of the electron cloud is zero, we note $\vec{I}_f^{at}$ the nuclear spin of an atom initially in such a state. In the metastable state, the spin configuration is 2^3S_1. In addition to the nuclear spin, which is noted $\vec{I}_m^{at}$, the atom then has an electron spin of quantum number $S = 1$, which is noted $\vec{\Sigma}_m^{at}$. We also note $\vec{J}_m^{at}$ and $\vec{K}_m^{at}$ the spins associated with the hyperfine multiplicities $F = 3/2$ and $F = 1/2$ of $\vec{I}_m^{at} + \vec{\Sigma}_m^{at}$, the total spin of an atom in the metastable state. We should not forget $\vec{\vec{Q}}_m^{at}$ the alignment tensor in $F = 3/2$, of Cartesian coordiantes $Q_{\alpha\beta}^{(at)}$. The elements of the alignment tensor can be written as

$$Q_{\alpha\beta}^{(at)} = \frac{1}{6}\left[3\frac{\Sigma_\alpha^{(at)}\Sigma_\beta^{(at)} + \Sigma_\beta^{(at)}\Sigma_\alpha^{(at)}}{2} - S(S+1)\delta_{\alpha\beta}\right] \tag{2.1}$$

with $\alpha, \beta = x, y, z$ and $\delta_{\alpha\beta}$ the non-zero Kroenecker symbol equal to 1 only for $\alpha = \beta$. Finally, these two configurations have zero orbital angular momentum. The one-body collective variables can be defined as the direct sum of the operator of this variable, over all atoms of a population. Thus, we note $\vec{I} = \sum_{i=1}^{N_{\text{cell}}} \vec{I}_f^{at}(i)$ the collective nuclear spin of atoms in the ground state, where i runs from 1 to N_{cell} and designates the atom i in the ground state. We can do the same for $\vec{\Sigma}_m = \sum_{j=1}^{n_{\text{cell}}} \vec{\Sigma}_m^{at}(j)$, $\vec{J} = \sum_{j=1}^{n_{\text{cell}}} \vec{J}_m^{at}(j)$, $\vec{K} = \sum_{j=1}^{n_{\text{cell}}} \vec{K}_m^{at}(j)$ and $\vec{\vec{Q}} = \sum_{j=1}^{n_{\text{cell}}} \vec{\vec{Q}}_m^{at}(j)$ where this time the sum runs from 1 to n_{cell} and designates an atom in the metastable state.

2.2.1 Observables during the collision

During a metastability exchange collision, no magnetic interaction plays a role in the collision: indeed, the spin-orbit interactions are all zero because the two atoms are in an s configuration. As for the hyperfine spin-spin couplings, the speed of the atoms at room temperature makes them unable to affect the spins because the atoms only remain in proximity to each other for an extremely short time (of the order of a few hundred femtoseconds). As the electrostatic interaction dominates the interaction potential, we conclude that the spin operators commute with the Hamiltonian, establishing a conservation of the different magnetic moments during the collision. Thus, the electron spin is transferred without alteration, together with the electron cloud during the metastability exchange collision. It is easy to understand how these metastability exchanges allow the transfer of a spin polarisation: once the metastable population is created by electric discharge in the gas and then optically pumped to the $2^3S - 2^3P$ transition, the orientation is shared between the electronic and nuclear spin of the metastable atoms. When a metastable atom polarized in this way undergoes an exchange collision with an atom in the ground state, the electron clouds are exchanged between the nuclei. The nucleus that belonged to the metastable population and whose spin is polarized

	Ground state	Metastable
Before	$\rho_f^{(1)}$	$\rho_m^{(1)}$
After	$\mathrm{Tr}_e\, \rho_m^{(1)}$	$\rho_f^{(1)} \otimes \mathrm{Tr}_n\, \rho_m^{(1)}$

Table 2.1: $\rho_f^{(1)}$ represents the density matrix of an atom in the ground state, $\rho_m^{(1)}$ that of an atom in the metastable state and Tr_n, Tr_e the trace operations on the nuclear and electronic variables respectively.

no longer has an electron spin and now participates in the collective spin of the ground state. In the work presented in the article by J. Dupont-Roc, M. Leduc and F. Laloë of 1973 [24] as well as in the thesis of J. Dupont-Roc [27], the evolution equations of the observables are reconstructed without any cross-section calculation, simply by a careful study of the useful elements of the collision scattering matrix from the physical and symmetry remarks that we have just presented. We will limit ourselves here to recalling these equations without going into the details of their construction.

2.2.2 The evolution of the macroscopic gas observables

Description in terms of density matrix Let us note $\rho_f^{(1)}$ the density matrix of an atom in the ground state, $\rho_m^{(1)}$ that of an atom in the metastable state and Tr_n, Tr_e the trace operations on the nuclear and electronic variables respectively, we also note $\mathrm{Tr} = \mathrm{Tr}_n\, \mathrm{Tr}_e = \mathrm{Tr}_e\, \mathrm{Tr}_n$ the complete trace. We set $\mathrm{Tr}\, \rho_m^{(1)} = 1$ and $\mathrm{Tr}\, \rho_f^{(1)} = 1$. Table 2.1 represents the exchange collsion from these matrices. We consider that there is no coherence between the metastable and ground states before or after the collision. [2] The one-body density operators for atoms in the ground state and metastable state are ρ_f and ρ_m respectively[3].

[2] Let us note the conservation of the total spin of the two atoms by these collision rules: Indeed, noting I_z, S_z, the spins of a nucleus and of the electron cloud respectively and $\Sigma_{\mathrm{total},z}$ this total spin in the z direction for example. We have

$$\langle \Sigma_{\mathrm{total},z}(\text{before collision}) \rangle = \mathrm{Tr}_n \left[\rho_f^{(1)} I_z \right] + \mathrm{Tr} \left[\rho_m^{(1)} (I_z + S_z) \right] \tag{2.2}$$

and recall that the initial state of the metastable atom $\rho_m^{(1)}$ runs on the nuclear and electronic variables. After the collision, we can write

$$\begin{aligned} \langle \Sigma_{\mathrm{total},z}(\text{after collision}) \rangle &= \mathrm{Tr}_n \left[\mathrm{Tr}_e\, \rho_m^{(1)} I_z \right] + \mathrm{Tr} \left[(\rho_f^{(1)} \otimes \mathrm{Tr}_n\, \rho_m^{(1)})(I_z + S_z) \right] && (2.3) \\ &= \mathrm{Tr} \left[\rho_m^{(1)} I_z \right] + \mathrm{Tr}_n \left[\rho_f^{(1)} (I_z + S_z) \right] + \mathrm{Tr}_e \left[(\mathrm{Tr}_n\, \rho_m^{(1)})(I_z + S_z) \right] && (2.4) \\ &= \mathrm{Tr} \left[\rho_m^{(1)} I_z \right] + \mathrm{Tr}_n \left[\rho_f^{(1)} I_z \right] + \mathrm{Tr} \left[\rho_m^{(1)} (I_z + S_z) \right] && (2.5) \end{aligned}$$

where $\mathrm{Tr}_n \left[\rho_f^{(1)} S_z \right] = 0$ and $\mathrm{Tr}_e \left[(\mathrm{Tr}_n\, \rho_m^{(1)})(I_z + S_z) \right] = \mathrm{Tr} \left[\rho_m^{(1)} (I_z + S_z) \right]$ were used. We then find (2.2) and so $\langle \Sigma_{\mathrm{total},z}(\text{after collision}) \rangle = \langle \Sigma_{\mathrm{total},z}(\text{before collision}) \rangle$.

[3] The one-body density matrix describing the helium gas is then of the form $\begin{pmatrix} \rho_m & 0 \\ 0 & \rho_f \end{pmatrix}$ with ρ_m a matrix of size 6×6 and ρ_f of size 2×2

For independent atoms, we can write

$$\rho_f = \sum_{i=1}^{N_{\text{cell}}} \rho_f^{(1)}(i) \quad \text{and} \quad \rho_m = \sum_{j=1}^{n_{\text{cell}}} \rho_m^{(1)}(j) \tag{2.6}$$

with $\rho_f^{(1)}(i), \rho_m^{(1)}(j)$ the density matrices of atom number i and j respectively. By definition, $\operatorname{Tr}\rho_f = N_{\text{cell}}$ and $\operatorname{Tr}\rho_m = n_{\text{cell}}$. We introduce the quantity $\frac{\mathrm{d}t}{T}$ which represents the fraction of ground state atoms undergoing a metastability exchange collision during a time interval $\mathrm{d}t$. T^{-1} is therefore a metastability exchange collision rate for a ground state atom. Similarly, we can define the ratio $\frac{\mathrm{d}t}{\tau}$ representing the fraction of metastable atoms undergoing an exchange collision in a time interval $\mathrm{d}t$, with τ^{-1} being an exchange rate of metastables. Since an equal number of ground-state atoms and metastable atoms have undergone an exchange collision, we can write:

$$\frac{N_{\text{cell}}}{T} = \frac{n_{\text{cell}}}{\tau}. \tag{2.7}$$

Thus the exchange rate ratio is equal to the population ratio $\frac{\tau}{T} = \frac{n_{\text{cell}}}{N_{\text{cell}}}$. From these rates and the 2.1 table, and considering only metastability exchange collisions, one can write evolution equations for the previously defined one-body density matrices:

$$\mathrm{d}\rho_f = -\frac{\mathrm{d}t}{T}\rho_f + \frac{\mathrm{d}t}{\tau}\operatorname{Tr}_e \rho_m \tag{2.8}$$

$$\mathrm{d}\rho_m = -\frac{\mathrm{d}t}{\tau}\rho_m + \frac{\mathrm{d}t}{T}\rho_f \otimes \operatorname{Tr}_n \rho_m. \tag{2.9}$$

From these evolution equations, it is possible to obtain those of the averages of the one-body observables of the gas. The mean of the one-body operator $\hat{O} = \sum_{i=1}^{\mathcal{N}} O_i$ is defined by $\langle\hat{O}\rangle = \operatorname{Tr}(\hat{O}\sigma)$, replacing σ by ρ_f or ρ_m depending on the nuclear or metastable nature of the observable. For its evolution, it is sufficient to consider the trace of one or other of the evolution equations of the density matrices (2.8) and (2.9) multiplied by the observable $\frac{\mathrm{d}}{\mathrm{d}t}\langle\hat{O}\rangle = \operatorname{Tr}(O\frac{d\sigma}{\mathrm{d}t})$. Finally, note that $\langle\hat{O}\rangle = \mathcal{N}\langle O\rangle_{\text{at}}$.

Evolution of internal variables Therefore, the contribution of the metastability exchange collisions (MEC) between ground-state and metastable atoms can be deduced directly from the master equation on the one-atom density operator of references [24, 27] by simply multiplying or dividing by the total number of ground-states N_{cell} or metastables n_{cell} in the cell:

$$\left.\frac{\mathrm{d}\langle\vec{K}\rangle}{\mathrm{d}t}\right|_{\text{ECH}} = -\frac{7}{9\tau}\langle\vec{K}\rangle + \frac{1}{9\tau}\langle\vec{J}\rangle - \frac{1}{9\tau}\frac{n_{\text{cell}}}{N_{\text{cell}}}\langle\vec{I}\rangle - \frac{4}{3\tau}\frac{1}{N_{\text{cell}}}\langle\vec{\vec{Q}}\rangle \cdot \langle\vec{I}\rangle \tag{2.10}$$

$$\left.\frac{\mathrm{d}\langle\vec{J}\rangle}{\mathrm{d}t}\right|_{\text{ECH}} = -\frac{4}{9\tau}\langle\vec{J}\rangle + \frac{10}{9\tau}\langle\vec{K}\rangle + \frac{10}{9\tau}\frac{n_{\text{cell}}}{N_{\text{cell}}}\langle\vec{I}\rangle + \frac{4}{3\tau}\frac{1}{N_{\text{cell}}}\langle\vec{\vec{Q}}\rangle \cdot \langle\vec{I}\rangle \tag{2.11}$$

$$\left.\frac{\mathrm{d}\langle Q_{\alpha\beta}\rangle}{\mathrm{d}t}\right|_{\text{ECH}} = -\frac{2}{3\tau}\langle Q_{\alpha\beta}\rangle + \frac{1}{9\tau}\frac{1}{N_{\text{cell}}}\left(3\frac{\langle I_\alpha\rangle\langle\Sigma_\beta\rangle + \langle I_\beta\rangle\langle\Sigma_\alpha\rangle}{2} - \delta_{\alpha\beta}\langle\vec{I}\rangle \cdot \langle\vec{\Sigma}\rangle\right) \tag{2.12}$$

$$\left.\frac{\mathrm{d}\langle\vec{I}\rangle}{\mathrm{d}t}\right|_{\text{ECH}} = -\frac{1}{T}\langle\vec{I}\rangle + \frac{1}{3T}\frac{N_{\text{cell}}}{n_{\text{cell}}}(\langle\vec{J}\rangle - \langle\vec{K}\rangle) \tag{2.13}$$

where $\langle\vec{\Sigma}\rangle = \frac{2}{3}\left[\langle\vec{J}\rangle + 2\langle\vec{K}\rangle\right]$ is the average value of the electron spin in the metastable state. Reference is made to equations (1.37b), (1.37a), (1.39) and (1.25) of reference [24] (taking into account a deviation of a factor 6 on the definition of the alignment tensor), or to equations (VIII.30), (VIII.29), (VIII.32) and (VIII.15) of reference [27] [adding a Kronecker factor $\delta_{\alpha\beta}$ omitted in (VIII.32)]. Note that this description neglects the hyperfine correlations between the $F = 3/2$ and $F = 1/2$ hyperfine levels of the metastable state. In general, collisions create such coherences via the $\rho_f \otimes \mathrm{Tr}_n\, \rho_m$ term in (2.9) but these evolve with a very large natural frequency (of the order of GHz) compared to the $1/\tau$ evolution rate (several MHz) which allows to decouple the evolution of coherences and hyperfine populations and to ignore the former (see part D of chapter VII of [27]).

2.3 Study of the two $1/2$-spins simplified model

To illustrate the effect of metastability exchange collisions on the collective variables of the gas, let us consider a simplified case where the ground state is characterised by a nuclear spin $I = 1/2$ and the metastable state by an electron spin $K = 1/2$. This simple model will reveal its physical interest when we adiabatically eliminate the fluctuations of the spin $\vec{J}$ as well as the alignment tensor $\vec{\vec{Q}}$ in chapter 3. Especially since the mathematical approaches used are the same. To facilitate comparison with the discussions in this chapter 3, we note N and n the numbers of atoms in the ground and metastable states respectively, $N = N_{\mathrm{cell}}$, $n = n_{\mathrm{cell}}$ and $\gamma_f = 1/T$, $\gamma_m = 1/\tau$ the collision rates. We always have the relation $\frac{\gamma_f}{\gamma_m} = \frac{n}{N}$ between rates and populations. In chapter 3, these quantities will correspond to the effective numbers in the case where the spins are not fully polarised initially. For the rest of this section, they represent only a change in notation.

2.3.1 Definitions and equations for quantum fluctuations

In the case of $I = \frac{1}{2}$ and $K = \frac{1}{2}$ the exchange collision has the only effect of exchanging the two spins and it is possible to convince oneself that the collective averages in an $\alpha = x, y, z$ direction reduce to

$$\frac{\mathrm{d}}{\mathrm{d}t}\langle K_\alpha\rangle = -\gamma_m\langle K_\alpha\rangle + \gamma_f\langle I_\alpha\rangle \tag{2.14}$$

$$\frac{\mathrm{d}}{\mathrm{d}t}\langle I_\alpha\rangle = -\gamma_f\langle I_\alpha\rangle + \gamma_m\langle K_\alpha\rangle. \tag{2.15}$$

Let us consider a stationary solution of this system of equations :

$$\langle K_x\rangle_s = \frac{n}{2}, \quad \langle I_x\rangle_s = \frac{N}{2}, \quad \langle K_{y,z}\rangle_s = \langle I_{y,z}\rangle_s = 0. \tag{2.16}$$

This solution corresponds to a perfectly polarized gas along the Ox axis, both ground-state and metastable atoms. The quantum fluctuation operators $\delta K_\alpha = K_\alpha - \langle K_\alpha\rangle_s$ and $\delta I_\alpha = I_\alpha - \langle I_\alpha\rangle_s$ are introduced for a spin component α orthogonal to the direction of polarisation.[4] These fluctuations obey the Langevin equations linearised around the stationary state. For

[4] By definition, $\langle\delta K_\alpha\rangle_s = 0$ and $\langle\delta K_\alpha^2\rangle = \mathrm{Var}_s K_\alpha$ and similarly for δI_α

example Oy, we have

$$\frac{\mathrm{d}}{\mathrm{d}t}\delta K_y = -\gamma_m \delta K_y + \gamma_f \delta I_y + f_{K_y} \tag{2.17}$$

$$\frac{\mathrm{d}}{\mathrm{d}t}\delta I_y = -\gamma_f \delta I_y + \gamma_m \delta K_y + f_{I_y}. \tag{2.18}$$

The operators f_{K_y} and f_{I_y}, Langevin forces, are zero mean and have a variance deduced to correctly reproduce the variances of the spins in the steady state for a set of independent atoms. If we note x_i, x_j two fluctuation operators (of zero means) with as evolution equation:

$$\frac{dx_i}{\mathrm{d}t} = \mathcal{E}_{x_i} + f_i \tag{2.19}$$

where $\mathcal{E}_{x_i}$ is a "deterministic" evolution operator and f_i a Langevin force, then we can calculate the average of a second moment with the relation:

$$\frac{\mathrm{d}}{\mathrm{d}t}\langle x_i x_j\rangle = \langle x_i \mathcal{E}_{x_j}\rangle + \langle \mathcal{E}_{x_i} x_j\rangle + D_{ij} \tag{2.20}$$

with $D_{ij} = \langle f_i f_j\rangle$ an element of the scattering matrix which is calculated in the polarized steady state (2.16) with the formula

$$D_{ij} = -\langle x_i \mathcal{E}_{x_j}\rangle_s - \langle \mathcal{E}_{x_i} x_j\rangle_s. \tag{2.21}$$

With respect to the elements of the scattering matrix defined by equations (2.17)-(2.18) :

$$D_{K_\alpha,K_\alpha} = D_{I_\alpha,I_\alpha} = -D_{K_\alpha,I_\alpha} = -D_{I_\alpha,K_\alpha} = \frac{1}{2}\gamma_m n = \frac{1}{2}\gamma_f N \tag{2.22}$$

with $\alpha = y, z$ and where all other elements are null.

2.3.2 Dynamics of quantum correlations

From equations (2.17)-(2.18) one can describe the transfer of quantum correlations between the ground state and the metastable state. Indeed, they allow to obtain a closed system of equations for the variances of the spin fluctuations:

$$\frac{\mathrm{d}}{\mathrm{d}t}\langle \delta K_y^2\rangle = -2\gamma_m \langle \delta K_y^2\rangle + \gamma_f \langle \{\delta K_y, \delta I_y\}\rangle + \frac{n\gamma_m}{2} \tag{2.23}$$

$$\frac{\mathrm{d}}{\mathrm{d}t}\langle \delta I_y^2\rangle = -2\gamma_f \langle \delta I_y^2\rangle + \gamma_m \langle \{\delta K_y, \delta I_y\}\rangle + \frac{n\gamma_m}{2} \tag{2.24}$$

$$\frac{\mathrm{d}}{\mathrm{d}t}\langle \{\delta K_y, \delta I_y\}\rangle = -(\gamma_m + \gamma_f)\langle \{\delta K_y, \delta I_y\}\rangle + 2\gamma_m \langle \delta K_y^2\rangle + 2\gamma_f \langle \delta I_y^2\rangle - n\gamma_m. \tag{2.25}$$

System that can be solved without difficulty for any initial state. Consider the case of an initial state where the nuclear spin is fully polarised in the Ox direction and the metastable spin is polarised in the same direction but squeezed in the Oy direction:

$$\langle \delta K_y^2\rangle(0) = \frac{n}{4}e^{-2r} \tag{2.26}$$

$$\langle \delta I_y^2\rangle(0) = \frac{N}{4} \tag{2.27}$$

$$\langle \{\delta K_y, \delta I_y\}\rangle(0) = 0 \tag{2.28}$$

with r a positive parameter. Integrating the differential equations (2.23)-(2.25) we obtain

$$\begin{pmatrix} \langle \delta K_y^2 \rangle \\ \langle \delta I_y^2 \rangle \\ \langle \{\delta K_y, \delta I_y\} \rangle \end{pmatrix} = \begin{pmatrix} \frac{n}{4}\left[1 - \frac{\gamma_f^2}{\gamma_m^2} C\right] \\ \frac{N}{4}\left[1 - \frac{\gamma_f}{\gamma_m} C\right] \\ -\frac{n}{2}\frac{\gamma_f}{\gamma_m} C \end{pmatrix} - \frac{n}{2} C e^{-(\gamma_m+\gamma_f)t} \begin{pmatrix} \gamma_f/\gamma_m \\ -1 \\ 1 - \frac{\gamma_f}{\gamma_m} \end{pmatrix} - \frac{n}{4} C e^{-2(\gamma_m+\gamma_f)t} \begin{pmatrix} 1 \\ 1 \\ -2 \end{pmatrix} \tag{2.29}$$

with $C = \frac{1-e^{-2r}}{1+(\frac{\gamma_f}{\gamma_m})^2}$. In the limit of a long time, this system admits a stationary state (which is reached after a time of order $(\gamma_m + \gamma_f)^{-1}$):

$$\Delta K_y^2 = \frac{n}{4}\left[1 - \left(\frac{\gamma_f}{\gamma_m}\right)^2 \frac{1 - e^{-2r}}{1 + (\frac{\gamma_f}{\gamma_m})^2}\right] \tag{2.30}$$

$$\Delta I_y^2 = \frac{N}{4}\left[1 - \frac{\gamma_f}{\gamma_m} \frac{1 - e^{-2r}}{1 + (\frac{\gamma_f}{\gamma_m})^2}\right]. \tag{2.31}$$

We can notice that the initial squeezing of the metastable spin parametrized by r is partly transferred to the nuclear spin because the term $\frac{\gamma_f}{\gamma_m}\frac{1-e^{-2r}}{1+(\gamma_f/\gamma_m)^2}$ is greater than 0 and thus $\Delta I_y^2 < \frac{N}{4}$. This transfer is fixed by the ratio of the populations $\gamma_f/\gamma_m = n/N \sim 10^{-6}$. Let us introduce the two-body correlation functions C_J and C_I in the metastable level and the ground-state level respectively:

$$C_J \equiv \sum_{l \neq k} \langle K_y^{at}(l) K_y^{at}(k) \rangle = \frac{1}{4(n-1)}\left(\frac{\Delta K_y^2}{n/4} - 1\right) \tag{2.32}$$

$$C_I \equiv \sum_{l \neq k} \langle I_y^{at}(l) I_y^{at}(k) \rangle = \frac{1}{4(N-1)}\left(\frac{\Delta I_y^2}{N/4} - 1\right) \tag{2.33}$$

where we sum over all atoms. We find an already known property of metastability exchange collisions [10] which tend to equalise the correlation functions C_J and C_I. Indeed, starting from (2.30) and (2.31)

$$1 - \frac{\Delta K_y^2}{n/4} = \left(\frac{\gamma_f}{\gamma_m}\right)^2 \frac{1 - e^{-2r}}{1 + (\frac{\gamma_f}{\gamma_m})^2} \underset{\gamma_f \ll \gamma_m}{\simeq} \left(1 - e^{-2r}\right)\left(\frac{\gamma_f}{\gamma_m}\right)^2 \tag{2.34}$$

$$1 - \frac{\Delta I_y^2}{N/4} = \frac{\gamma_f}{\gamma_m} \frac{1 - e^{-2r}}{1 + (\frac{\gamma_f}{\gamma_m})^2} \underset{\gamma_f \ll \gamma_m}{\simeq} \left(1 - e^{-2r}\right)\frac{\gamma_f}{\gamma_m}. \tag{2.35}$$

Thus

$$1 - \frac{\Delta K_y^2}{n/4} = \frac{\gamma_f}{\gamma_m}\left(1 - \frac{\Delta I_y^2}{N/4}\right) \tag{2.36}$$

$$C_J \frac{n-1}{n} = C_I \frac{N-1}{N} \quad \longrightarrow \quad C_J \simeq C_I. \tag{2.37}$$

This equalization of the correlation functions confirms that they do not reduce to an "inconsistent" exchange of polarizations by transferring excitations in the ground-state population, they also transfer quantum correlations between the atoms of the gas. As an illustration,

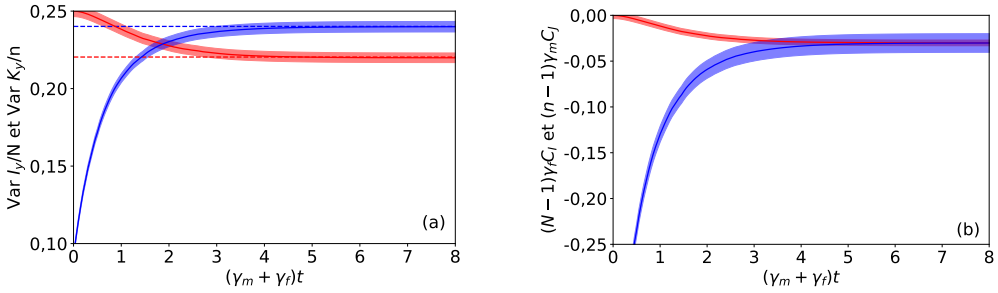

Figure 2.1: Quantity obtained from a Monte Carlo simulation of two collective spins, metastable and ground-state, coupled by metastability exchange collisions. Averaged over 10,000 Monte Carlo trajectories. $\gamma_f/\gamma_m = 1/3$. Initially, both spins are polarised in the Ox direction, the nuclear spin (in red) is in a coherent state while the metastable spin (in blue) is squeezed in the Oy direction as defined by the equation (2.26) with $r = 1/2$. The filled area represents the uncertainty on the Monte Carlo average. (a) As a solid line, the variance of the Oy components of each spin normalized by their respective population. The dotted lines indicate the long time limit. (b) Two-body correlation functions (by one factor) defined by the equations (2.32)-(2.33). The red line represents $(N-1)\gamma_f C_I$ and the blue $(n-1)\gamma_m C_J$. Recall that $n\gamma_m = N\gamma_f$ and that this quantity represents the number of metastability exchange collisions per unit time.

we show in figure 2.1 the correlation functions as well as the variances in the Oy direction of two collective spins, one of which is initially squeezed in this direction (parameter r non-zero). We have taken $\frac{\gamma_f}{\gamma_m} = \frac{1}{3}$ and $r = 0.5$. [5] On these illustrations, the convergence of the correlation functions under the effect of collisions is clearly visible as well as the partition of the variances between the two spins in the course of time.

Let us conclude this discussion of the transfer of correlations with a final remark : although equation (2.35) indicates that the squeezing of the nuclear spin is non-zero in the asymptotic state, we can see the presence of a factor $\frac{\gamma_f}{\gamma_m}$ with respect to the normalized squeezing initially present in the metastable $(1 - e^{-2r})$. However, this factor is very small in practice, of the order of 10^{-6}. Thus the nuclear and metastable spins [the latter with an additional factor $\frac{\gamma_f}{\gamma_m}$ in (2.34)] are only weakly squeezed. This is because even with a very strong squeezing of the metastable population initially, the transferred excitations represent only a small fraction of the atoms in the ground-state population. To create a significant squeezing of the nuclear spin, we then need to continuously bring correlations into the system. Therefore, we consider a *continuous* nondemolition quantum measurement as the source of correlation. From then on, the factor $\frac{\gamma_f}{\gamma_m}$ will intervene in the characteristic squeezing time and not in the asymptotic squeezing level, as we will see.

[5] Parameters disconnected from real experiments. In particular, these parameters imply that one third of the atoms in the gas are in the metastable state. But there is an upper limit to the fraction of metastable that can exist in the gas. Above a certain metastable density, the collisions $He^* + He^*$, called Penning, ionise the atoms and destroy the metastable populatio [39].

2.3.3 Master equation for the metastability exchange collisions

To conclude this chapter, we introduce a master equation description of the collisional evolution of metastability exchange. This description will prove very useful in the following chapters. Under the assumption that metastability exchange collisions occur independently for each atom in the gas, as one would describe for example out-of-phase collisions, their contribution to the evolution of the density operator ρ describing the spin degrees of freedom in the gas can be described by a Lindblad master equation:

$$\frac{d}{dt}\rho = \sum_{i}^{n_{\text{cell}}+N_{\text{cell}}} C_i \rho C_i^\dagger - \frac{1}{2}(C_i^\dagger C_i \rho + \rho C_i^\dagger C_i) \tag{2.38}$$

where $n_{\text{cell}} + N_{\text{cell}}$ is the total number of atoms, and C_i a jump operator acting only on the atom i :

$$C = \begin{pmatrix} 0 & \sqrt{\frac{1}{T}}\mathbb{1}_f \\ \sqrt{\frac{1}{\tau}}\mathbb{1}_m & 0 \end{pmatrix}. \tag{2.39}$$

where $\mathbb{1}_f$ and $\mathbb{1}_m$ denote the identity matrices in the subspaces describing an atom in the ground state and in the metastable state, respectively. As an example, let us give some indications that allow us to find equations (2.14)-(2.15) in the case of the simple model $I = \frac{1}{2}$ and $K = \frac{1}{2}$, starting from (2.38). We sought, for a one-body observable $\hat{O} = \sum_i^{\mathcal{N}} O_i$ with $\mathcal{N} = n+N$ and O_i an operator acting only on the atom i, the evolution equation of its mean $\frac{\mathrm{d}}{\mathrm{d}t}\langle\hat{O}\rangle = \mathrm{Tr}\left[\hat{O}\frac{\mathrm{d}\rho}{\mathrm{d}t}\right] = \mathrm{Tr}\left[\sum_i C_i^\dagger \hat{O} C_i \rho - \frac{1}{2}(C_i^\dagger C_i \hat{O} + \hat{O} C_i^\dagger C_i)\rho\right]$ with C_i an operator of the form (2.39) acting only on the atom i. We will take as an example the metastable spin operator in the direction Oy, $K_y = \sum_i^{\mathcal{N}} K_y^{at}(i)$ with $K_y^{at}(i) = \frac{i}{2}\left(|m;+\rangle\langle m;-| - |m;-\rangle\langle m;+|\right)$ and $|m;+\rangle, |m;-\rangle$ the two states composing the metastable spin 1/2, not to be confused with $|f;+\rangle, |f;-\rangle$ the nuclear spin 1/2. Note that two operators acting on two different atoms commute. Hence, we can write

$$\frac{\mathrm{d}}{\mathrm{d}t}\langle K_y\rangle = \mathrm{Tr}\left[\sum_i C_i^\dagger K_y^{at}(i) C_i \rho - \frac{1}{2}(C_i^\dagger C_i K_y^{at}(i) + K_y^{at}(i) C_i^\dagger C_i)\rho\right]. \tag{2.40}$$

Thus each term of the sum relates to only one atom, which allows us to write

$$\frac{\mathrm{d}}{\mathrm{d}t}\langle K_y\rangle = \mathrm{Tr}_1\left[C_1^\dagger K_y^{at}(1) C_1 \rho^{(1)} - \frac{1}{2}(C_1^\dagger C_1 K_y^{at}(1) + K_y^{at}(1) C_1^\dagger C_1)\rho^{(1)}\right] \tag{2.41}$$

with Tr_1 is the trace on the states of atom 1 and $\rho^{(1)} = \mathcal{N}\mathrm{Tr}_{2,3,4,\ldots,\mathcal{N}}\rho$. From an expression of C_1 in the base $\{|m;+\rangle, |m;-\rangle, |f;+\rangle, |f;-\rangle\}$, it only remains to calculate the products of matrices $C_1^\dagger K_y^{at}(1) C_1$, $C_1^\dagger C_1 K_y^{at}(1)$ and $K_y^{at}(1) C_1^\dagger C_1$ and then to recognise the expressions of $K_y^{at}(1)$ and $I_y^{at}(1) = \frac{i}{2}\left(|f;+\rangle\langle f;-| - |f;-\rangle\langle f;+|\right)$. We then come back to (2.14) for $\alpha = y$.

Chapter 3

Three-spin coupled model

Foreword

In this chapter we describe the equations of the complete cell and cavity system. The aim will be to set up a quantum description of the system suitable for our problem from which we can explore the dynamics when subjected to continuous quantum nondemolition measurement. These measurements will not be discussed in this chapter, as they are covered in chapters 4 and 5. On the one hand we have the atoms, the coupling between the atoms in the ground state and those in the metastable state, and on the other hand the light in the optical cavity and its coupling with the metastable. To describe these different elements, this chapter opens with a semiclassical approach, i.e. ignoring quantum fluctuations, where the evolution equations are derived only for the averages of the observables. To the equations of section 2.2.2 of chapter 2 which describe in such a way the metastability exchange collisions, we will have to add the macroscopic observables describing the light (a Stokes spin) and its coupling with the metastable spin observables. After having described the stationary state of these equations in which we initially place the system, which corresponds to a state where each of the spins is polarised in the same direction, we describe in the next section the evolution of the quantum fluctuation operators around this stationary state. These fluctuation operators are only the spin operators in the directions perpendicular to the polarisation. But this description allows us to adiabatically eliminate the metastable spin operators related to the $F = 3/2$ multiplicity of the total metastable spin, namely the $\vec{J}$ spin and the $\vec{\vec{Q}}$ alignment tensor. This results in a description of the system reduced to three coupled spins. In the section that closes the chapter, the model that will be considered during the rest of this part is introduced. This model is that of three coupled bosonic modes, directly derived from the three-spin model, where each of the modes is related to one of the three spins. This transformation is done by the so-called Holstein-Primakoff approximation. For a very large and polarised spin, this allows the spin operators perpendicular to the direction of polarisation to be described as bosonic modes, via a normalisation of the operators. Following this, the section concludes with a three-mode master equation, where the Hamiltonian part corresponds to the light-metastable coupling and the jump operators to the metastability exchange collisions rewritten in the framework of this Primakoff approximation.

3.1 Semi-classical description of the evolution of the system

Recall the notations for the observables already introduced in section 2.2: $\vec{I}$ the collective nuclear spin in the ground state, $\vec{J}$ and $\vec{K}$ the collective spins associated with the hyperfine multiplicities $F = 3/2$ and $F = 1/2$ in the metastable state and $\vec{\vec{Q}}$ the collective alignment tensor in $F = 3/2$. For light propagating along Oz, we introduce the Stokes spin [26] constructed from the creation and annihilation operators of a photon in the linearly polarised cavity modes along Ox and Oy[1] :

$$S_x = \frac{1}{2}\left(c_x^\dagger c_x - c_y^\dagger c_y\right), \quad S_y = \frac{1}{2}\left(c_x^\dagger c_y + c_y^\dagger c_x\right), \quad S_z = \frac{1}{2\mathrm{i}}\left(c_x^\dagger c_y - c_y^\dagger c_x\right). \tag{3.1}$$

For simplicity we assume that the cell is uniformly illuminated by the cavity mode. In the limit of large detuning and small saturation of the atomic transition by the field, the excited state 2^3P can be eliminated adiabatically and the Hamiltonian interaction between the spin of the metastable $\vec{K}$ and the Stokes spin $\vec{S}$ takes the Faraday form [26]:

$$H = \hbar\chi K_z S_z \tag{3.2}$$

which is none other than the light displacement operator of the Zeeman sublevels in the metastable level $F = 1/2$, as can be clearly seen on the form of S_z in note 1.

3.1.1 Nonlinear semiclassical equations

In this subsection we describe the coupled nonlinear equations that govern the evolution of mean spins. In addition to the evolution due to the Faraday Hamiltonian (3.2) and the metastability exchange collisions, we need to include the contribution of the usual Liouvillian terms in the master equation describing the injection of a Ox polarised coherent field into the cavity and the losses due to the output mirror, the combined effect of which leads to $\langle S_x\rangle_s = n_{\mathrm{ph}}/2$ in the stationary state in the absence of atoms, where n_{ph} is the average photon number in the Ox polarised mode. This leads to

$$\frac{\mathrm{d}\langle\vec{S}\rangle}{\mathrm{d}t} = -\frac{\kappa}{2}\left(\langle\vec{S}\rangle - \frac{n_{\mathrm{ph}}}{2}\vec{u}_x\right) + \chi\langle K_z\rangle\left(\langle\vec{S}\rangle\times\vec{u}_z\right) \tag{3.3}$$

$$\frac{\mathrm{d}\langle\vec{K}\rangle}{\mathrm{d}t} = \left.\frac{\mathrm{d}\langle\vec{K}\rangle}{\mathrm{d}t}\right|_{\mathrm{ECH}} + \chi\langle S_z\rangle\left(\langle\vec{K}\rangle\times\vec{u}_z\right) \tag{3.4}$$

$$\frac{\mathrm{d}\langle\vec{J}\rangle}{\mathrm{d}t} = \left.\frac{\mathrm{d}\langle\vec{J}\rangle}{\mathrm{d}t}\right|_{\mathrm{ECH}}, \quad \frac{\mathrm{d}\langle Q_{\alpha\beta}\rangle}{\mathrm{d}t} = \left.\frac{\mathrm{d}\langle Q_{\alpha\beta}\rangle}{\mathrm{d}t}\right|_{\mathrm{ECH}}, \quad \frac{\mathrm{d}\langle\vec{I}\rangle}{\mathrm{d}t} = \left.\frac{\mathrm{d}\langle\vec{I}\rangle}{\mathrm{d}t}\right|_{\mathrm{ECH}} \tag{3.5}$$

with $\vec{u}_{\alpha=x,y,z}$ the unit vector of axis $O\alpha$. We have performed the $\langle AB\rangle \simeq \langle A\rangle\langle B\rangle$ approximation where A and B are two operators, known as semiclassical quantum optics. The terms proportional to the loss rate κ of the cavity output mirror cause $\langle S_x\rangle$ to relax to its stationary value $\langle S_x\rangle_s = n_{\mathrm{ph}}/2$ forced by the Ox line-polarised laser field injected into the cavity, and the transverse averages $\langle S_y\rangle$ and $\langle S_z\rangle$ to zero. The terms denoted by "ECH" are the metastability exchange terms described by (2.10)-(2.13) in Chapter 2.

[1] Equivalently, one can construct the Stokes spin $\vec{S}$ using the annihilation operators in the circularly polarised modes, $c_1 = \frac{1}{\sqrt{2}}(c_x - \mathrm{i}c_y)$, $c_2 = \frac{1}{\sqrt{2}}(c_x + \mathrm{i}c_y)$ [40], in which case $S_z = \frac{1}{2}\left(c_1^\dagger c_1 - c_2^\dagger c_2\right)$.

3.1.2 Partially polarised stationary solution

We now linearise these equations around a partially polarised stationary solution. The aim is to adiabatically eliminate the fluctuations of the spin $\vec{J}$ and the collective alignment tensor in $F = 3/2$. We believe that this non-mathematically controlled approximation is reasonable for the proposed experiment, as spin $\vec{J}$ is not directly coupled to light and therefore not directly affected by the continuous field measurement. On the other hand, eliminating the fluctuations of the spin $\vec{K}$, directly coupled to the field, would lead to a non-negligible error in the spin squeezing dynamics in the case of photon counting detection (i.e. omitting the double jump C_d in the master equation (4.18) and the rate Γ_0 in the average number of counted photons (4.27), and thus strongly underestimating the number of photodetections required to achieve a given squeezing level), but a negligible error in the case of homodyne detection, as we have verified on the single-mode model in section 4.2.

If we look for a partially polarised steady state from a nuclear polarisation $\eta \in [-1, 1]$,

$$\langle I_x\rangle_s = \eta\frac{N_{\text{cell}}}{2}, \quad \langle I_y\rangle_s = \langle I_z\rangle_s = 0, \quad \langle S_x\rangle_s = \frac{n_{\text{ph}}}{2}, \quad \langle S_y\rangle_s = \langle S_z\rangle_s = 0, \tag{3.6}$$

the rotational invariance of axis Ox of this polarisation and the system (3.3)-(3.5) forces the mean spins in the metastable state to be aligned along Ox, and the mean alignment tensor to be diagonal in the Cartesian basis, with equal eigenvalues along directions Oy and Oz. The system (3.3)-(3.5) thus admits a stationary solution with the only non-zero means in the metastable state:

$$\langle K_x\rangle_s = \frac{\eta}{2}\frac{1-\eta^2}{3+\eta^2}n_{\text{cell}}, \quad \langle J_x\rangle_s = \eta\frac{5+\eta^2}{3+\eta^2}n_{\text{cell}}, \quad \langle \Sigma_x\rangle_s = \frac{4\eta}{3+\eta^2}n_{\text{cell}}, \tag{3.7}$$

$$\langle Q_{yy}\rangle_s = \langle Q_{zz}\rangle_s = -\frac{1}{2}\langle Q_{xx}\rangle_s = -\frac{\eta}{12}\langle \Sigma_x\rangle_s\,. \tag{3.8}$$

3.2 Description of the quantum fluctuations

3.2.1 Linearised semiclassical equations

We now linearise the equations (3.3)-(3.5) in the classical fluctuations around the stationary solution (3.6)-(3.8) by making the substitution $\langle A\rangle \to \langle A\rangle_s + \delta A$ and treating δA to first order. By restricting ourselves to the subspace of the transverse fluctuations, i.e. to the directions $\alpha = y, z$ orthogonal to the mean spins, we obtain a closed system:

$$\frac{\mathrm{d}}{\mathrm{d}t}\delta S_\alpha = -\frac{\kappa}{2}\delta S_\alpha + \chi\delta_{\alpha y}\langle S_x\rangle_s\delta K_z \tag{3.9}$$

$$\frac{\mathrm{d}}{\mathrm{d}t}\delta K_\alpha = -\frac{7}{9\tau}\delta K_\alpha + \frac{1}{9\tau}\delta J_\alpha - \frac{2\eta}{3\tau}\delta Q_{\alpha x} - \frac{1}{9T}\left(1 + \frac{12}{n_{\text{cell}}}\langle Q_{\alpha\alpha}\rangle_s\right)\delta I_\alpha + \chi\delta_{\alpha y}\langle K_x\rangle_s\delta S_z \tag{3.10}$$

$$\frac{\mathrm{d}}{\mathrm{d}t}\delta J_\alpha = -\frac{4}{9\tau}\delta J_\alpha + \frac{10}{9\tau}\delta K_\alpha + \frac{2\eta}{3\tau}\delta Q_{\alpha x} + \frac{10}{9T}\left(1 + \frac{6}{5n_{\text{cell}}}\langle Q_{\alpha\alpha}\rangle\right)\delta I_\alpha \tag{3.11}$$

$$\frac{\mathrm{d}}{\mathrm{d}t}\delta Q_{\alpha x} = -\frac{2}{3\tau}\delta Q_{\alpha x} + \frac{\eta}{12\tau}\delta\Sigma_\alpha + \frac{1}{6Tn_{\text{cell}}}\langle\Sigma_x\rangle_s\delta I_\alpha \tag{3.12}$$

$$\frac{\mathrm{d}}{\mathrm{d}t}\delta I_\alpha = -\frac{1}{T}\delta I_\alpha + \frac{1}{3\tau}(\delta J_\alpha - \delta K_\alpha). \tag{3.13}$$

We recall the notations of chapter 2 where $N_{\rm cell}$ and $n_{\rm cell}$ are the number of atoms in the ground state and metastable state respectively while $1/T$ and $1/\tau$ are the rate of exchange collisions seen by the atoms in the ground state and metastable state respectively. [2]

3.2.2 Reduction with three coupled collective spins

By positing $\frac{\rm d}{{\rm d}t}\delta J_\alpha = 0$ in equation (3.11) and $\frac{\rm d}{{\rm d}t}\delta Q_{\alpha x} = 0$ in equation (3.12), we adiabatically eliminate the fluctuations of the collective spin $\vec{J}$ and the collective alignment tensor whose evolutions are governed by the metastability exchange only.

$$\delta J_\alpha^{\rm adiab} = 2\frac{10+\eta^2}{8-\eta^2}\delta K_\alpha + \frac{12\tau}{T}\frac{5+2\eta^2}{(3+\eta^2)(8-\eta^2)}\delta I_\alpha \tag{3.14}$$

$$\delta Q_{\alpha x}^{\rm adiab} = \frac{3\eta}{8-\eta^2}\delta K_\alpha + \frac{\tau}{T}\frac{\eta(13+\eta^2)}{(3+\eta^2)(8-\eta^2)}\delta I_\alpha. \tag{3.15}$$

Carrying over the adiabatic expressions (3.14)-(3.15) in equations (3.10) and (3.13) to δK_α and δI_α leads to a reduced system coupling the three collective spins $\vec{I}$, $\vec{K}$ and $\vec{S}$. The stationary mean values are redefined by :

$$\langle\vec{I}\rangle_s = \frac{N}{2}\,\vec{u}_x\,, \quad \langle\vec{K}\rangle_s = \frac{n}{2}\,\vec{u}_x\,, \quad \langle\vec{S}\rangle_s = \frac{n_{\rm ph}}{2}\,\vec{u}_x\,. \tag{3.16}$$

Here $\vec{u}_x$ is the unit vector according to Ox, N and n are the effective numbers of fundamental and metastable atoms participating in the collective spin dynamics. They are renormalized with respect to the true total numbers $N_{\rm cell}$ and $n_{\rm cell}$ in the cell, by factors depending on the nuclear polarization η[3] :

$$N = \eta\, N_{\rm cell}\,, \quad n = \left(\frac{1-\eta^2}{3+\eta^2}\right)\eta\, n_{\rm cell}\,. \tag{3.17}$$

The semiclassical equations on the fluctuations of the three collective spins are then written :

$$\frac{\rm d}{{\rm d}t}\delta S_z = -\frac{\kappa}{2}\delta S_z\,, \qquad \frac{\rm d}{{\rm d}t}\delta S_y = -\frac{\kappa}{2}\delta S_y + \chi\langle S_x\rangle_s\delta K_z \tag{3.18}$$

$$\frac{\rm d}{{\rm d}t}\delta I_z = -\gamma_{\rm f}\delta I_z + \gamma_{\rm m}\delta K_z\,, \qquad \frac{\rm d}{{\rm d}t}\delta I_y = -\gamma_{\rm f}\delta I_y + \gamma_{\rm m}\delta K_y \tag{3.19}$$

$$\frac{\rm d}{{\rm d}t}\delta K_z = -\gamma_{\rm m}\delta K_z + \gamma_{\rm f}\delta I_z\,, \qquad \frac{\rm d}{{\rm d}t}\delta K_y = -\gamma_{\rm m}\delta K_y + \gamma_{\rm f}\delta I_y + \chi\langle K_x\rangle_s\delta S_z\,. \tag{3.20}$$

Recall that $\gamma_{\rm m}$ and $\gamma_{\rm f}$ are the effective rates of metastability exchange in the metastable state and in the ground state. These depend on the nuclear polarisation as below and in figure 3.1a, and are in the same ratio as the numbers of effective atoms N and n (3.17) constituting the collective spins:

$$\gamma_{\rm f} = \frac{4+\eta^2}{8-\eta^2}\,\frac{1-\eta^2}{3+\eta^2}\,\frac{1}{T}\,, \quad \gamma_{\rm m} = \frac{4+\eta^2}{8-\eta^2}\,\frac{1}{\tau}\,, \quad \frac{\gamma_{\rm m}}{\gamma_{\rm f}} = \frac{N}{n} \gg 1\,. \tag{3.21}$$

[2] Thus $\frac{N_{\rm cell}}{T}dt = \frac{n_{\rm cell}}{\tau}dt$ and this quantity represents the number of atoms undergoing a metastability exchange collision during an interval dt. This relation implies $\frac{\tau}{T} = \frac{n_{\rm cell}}{N_{\rm cell}}$.

[3] Note that $n = 0$ in the fully polarized case $\eta = 1$. Indeed, the entire population of the metastable state is then in the extreme Zeeman sublevel $m_x = 3/2$ of the hyperfine state $F = 3/2$ and the multiplicity $F = 1/2$ is empty. This is also the reason why we have considered a partially polarized state since the beginning of this chapter.

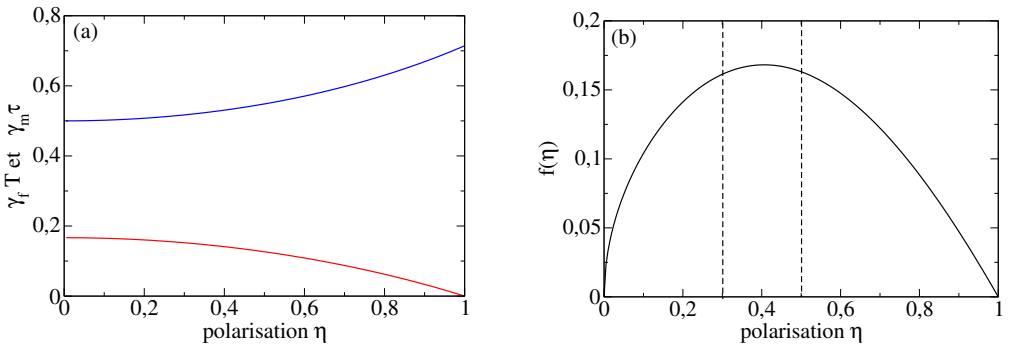

Figure 3.1: (a) Effective metastability exchange rates γ_f (bottom curve, red) and γ_m (top curve, blue) from the equation (3.21) in the ground state and metastable as a function of nuclear polarisation η, normalised by the rates of metastability exchange collisions $1/T$ and $1/\tau$ experienced by a ground state and metastable atoms in the gas. (b) Nuclear polarisation dependence of the Faraday pulsation Ω_α entering the rate of excitation creation by Faraday coupling in the hybrid nuclear bosonic mode (4.13) and in the spin compression rates (4.32) and (5.51) in the $\gamma_\mathrm{f} \ll \gamma_\mathrm{m}$ limit; more precisely, we represent the factor $f(\eta) = \sqrt{\eta}\frac{1-\eta^2}{3+\eta^2}$ such that $\Omega_\alpha \simeq \Omega(\gamma_\mathrm{f}/\gamma_\mathrm{m})^{1/2} = \chi\sqrt{n_\mathrm{ph} n_\mathrm{cell}}\sqrt{\frac{n_\mathrm{cell}}{N_\mathrm{cell}}} f(\eta)$. When the polarisation varies between 0.3 and 0.5 (vertical dashed lines), $f(\eta)$ deviates by 4% from its maximum $\simeq 0.17$ reached at $\eta = 0.42$. It is therefore advantageous to place oneself close to this value of η in order to reduce the temporal drift of Ω_α due to a slight damping of the nuclear polarisation during the spin compression (indeed, the optical pumping process is then interrupted and the lifetime of the polarisation is reduced by the presence of the discharge, it becomes of the order of γ_α^{-1}, where γ_α is the reduced decoherence rate from section 5.4).

Note that the system of equations coupling the δI_y and δK_y fluctuations, ignoring the Faraday term in χ, is the one previously studied in section 2.3 describing the simple model of two 1/2-spins coupled by the metastability exchange collisions. In figure 3.1b, we also show the nuclear polarisation dependence of the effective Ω_α (4.5) Faraday coupling between light and the metastable hybridised nuclear spin, which controls the spin squeezing rate as we shall see.

3.3 Three bosonic mode models

The stationary, polarised state of the system we have just presented allows the implementation of the Holstein-Primakoff approximation, introducing a representation of the system via three bosonic modes. In this section, the introduction of this approximation will be followed by the writing of a master equation for such a system, taking into account the Faraday coupling as well as the metastability exchange collisions.

3.3.1 Holstein-Primakoff approximation

Initially, the collective nuclear spin $\vec{I}$, the collective spin of the metastable $\vec{K}$ and the Stokes spin $\vec{S}$ of the light are polarised according to Ox, and will remain so throughout the experimental procedure. In the Holstein-Primakoff approximation, which assimilates the macro-

scopic spin components according to Ox to classical variables, the remaining Oy and Oz components, orthogonal to the mean spins, behave as the quadrature operators (hermitian and antihermitian parts of annihilation operators and thus canonically conjugate, $[X, P] = \mathrm{i}/2$) of three bosonic modes a, b, c : [4]

$$\frac{I_y}{\sqrt{N}} \overset{\text{Primakoff}}{\simeq} X_a = \frac{a + a^\dagger}{2}, \quad \frac{K_y}{\sqrt{n}} \overset{\text{Primakoff}}{\simeq} X_b = \frac{b + b^\dagger}{2}, \quad \frac{S_y}{\sqrt{n_{\text{ph}}}} \overset{\text{Primakoff}}{\simeq} X_c = \frac{c + c^\dagger}{2}, \tag{3.22}$$

$$\frac{I_z}{\sqrt{N}} \overset{\text{Primakoff}}{\simeq} P_a = \frac{a - a^\dagger}{2\mathrm{i}}, \quad \frac{K_z}{\sqrt{n}} \overset{\text{Primakoff}}{\simeq} P_b = \frac{b - b^\dagger}{2\mathrm{i}}, \quad \frac{S_z}{\sqrt{n_{\text{ph}}}} \overset{\text{Primakoff}}{\simeq} P_c = \frac{c - c^\dagger}{2\mathrm{i}}. \tag{3.23}$$

We have taken into account the mean values (3.16) in the normalization. Let's make the link with the exact bosonic (3.1) representation of the Stokes spin by writing:

$$\frac{S_y}{\sqrt{n_{\text{ph}}}} - \mathrm{i}\frac{S_z}{\sqrt{n_{\text{ph}}}} = \frac{1}{\sqrt{n_{\text{ph}}}} c_y^\dagger c_x \overset{\text{Primakoff}}{\simeq} c_y^\dagger, \quad \frac{S_y}{\sqrt{n_{\text{ph}}}} + \mathrm{i}\frac{S_z}{\sqrt{n_{\text{ph}}}} = \frac{1}{\sqrt{n_{\text{ph}}}} c_x^\dagger c_y \overset{\text{Primakoff}}{\simeq} c_y. \tag{3.24}$$

This shows that the $c^\dagger$ creation operator in (3.22)-(3.23), identified with $c_y^\dagger$ in the Primakoff approximation, transfers a photon from the cavity mode strongly populated by an Ox-polarised coherent state into the initially empty Oy-polarised cavity mode. In the Primakoff approximation, the Hamiltonian of the Faraday atom-field coupling (3.2) is written:

$$H = \hbar\Omega P_b P_c \qquad \text{with} \qquad \Omega = \chi\sqrt{n n_{\text{ph}}}. \tag{3.25}$$

Since χ does not depend on the field strength in the cavity, Ω^2 is proportional to the field strength.

Metrological gain due to squeezing Let us write in terms of Primakoff variables the parameter ξ of reference [25] quantifying the level of spin squeezing usable in an interferometer (the metrological gain is all the higher as ξ is lower) previously introduced in chapter 1, Oz being the direction transverse to the average spin of highest squeezing and the collective nuclear spin being of quantum number $I = N_{\text{cell}}/2$:

$$\boxed{\xi^2 \equiv \frac{2I\,\mathrm{Var}(I_z)}{\langle I_x\rangle^2} = \frac{4\,\mathrm{Var}(P_a)}{\eta}.} \tag{3.26}$$

The nuclear polarisation η being fixed, and a quantum nondemolition measurement being carried out continuously on the nuclear spin, it is necessary to seek to minimise the variance of P_a conditional on the measurement signal to be defined, by making it fall as far as possible below its initial value 1/4. Note how partial polarization "works against us" in this respect because it increases by a factor of η the value below which $\mathrm{Var}(P_a)$ must fall to obtain the same gain as for a fully polarized spin.

[4] If we consider a large spin $\vec{S}$ polarized along Ox, we can approximate the spin component in this direction by a classical variable, positing $\hat{S}_x \simeq \langle \hat{S}_x \rangle$ so that $[\hat{S}_y/\sqrt{2\langle \hat{S}_x\rangle}\,,\ \hat{S}_z/\sqrt{2\langle \hat{S}_x\rangle}] \simeq \mathrm{i}/2$.

3.3.2 Three-mode master equation for metastability exchange

Let us consider in this subsection the evolution of the system due to metastability exchange ($\chi = 0$) alone. Unlike in section 2.3, we formulate the equations in terms of the bosonic operators from the Primakoff approximation. In a quantum treatment, the classical equations (3.19)-(3.20) become stochastic equations including quantum fluctuations. In the Primakoff approximation, this gives for the X quadratures in the metastable and ground state:

$$\mathrm{d}X_a = -\gamma_\mathrm{f} X_a \mathrm{d}t + \sqrt{\gamma_\mathrm{m}\gamma_\mathrm{f}} X_b \mathrm{d}t + \mathrm{d}X_a^\mathrm{stoch}\,, \quad \mathrm{d}X_b = -\gamma_\mathrm{m} X_b \mathrm{d}t + \sqrt{\gamma_\mathrm{m}\gamma_\mathrm{f}} X_a \mathrm{d}t + \mathrm{d}X_b^\mathrm{stoch} \tag{3.27}$$

where the equality of the ratios between collision rates and populations of the two states (3.21) has been used. The Langevin noises $\mathrm{d}X_i^\mathrm{stoch}$, together with $i \in \{a, b\}$, have zero mean, are independent random variables at different times and have equal time variances and covariances that reproduce the variances of a set of independent atoms. They have already been calculated in chapter 2, see equation (2.22) and the corresponding section in general.

$$\langle \mathrm{d}X_i^\mathrm{stoch} \mathrm{d}X_j^\mathrm{stoch} \rangle = D_{ij}\mathrm{d}t \quad \text{with} \quad \underline{\underline{D}} = \frac{1}{2}\begin{pmatrix} \gamma_\mathrm{f} & -\sqrt{\gamma_\mathrm{m}\gamma_\mathrm{f}} \\ -\sqrt{\gamma_\mathrm{m}\gamma_\mathrm{f}} & \gamma_\mathrm{m} \end{pmatrix}. \tag{3.28}$$

We have equations of the same form as (3.27) for the P_i quadratures, with other Langevin noises $\mathrm{d}P_i^\mathrm{stoch}$, of the same covariance matrix as equation (3.28) between them but of covariance matrix with the $\mathrm{d}X_i^\mathrm{stoch}$ noises given by

$$\langle \mathrm{d}X_i^\mathrm{stoch} \mathrm{d}P_j^\mathrm{stoch} \rangle = \mathcal{D}_{ij}\mathrm{d}t \quad \text{with} \quad \underline{\underline{\mathcal{D}}} = \mathrm{i}\underline{\underline{D}}. \tag{3.29}$$

For the computation of the mean values and variances of the atomic observables, this stochastic formulation is equivalent to a master equation on the ρ_at atomic density operator of the two bosonic modes a and b:

$$\frac{\mathrm{d}\rho_\mathrm{at}}{\mathrm{d}t} = C\rho_\mathrm{at}C^\dagger - \frac{1}{2}\{C^\dagger C, \rho_\mathrm{at}\} \quad \text{with} \quad C = \sqrt{2\gamma_\mathrm{f}}a - \sqrt{2\gamma_\mathrm{m}}b. \tag{3.30}$$

Indeed, the stochastic Langevin representation of the master equation (3.30) for any operator A is written

$$\mathrm{d}A = \frac{\mathrm{d}t}{2}\Big\{C^\dagger[A,C] - [A,C^\dagger]C\Big\} + \mathrm{d}A^\mathrm{stoch} \quad \text{where} \quad \mathrm{d}A^\mathrm{stoch} = [C^\dagger, A]\mathrm{d}B + \mathrm{d}B^\dagger[A,C] \tag{3.31}$$

and $\mathrm{d}B$ is a stochastic Markovian operator of zero mean, equal time covariance matrix

$$\langle \mathrm{d}B\,\mathrm{d}B^\dagger \rangle = \mathrm{d}t\,, \quad \langle \mathrm{d}B\,\mathrm{d}B \rangle = \langle \mathrm{d}B^\dagger \mathrm{d}B^\dagger \rangle = \langle \mathrm{d}B^\dagger \mathrm{d}B \rangle = 0\,. \tag{3.32}$$

3.3.3 Complete three-mode master equation

The complete evolution, including the atom-field interaction of Hermitian Hamiltonian H (3.25), metastability exchange and cavity losses, is described by the master equation. [5]

$$\frac{\mathrm{d}\rho}{\mathrm{d}t} = \frac{1}{\mathrm{i}\hbar}[H,\rho] + \kappa\left(c\rho c^\dagger - \frac{1}{2}\{c^\dagger c, \rho\}\right) + C\rho C^\dagger - \frac{1}{2}\{C^\dagger C, \rho\} \tag{3.33}$$

[5] We neglect here the internal evolution of the atomic modes (spin precession) by assuming that the Zeeman sublevels are degenerate in the ground state and in the metastable $F = 1/2$ level, thus the external magnetic field is zero, $\vec{B} = \vec{0}$. This simplifying assumption calls for some comments which we develop in section 5.5.2.

where C is the jump operator for the (3.30) metastability exchange, κ is the cavity loss rate, γ_{m} and γ_{f} are the effective metastability exchange rates in the metastable and ground state.

In this thesis, we consider that the three modes are in the empty state corresponding to a polarised coherent state for the three spins [6]:

$$\langle X_a\rangle(0) = \langle X_b\rangle(0) = \langle X_c\rangle(0) = 0\,, \quad \langle X_a^2\rangle(0) = \langle X_b^2\rangle(0) = \langle X_c^2\rangle(0) = \frac{1}{4} \tag{3.34}$$

and similarly for the quadratures P. For this initial state, the first moments of the quadratures remain zero, and a closed system of second moment equations can be obtained. It is found that the quadratures P remain with constant variances and zero covariances in all three modes,

$$\langle P_a^2\rangle(t) = \langle P_b^2\rangle(t) = \langle P_c^2\rangle(t) = \frac{1}{4}\,, \quad \langle P_aP_b\rangle(t) = \langle P_aP_c\rangle(t) = \langle P_bP_c\rangle(t) = 0 \tag{3.35}$$

that the variance $\langle X_c^2\rangle$ remains bounded and the covariances $\langle X_aX_c\rangle$ and $\langle X_bX_c\rangle$ remain zero, while the variances and covariance of the quadratures X_a and X_b, and thus the number of excitations in the atomic modes, [7] diverge linearly in time, at least as long as the Primakoff approximation is applicable. We give here explicitly only the behaviour at long times:

$$\langle X_a^2\rangle(t) \underset{t\to+\infty}{=} \frac{\gamma_{\mathrm{m}}\gamma_{\mathrm{f}}}{(\gamma_{\mathrm{m}}+\gamma_{\mathrm{f}})^2}\frac{\Omega^2 t}{4\kappa} + O(1) \tag{3.36}$$

$$\langle X_b^2\rangle(t) \underset{t\to+\infty}{=} \frac{\gamma_{\mathrm{f}}^2}{(\gamma_{\mathrm{m}}+\gamma_{\mathrm{f}})^2}\frac{\Omega^2 t}{4\kappa} + O(1) \tag{3.37}$$

$$\langle X_aX_b\rangle(t) \underset{t\to+\infty}{=} \frac{\gamma_{\mathrm{m}}^{1/2}\gamma_{\mathrm{f}}^{3/2}}{(\gamma_{\mathrm{m}}+\gamma_{\mathrm{f}})^2}\frac{\Omega^2 t}{4\kappa} + O(1) \tag{3.38}$$

$$\langle X_c^2\rangle(t) - \frac{1}{4} \underset{t\to+\infty}{=} \left(\frac{\Omega}{2\kappa}\right)^2\left(1 - \frac{2\gamma_{\mathrm{m}}}{\kappa + 2(\gamma_{\mathrm{m}}+\gamma_{\mathrm{f}})}\right). \tag{3.39}$$

[6] We make here a new approximation which amounts to ignoring the fact that the polarisations of the nuclear and metastable spins are only partials in the definition of the ground state. Indeed, in all rigour $\langle X_a^2(0)\rangle = \langle P_a^2(0)\rangle = \frac{1}{4\eta}$ and $\langle X_b^2(0)\rangle = \langle P_b^2(0)\rangle = \frac{1}{4p}$ with $p = \eta\frac{1-\eta^2}{3+\eta^2}$. The approximation therefore amounts to neglecting part of the noise in the initial state. Here, our simplification allows us to consider an initial Gaussian state, a property that will prove crucial in chapter 5. The question then becomes whether the true coherent but non-Gaussian initial state is similarly affected by the measurement. In the literature, this situation is not unknown. It arises in any attempt to compress a collective spin from a non-polarised state, or in the presence of decoherence. The theoretical work undertaken by Baragiola, Chase and Geremia in reference [41] for example seems to confirm our argument. In an extensive study of collective states of atomic ensembles in standard quantum optics experimental procedures, the authors show that squeezed spin states (in any case with reduced variances) can be constructed even from states that are not fully polarized or in the presence of decoherence. In the experimental work, we can cite [15] where a squeezing of $2,2$ dB on a spin of a set of atoms polarised at 98% is obtained by quantum nondemolition measurement via a Faraday cavity interaction like the work presented here. Reference [11] also refers to correlations in the nuclear spin of a noble gas by continuous measurement of the cavity light that has interacted with the atomic ensemble by the Faraday effect, and discusses the fact that a partially polarised set of $1/2$ spins is similar to a mixture of two sets, one polarised and one unpolarised, which would only have the overall effect of reducing the coupling strength between the light and the atoms. An alternative scheme in which one can achieve (at least in theory), $\eta = 1$ and where such a problem disappears, is described as a perspective in section 5.5.1 at the end of this part.

[7] For the initial state considered, one has at all times $\langle X_a\rangle = 0$ and $\langle X_a^2\rangle - \frac{1}{4} = \langle a^\dagger a\rangle$, where $\langle a^\dagger a\rangle$ is the average number of excitations in the nuclear spin mode, so that $\mathrm{Var}\, X_a = \langle a^\dagger a\rangle + \frac{1}{4}$; in effect, one has $a^\dagger a + 1/2 = X_a^2 + P_a^2$. The same relations hold for the other two modes.

Chapter 4

Nuclear spin squeezing by photon counting

Foreword

Having introduced the metastability exchange collisions (chapter 2), coupling the atoms of the ground state to those of the metastable state, we added the coupling with the cavity light (chapter 3) and developed an effective model of 3 coupled bosonic modes describing by a master equation (3.33) the fluctuations of the spins around the stationary state in which we initially place the system. For the scheme to be complete, and to induce a nuclear spin squeezing, all that remains is the description of the quantum nondemolition measurement of the light at the cavity exit and its effect on the state of the three-mode system. Indeed, the quantum averages calculated in chapter 3, equations (3.36)-(3.39), correspond to ensemble averages over an infinite number of realisations of the experiment. In the present and next chapters, we study what we are really interested in, the evolution of the system in one or more given realisations, conditional on the results of a continuous measurement on the Oy polarised light coming out of the cavity. For this, we take advantage of the formulation in terms of Monte Carlo wave functions where stochastic trajectories $|\psi(t)\rangle$ corresponding to a particular succession of quantum jumps reconstruct the density operator of the system conditional on measurement results [42]. The precise form of the Monte Carlo jump operators, which is not unique in the stochastic reformulation of a master equation, is then determined by the particular measurements made. Here, the case of a photon counting measurement at the cavity exit will be considered, with an analytical study in the one-mode model and a numerical study in the full three-mode model. The first section of this chapter is dedicated to the introduction of this Monte Carlo wavefunction formalism. Subsequently, we perform a first analysis in a limit, which we call "one-mode", that allows us to describe the (slow) evolution of the nuclear spin during the experiment. This analysis is first limited to the quantum averages and then in the following section 4.3, we introduce the cavity output measurement and its effect on the system. We take it into account, with the same formalism introduced in 4.1, by conditioning the mode states and the observable averages on the measurement results. The last section thus proposes an analytical development in the framework of the one-mode limit already introduced and then in the complete three-mode model, but only numerically. These two analyses confirm that this counting scheme produces a collective nu-

clear spin state with a narrower structure than the standard quantum limit, a priori allowing a metrological gain.

4.1 Monte-Carlo wavefunction principle

In the Monte-Carlo wavefunction formalism [42, 43], the general master equation of the Lindblad form [44]

$$\frac{\mathrm{d}\rho}{\mathrm{d}t} = \frac{1}{\mathrm{i}\hbar}[H,\rho] + \sum_m C_m^\dagger \rho C_m - \frac{1}{2}\{C_m^\dagger C_m, \rho\} \tag{4.1}$$

is reinterpreted in terms of a corresponding Hilbert space vector that undergoes a stochastic evolution. The Monte Carlo (MC) wave vector is considered to evolve according to a non-Hermitian Hamiltonian $H_{MC} = H - \frac{i\hbar}{2}\sum_m C_m C_m^\dagger$, which is stochastically interrupted by quantum jumps due to operators C_m such that $|\phi\rangle \to C_m|\phi\rangle$. Concretely, calculating the evolution during δt of a Monte-Carlo wave vector $|\phi(t)\rangle$ can be done in two steps, assuming δt sufficiently small: one defines beforehand the quantities $\delta p_m = \delta t \langle\phi(t)|C_m^\dagger C_m|\phi(t)\rangle$ and $\delta p = \sum_m p_m$ (these different quantities are assumed to be small compared to 1). We then use δp as the probability that the MC wave vector undergoes a quantum jump. We draw a number ϵ uniformly between 0 and 1, if this number is greater than δp then we take as wave vector at $t+\delta t$ the vector $|\phi(t)\rangle$ evolved under the action of H_{MC} during δt : $|\phi(t+\delta t)\rangle = \mathcal{N}\left(1 - \frac{i\delta t}{\hbar} H_{MC}\right)|\phi(t)\rangle$ with $\mathcal{N}$ a constant to normalize the vector. If, on the other hand, $\epsilon < \delta p$ then $|\phi(t+\delta t)\rangle = \mathcal{N} C_m|\phi(t)\rangle$ where the jump operator C_m was randomly drawn with probability law $P(m) = \frac{\delta p_m}{\delta p}$. It can be shown that, for a sufficiently small δt, the quantity $|\phi(t+\delta t)\rangle\langle\phi(t+\delta t)|$ averaged over the realisations and quantum jump choices is exactly equivalent to $\rho(t+\delta t)$ evolved according to the master equation (4.1). Similarly, for an operator A, any quantity $\langle\phi(t)|A|\phi(t)\rangle$, similarly averaged, is equivalent to $\mathrm{Tr}(A\rho)$. Finally, if we take care to take for C_m operators that have a physical meaning,[1] i.e. that are related to real processes accessible in the experiment, it is possible to physically interpret the trajectory of a Monte-Carlo wave vector. Consider a two-level atom coupled to a coherent laser and the vacuum of the electromagnetic field. A Monte Carlo trajectory of such an atom is simply interpreted as the Rabi oscillation sporadically returned to the ground state by the production of a photon. By averaging over all possible trajectories, we come back to the characteristic damped oscillation [42]. We can see how this approach makes it possible to address the question of the impact of a measurement on a quantum system, via an operator that represents the measurement over time, since we can calculate the averages of the system's operators by averaging them over the vectors of states conditional on a certain measurement history. For example, one can imagine a cavity system, from which photons escape and are counted, if one notes C the jump operator associated with the exit of a photon from the cavity, one can imagine calculating the average of an operator A in the set of MC wave vectors that have undergone n cavity jumps. One would then obtain an average of A conditional on observing n photons at the cavity exit.

[1] The precise form of the jump operators is not unique in the stochastic reformulation of a master equation.

4.2 Analysis of the one-mode limit

In this subsection, we establish a one-mode master equation describing the slow evolution of the nuclear spin in the

$$\Gamma_{\rm ex} \ll \gamma_{\rm f} < \gamma_{\rm m} \quad \text{and} \quad \Gamma_{\rm ex} \ll \kappa \tag{4.2}$$

limit where $\Gamma_{\rm ex}$ is a rate of creation of excitations in the α hybrid nuclear bosonic mode defined below (4.13) under the effect of Faraday coupling (it is sufficient to know here that $\Gamma_{\rm ex} \propto \Omega^2$ so that (4.2) is a weak Faraday coupling limit $\Omega \to 0$). For this purpose, the bosonic annihilation operators have to be introduced in a cleverly rotated basis, by means of the following linear combinations of the operators a and b:

$$\alpha = \sqrt{\frac{\gamma_{\rm m}}{\gamma_{\rm m}+\gamma_{\rm f}}}a + \sqrt{\frac{\gamma_{\rm f}}{\gamma_{\rm m}+\gamma_{\rm f}}}b\,, \quad \beta = \sqrt{\frac{\gamma_{\rm m}}{\gamma_{\rm m}+\gamma_{\rm f}}}b - \sqrt{\frac{\gamma_{\rm f}}{\gamma_{\rm m}+\gamma_{\rm f}}}a \tag{4.3}$$

α and β correspond indeed to the eigenmodes of the metastability exchange part of the three-mode master equation (3.33). [2] While the α mode undergoes a divergence in time of its mean number of excitations (hence the possibility of defining a $\Gamma_{\rm ex}$ rate), the β mode is strongly damped and tends towards a stationary value,[3] which will allow it to be eliminated adiabatically, just like the cavity field. In this new basis, the three-mode master equation (3.33) takes the form

$$\boxed{\frac{{\rm d}\rho}{{\rm d}t} = \frac{1}{{\rm i}\hbar}\,[H,\rho] + \kappa\left(c\rho c^\dagger - \frac{1}{2}\{c^\dagger c,\rho\}\right) + \gamma_\beta\left(\beta\rho\beta^\dagger - \frac{1}{2}\{\beta^\dagger\beta,\rho\}\right)} \tag{4.4}$$

where $\gamma_\beta \equiv 2(\gamma_{\rm m}+\gamma_{\rm f})$ and

$$H = \hbar(\Omega_\alpha P_\alpha + \Omega_\beta P_\beta)P_c \quad \text{with} \quad \Omega_\alpha \equiv \Omega\sqrt{\frac{\gamma_{\rm f}}{\gamma_{\rm m}+\gamma_{\rm f}}} \quad \text{and} \quad \Omega_\beta \equiv \Omega\sqrt{\frac{\gamma_{\rm m}}{\gamma_{\rm m}+\gamma_{\rm f}}}\,i. \tag{4.5}$$

Reference [45] explains in general terms how to perform adiabatic elimination at the master equation. Here we prefer to perform it, as in reference [46], in weak Faraday coupling $\Omega \to 0$ in the Monte Carlo wave function formalism. We write the effective non-Hermitian Hamiltonian that we will make act on the state vector $|\psi(t)\rangle$ as

$$H_{\rm eff} = H - \frac{{\rm i}\hbar}{2}\left(\kappa c^\dagger c + \gamma_\beta \beta^\dagger\beta\right) \tag{4.6}$$

and the quantum jumps, randomly interrupting (discontinuous evolutions $|\psi\rangle \to C|\psi\rangle$) the trajectory, of jump operators

$$C_c = \sqrt{\kappa}c \quad \text{and} \quad C_\beta = \sqrt{\gamma_\beta}\beta. \tag{4.7}$$

In the absence of the coherent coupling Ω in (4.5) the hybridized metastable mode and the cavity mode remain in the initial empty state. At first order in Ω, this state is coupled to

[2] In practice, we have $\gamma_{\rm m} \gg \gamma_{\rm f}$, see equation (3.21), so that the β mode corresponds to the spin of the metastable slightly hybridised with the spin of the ground state, and α to the nuclear spin slightly hybridised with the spin of the metastable

[3] See results (3.35)-(3.39), which show that $\langle P_\beta^2\rangle = 1/4$ and $\langle X_\beta^2\rangle = O(1)$ where $X_\beta = (\beta+\beta^\dagger)/2$ and $P_\beta = (\beta-\beta^\dagger)/2i$, we define similarly the quadratures X_α, P_α.

one-excited states in the cavity (through the action of P_c) and zero or one-excited states in the hybrid metastable mode (through the action of P_α or P_β). We can then truncate the Monte Carlo state vector $|\psi\rangle$ in the Fock basis $\{|n_\alpha\rangle_{\rm fond}|n_\beta\rangle_{\rm meta}|n_c\rangle_{\rm cav}\}$ as follows,

$$|\psi\rangle = |\psi_\alpha^{00}\rangle|0\rangle|0\rangle + |\psi_\alpha^{01}\rangle|0\rangle|1\rangle + |\psi_\alpha^{11}\rangle|1\rangle|1\rangle \tag{4.8}$$

with a norm error $O(\Omega^2)$. Under the effect of the effective Hamiltonian (4.6) the fast components $|\psi_\alpha^{01}\rangle$ and $|\psi_\alpha^{11}\rangle$ exponentially join a regime adiabatically following the slow component $|\psi_\alpha^{00}\rangle$ with rates $\kappa/2$ or $(\kappa+\gamma_\beta)/2$. Indeed, in the adiabatic following regime, the occupation probabilities of the excited components are

$$\langle\psi_\alpha^{11}|\psi_\alpha^{11}\rangle_{\rm adiab}/\langle\psi|\psi\rangle = [\Omega_\beta^2/4(\kappa+\gamma_\beta)^2]\langle\psi_\alpha^{00}|\psi_\alpha^{00}\rangle/\langle\psi|\psi\rangle \tag{4.9}$$

$$\langle\psi_\alpha^{01}|\psi_\alpha^{01}\rangle_{\rm adiab}/\langle\psi|\psi\rangle = (\Gamma_{\rm ex}/\kappa)\langle\psi_\alpha^{00}|P_\alpha^2|\psi_\alpha^{00}\rangle/\langle\psi|\psi\rangle \tag{4.10}$$

where definitions (4.13) have been used in advance. In the (4.2) limit, it is easy to check that they are $\ll 1$, so that almost the whole population is in the $|\psi_\alpha^{00}\rangle|0\rangle|0\rangle$ component as it should be, which will allow us in the following to replace $\langle\psi|\psi\rangle$ by $\langle\psi_\alpha^{00}|\psi_\alpha^{00}\rangle$ and justifies the adiabatic elimination of the excited components in this limit [4]

$$|\psi_\alpha^{11}\rangle_{\rm adiab} \simeq \frac{{\rm i}\Omega_\beta}{2(\kappa+\gamma_\beta)}|\psi_\alpha^{00}\rangle \quad \text{and} \quad |\psi_\alpha^{01}\rangle_{\rm adiab} \simeq \frac{\Omega_\alpha}{\kappa}P_\alpha|\psi_\alpha^{00}\rangle. \tag{4.11}$$

The expressions for $|\psi_\alpha^{11}\rangle_{\rm adiab}$, $|\psi_\alpha^{01}\rangle_{\rm adiab}$ into the Hamiltonian evolution equation of $|\psi_\alpha^{00}\rangle$ to obtain

$${\rm i}\hbar\frac{{\rm d}}{{\rm d}t}|\psi_\alpha^{00}\rangle = -\frac{{\rm i}\hbar}{2}\left(\Gamma_{\rm ex}P_\alpha^2 + \Gamma_0\right)|\psi_\alpha^{00}\rangle \equiv H_{\rm eff}^{00}\,|\psi_\alpha^{00}\rangle \tag{4.12}$$

where we have introduced the rates

$$\boxed{\Gamma_{\rm ex} = \frac{\Omega_\alpha^2}{\kappa} \quad \text{and} \quad \Gamma_0 = \frac{\Omega_\beta^2}{4(\kappa+\gamma_\beta)}.} \tag{4.13}$$

By studying the effect of the cavity jump operator C_c and the metastability exchange jump operator C_β on the state vector (4.8), we can interpret the effective Hamiltonian of equation (4.12).

[4] in a similar way. We also check that another condition for the validity of the adiabatic elimination, namely the slowness of the evolution of the hybridized nuclear spin α with respect to the fast variables, which is written here $\Gamma_{\rm ex}, \Gamma_0 \ll \kappa, \kappa+\gamma_\beta$, is satisfied. These considerations do not, however, show that the condition $\Gamma_{\rm ex} \ll \gamma_{\rm f}$ is necessary (unless $\kappa \ll \gamma_\beta$). To see this in all generality, we push to order Ω^4 the computation of the effective Hamiltonian $H_{\rm eff}^{00} = PH_{\rm eff}P + PHQ(zQ - QH_{\rm eff}Q)^{-1}QHP$ in the subspace $n_\beta = n_c = 0$ on which P projects (here $Q = \mathbb{1} - P$ and $z = O(\Omega^2)$). Qualitatively, at this order, by action of H_α and then H_β on $|\psi_\alpha^{00}\rangle|0\rangle|0\rangle$ (with the obvious notation $H = H_\alpha + H_\beta$), we virtually create an excitation β alone, relaxing at the rate $\gamma_\beta/2$, hence the additional adiabaticity condition $\Gamma_0 \ll \gamma_\beta$; joined to $\Gamma_0 \ll \kappa$ and $\gamma_{\rm f} < \gamma_{\rm m}$, it implies $\Gamma_{\rm ex} \ll \gamma_{\rm f}$ since $\Gamma_{\rm ex}/\gamma_{\rm f} = (\Gamma_0/\kappa + \Gamma_0/\gamma_\beta)(4\gamma_\beta/\gamma_{\rm m}) < 16(\Gamma_0/\kappa + \Gamma_0/\gamma_\beta)$. Quantitatively, we find a correction to the coefficient of P_α^2 in $H_{\rm eff}^{00}$ of type $H_\alpha G_0 H_\beta G_0 H_\beta G_0 H_\alpha$ (G_0 is the resolvent of $H_{\rm eff}$ for $\Omega = 0$) of the form $\hbar\Gamma_{\rm ex}\Omega_\beta^2/\gamma_\beta\kappa$, which must be negligible, which imposes $\Omega_\beta^2/\gamma_\beta\kappa \ll 1$, i.e. $\Gamma_{\rm ex} \ll \gamma_{\rm f}$ given $\gamma_{\rm f} < \gamma_{\rm m}$. The corrections to the scalar term are negligible as soon as $\Gamma_0 \ll \gamma_\beta, \kappa$, and the new term in P_α^4 that appears is negligible in front of $\hbar\Gamma_{\rm ex}P_\alpha^2$ for $P_\alpha = O(1)$ if $\Gamma_{\rm ex} \ll \kappa$.

(i) Consider first the effect of a cavity jump, which occurs at time t with a rate $\kappa(\langle\psi_\alpha^{11}|\psi_\alpha^{11}\rangle + \langle\psi_\alpha^{01}|\psi_\alpha^{01}\rangle)_{\rm adiab}/\langle\psi_\alpha^{00}|\psi_\alpha^{00}\rangle$. Immediately after the jump, the state vector, initially in the adiabatic following regime, becomes

$$|\psi(t^+)\rangle = C_c|\psi(t^-)\rangle_{\rm adiab} \propto |\psi_\alpha^{01}(t^-)\rangle_{\rm adiab}|0\rangle|0\rangle + |\psi_\alpha^{11}(t^-)\rangle_{\rm adiab}|1\rangle|0\rangle. \tag{4.14}$$

This is the superposition of an unstable component $|1\rangle|0\rangle$ and a stable component $|0\rangle|0\rangle$. With probability $\langle\psi_\alpha^{11}|\psi_\alpha^{11}\rangle_{\rm adiab}/(\langle\psi_\alpha^{01}|\psi_\alpha^{01}\rangle + \langle\psi_\alpha^{11}|\psi_\alpha^{11}\rangle)_{\rm adiab}$ the cavity jump is then followed by a metastability exchange jump before the state vector of the system has time to reach its adiabatic value. In this case we have a "double jump", which ultimately does not affect the $|\psi_\alpha^{00}(t^-)\rangle$ component since

$$C_\beta C_c|\psi(t^-)\rangle_{\rm adiab} \propto |\psi_\alpha^{00}(t^-)\rangle|0\rangle|0\rangle \tag{4.15}$$

This process contributes to the scalar term (proportional to the identity) in the effective Hamiltonian of equation (4.12). With the complementary probability $\langle\psi_\alpha^{01}|\psi_\alpha^{01}\rangle_{\rm adiab}/(\langle\psi_\alpha^{01}|\psi_\alpha^{01}\rangle + \langle\psi_\alpha^{11}|\psi_\alpha^{11}\rangle)_{\rm adiab}$ the state vector joins its adiabatic value before any further jumps occur, and is slaved to $|\psi_\alpha^{(01)}(t^-)\rangle_{\rm adiab} \propto P_\alpha|\psi_\alpha^{00}(t^-)\rangle$, i.e. the slow component $|\psi_\alpha^{00}(t^-)\rangle$ has effectively undergone a single quantum jump with a jump operator proportional to P_α. This process corresponds to the first term, proportional to P_α^2, in the effective Hamiltonian of equation (4.12).

(ii) Next assume that the jump at time t is a metastability exchange jump, which occurs with a rate $\gamma_\beta\langle\psi_\alpha^{11}|\psi_\alpha^{11}\rangle_{\rm adiab}/\langle\psi_\alpha^{00}|\psi_\alpha^{00}\rangle$. We verify in this case that the state vector after the jump, $C_\beta|\psi(t^-)\rangle$, is fully unstable and almost immediately undergoes a second jump, a cavity jump. The total effect again corresponds to a double jump and the action of a scalar operator on the slow component. From this discussion we derive the following single and double jump rates:

$$\Gamma_s = \frac{\kappa(\langle\psi_\alpha^{11}|\psi_\alpha^{11}\rangle + \langle\psi_\alpha^{01}|\psi_\alpha^{01}\rangle)_{\rm adiab}}{\langle\psi_\alpha^{00}|\psi_\alpha^{00}\rangle} \frac{\langle\psi_\alpha^{01}|\psi_\alpha^{01}\rangle_{\rm adiab}}{(\langle\psi_\alpha^{01}|\psi_\alpha^{01}\rangle + \langle\psi_\alpha^{11}|\psi_\alpha^{11}\rangle)_{\rm adiab}} = \Gamma_{\rm ex}\frac{\langle\psi_\alpha^{00}|P_\alpha^2|\psi_\alpha^{00}\rangle}{\langle\psi_\alpha^{00}|\psi_\alpha^{00}\rangle} \equiv \Gamma_{\rm ex}\langle P_\alpha^2\rangle \tag{4.16}$$

$$\Gamma_d = \frac{\kappa(\langle\psi_\alpha^{11}|\psi_\alpha^{11}\rangle + \langle\psi_\alpha^{01}|\psi_\alpha^{01}\rangle)_{\rm adiab}}{\langle\psi_\alpha^{00}|\psi_\alpha^{00}\rangle} \frac{\langle\psi_\alpha^{11}|\psi_\alpha^{11}\rangle_{\rm adiab}}{(\langle\psi_\alpha^{01}|\psi_\alpha^{01}\rangle + \langle\psi_\alpha^{11}|\psi_\alpha^{11}\rangle)_{\rm adiab}} + \frac{\gamma_\beta\langle\psi_\alpha^{11}|\psi_\alpha^{11}\rangle_{\rm adiab}}{\langle\psi_\alpha^{00}|\psi_\alpha^{00}\rangle} = \Gamma_0\,. \tag{4.17}$$

Finally, we obtain the one-mode master equation describing the slow evolution of the ρ_α density operator of the α bosonic mode (hybridised but almost purely nuclear spin):

$$\boxed{\frac{{\rm d}\rho_\alpha}{{\rm d}t} = C_s\rho_\alpha C_s^\dagger - \frac{1}{2}\{C_s^\dagger C_s, \rho_\alpha\} + C_d\rho_\alpha C_d^\dagger - \frac{1}{2}\{C_d^\dagger C_d, \rho_\alpha\}} \tag{4.18}$$

in terms of two quantum jumps, the single (cavity-only) C_s jump and the double (cavity and metastability exchange in this or the other order) C_d jump:

$$C_s = \sqrt{\Gamma_{\rm ex}}P_\alpha\,, \quad C_d = \sqrt{\Gamma_0}\mathbb{1}\,. \tag{4.19}$$

From the integrated (4.18) equation for the initial empty state of α, we derive:

$$\langle X_\alpha^2\rangle = \frac{1}{4}(1+\Gamma_{\rm ex}t)\,, \quad \langle P_\alpha^2\rangle = \frac{1}{4} \tag{4.20}$$

which effectively designates Γ_{ex} as an excitations creation rate in the α mode. Returning to the initial (unrotated) atomic basis and restricting the (4.8) state vector to its first term, we find the (3.35)-(3.38) results of the three-mode model, yet valid at any Ω Faraday coupling, not necessarily infinitesimal. Finally, the average number of Oy polarised photons leaving the cavity per unit time, given in the one-mode model by $\Gamma_0 + \Gamma_{\text{ex}}/4$ as will be shown by equation (4.27), agrees with the exact value $\kappa\langle c^\dagger c\rangle_s$ where the stationary average number of Oy polarised photons in the cavity $\langle c^\dagger c\rangle_s = \langle X_c^2\rangle_s - 1/4$ is the result (3.39). [5]

4.3 Dynamics conditional on counting result

Suppose that one counts continuously and directly (by photodetection) the number of Oy polarized photons exiting the cavity (see Figure 1.1b), as proposed in reference [47]. The jump operator associated with this measurement is $\sqrt{\kappa}c$, so the three-mode master equation (3.33) is already in the right form to analyse the evolution of the state vector $|\psi(t)\rangle$ conditional on the measurement. Let us start by studying the situation of a weak Faraday coupling, the $\Omega \to 0$ limit, which leads to the one-mode model of the 4.2 section. This will be followed by a numerical verification of these analytical predictions in the three-mode model.

4.3.1 One-mode analytical results

Since the jump operators C_d and C_s of the master equation (4.18) both correspond to the cavity loss of a polarised photon according to Oy (recall that C_d results from a cavity jump immediately followed or preceded by a metastability exchange jump, and C_s a single cavity jump), the measurement cannot distinguish between the two, and the density operator conditional on a given number n of detected photons is obtained by averaging over realizations having this same *total* n number of jumps. An unnormalized Monte Carlo state vector having undergone these n jumps for the duration t is written

$$|\psi(t)\rangle = \mathrm{e}^{-\frac{\mathrm{i}}{\hbar}H_{\text{eff}}^{00}(t-t_n)}\, C_{\epsilon_n}\, \mathrm{e}^{-\frac{\mathrm{i}}{\hbar}H_{\text{eff}}^{00}(t_n-t_{n-1})}\, C_{\epsilon_{n-1}} \dots C_{\epsilon_1}\, \mathrm{e}^{-\frac{\mathrm{i}}{\hbar}H_{\text{eff}}^{00}t_1}|\psi(0)\rangle \tag{4.21}$$

where $\epsilon_k \in \{s,d\}$ and t_k are the type and time of the krd jump, H_{eff}^{00} is the effective Hamiltonian (4.12) and we denote the state vector of the single-mode model $|\psi\rangle$ rather than $|\psi_\alpha^{00}\rangle$ for the sake of simplicity. The quantum average of an observable O is obtained by averaging over all possible trajectories, thus summing over the number and type of jumps and integrating over their times:

$$\langle O\rangle(t) = \sum_n \int_{0<t_1<t_2\dots<t_n<t} \mathrm{d}t_1\, \mathrm{d}t_2 \dots \mathrm{d}t_n \sum_{(\epsilon_k)_{1\le k\le n}\in\{s,d\}^n} \langle\psi(t)|O|\psi(t)\rangle \tag{4.22}$$

where the squared norm of each unnormalized state vector $|\psi(t)\rangle$ automatically gives its probability density [48]. Taking $O = \mathbb{1}$, we derive the probability that n jumps occurred in the time interval $[0,t]$:

$$\Pi_n(t) = \int_{0<t_1<t_2\dots<t_n<t} \mathrm{d}t_1\, \mathrm{d}t_2 \dots \mathrm{d}t_n \sum_{(\epsilon_k)_{1\le k\le n}\in\{s,d\}^n} \langle\psi(t)|\psi(t)\rangle. \tag{4.23}$$

[5] In contrast, the value of $\langle c^\dagger c\rangle_{\text{adiab}}$ in the adiabatic form (4.11) of the state vector does not represent this number. The solution to the paradox lies in the existence of the de-excitation pathway (ii), that of the first-jump annihilation of the $n_\beta = 1$ excitation in the metastable mode immediately followed by the loss of a cavity photon. The true exit rate of polarised photons according to Oy is therefore $\kappa\langle c^\dagger c\rangle_{\text{adiab}} + \gamma_\beta\langle\beta^\dagger\beta\rangle_{\text{adiab}}$.

To evaluate (4.23), we take advantage of the fact that all jump operators in (4.21) and their Hermitian conjugates commute with each other and with $H_{\rm eff}^{00}$. [6] Using the identities

$$\sum_{\epsilon_n=s,d}\dots\sum_{\epsilon_1=s,d}\left(C_{\epsilon_n}^\dagger C_{\epsilon_n}\dots C_{\epsilon_1}^\dagger C_{\epsilon_1}\right)=\left(\sum_{\epsilon_n=s,d}C_{\epsilon_n}^\dagger C_{\epsilon_n}\right)\dots\left(\sum_{\epsilon_n=s,d}C_{\epsilon_1}^\dagger C_{\epsilon_1}\right)=\left(\Gamma_{\rm ex}P_\alpha^2+\Gamma_0\mathbb{1}\right)^n \tag{4.24}$$

and injecting a closure relation into the eigenbasis of P_α such that $P_\alpha|p_\alpha\rangle=p_\alpha|p_\alpha\rangle$, after integrating over times t_k as allowed by the telescopic product of the evolution operators, we obtain

$$\Pi_n(t)=\frac{t^n}{n!}\int_{-\infty}^{+\infty}{\rm d}p_\alpha\,\left(\Gamma_{\rm ex}p_\alpha^2+\Gamma_0\right)^n{\rm e}^{-\Gamma_{\rm ex}p_\alpha^2t}{\rm e}^{-\Gamma_0t}\Pi(p_\alpha,0) \tag{4.25}$$

$$=\binom{2n}{n}\frac{(\Gamma_{\rm ex}t/8)^n\,{\rm e}^{-\Gamma_0t}}{(1+\Gamma_{\rm ex}t/2)^{n+1/2}}\,\Phi\left(-n,\frac{1}{2}-n;\Gamma_0t+\frac{2\Gamma_0}{\Gamma_{\rm ex}}\right) \tag{4.26}$$

where $\Pi(p_\alpha,0)$ is the initial probability distribution of p_α (a Gaussian of mean zero and variance $1/4$) and Φ is the confluent hypergeometric Kummer function ${}_1F_1$. Note that (4.26) is in fact a Gaussian mean over p_α of a Poisson distribution of parameter $\lambda=(\Gamma_{\rm ex}p_\alpha^2+\Gamma_0)t$. We deduce the mean and the variance of the number of photodetections during the time t:

$$\langle n\rangle=\left(\Gamma_0+\frac{1}{4}\Gamma_{\rm ex}\right)t\,,\quad {\rm Var}\,n=\langle n\rangle+\frac{(\Gamma_{\rm ex}t)^2}{8}\,. \tag{4.27}$$

Still using equation (4.26), we access the probability distribution of p_α knowing that n photons have been detected in the time interval $[0,t]$:

$$\Pi_t(p_\alpha|n)=\frac{1}{\Pi_n(t)}\frac{t^n}{n!}\left(\Gamma_{\rm ex}p_\alpha^2+\Gamma_0\right)^n{\rm e}^{-\Gamma_{\rm ex}p_\alpha^2t}{\rm e}^{-\Gamma_0t}\Pi(p_\alpha,0). \tag{4.28}$$

As expected, this is an even function of p_α, as photodetection only gives access to the polarized outgoing field intensity according to Oy and cannot distinguish between opposite values $\pm p_\alpha$ of the P_α quadrature of the hybridized nuclear spin according to Oz. This results in a squeezing of the fluctuations of P_α^2 rather than P_α, which we characterise by the conditional mean and variance of P_α^2 given that n photons were detected during t, deduced from (4.28):

$$\langle P_\alpha^2\rangle_n=\frac{(n+1)}{\Gamma_{\rm ex}t}\frac{\Pi_{n+1}(t)}{\Pi_n(t)}-\frac{\Gamma_0}{\Gamma_{\rm ex}} \tag{4.29}$$

$${\rm Var}_n(P_\alpha^2)\equiv\langle P_\alpha^4\rangle_n-\langle P_\alpha^2\rangle_n^2=\frac{(n+1)^2}{(\Gamma_{\rm ex}t)^2}\left[\frac{(n+2)\Pi_{n+2}(t)}{(n+1)\Pi_n(t)}-\frac{\Pi_{n+1}^2(t)}{\Pi_n^2(t)}\right]. \tag{4.30}$$

Finally, using equation (4.28), we find that for $\Gamma_{\rm ex}t\to+\infty$, the probability distribution of p_α^2 conditional on the number n of photodetections is pitted around a value p_0^2 with a

[6] For this reason, keeping the information on the jump times does not allow, by post-selection, to increase the efficiency of the spin squeezing. Indeed, the density operator $\rho_\alpha(t)|_{t_1,\dots,t_n}$ knowing that n jumps occurred at times $t_1,\dots,t_n$ leads to the same probability distribution of P_α as the density operator $\rho_\alpha(t)|_n$ knowing only that there were n jumps during $[0,t]$.

conditional variance tending to zero: [7]

$$\boxed{p_0^2 - \frac{1}{4} = \frac{n - \langle n\rangle}{\Gamma_{\rm ex} t} \quad \text{hence} \quad \langle P_\alpha^2\rangle_n \underset{\Gamma_{\rm ex}t\to+\infty}{\sim} p_0^2} \quad ; \quad \boxed{{\rm Var}_n(P_\alpha^2) \underset{\Gamma_{\rm ex}t\to+\infty}{\sim} \frac{n}{(\Gamma_{\rm ex}t)^2} \to 0.} \tag{4.31}$$

Replacing in this expression n by its mean value and taking into account the value $1/8$ of the variance of P_α^2 in the initial state, we end up with the nuclear spin squeezing rate by photon counting:

$$\boxed{\Gamma_{\rm sq} = \frac{\Gamma_{\rm ex}^2}{8(\Gamma_0 + \frac{1}{4}\Gamma_{\rm ex})}\,.} \tag{4.32}$$

Similarly, the conditional probability distribution of p_α has two peaks at $\pm p_0$ as can be seen in the Wigner function of figure 4.2b, obtained by numerical simulation of the conditional evolution of the system at long times in the one-mode model (4.18). This shows that, in a given run of the experiment, continuous photodetection of the Oy-polarized photons exiting the cavity makes the value of P_α^2, and thus to a large extent of I_z^2, the square of the Oz component of the collective nuclear spin, increasingly certain, as seen by linking in the $\Omega \to 0$ limit the conditional moments of P_a^2, i.e., of I_z^2, to those of P_α^2:

$$\langle P_a^2\rangle_n = \frac{\gamma_{\rm m}}{\gamma_{\rm f}+\gamma_{\rm m}}\langle P_\alpha^2\rangle_n + \frac{\gamma_{\rm f}/4}{\gamma_{\rm f}+\gamma_{\rm m}} \tag{4.33}$$

$${\rm Var}_n(P_a^2) = \frac{\gamma_{\rm m}^2}{(\gamma_{\rm f}+\gamma_{\rm m})^2}{\rm Var}_n(P_\alpha^2) + \frac{\gamma_{\rm f}\gamma_{\rm m}}{(\gamma_{\rm f}+\gamma_{\rm m})^2}\langle P_\alpha^2\rangle_n + \frac{\gamma_{\rm f}^2/8}{(\gamma_{\rm f}+\gamma_{\rm m})^2}\,. \tag{4.34}$$

Since the squeezing is on P_a^2 rather than P_a, the conditional angular distribution of the collective nuclear spin is bimodal (it has, like that of P_α, two well-separated peaks provided that $\gamma_{\rm f}/\gamma_{\rm m} \ll (2p_0)^2$); these narrower structures than the standard quantum limit still allow for more accurate angular pointing than with an unsqueezed state. We therefore redefine the metrological gain (3.26) by replacing in the third member of this equation the conditional variance of P_a by the square of the half-width δP_a of the peaks centred in $\pm P_{a,0}$ of the conditional probability distribution of P_a, and then equating the centre $P_{a,0}^2$ and width $\delta(P_a^2)$ of the distribution of P_a^2 with the conditional mean and standard deviation of P_a^2:

$$\xi^2 = \frac{4(\delta P_a)^2}{\eta} = \frac{(2P_{a,0}\delta P_a)^2}{\eta P_{a,0}^2} = \frac{[\delta(P_a^2)]^2}{\eta P_{a,0}^2} = \frac{{\rm Var}_n(P_a^2)}{\eta\langle P_a^2\rangle_n}. \tag{4.35}$$

Note that this expression is not deduced from the method of moments outlined in Section II. B.6 of reference [12] by taking P_a^2 as an estimator, because the effect of the unitary transformation $\exp(2{\rm i}\theta X_a)$ (in practice, a precession of the nuclear spin around a magnetic field according to Oy) is not to shift the peak in the distribution of P_a^2 but to split it into two peaks centred in $(P_{a,0} \pm \theta)^2$.

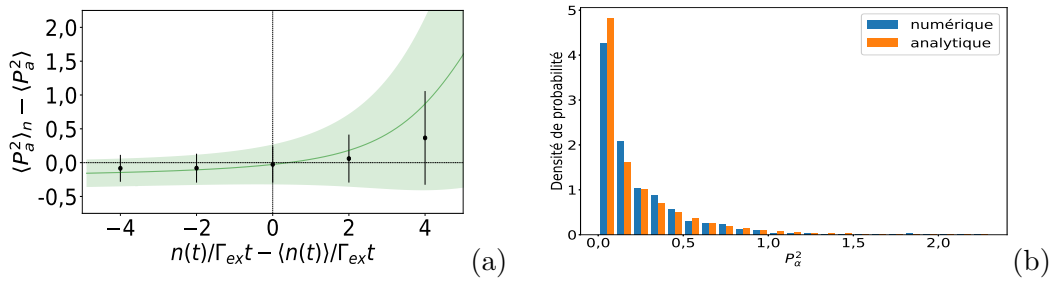

Figure 4.1: Squeezing of P_a^2 by photon counting at short times, $\Gamma_{\rm ex}t = 15$, where $\Gamma_{\rm ex}$ is the rate of excitation creation in the α hybrid nuclear bosonic mode. (a) Conditional mean and standard deviation of the nuclear spin squared P_a^2 given n photodetections in the time interval $[0, t]$, as a function of this number n. The standard deviation is represented as a confidence interval. The unconditional mean $\langle P_a^2\rangle = 1/4$ is independent of time, see equation (3.35). Black dots and error bars : numerical simulation of the three-mode model with 3000 realisations; green line and coloured area: analytical predictions from equations (4.26), (4.29), (4.30) and (4.33), (4.34) of the one-mode model. In practice, the black points are obtained after averaging over classes of n values centred on these points (within a given class, the trajectories have close photodetection numbers but independent histories for metastability exchange jumps to which the experimentalist has no access). Parameters of the three-mode model : $\Omega/\kappa = 1/3$, $\gamma_{\rm m}/\kappa = 1/10$, $\gamma_{\rm f}/\kappa = 1/1000$ (so that $\Gamma_{\rm ex}/\kappa = 1/909$), $n_a^{\max} = 64, n_b^{\max} = n_c^{\max} = 8$. This corresponds to $\Gamma_0/\Gamma_{\rm ex} = 12\,500/601 \simeq 20,8$ and $\Gamma_{\rm sq}/\Gamma_{\rm ex} = 601/101\,202 \simeq 1/168$ where $\Gamma_{\rm sq}$ is the squeezing rate (4.32). (b) For the class centred on $n = \langle n(t)\rangle$, histogram of conditional values of P_α^2. Blue bars: numerical simulation of the three-mode model; orange bars: analytical predictions from the equation (4.28) of the one-mode model.

4.3.2 Numerical results with three modes

Finally, let us perform a numerical verification of these analytical predictions in the three-mode model. In Figure 4.1a, we plot the conditional mean of the P_a^2 square of the nuclear spin quadrature knowing that n photodetections occurred in the $[0, t]$ time interval, with $\Gamma_{\rm ex}t = 15$ (black dots), as a function of this number n. The set of realizations is divided into 5 classes corresponding to a number of photodetections falling in a given interval, and the black dots are obtained by averaging over the realizations in the same class. The numerical results are close to the analytical predictions derived from (4.33) and (4.34) and shown in green, except in the extreme classes where the number of realisations is too small. On the other hand, the asymptotic analytical predictions (4.31), not shown, would disagree with the simulations of the two models because the time $t = 15/\Gamma_{\rm ex}$ is not long enough, it is much less than the squeezing time $1/\Gamma_{\rm sq}$. In Figure 4.1b we show the conditional probability distribution of P_α^2 corresponding to the middle class of Figure 4.1a; there is also good agreement between one-mode analytical and three-mode numerical predictions.

[7] According to equation (4.27), the second member of the first equation (4.31) is asymptotically of the order of unity for a typical photodetection sequence. This equation actually only makes sense for p_0^2 positive so $n > \Gamma_0 t$; then the (4.31) equivalents apply when the gap between the two peaks in $\Pi_t(p_\alpha|n)$ is much greater than their width, which imposes $2p_0^2 \gg n^{1/2}/\Gamma_{\rm ex}t = (\Gamma_0 + \Gamma_{\rm ex}p_0^2)^{1/2}/\Gamma_{\rm ex}t^{1/2}$. To obtain them, we pose $n = \gamma t$ with $\gamma > \Gamma_0$, then write (4.28) in the form $\exp[-tS(p_\alpha)]\Pi(p_\alpha, 0)$ and quadratize $S(p_\alpha)$ around its minima.

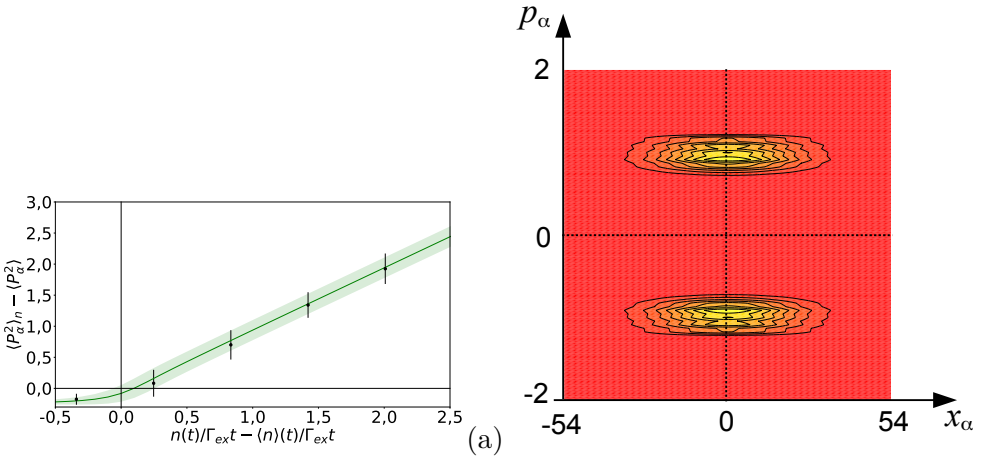

Figure 4.2: Squeezing of P_α^2 by counting photons at long times in the one-mode model (4.18). (a) Conditional mean and standard deviation of P_α^2 given that the number of photodetections n falls within a given class of values, similar to Figure 4.1a but for $\Gamma_{ex}t = 1000$ and 2000 realisations (this long time would make it difficult to simulate in the three-mode model). (b) Wigner distribution of the hybridised nuclear bosonic mode in the quadrature space (X_α, P_α) at $\Gamma_{ex}t = 1000$, obtained by averaging the dyads $|\psi(t)\rangle\langle\psi(t)|$ whose number of photodetections falls into the third class of (a) (302 trajectories out of 5000 realisations). It has two lines of peaks but no interference fringes.

In Figure 4.2, we explore the long times in the one-mode model, with $\Gamma_{ex}t = 1000$ i.e. $\Gamma_{sq}t \simeq 5,94$. Figure 4.2a, which is the equivalent of Figure 4.1a, shows that $\langle P_\alpha^2\rangle_n$ is then related to the number of photodetections n as in the analytical prediction (4.31), i.e. along the first bisector in the units of the figure, with a conditional standard deviation in (4.31) that is approximately constant $\simeq (\Gamma_0 t)^{1/2}/\Gamma_{ex}t \simeq 1/(\Gamma_{sq}t)^{1/2}$ because Γ_0 is here $\gg \Gamma_{ex}$. The absence of fringes shows that a statistical mixture rather than a coherent superposition of two states squeezed into the P_α quadrature has been prepared. In figure 4.2b, we find from equation (4.22) that

$$\langle p_0|\rho_n(t)|-p_0\rangle/\langle p_0|\rho_n(t)|p_0\rangle = [(\Gamma_0 - \Gamma_{ex}p_0^2)/(\Gamma_0 + \Gamma_{ex}p_0^2)]^n \simeq \exp(-2\Gamma_{ex}tp_0^2) \lll 1 \quad (4.36)$$

$\rho_n(t)$ is the conditional density operator. The Laplace method gives at long times the conditional Wigner distribution

$$W_t(x_\alpha, p_\alpha|n) \sim \pi\Pi_t(p_\alpha|n)\exp[-2x_\alpha^2/\Gamma_{ex}ts(p_\alpha)]/\sqrt{\pi\Gamma_{ex}ts(p_\alpha)/2} \quad (4.37)$$

with $s(p_\alpha) = [1+(\Gamma_0+\Gamma_{ex}p_0^2)/(\Gamma_0+\Gamma_{ex}p_\alpha^2)]/2$. We notice that $s(\pm p_0) = 1$ and $s(p_\alpha) \simeq 1$ for $\Gamma_0 \gg \Gamma_{ex}$. While $W_t(0,0|n)$ is crushed exponentially in time (in the limit $\Gamma_{ex} \ll \Gamma_0$, there comes $W_t(0,0|n) \sim (\Gamma_{ex}/\Gamma_0)^{1/2}p_0\exp(2p_0^2)\exp(-4p_0^4\Gamma_{sq}t)$), we also have $W_t(0,0|n) = \langle 2\varepsilon\rangle_n$ where $\varepsilon = \pm 1$ is the parity of the Monte Carlo wave function $\psi(p_\alpha, t)$. In a numerical simulation, we therefore only have a slow decay $\langle\varepsilon\rangle_n \approx 1/\sqrt{\mathcal{N}_n}$ where $\mathcal{N}_n$ is the number of trajectories that have undergone n jumps during t; this leads to unphysical fringes with negative values in the Wigner distribution near the Ox_α axis. To minimise this effect and make it imperceptible at a not too high p_α resolution ($\mathrm{d}p_\alpha = 0,044$ in figure 4.2b), the Monte

Carlo simulation is stopped at a stage where there are exactly the same number $\mathcal{N}_n/2$ of even and odd wave functions. To obtain a coherent superposition of squeezed states, one would have to perform an additional post-selection, restricting oneself to Monte Carlo realisations of wavefunction $\psi(p_\alpha, t)$ of fixed parity ε (having undergone an even number of single jumps if $\varepsilon = 1$, an odd number otherwise, the jump operator C_s changing the parity). In the corresponding conditional density operator, we then have $\langle p_0|\rho_{n,\varepsilon}(t)|-p_0\rangle/\langle p_0|\rho_{n,\varepsilon}(t)|p_0\rangle = \overline{\psi(-p_0,t)\psi(p_0,t)}^{n,\varepsilon}/\overline{\psi(p_0,t)\psi(p_0,t)}^{n,\varepsilon} = \varepsilon$ without the two-peak structure of the distribution of P_α being affected at long times because $\Pi_t(p_\alpha|n,\varepsilon)/\Pi_t(p_\alpha|n) \propto 1 + \varepsilon[(\Gamma_0 - \Gamma_{\rm ex}p_\alpha^2)/(\Gamma_0 + \Gamma_{\rm ex}p_\alpha^2)]^n \to 1$ when $n \to +\infty$ to p_α non-zero fixed. The Wigner distribution $W_t(x_\alpha, p_\alpha|n,\varepsilon)$ now has positive and negative fringes of maximum amplitude 2 on the $p_\alpha = 0$ axis. This filtering technique also overcomes the decoherence mechanisms of section 5.4 because the Monte Carlo wave functions remain of well-defined parity after action of the corresponding jump operator $\gamma_\alpha^{1/2}\alpha$. [8]

[8] This idea of controlling decoherence through parity measurements is well known in cavity quantum electrodynamics [49].

Chapter 5

Nuclear spin squeezing by homodyne detection

Foreword

We now assume that the photons leaving the cavity polarised along Oy are measured continuously by homodyne detection [50], as in figure 1.1c, i.e. from the measurement of one of the quadratures of the field at the cavity exit. In this situation, we are able to calculate, analytically, the evolution of the variance of the Oz direction of the nuclear spin over time in the one-mode model and in the full three-mode model, with the explicit expression of squeezing rates in terms of the system rates. We will push the analysis to solve, with the same analytical method, the case of a decoherence in the metastable population[1], whether in the one-mode or three-mode model, finally obtaining the expression of the squeezing rate modified by this atom loss. To do this, we first need to find the right stochastic equations giving the evolution of the state vector of the system conditional on the homodyne detection, since the jump operators appearing naturally in the (4.4) or (4.18) writing of the three-mode or one-mode master equation are inadequate. In order to obtain these results, we used the fact that, for the empty initial state considered here, the conditional state vector is given exactly at all times by a Gaussian ansatz [51], whatever the number of modes in the model, in the presence or absence of decoherence. The results show that this configuration allows us to obtain a deterministic equation giving the reduction of the variance of a transverse component of the nuclear spin, although the results are a priori conditional on the results of the homodyne measurement. Several arguments lead us to consider this configuration as more suitable for a real experimental realisation in the framework of the construction of a metrological state going beyond the standard quantum limit. Firstly, as we have seen in the previous chapter, the rate of squeezing of the nuclear spin by photon counting is proportional to the rate of excitation in the nuclear mode Γ_{ex}, related to the "single jump" process where a photon leaves the cavity correlated to an excitation created in the nuclear spin, and inversely proportional to that of the "double jump" rate Γ_0, which corresponds to a photon leaving the cavity with no excitation created. As the photons from these two processes are

[1] The only decoherence process having a significant impact on the system, it corresponds to the collision of the metastable atoms on the cell walls, which brings them back to the ground state while losing all information of the electronic cloud.

indistinguishable, the photons from the "double jump" pollute the measurement and reduce the accessible spin squeezing. As we will see in this chapter, the advantage of homodyne detection is that it suppresses the contribution of these double jumps to the nuclear spin dynamics, thus accelerating the squeezing rate. Another advantage is that the conditional probability distribution of I_z obtained is no longer bimodal as in chapter 4, i.e. it converges well to a value of I_z and not I_z^2. This ensures that the nature of the spin state at the end of the procedure is indeed that of a standard squeezed spin state, as understood in quantum metrology work. Therefore, to conclude this chapter and this section, we use this homodyne detection configuration to propose a proff-of-concept experiment. Values are given for the parameters defining the configuration, which are realistic in the literature today, and it is shown that based on the analytical results of this chapter, we can expect a squeezing of a few decibels with respect to the standard quantum limit of a fully polarised state, as well as a metrological gain of $\xi^2 < 1$. [2]

5.1 Adjusted stochastic formulation of the master equation

A general master equation of the Lindblad form [44]

$$\frac{\mathrm{d}\rho}{\mathrm{d}t} = \frac{1}{\mathrm{i}\hbar}[H,\rho] + \sum_m C_m \rho C_m^\dagger - \frac{1}{2}\{C_m^\dagger C_m, \rho\} \tag{5.1}$$

with H the Hermitian part of the Hamiltonian and C_m the jump operators, can be rewritten in an equivalent way by adding an arbitrary constant to the jump operators and/or mixing them by some unitary linear combination. In order to take into account a homodyne detection on the outgoing field, we form, from a jump operator C_m corresponding to a photodetection, the two "homodyne" jump operators $D_{m,\pm}$ [42]

$$D_{m,+} = \frac{\mu\mathbb{1} + C_m}{\sqrt{2}}, \quad D_{m,-} = \frac{\mu\mathbb{1} - C_m}{\sqrt{2}} \tag{5.2}$$

where μ^2 has the dimensions of a momentum. Measuring the difference in jump rates $D_+^\dagger D_+ - D_-^\dagger D_-$ then gives access to a quadrature of C_m. Thus, for μ real and C_m corresponding to the cavity jump operator C_c, see equation (4.7), the difference between the numbers of photons $N_\pm$ detected during the short time interval Δt in the two output channels of figure 1.1c, which by definition constitutes the homodyne signal,

$$N_+ = (D_{c,+}^\dagger D_{c,+})\,\Delta t\,, \quad N_- = (D_{c,-}^\dagger D_{c,-})\,\Delta t\,, \quad \frac{N_+ - N_-}{2\,\mu} = \frac{c + c^\dagger}{2}\sqrt{\kappa}\Delta t \tag{5.3}$$

gives access to X_c ; it is indeed the quadrature of the field conjugated to P_c and thus translated by an amount proportional to P_b and time under the action of the Hamiltonian H (3.25), which gives information on P_a through the metastability exchange collisions. In the case of the three-mode master equation (4.4), we must apply the splitting procedure (5.2)

[2] Recall that the squeezing of the nuclear spin in the Oz direction is defined by the relation $\frac{\Delta I_z}{N/4}$, which is less than 1 if the variance in this direction is less than that of the fully polarised coherent state, this squeezing will be expressed in decibels. The metrological gain is defined by the relation $\xi^2 = (2I)^{1/2}\Delta I_z/|I_z|$, which is less than 1 if the nuclear spin state is more sensitive to the magnetic field than the fully polarised coherent state. We borrow this measurement from reference [25].

a priori only to the cavity jump operator. In practice, we will also apply it to the jump operator C_β, i.e. we will split by "homodyning" *all* the jump operators C_m, in order to avoid the discomfort of a mixed representation mixing discrete quantum jumps and continuous stochastic evolution, see the upcoming equation (5.4). In the case of the one-mode master equation (4.18), the two jump operators C_s and C_d must be "homodyned" anyway, since each is accompanied by the loss of a photon in cavity, as explained in section 4.2.

In the limit of a large-amplitude local oscillator μ, one can pretend that Δt is infinitesimal [3] and represent the evolution of the Monte Carlo wavefunction, this time normalized to unity, by a continuous nonlinear stochastic equation without quantum jumps [42, 52, 53] in Ito's point of view :

$$\boxed{\begin{aligned}\mathrm{d}|\phi(t)\rangle = &-\frac{\mathrm{i}}{\hbar}H|\phi(t)\rangle\mathrm{d}t\\ &-\frac{1}{2}\sum_m\left(C_m^\dagger C_m - \langle\phi(t)|C_m+C_m^\dagger|\phi(t)\rangle C_m + \frac{1}{4}\langle\phi(t)|C_m+C_m^\dagger|\phi(t)\rangle^2\right)|\phi(t)\rangle\mathrm{d}t\\ &+\sum_m\left(C_m - \frac{1}{2}\langle\phi(t)|C_m+C_m^\dagger|\phi(t)\rangle\right)|\phi(t)\rangle\,\mathrm{d}\zeta_m(t)\end{aligned}} \tag{5.4}$$

where, to each jump operator C_m in the initial writing of the master equation, we associate a real-valued Gaussian continuous-time stochastic process $\mathrm{d}\zeta_m(t)$, of zero-mean and variance $\mathrm{d}t$, statistically independent of the other processes and memory-free. At the same level of approximation, the homodyne signal operator (5.3) is replaced by the sum of its mean and a classical noise representing its fluctuations, which is no other than the corresponding $\mathrm{d}\zeta_m$ [42]:

$$\frac{N_+ - N_-}{2\mu} = \frac{\sqrt{\kappa}\langle\phi|c+c^\dagger|\phi\rangle}{2}\mathrm{d}t + \frac{1}{2}\mathrm{d}\zeta_c. \tag{5.5}$$

In practice, more than the homodyning history, i.e. the detailed time dependence of the homodyne detection signal, it is its temporal average over a time interval $[0,t]$ that is easily accessible in an experiment (and allows a post-selection of the states i.e. the experimental realizations) over a non-negligible set of statistical weights. We therefore introduce the integrated signal having the dimension of the root of a momentum,

$$\boxed{\sigma(t) \equiv \frac{N_+^{\mathrm{tot}} - N_-^{\mathrm{tot}}}{2\mu t} = \frac{1}{t}\int_0^t \mathrm{d}t'\left[\sqrt{\kappa}\langle\phi(t')|X_c|\phi(t')\rangle + \frac{1}{2}\frac{\mathrm{d}\zeta_c(t')}{\mathrm{d}t'}\right]} \tag{5.6}$$

and in the following we will calculate the mean and variance of the P_a quadrature of the nuclear spin conditioned on σ. Recall that the mean and variance of an observable (here P_a) in a single realisation $|\phi(t)\rangle$ of the stochastic equation, hence of the experiment, do not in general have any physical meaning, because there is no possible measurement of the mean value of an observable in a single realisation, one has instead to average over a large number of realisations of the experiment that have evolved during t from the same pure case or initial density operator. A counter-example is the case where one can, by continuous measurements, trace the time dependence of *all* the stochastic processes $\mathrm{d}\zeta_m$; this is the case

[3] This approximation is valid for a time resolution, i.e. a time step Δt, such as $\mu^{-2} \ll \Delta t \ll \kappa^{-1}$, where κ is in practice the fastest rate of evolution of the system in the experiment.

of the one-mode model subjected to homodyne detection, the time dependence of the signal (5.5) fixing that of the single stochastic process $\mathrm{d}\zeta_c$. This would then allow, in principle, to select, among a large number of realisations of the experiment, those leading to the chosen state $|\phi(t)\rangle$, and to deduce the averages of observables in $|\phi(t)\rangle$; in practice, this would be unrealistic, given the infinitesimal statistical weight of the realisations to keep.

5.2 Analytic solutions in the one-mode model

Let us explicitly write the stochastic equation (5.4) for the one-mode model (4.18) :

$$\mathrm{d}|\phi(t)\rangle = -\frac{\mathrm{d}t}{2}\Gamma_{\mathrm{ex}}[P_\alpha - \bar{P}_\alpha(t)]^2|\phi(t)\rangle + \sqrt{\Gamma_{\mathrm{ex}}}\mathrm{d}\zeta_s(t)[P_\alpha - \bar{P}_\alpha(t)]|\phi(t)\rangle \tag{5.7}$$

with $\bar{P}_\alpha(t) \equiv \langle\phi(t)|P_\alpha|\phi(t)\rangle$. The striking fact is that the jumps associated with the identity-proportional operator C_d, which added noise to the photon-counting detection of section 4.3, do not contribute, as the operator C_d disappears from the conditional evolution equation in the homodyne case. Indeed, the photons emitted during these jumps come from the $|1\rangle|1\rangle$ component of the (4.8) state vector containing an β excitation, which makes them optically incoherent with the light field injected into the cavity, i.e. with the $|0\rangle|0\rangle$ component of (4.8), in the sense that $|1\rangle|1\rangle$ contributes to $\langle c^\dagger c\rangle$ but not to $\langle c + c^\dagger\rangle$. This leaves only the stochastic process $\mathrm{d}\zeta_s$ associated with the jump operator C_s. This process merges with the process $\mathrm{d}\zeta_c$ appearing in the homodyne detection signal (5.5), $\mathrm{d}\zeta_s \equiv \mathrm{d}\zeta_c$, a fact admitted here but which will be established by returning to the three-mode model in section 5.3.

The stochastic equation (5.7) has a linear noise term and a deterministic quadratic term in the P_α operator, which are real in Fourier space. For the initial state considered here, it is therefore solved exactly by a Gaussian ansatz on the wave function in momentum representation, real and correctly normalised to the $[X_\alpha, P_\alpha] = \mathrm{i}/2$:

$$\langle p_\alpha|\phi(t)\rangle = [2\pi u(t)]^{1/4}\exp\{-u(t)[p_\alpha - \bar{P}_\alpha(t)]^2\}. \tag{5.8}$$

In contrast, gaussianity is lost in the photodetection squeezing of section 4.3. Using Ito calculus,[4] we find that u follows a deterministic evolution equation, to be integrated with the initial condition $u(0) = 1$:

$$\mathrm{d}u(t) = \Gamma_{\mathrm{ex}}\mathrm{d}t \quad \text{hence} \quad u(t) = 1 + \Gamma_{\mathrm{ex}}t \quad \text{and} \quad \mathrm{Var}_\phi P_\alpha(t) \equiv \frac{1}{4u(t)} = \frac{1}{4}\frac{1}{1+\Gamma_{\mathrm{ex}}t} \tag{5.9}$$

where we have also given the variance of P_α in the $|\phi\rangle$ state. In contrast, the equation on the mean value of P_α in $|\phi\rangle$ is purely stochastic, with a time-dependent diffusion coefficient $D(t)$ and the initial condition $\bar{P}_\alpha(0) = 0$:

$$\mathrm{d}\bar{P}_\alpha(t) = [2D(t)]^{1/2}\mathrm{d}\zeta_s(t) \quad \text{with} \quad D(t) = \frac{\Gamma_{\mathrm{ex}}}{8u(t)^2} = \frac{\Gamma_{\mathrm{ex}}}{8(1+\Gamma_{\mathrm{ex}}t)^2}. \tag{5.10}$$

Since $D(t)$ is of finite integral, $\bar{P}_\alpha(t)$ stabilises asymptotically (at long times) at a fixed value on a single realisation, as seen in figure 5.1, with a variance in the quantum state $\mathrm{Var}_\phi P_\alpha$ tending towards 0. This phenomenon of "stochastic convergence" towards an eigenstate

[4] Keeping only the linear terms in $\mathrm{d}t$ or in the noise, and systematically replacing the quadratic terms $\mathrm{d}\zeta_s^2$ by their mean $\mathrm{d}t$.

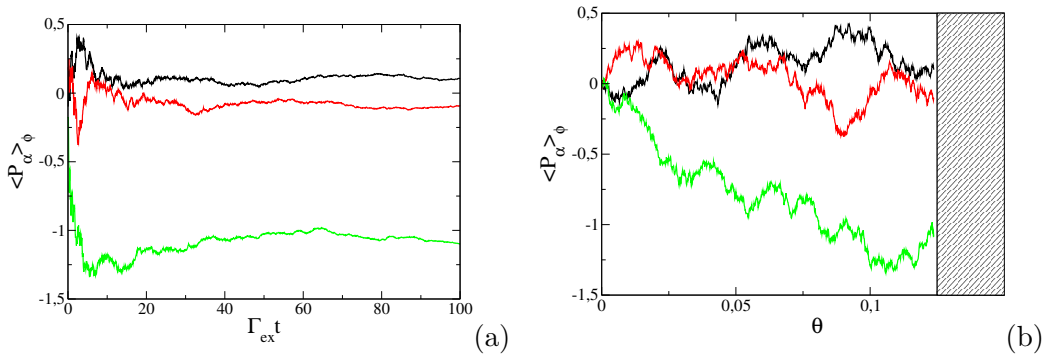

Figure 5.1: In the case of squeezing by continuous homodyne detection, random walk (5.10) in the one-mode model performed by the quantum average value of the nuclear spin quadrature P_α in a given realisation of the experiment. (a) Mean value as a function of true time t scaled by the rate (4.13) of excitation creation for three realisations of the experiment; this is a stretched Brownian motion converging at long times to a fixed but unpredictable value. (b) Idem but as a function of the compact renormalized time θ (5.11); this time it is an ordinary Brownian motion but limited to $\theta \leq 1/8$.

of the measured observable (in this case P_α) is expected in the description of a quantum measurement by a diffusion equation of the state vector [52, 53, 54]. To show this here, we introduce a renormalized time θ with respect to which $\bar{P}_\alpha$ performs an ordinary Brownian motion with a unit diffusion coefficient, and we notice that this time is bounded:

$$\theta = \int_0^t \mathrm{d}t' D(t') = \frac{\Gamma_{\mathrm{ex}} t}{8(1+\Gamma_{\mathrm{ex}} t)} \underset{t\to+\infty}{\to} \theta_\infty = \frac{1}{8}. \tag{5.11}$$

At the renormalized time θ_∞, $\bar{P}_\alpha$ follows a Gaussian distribution of mean zero and variance $1/4$: $\bar{P}_\alpha$ thus has the same asymptotic probability distribution ($t \to +\infty$) as that of the observable P_α in the initial quantum state of the nuclear spin.

Let us now turn to the mean and variance of P_α conditional on the value $\mathcal{S}$ of the time-integrated homodyne signal σ (5.6). Remarkably, we find that the conditional mean is always proportional to the signal, with a time-dependent proportionality coefficient, and that the conditional variance is time-dependent but not signal-dependent :

$$\boxed{\begin{array}{c} \langle P_\alpha \rangle_{\sigma=\mathcal{S}} = m(t) \dfrac{\mathcal{S}}{\sqrt{\Gamma_{\mathrm{ex}}}} \quad ; \quad \mathrm{Var}_{\sigma=\mathcal{S}}(P_\alpha) = \mathcal{V}(t) \\ \text{where} \quad m(t) = \dfrac{\Gamma_{\mathrm{ex}} t}{1+\Gamma_{\mathrm{ex}} t} \quad \text{and} \quad \mathcal{V}(t) = \dfrac{1}{4(1+\Gamma_{\mathrm{ex}} t)}. \end{array}} \tag{5.12}$$

These expressions designate Γ_{ex} as the nuclear spin squeezing rate by homodyning in the one-mode model and thus with weak Faraday coupling :

$$\boxed{\Gamma_{\mathrm{sq}} \underset{\Omega\to 0}{\sim} \Gamma_{\mathrm{ex}} = \frac{\Omega^2}{\kappa} \frac{\gamma_{\mathrm{f}}}{\gamma_{\mathrm{m}} + \gamma_{\mathrm{f}}}.} \tag{5.13}$$

In figure 5.2a, we plot $m(t)$ and $\mathcal{V}(t)$ as a function of the reduced time $\Gamma_{\mathrm{ex}} t$. Like the quantum variance on a realization $\mathrm{Var}_\phi P_\alpha$, with which it actually coincides, the conditional variance

tends asymptotically to zero as the inverse of time. In the conditional mean, the coefficient $m(t)$ tends towards 1 at long times. To understand this, let us relate the integrated signal (5.6) to $\bar{P}_\alpha$ using the adiabatic expressions (4.11) in the truncated state vector (4.8) :

$$\sigma(t) = \frac{1}{t}\int_0^t \mathrm{d}t' \left[\sqrt{\Gamma_{\mathrm{ex}}}\bar{P}_\alpha(t') + \frac{1}{2}\frac{\mathrm{d}\zeta_s(t')}{\mathrm{d}t'}\right]. \tag{5.14}$$

Since $\bar{P}_\alpha(t)$ stabilizes asymptotically on a single realization, and the time-averaged noise $\mathrm{d}\zeta_s$ tends to zero as $1/t^{1/2}$ almost surely, $\sigma(+\infty)$ directly yields the value of $\bar{P}_\alpha(+\infty)$ to within a constant factor $\sqrt{\Gamma_{\mathrm{ex}}}$.

To establish the results (5.12), let us first relate the conditional variance of the operator P_α to that of its quantum average over a realization $\bar{P}_\alpha$ as follows:

$$\begin{aligned}
\mathrm{Var}_{\sigma=\mathcal{S}}(P_\alpha) &\equiv \langle\, \langle\phi|P_\alpha^2|\phi\rangle \,\rangle_{\sigma=\mathcal{S}} - \langle\, \langle\phi|P_\alpha|\phi\rangle \,\rangle^2_{\sigma=\mathcal{S}} &(5.15)\\
&= \langle\, \langle\phi|P_\alpha^2|\phi\rangle - \langle\phi|P_\alpha|\phi\rangle^2 \,\rangle_{\sigma=\mathcal{S}} + \langle\bar{P}_\alpha^2\rangle_{\sigma=\mathcal{S}} - \langle\bar{P}_\alpha\rangle^2_{\sigma=\mathcal{S}}\\
&= \langle\mathrm{Var}_\phi P_\alpha\rangle_{\sigma=\mathcal{S}} + \mathrm{Var}_{\sigma=\mathcal{S}}(\bar{P}_\alpha)\\
&= \frac{1}{4}\frac{1}{1+\Gamma_{\mathrm{ex}}t} + \mathrm{Var}_{\sigma=\mathcal{S}}(\bar{P}_\alpha) &(5.16)
\end{aligned}$$

where we have used the expression (5.9) for the quantum variance of P_α in the $|\phi\rangle$ state. It therefore remains to determine the conditional probability distribution of $\bar{P}_\alpha$ knowing that $\sigma = \mathcal{S}$,

$$P(\bar{P}_\alpha = p_\alpha|\sigma=\mathcal{S}) \equiv \frac{P(\bar{P}_\alpha = p_\alpha, \sigma=\mathcal{S})}{P(\sigma=\mathcal{S})}. \tag{5.17}$$

Now, the random variable $\bar{P}_\alpha(t)$, resulting from a Brownian motion (5.10), has a Gaussian probability distribution; the same is true for the time integral of $\bar{P}_\alpha$ and the noise $\mathrm{d}\zeta_s$, and therefore of the signal σ (5.14) which is the sum of them. As the variables $\bar{P}_\alpha$ and σ have zero means, their joint probability distribution is characterised by their covariance matrix, or more directly by its inverse matrix, so that

$$P(\bar{P}_\alpha = p_\alpha|\sigma=\mathcal{S}) = \frac{\frac{1}{2\pi\sqrt{\langle\bar{P}_\alpha^2\rangle_{\mathrm{stoch}}\langle\sigma^2\rangle_{\mathrm{stoch}} - \langle\sigma\bar{P}_\alpha\rangle^2_{\mathrm{stoch}}}}\exp\left(-\frac{1}{2}\frac{p_\alpha^2\langle\sigma^2\rangle_{\mathrm{stoch}} + \mathcal{S}^2\langle\bar{P}_\alpha^2\rangle_{\mathrm{stoch}} - 2p_\alpha\mathcal{S}\langle\sigma\bar{P}_\alpha\rangle_{\mathrm{stoch}}}{\langle\bar{P}_\alpha^2\rangle_{\mathrm{stoch}}\langle\sigma^2\rangle_{\mathrm{stoch}} - \langle\sigma\bar{P}_\alpha\rangle^2_{\mathrm{stoch}}}\right)}{\frac{1}{\sqrt{2\pi\langle\sigma^2\rangle_{\mathrm{stoch}}}}\exp\left(-\frac{\mathcal{S}^2}{2\langle\sigma^2\rangle_{\mathrm{stoch}}}\right)} \tag{5.18}$$

$$P(\bar{P}_\alpha = p_\alpha|\sigma=\mathcal{S}) = \frac{1}{\sqrt{2\pi\left[\langle\bar{P}_\alpha^2\rangle_{\mathrm{stoch}} - \langle\sigma\bar{P}_\alpha\rangle^2_{\mathrm{stoch}}/\langle\sigma^2\rangle_{\mathrm{stoch}}\right]}}\exp\left[-\frac{1}{2}\frac{\left(p_\alpha - \mathcal{S}\langle\sigma\bar{P}_\alpha\rangle_{\mathrm{stoch}}/\langle\sigma^2\rangle_{\mathrm{stoch}}\right)^2}{\langle\bar{P}_\alpha^2\rangle_{\mathrm{stoch}} - \langle\sigma\bar{P}_\alpha\rangle^2_{\mathrm{stoch}}/\langle\sigma^2\rangle_{\mathrm{stoch}}}\right] \tag{5.19}$$

where $\langle\ldots\rangle_{\mathrm{stoch}}$ at time t is the mean taken over all realisations of the stochastic process $\mathrm{d}\zeta_s(t')$ over the time interval $[0,t]$. From this, it can be deduced that in equations (5.12),

$$m(t) = \sqrt{\Gamma_{\mathrm{ex}}}\frac{\langle\sigma(t)\bar{P}_\alpha(t)\rangle_{\mathrm{stoch}}}{\langle\sigma^2(t)\rangle_{\mathrm{stoch}}} \tag{5.20}$$

$$\mathcal{V}(t) = \frac{1}{4(1+\Gamma_{\mathrm{ex}}t)} + \langle\bar{P}_\alpha^2(t)\rangle_{\mathrm{stoch}} - \frac{\langle\sigma(t)\bar{P}_\alpha(t)\rangle^2_{\mathrm{stoch}}}{\langle\sigma^2(t)\rangle_{\mathrm{stoch}}}\,. \tag{5.21}$$

In order to determine their variances and covariance, $\sigma(t)$ and $\bar{P}_\alpha(t)$ are written as linear functionals of the stochastic process $\mathrm{d}\zeta_s$ and the fact that the Langevin forces $\mathrm{d}\zeta_s(t)/\mathrm{d}t$ and $\mathrm{d}\zeta_s(t')/\mathrm{d}t'$ have a Dirac correlation function $\delta(t-t')$ is used. Let us give the example of the first contribution to $\sigma(t)$:

$$\begin{aligned}\int_0^t \mathrm{d}t''\bar{P}_\alpha(t'') &= \int_0^t \mathrm{d}t'' \int_0^{t''} \mathrm{d}t'[2D(t')]^{1/2}\frac{\mathrm{d}\zeta_s(t')}{\mathrm{d}t'} \\ &= \int_0^t \mathrm{d}t' \int_{t'}^t \mathrm{d}t''[2D(t')]^{1/2}\frac{\mathrm{d}\zeta_s(t')}{\mathrm{d}t'} \\ &= \int_0^t \mathrm{d}t'(t-t')[2D(t')]^{1/2}\frac{\mathrm{d}\zeta_s(t')}{\mathrm{d}t'} \end{aligned} \tag{5.22}$$

where we have changed the order of integration on t' and t'' and then integrated explicitly on t''. This leads to the searched expressions (5.12), whose simplicity follows from the fact that, on a realization of the experiment, we always have

$$\boxed{\sigma(t) = \sqrt{\Gamma_{\mathrm{ex}}}\frac{1+\Gamma_{\mathrm{ex}}t}{\Gamma_{\mathrm{ex}}t}\bar{P}_\alpha(t).} \tag{5.23}$$

Remarkably, the knowledge of the only integrated signal $\sigma(t)$ in a realization of the experiment of duration t is enough to prepare the nuclear spin in a well-defined pure Gaussian case (5.8), with a parameter u given by the equation (5.9) and a mean quadrature $\bar{P}_\alpha$ related to the signal by the equation (5.23).

Finally, let us return to the P_a quadrature of the unhybridized nuclear spin, which is the one actually usable in the experiment once the discharge is turned off in the cell, as shown by the (3.26) expression for the metrological gain in a precession measurement. Leaving the rotated basis by reversing the (4.3) transformation and restricting the (4.8) equation to its first term (to the leading order in Ω), it comes

$$\langle P_a\rangle_{\sigma=\mathcal{S}} = \left(\frac{\gamma_{\mathrm{m}}}{\gamma_{\mathrm{f}}+\gamma_{\mathrm{m}}}\right)^{1/2}\langle P_\alpha\rangle_{\sigma=\mathcal{S}} \tag{5.24}$$

$$\mathrm{Var}_{\sigma=\mathcal{S}}(P_a) = \frac{\gamma_{\mathrm{f}}}{4(\gamma_{\mathrm{f}}+\gamma_{\mathrm{m}})} + \frac{\gamma_{\mathrm{m}}}{\gamma_{\mathrm{f}}+\gamma_{\mathrm{m}}}\mathrm{Var}_{\sigma=\mathcal{S}}(P_\alpha)\,. \tag{5.25}$$

The conditional variance of P_a at long times tends to a non-zero value, although small in practice : this is the intrinsic limit of this nuclear spin squeezing scheme, which uses the metastable ^{3}He state as an intermediate.

5.3 Analytical solutions in the three-mode model

The study of spin squeezing in the framework of the one-mode model is limited to the (4.2) regime where the squeezing rate $\Gamma_{\mathrm{sq}} \sim \Gamma_{\mathrm{ex}}$ corresponds to the longest time scale of the system. However, it is crucial for applications to see how far the squeezing process can be accelerated by increasing Γ_{ex} so, for example, the Faraday Ω coupling of metastable atoms to the cavity field. To this end, we obtain the analytical solution of the three-mode model by using the Gaussian character of the state vector which results, as for the one-mode model, from the initial state considered (vacuum), the linearity of the jump operators C_m and the

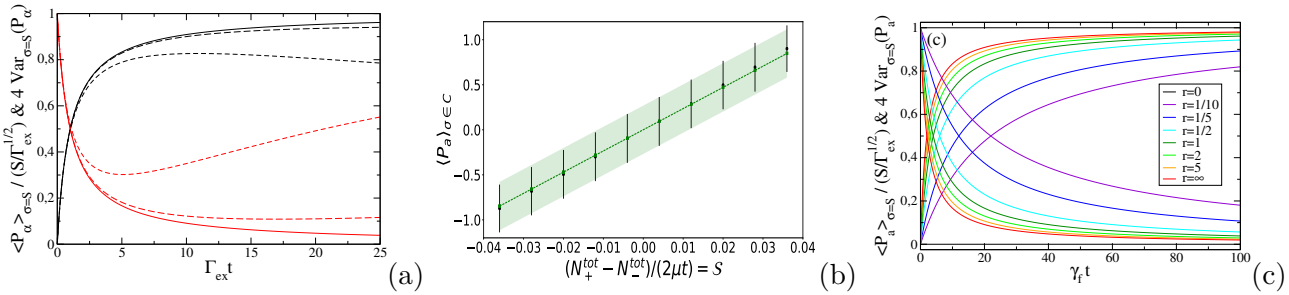

Figure 5.2: Nuclear spin squeezing by continuous homodyne measurement. (a) In the one-mode model, mean (black) and variance (multiplied by 4, red) of the quadrature P_α of the hybridised nuclear spin conditional on the integrated homodyning signal σ, as a function of the integration time t. Solid lines: analytical expressions (5.12). Dashed lines: expressions (5.60) in the presence of decoherence by de-excitation of the metastables on the cell walls (long dashed line: $\epsilon = 1/100$, short dashed line: $\epsilon = 1/10$, with $\epsilon = \gamma_\alpha/\Gamma_{\rm ex}$ and γ_α the decoherence rate brought back to (5.56)). (b) In the three-mode model, for $\Gamma_{\rm ex}t = 5$, mean and standard deviation of the nuclear spin quadrature P_a conditional on the σ signal belonging to a C class, the interval of σ values having been divided into 10 classes of equal width (the $\mathcal{S}$ values of σ are in units of $\Gamma_{\rm ex}^{1/2}$ on the x-axis). The standard deviation is represented as a confidence interval. In black: numerical simulation of the stochastic equation (5.4) with 1079 realisations. Green dashed line and coloured area: exact results from the (5.38) and (5.39) relationships, and from the analytical expression of the conditional probability distribution of $\bar{P}_a$ in terms of the variances and covariance (5.46)-(5.48) on the model of the equation (5.19). The discrepancy between numerical and analytical in the extreme classes is due to the small number of realisations falling into these classes. Values of the parameters: $\Omega/\kappa = 1/10$, $\gamma_{\rm m}/\kappa = 1/10$, $\gamma_{\rm f}/\kappa = 1/100$, $\Gamma_{\rm ex}/\kappa = 1/1000$. (c) In the limit $\Gamma_{\rm ex} \to 0$ to $\Gamma_{\rm ex}/2\gamma_{\rm f}$ fixed of the three-mode model, conditional mean and variance of P_a (5.50) as a function of the reduced time $\gamma_{\rm f}t$, for different values of the rate $r = 2\Gamma_{\rm ex}/\gamma_{\rm f}$ (increasing curves: mean, decreasing curves: variance).

quadraticity of the Hamiltonian H in the quadratures of the modes. The stochastic equation (5.4) thus admits as an exact solution the Gaussian ansatz generalising that of the equation (5.8),

$$\langle p_\alpha, p_\beta, x_c|\phi(t)\rangle = \phi(\mathbf{q},t) = [8\pi \det \underline{\underline{u}}(t)]^{1/4} \exp\left\{-[\mathbf{q}-\bar{\mathbf{q}}(t)]\cdot \underline{\underline{u}}(t)\,[\mathbf{q}-\bar{\mathbf{q}}(t)]\right\} \equiv \mathrm{e}^{-S} \tag{5.26}$$

where $\underline{\underline{u}}$ is a real symmetric 3×3 matrix, $\bar{\mathbf{q}}$ is a real three-component vector, the coordinates $q_\alpha = p_\alpha$ and $q_\beta = p_\beta$ are in Fourier space (eigenbasis of the P quadrature) and the $q_c = x_c$ coordinate is in "positions" space (eigenbasis of the X quadrature). The only trick here was to choose as the metastability exchange jump operator $C_\beta = \sqrt{\gamma_\beta}\,\mathrm{i}\beta$; this phase choice, which of course does not change the master equation (4.4), remains legitimate for the evolution conditional on the homodyne detection of the field because metastability jumps are not measured. In the mixed representation of the wave function (5.26), the Hamiltonian H is

then pure imaginary and the jump operators are real, hence the real ansatz (5.26). [5]

To obtain the equations of motion on $\underline{\underline{u}}$ and $\bar{\mathbf{q}}$, we calculate the relative variation $\mathrm{d}\phi(\mathbf{q},t)/\phi(\mathbf{q},t)$ of the wave function in two different ways, on the one hand by relating it to the variation $\mathrm{d}S$ of the quantity S in (5.26), separated into a deterministic part $\mathrm{d}S_d$ and a noise part $\mathrm{d}S_b$, and on the other hand by carrying over the ansatz (5.26) into the stochastic equation (5.4). By identifying the deterministic and noisy parts of the two resulting forms, we obtain

$$-\mathrm{d}S_b = \gamma_\beta^{1/2}\left(\frac{1}{2}\partial_{q_\beta}S - q_\beta + \bar{q}_\beta\right)\mathrm{d}\zeta_\beta - \kappa^{1/2}\left(\frac{1}{2}\partial_{q_c}S - q_c + \bar{q}_c\right)\mathrm{d}\zeta_c \tag{5.27}$$

$$\begin{aligned}-\mathrm{d}S_d + \frac{1}{2}(\mathrm{d}S_b)^2 =&(\Omega_\alpha q_\alpha + \Omega_\beta q_\beta)\frac{\mathrm{d}t}{2}\partial_{q_c}S \\ &- \frac{\gamma_\beta \mathrm{d}t}{2}\left\{q_\beta^2 - \frac{1}{2} + \frac{1}{4}\left[\partial_{q_\beta}^2 S - \left(\partial_{q_\beta}S\right)^2\right] + \bar{q}_\beta\left(\partial_{q_\beta}S - 2q_\beta\right) + \bar{q}_\beta^2\right\} \\ &- \frac{\kappa \mathrm{d}t}{2}\left\{q_c^2 - \frac{1}{2} + \frac{1}{4}\left[\partial_{q_c}^2 S - (\partial_{q_c}S)^2\right] + \bar{q}_c\left(\partial_{q_c}S - 2q_c\right) + \bar{q}_c^2\right\}.\end{aligned} \tag{5.28}$$

It remains to transfer the expression of $\mathrm{d}S_b$ from (5.27) into (5.28), applying Ito's rule of replacing the squares of the noises by their mean, and then to identify the terms of degree 2 in $\mathbf{q}-\bar{\mathbf{q}}$ to obtain the purely deterministic linear equation on $\underline{\underline{u}}$: [6]

$$\begin{array}{ll}\mathrm{d}u_{\alpha\alpha} = -\Omega_\alpha \mathrm{d}t\, u_{\alpha c} & \mathrm{d}u_{\alpha\beta} = -\frac{\mathrm{d}t}{2}(\gamma_\beta u_{\alpha\beta} + \Omega_\beta u_{\alpha c} + \Omega_\alpha u_{\beta c}) \\ \mathrm{d}u_{\beta\beta} = -\Omega_\beta \mathrm{d}t\, u_{\beta c} + \gamma_\beta \mathrm{d}t(1-u_{\beta\beta}) & \mathrm{d}u_{\alpha c} = -\frac{\mathrm{d}t}{2}(\kappa u_{\alpha c} + \Omega_\alpha u_{cc}) \\ \mathrm{d}u_{cc} = \kappa \mathrm{d}t(1-u_{cc}) & \mathrm{d}u_{\beta c} = -\frac{\mathrm{d}t}{2}[(\gamma_\beta+\kappa)u_{\beta c} + \Omega_\beta u_{cc}]\end{array} \tag{5.29}$$

and the terms of degree 1 in $\mathbf{q}-\bar{\mathbf{q}}$ to obtain the stochastic linear equation on $\bar{\mathbf{q}}$:

$$\mathrm{d}\bar{\mathbf{q}} = \frac{1}{2}\begin{pmatrix}0 & 0 & 0\\ 0 & -\gamma_\beta & 0\\ \Omega_\alpha & \Omega_\beta & -\kappa\end{pmatrix}\mathrm{d}t\,\bar{\mathbf{q}} + \frac{1}{2}[\mathbb{1} - \underline{\underline{c}}(t)]\begin{pmatrix}0\\ \gamma_\beta^{1/2}\mathrm{d}\zeta_\beta(t)\\ -\kappa^{1/2}\mathrm{d}\zeta_c(t)\end{pmatrix}. \tag{5.30}$$

It is necessary to specify that $\bar{\mathbf{q}}$ is the vector of the quantum means of the variables q in the state vector (5.26)[7]; moreover, the notation $\underline{\underline{c}}$ has been introduced for the inverse matrix of $\underline{\underline{u}}$, which is none other than the quantum covariance matrix of the qs, except for one numerical factor. Thus we have:

$$\begin{gathered}\langle\phi(t)|q_i|\phi(t)\rangle = \bar{q}_i(t) \quad \text{and} \quad \langle\phi(t)|q_iq_j|\phi(t)\rangle = \bar{q}_i(t)\bar{q}_j(t) + \frac{1}{4}c_{ij}(t) \\ \forall i,j \in \{\alpha,\beta,c\} \quad \text{with} \quad \underline{\underline{c}}(t) = [\underline{\underline{u}}(t)]^{-1}.\end{gathered} \tag{5.31}$$

[5] For example, $\mathrm{i}\beta = \mathrm{i}(X_\beta + \mathrm{i}P_\beta)$ is represented in momentum by the real operator $-\partial_{p_\beta}/2 - p_\beta$, and $\beta^\dagger\beta$ by $-\partial_{p_\beta}^2/4 + p_\beta^2 - 1/2$.

[6] Note that the quadratic terms in $\underline{\underline{u}}$ in the second member of (5.28) compensate for those in $(\mathrm{d}S_b)^2/2$ in the first member.

[7] We can therefore recover equation (5.30) from the stochastic equation deduced from (5.4) on the mean of an observable O, $\mathrm{d}\langle O\rangle = (\mathrm{d}t/\mathrm{i}\hbar)\langle[O,H]\rangle + (\mathrm{d}t/2)\sum_m\langle C_m^\dagger[O,C_m] + \mathrm{h.c.}\rangle + \sum_m[\langle OC_m + \mathrm{h.c.}\rangle - \langle C_m + C_m^\dagger\rangle\langle O\rangle]\mathrm{d}\zeta_m$, where $\langle\ldots\rangle$ is taken in state $|\phi(t)\rangle$, by specializing it to cases $O = P_\alpha$, $O = P_\beta$ and $O = X_c$.

The differential system (5.29) integrates easily for the initial condition $\underline{\underline{u}}(0) = \mathbb{1}$:

$$u_{\alpha\alpha}(t) = 1 + \frac{\Omega_\alpha^2 t}{\kappa} - \frac{2\Omega_\alpha^2}{\kappa^2}\left(1 - \mathrm{e}^{-\kappa t/2}\right) \tag{5.32}$$

$$u_{\alpha\beta}(t) = \frac{\Omega_\alpha\Omega_\beta}{\gamma_\beta}\left(\frac{1}{\gamma_\beta+\kappa} + \frac{1}{\kappa}\right)\left(1 - \mathrm{e}^{-\gamma_\beta t/2}\right) + \frac{\Omega_\alpha\Omega_\beta}{\kappa(\kappa-\gamma_\beta)}\left(\mathrm{e}^{-\kappa t/2} - \mathrm{e}^{-\gamma_\beta t/2}\right) + \frac{\Omega_\alpha\Omega_\beta}{\kappa(\gamma_\beta+\kappa)}\left(\mathrm{e}^{-(\gamma_\beta+\kappa)t/2} - \mathrm{e}^{-\gamma_\beta t/2}\right) \tag{5.33}$$

$$u_{\alpha c}(t) = -\frac{\Omega_\alpha}{\kappa}\left(1 - \mathrm{e}^{-\kappa t/2}\right) \tag{5.34}$$

$$u_{\beta\beta}(t) = 1 + \frac{\Omega_\beta^2}{\gamma_\beta(\gamma_\beta+\kappa)}\left(1 - \mathrm{e}^{-\gamma_\beta t}\right) - \frac{2\Omega_\beta^2}{\kappa^2-\gamma_\beta^2}\left(\mathrm{e}^{-\gamma_\beta t} - \mathrm{e}^{-(\gamma_\beta+\kappa)t/2}\right) \tag{5.35}$$

$$u_{\beta c}(t) = -\frac{\Omega_\beta}{\gamma_\beta+\kappa}\left(1 - \mathrm{e}^{-(\gamma_\beta+\kappa)t/2}\right) \tag{5.36}$$

$$u_{cc}(t) = 1. \tag{5.37}$$

It would have been different if we had taken as unknown the covariance matrix $\underline{\underline{c}}(t)$, which obeys a nonlinear Riccati differential system [55]. Since $\bar{\mathbf{q}}$ describes a Brownian motion (partially damped because the friction matrix in (5.30) has eigenvalues 0, $\gamma_\beta/2$ and $\kappa/2$), and since the homodyne signal averaged over the time interval $[0,t]$ σ can be deduced by integration, these random variables have a Gaussian statistic and we can reproduce the reasoning of section 5.2. We find for the conditional mean and variance of the nuclear spin quadrature P_a knowing $\sigma = \mathcal{S}$, this variance determining the metrological gain (3.26) :

$$\langle P_a\rangle_{\sigma=\mathcal{S}} = \frac{\langle\sigma(t)\bar{P}_a(t)\rangle_{\mathrm{stoch}}}{\langle\sigma^2(t)\rangle_{\mathrm{stoch}}}\mathcal{S} \tag{5.38}$$

$$\mathrm{Var}_{\sigma=\mathcal{S}}(P_a) = \frac{1}{4}\left[\frac{\Omega_\beta^2}{\Omega^2}c_{\alpha\alpha}(t) + \frac{\Omega_\alpha^2}{\Omega^2}c_{\beta\beta}(t) - 2\frac{\Omega_\alpha\Omega_\beta}{\Omega^2}c_{\alpha\beta}(t)\right] + \langle\bar{P}_a^2(t)\rangle_{\mathrm{stoch}} - \frac{\langle\sigma(t)\bar{P}_a(t)\rangle^2_{\mathrm{stoch}}}{\langle\sigma^2(t)\rangle_{\mathrm{stoch}}}. \tag{5.39}$$

The bracketed expression in equation (5.39) is the matrix element of $\underline{\underline{c}}(t)$ in the vector $(\Omega_\beta/\Omega, -\Omega_\alpha/\Omega, 0)$ of the coordinates of the direction a in the rotated basis, thus, to within a factor 4, the quantum variance of P_a in the stochastic state $\phi(t)$, time-dependent but, recall, independent of the particular realization of $\phi(t)$. From the chain of equalities

$$\begin{aligned}\langle P_a^2\rangle(t) &= \langle\ \langle\phi(t)|P_a^2|\phi(t)\rangle\ \rangle_{\mathrm{stoch}} \\ &= \langle\ \langle\phi(t)|P_a^2|\phi(t)\rangle - \langle\phi(t)|P_a|\phi(t)\rangle^2 + \langle\phi(t)|P_a|\phi(t)\rangle^2\ \rangle_{\mathrm{stoch}} \\ &= \langle\mathrm{Var}_{\phi(t)}P_a\rangle_{\mathrm{stoch}} + \langle\bar{P}_a^2(t)\rangle_{\mathrm{stoch}}\end{aligned} \tag{5.40}$$

as well as the property (3.35) on the unconditional mean $\langle P_a^2\rangle(t) = 1/4$, we derive the simplified expression

$$\mathrm{Var}_{\sigma=\mathcal{S}}(P_a) = \frac{1}{4} - \frac{\langle\sigma(t)\bar{P}_a(t)\rangle^2_{\mathrm{stoch}}}{\langle\sigma^2(t)\rangle_{\mathrm{stoch}}}. \tag{5.41}$$

It remains, in order to determine the variances and covariances of the random variables $\bar{P}_a(t)$ and $\sigma(t)$, to calculate their amplitudes on the stochastic processes $\mathrm{d}\zeta_\beta(t')$ and $\mathrm{d}\zeta_c(t')$, by formally integrating equation (5.30) by the method of variation of the constant for $\bar{P}_a$ and $\bar{X}_c$, and by proceeding as in equation (5.22) for σ

$$p_\beta(t,t') = -\frac{1}{2}\gamma_\beta^{1/2}\left\{\frac{\Omega_\beta}{\Omega}c_{\alpha\beta}(t') + \frac{\Omega_\alpha}{\Omega}[1-c_{\beta\beta}(t')]\mathrm{e}^{-\gamma_\beta(t-t')/2}\right\} \tag{5.42}$$

$$p_c(t,t') = \frac{1}{2}\kappa^{1/2}\left\{\frac{\Omega_\beta}{\Omega}c_{\alpha c}(t') - \frac{\Omega_\alpha}{\Omega}c_{\beta c}(t')\mathrm{e}^{-\gamma_\beta(t-t')/2}\right\} \tag{5.43}$$

$$\begin{aligned}\sigma_\beta(t,t') =& \frac{(\gamma_\beta\kappa)^{1/2}}{2t}\left\{-c_{\alpha\beta}(t')[t-t'-f_\kappa(t-t')]\frac{\Omega_\alpha}{\kappa} - c_{\beta c}(t')f_\kappa(t-t')\right.\\ &\left.+[1-c_{\beta\beta}(t')][f_{\gamma_\beta}(t-t') - f_\kappa(t-t')]\frac{\Omega_\beta}{\kappa-\gamma_\beta}\right\}\end{aligned} \tag{5.44}$$

$$\begin{aligned}\sigma_c(t,t') =& \frac{1}{2t} - \frac{\kappa}{2t}\left\{-c_{\alpha c}(t')[t-t'-f_\kappa(t-t')]\frac{\Omega_\alpha}{\kappa} + [1-c_{cc}(t')]f_\kappa(t-t')\right.\\ &\left.-c_{\beta c}(t')[f_{\gamma_\beta}(t-t') - f_\kappa(t-t')]\frac{\Omega_\beta}{\kappa-\gamma_\beta}\right\}\end{aligned} \tag{5.45}$$

where $f_\lambda(\tau) \equiv [1-\exp(-\lambda\tau/2)]/(\lambda/2)$. We obtain:

$$\langle\sigma(t)\bar{P}_a(t)\rangle_{\mathrm{stoch}} = \int_0^t \mathrm{d}t'\,[p_\beta(t,t')\sigma_\beta(t,t') + p_c(t,t')\sigma_c(t,t')] \tag{5.46}$$

$$\langle\sigma^2(t)\rangle_{\mathrm{stoch}} = \int_0^t \mathrm{d}t'\,[\sigma_\beta^2(t,t') + \sigma_c^2(t,t')] \tag{5.47}$$

$$\langle\bar{P}_a^2(t)\rangle_{\mathrm{stoch}} = \int_0^t \mathrm{d}t'\,[p_\beta^2(t,t') + p_c^2(t,t')]\,. \tag{5.48}$$

From these results we derive the long-time limits [8]

$$\langle P_a\rangle_{\sigma=\mathcal{S}} \underset{t\to+\infty}{\to} \left(\frac{\gamma_{\mathrm{m}}}{\gamma_{\mathrm{f}}+\gamma_{\mathrm{m}}}\right)^{1/2}\frac{\mathcal{S}}{\Gamma_{\mathrm{ex}}^{1/2}}\,, \quad \mathrm{Var}_{\sigma=\mathcal{S}}(P_a) \underset{t\to+\infty}{\to} \frac{1}{4}\frac{\gamma_{\mathrm{f}}}{\gamma_{\mathrm{f}}+\gamma_{\mathrm{m}}} \tag{5.49}$$

with which the predictions (5.24) and (5.25) of the one-mode model, though obtained in the weak coupling limit (4.2), are in perfect agreement.

In application of our analytical solution of the three-mode model, let us tend the rate Γ_{ex} towards zero at reduced time $\tau = \Gamma_{\mathrm{ex}}t$ fixed by keeping (unlike the one-mode model) the

[8] Let us give some intermediate results and considerations. *(i)* While $c_{\beta\beta}(t')$, $c_{\beta c}(t')$ and $c_{cc}(t')$ have a finite limit when $t'\to+\infty$ [we will need $c_{\beta\beta}(+\infty) = (1+\rho)^{-1}$, $c_{\beta c}(+\infty) = \Omega_\beta/((\gamma_\beta+\kappa)(1+\rho))$ with $\rho = \Omega_\beta^2\kappa/(\gamma_\beta(\gamma_\beta+\kappa)^2)$], $c_{\alpha\alpha}(t')$, $c_{\alpha\beta}(t')$ and $c_{\alpha c}(t')$ tend to zero as $1/t'$. *(ii)* In an integral over t' containing the exponential factor $\exp[-\gamma_\beta(t-t')/2]$ or its square, we can replace the function which multiplies it by its limit in $t'=+\infty$. *(iii)* For any uniformly bounded function $w(t,t')$, we can show for $\nu\in\{\beta,c\}$ that $\int_0^t \mathrm{d}t'[(t-t')c_{\alpha\nu}(t')+w(t,t')]^2/t^2 \to \int_0^{+\infty}\mathrm{d}t' c_{\alpha\nu}^2(t')$. *(iv)* We then obtain the asymptotic limits $\langle P_a^2(t)\rangle_{\mathrm{stoch}} \to (\Omega_\beta/2\Omega)^2\mathcal{I} + (\Omega_\alpha/2\Omega)^2\rho/(1+\rho)$, $\langle\sigma^2(t)\rangle_{\mathrm{stoch}} \to (\Omega_\alpha^2/4\kappa)\mathcal{I}$, $\langle\sigma(t)\bar{P}_a(t)\rangle_{\mathrm{stoch}} \to (\Omega_\alpha\Omega_\beta/4\Omega\kappa^{1/2})\mathcal{I}$ or $\mathcal{I} \equiv \int_0^{+\infty}\mathrm{d}t'[\gamma_\beta c_{\alpha\beta}^2(t') + \kappa c_{\alpha c}^2(t')]$. We thus deduce (5.49) from (5.38) and from the first equality in (5.39), without needing to know the value of $\mathcal{I}$. From the second equality in (5.39) we get the result $\mathcal{I}=1$, which can also be deduced from the equation of motion $\mathrm{d}c_{\alpha\alpha}/\mathrm{d}t = -\gamma_\beta c_{\alpha\beta}^2 - \kappa c_{\alpha c}^2$ embedded between $t=0$ and $t=+\infty$.

rate $\Gamma_{\rm ex}/\gamma_{\rm f}$ at a non-infinitesimal constant value. The physical motivation is clear: in the projected experiments, [9] $\gamma_{\rm f}$ and $\Gamma_{\rm ex}$ are of the same order of magnitude but are really much smaller than $\gamma_{\rm m}$ and κ (by factors $\approx 10^{-6}$ and 10^{-9}). We find in this limit: [10]

$$\boxed{\langle P_a\rangle_{\sigma=\mathcal{S}} \sim \frac{\Gamma_{\rm sq}t}{1+\Gamma_{\rm sq}t}\frac{\mathcal{S}}{\Gamma_{\rm ex}^{1/2}} \quad \text{and} \quad \mathrm{Var}_{\sigma=\mathcal{S}}(P_a) \sim \frac{1}{4}\frac{1}{1+\Gamma_{\rm sq}t}} \tag{5.50}$$

where the nuclear spin squeezing rate has been introduced in the three-mode model and

$$\boxed{\Gamma_{\rm sq} \equiv \left(\frac{1}{\Gamma_{\rm ex}}+\frac{2}{\gamma_{\rm f}}\right)^{-1}.} \tag{5.51}$$

We find the natural scaling of the signal by $\Gamma_{\rm ex}^{1/2}$ already seen in the one-mode model and the same functional forms in time, but we lose any (5.23) type proportionality relation between integrated signal and quadrature average over a realisation, the conditional variance of $\bar{P}_a$ now being $\not\equiv 0$. [11] In Figure 5.2c we show the time dependence $\gamma_{\rm f}t$ of the conditional mean and variance (5.50) for different values of the rate $r = 2\Gamma_{\rm ex}/\gamma_{\rm f}$. It can be seen that the squeezing process is faster the larger r is, and that it saturates at a limit behaviour. This is to be expected, as $\Gamma_{\rm sq}$ is an increasing function of r of finite limit; at fixed time, the conditional mean (in units of $\mathcal{S}/\Gamma_{\rm ex}^{1/2}$) is therefore an increasing function and the conditional variance a decreasing function of r, as can be seen in Figure 5.2c. Specifically, in the weak coupling limit $\Omega \to 0$, where $r \to 0$, the squeezing rate is equivalent to the excitation creation rate $\Gamma_{\rm ex}$, in agreement with the one-mode model, and in the limit $r \to +\infty$, it saturates at the value $\gamma_{\rm f}/2$. Therefore, it is not possible to squeeze faster than at the rate $\gamma_{\rm f}$, which is not surprising: one cannot expect to reduce nuclear spin fluctuations until each atom in the ground state has undergone on average at least one metastability exchange collision, the effective rate $\gamma_{\rm f}$ being in practice of the same order of magnitude as the individual rate $1/T$ in equation (3.21) except in the case of extreme polarization (see figure 3.1a).

5.4 Decoherence effects

For completeness, we take into account, in the homodyne squeezing scheme, the finite lifetime $(2\gamma_0)^{-1}$ of the metastable atoms, which de-excite when they reach the cell walls after a diffusive motion in the gas. To this end, we add a jump operator $\sqrt{2\gamma_0}b$ to the three-mode master equation (3.33). Since the non-Hermitian Hamiltonian part remains quadratic in the quadratures of the modes, it can be put into reduced form by an appropriate rotation of the atomic modes, as we have already done in section 4.2: we need to decompose the vector (a, b) into the orthonormal eigenbase of the rate matrix

$$\underline{\underline{\Gamma}} = \begin{pmatrix} 2\gamma_{\rm f} & -2\sqrt{\gamma_{\rm f}\gamma_{\rm m}} \\ -2\sqrt{\gamma_{\rm f}\gamma_{\rm m}} & 2(\gamma_0+\gamma_{\rm m}) \end{pmatrix} \tag{5.52}$$

[9] See section 5.5 of this chapter for such propositions.

[10] In practice, it is sufficient to make Ω_α tend to zero at fixed $\tau = \Gamma_{\rm ex}t > 0$, Ω_β, γ_β and κ. In particular, this makes all exponential transients in equations (5.32)-(5.37) disappear. To simplify the calculations, it is useful to introduce the quantity $\rho = \Omega^2\kappa/[2\gamma_{\rm m}(\kappa+2\gamma_{\rm m})^2]$ so that $\rho = (\Gamma_{\rm ex}/2\gamma_{\rm f})(1+2\gamma_{\rm m}/\kappa)^{-2}$ in the limit $\gamma_{\rm f} \to 0$.

[11] We have indeed $\mathrm{Var}_{\sigma=\mathcal{S}}(\bar{P}_a) \sim \Gamma_{\rm ex}t/[4(1+\Gamma_{\rm ex}t)] - \Gamma_{\rm sq}t/[4(1+\Gamma_{\rm sq}t)]$.

with operator-valued coefficients α and β. The direction β remains that of the maximum eigenvalue γ_β of $\underline{\underline{\Gamma}}$, and α that of the minimum eigenvalue γ_α, now non-zero

$$\gamma_{\alpha,\beta} = \gamma_\mathrm{m} + \gamma_\mathrm{f} + \gamma_0 \mp [(\gamma_\mathrm{m} + \gamma_\mathrm{f} + \gamma_0)^2 - 4\gamma_\mathrm{f}\gamma_0]^{1/2}. \tag{5.53}$$

In terms of the Faraday momenta Ω_α and Ω_β, the corresponding normalized eigenvectors are written $(\Omega_\beta/\Omega, \Omega_\alpha/\Omega)$ and $(-\Omega_\alpha/\Omega, \Omega_\beta/\Omega)$, so that $\alpha = (\Omega_\beta a + \Omega_\alpha b)/\Omega$ and $\beta = (\Omega_\beta b - \Omega_\alpha a)/\Omega$ with

$$\Omega_\alpha = \frac{\Omega(\gamma_\mathrm{f} - \gamma_\alpha/2)}{[\gamma_\mathrm{m}\gamma_\mathrm{f} + (\gamma_\mathrm{f} - \gamma_\alpha/2)^2]^{1/2}}, \quad \Omega_\beta = \frac{\Omega\sqrt{\gamma_\mathrm{m}\gamma_\mathrm{f}}}{[\gamma_\mathrm{m}\gamma_\mathrm{f} + (\gamma_\mathrm{f} - \gamma_\alpha/2)^2]^{1/2}} \tag{5.54}$$

with a choice of sign ensuring that $\alpha \to a$ and $\beta \to b$ when $\gamma_\mathrm{f} \to 0$ and reproducing (4.5) when $\gamma_0 \to 0$. This leads to the master equation

$$\boxed{\begin{aligned}\frac{\mathrm{d}\rho}{\mathrm{d}t} = {} & \frac{1}{\mathrm{i}\hbar}\left[\hbar(\Omega_\alpha P_\alpha + \Omega_\beta P_\beta)P_c, \rho\right] + \kappa\left(c\rho c^\dagger - \frac{1}{2}\{c^\dagger c, \rho\}\right) \\ & + \gamma_\alpha\left(\alpha\rho\alpha^\dagger - \frac{1}{2}\{\alpha^\dagger\alpha, \rho\}\right) + \gamma_\beta\left(\beta\rho\beta^\dagger - \frac{1}{2}\{\beta^\dagger\beta, \rho\}\right).\end{aligned}} \tag{5.55}$$

Since the jump operator $C_\alpha \propto \alpha$ describes unmeasured processes, we can, as we did for C_β, take it of the form $\sqrt{\gamma_\alpha}\mathrm{i}\alpha$ and reuse the real Gaussian ansatz (5.26).

5.4.1 In the one-mode model

We restrict ourselves here to the physically useful limit $\gamma_0 \ll \gamma_\mathrm{m}$ (we still have $\gamma_\mathrm{f} < \gamma_\mathrm{m}$). At the lowest order in γ_0, the coefficients Ω_α, Ω_β and γ_β remain unchanged, and we have

$$\gamma_\alpha \simeq \frac{2\gamma_0\gamma_\mathrm{f}}{\gamma_\mathrm{m} + \gamma_\mathrm{f}} \tag{5.56}$$

which is nothing else than the decoherence rate brought back into the hybridised nuclear spin. Furthermore, we place ourselves in the one-mode limit (4.2), with $\gamma_\alpha = O(\Gamma_\mathrm{ex})$, which allows us to evaluate the effect of decoherence using the one-mode model, which remains the same as in section 4.2. The stochastic equation (5.7) is completed as follows

$$\begin{aligned}\mathrm{d}|\phi(t)\rangle = {} & -\frac{\Gamma_\mathrm{ex}\mathrm{d}t}{2}(P_\alpha - \bar{P}_\alpha)^2|\phi(t)\rangle + \sqrt{\Gamma_\mathrm{ex}}\mathrm{d}\zeta_s(t)(P_\alpha - \bar{P}_\alpha)|\phi(t)\rangle \\ & - \frac{\gamma_\alpha\mathrm{d}t}{2}(\alpha^\dagger\alpha + 2\mathrm{i}\bar{P}_\alpha\alpha + \bar{P}_\alpha^2)|\phi(t)\rangle + \sqrt{\gamma_\alpha}\mathrm{d}\zeta_\alpha(t)(\mathrm{i}\alpha + \bar{P}_\alpha)|\phi(t)\rangle.\end{aligned} \tag{5.57}$$

The choice of $\gamma_\alpha^{1/2}\mathrm{i}\alpha$ as the jump operator for the reduced decoherence allows the equation to be solved by the same real Gaussian ansatz (5.8). This time we find[12]

$$\mathrm{d}u = [\Gamma_{\rm ex} + \gamma_\alpha(1-u)]\mathrm{d}t \quad \Longrightarrow \quad u(\tau) = 1 + \frac{1-\exp(-\epsilon\tau)}{\epsilon} \tag{5.58}$$

$$\mathrm{d}\bar{P}_\alpha = -\frac{1}{2}\gamma_\alpha \bar{P}_\alpha \mathrm{d}t + \frac{\sqrt{\Gamma_{\rm ex}}\mathrm{d}\zeta_s + \sqrt{\gamma_\alpha}(u-1)\mathrm{d}\zeta_\alpha}{2u} \tag{5.59}$$

where we have posed $\tau = \Gamma_{\rm ex}t$ and $\epsilon = \gamma_\alpha/\Gamma_{\rm ex}$. The same Gaussianity arguments as in section 5.2 lead to the same dependencies in the signal $\mathcal{S}$ of the conditional mean and variance,[13]

$$\langle P_\alpha\rangle_{\sigma=\mathcal{S}} = m(\tau)\frac{\mathcal{S}}{\sqrt{\Gamma_{\rm ex}}}, \qquad \mathrm{Var}_{\sigma=\mathcal{S}}(P_\alpha) = \mathcal{V}(\tau) \tag{5.60}$$

$$\text{with} \quad m(\tau) = \sqrt{\Gamma_{\rm ex}}\frac{\langle\sigma(t)\bar{P}_\alpha(t)\rangle_{\rm stoch}}{\langle\sigma^2(t)\rangle_{\rm stoch}} \quad \text{and} \quad \mathcal{V}(\tau) = \frac{1}{4} - \frac{\langle\sigma(t)\bar{P}_\alpha(t)\rangle^2_{\rm stoch}}{\langle\sigma^2(t)\rangle_{\rm stoch}}$$

and the variance and covariance taken over the stochastic processes $\mathrm{d}\zeta_s \equiv \mathrm{d}\zeta_c$ and $\mathrm{d}\zeta_\alpha$,

$$\begin{aligned}\frac{\langle\sigma^2\rangle_{\rm stoch}}{\Gamma_{\rm ex}} &= \int_0^\tau \frac{\mathrm{d}\tau'}{\tau^2}\left\{\left[\frac{1}{2} + \frac{1-\mathrm{e}^{\epsilon(\tau'-\tau)/2}}{\epsilon u(\tau')}\right]^2 + \frac{[u(\tau')-1]^2}{u^2(\tau')}\frac{\left[1-\mathrm{e}^{\epsilon(\tau'-\tau)/2}\right]^2}{\epsilon}\right\} \qquad (5.61)\\ &= \frac{\epsilon\tau - 2(1-\mathrm{e}^{-\epsilon\tau/2})}{\epsilon^2\tau^2} + \frac{1}{4\tau}\\ \frac{\langle\sigma\bar{P}_\alpha\rangle_{\rm stoch}}{\sqrt{\Gamma_{\rm ex}}} &= \int_0^\tau \frac{\mathrm{d}\tau'}{\tau}\frac{\mathrm{e}^{\epsilon(\tau'-\tau)/2}}{2u(\tau')}\left\{\frac{1}{2} + \frac{1-\mathrm{e}^{\epsilon(\tau'-\tau)/2}}{\epsilon u(\tau')} + \frac{[u(\tau')-1]^2}{u(\tau')}\left[1-\mathrm{e}^{\epsilon(\tau'-\tau)/2}\right]\right\} \qquad (5.62)\\ &= \frac{1-\mathrm{e}^{-\epsilon\tau/2}}{2\epsilon\tau}.\end{aligned}$$

These expressions allow the effect of decoherence on spin squeezing to be easily evaluated through the metrological gain (3.26), see the dashed lines in figure 5.2a. For the practically useful case of a low decoherence $\epsilon \ll 1$ and a short time before $1/\gamma_\alpha$, they can be expanded to first order in ϵ :

$$\boxed{m(\tau) = \frac{\tau}{1+\tau} - \epsilon\frac{(\tau+3)\tau^2}{12(\tau+1)^2} + O(\epsilon^2\tau^2) \quad ; \quad \mathcal{V}(\tau) = \frac{1}{4(\tau+1)} + \epsilon\frac{(\tau+3/2)\tau^2}{12(\tau+1)^2} + O(\epsilon^2\tau^2)\,.} \tag{5.63}$$

From this we deduce that the optimal squeezing on P_α is obtained at a time $t_{\rm opt} \sim (3/\Gamma_{\rm ex}\gamma_\alpha)^{1/2}$ and corresponds to a conditional variance $\mathcal{V}_{\rm opt} \sim (\gamma_\alpha/12\Gamma_{\rm ex})^{1/2}$. Note that in studies of spin

[12] In the regime $\epsilon \ll 1$, the long-time limit of the variance of P_α on a single realisation depends strongly on the choice of phase in the jump operator of the reduced decoherence, which underlines the non-physical character of this variance (see section 5.1): if we take $\gamma_\alpha^{1/2}\alpha$ as the jump operator, we find $\mathrm{Var}_\phi P_\alpha \to \epsilon^{1/2}/4$ instead of $\mathrm{Var}_\phi P_\alpha \to 1/4\epsilon$ as in equation (5.58). More generally, the choice $\gamma_\alpha^{1/2}\exp(\mathrm{i}\theta)\,\alpha$, $-\pi/2 < \theta < \pi/2$, leads to the Riccati equation on parameter u of the (now complex) Gaussian ansatz $\mathrm{d}u = \Gamma_{\rm ex}\mathrm{d}t + \gamma_\alpha\mathrm{d}t\{\exp(2\mathrm{i}\theta)u + [1-\exp(2\mathrm{i}\theta)]/2 - u^2[1+\exp(2\mathrm{i}\theta)]/2\}$ so that $\mathrm{Var}_\phi P_\alpha \to (1/4)\epsilon^{1/2}\sqrt{\cos\theta}\cos(\theta/2)$ in a time $\tau \sim 1/\sqrt{2\epsilon[1+\exp(2\mathrm{i}\theta)]}$; the power law in ϵ obtained for $\theta = 0$ is thus the rule, the one obtained for $\theta = \pi/2$ is the exception.

[13] We have simplified the expression of $\mathcal{V}(\tau)$ in (5.60) using the identity $[4u(\tau)]^{-1} + \langle\bar{P}_\alpha^2\rangle_{\rm stoch} = 1/4$, which results as in equation (5.40) from the fact that the unconditional mean $\langle P_\alpha^2\rangle = 1/4$, even in the presence of decoherence.

squeezing in cavity alkali gases, the C cooperativity of the coupled atom-field system is often introduced, defined as the square of the coupling pulsation divided by the decay rates of the coupled states [56]. In this sense, the cooperativity of the nuclear spin-hybridized field system is

$$C \equiv \frac{\Omega_\alpha^2}{\kappa\gamma_\alpha} = \frac{\Gamma_{\rm ex}}{\gamma_\alpha} \simeq \frac{\Omega^2}{2\gamma_0\kappa} \tag{5.64}$$

so that we find the usual alkali scaling law of exponent $-1/2$ relating the optimal spin variance to C [56]. More generally, decoherence has a weak effect on the nuclear spin squeezing as long as we stay at short times in front of $t_{\rm opt}$.

5.4.2 In the three-mode model

The reuse of the real Gaussian ansatz (5.26) in order to solve the stochastic equation (5.4) on the state vector in full generality allows an extension of these scaling laws beyond the one-mode model, i.e. for any non-infinitesimal $\Gamma_{\rm ex}/\gamma_{\rm f}$ rate. As we shall see, the link between $\mathcal{V}_{\rm opt}$ and (5.64) cooperativity is then broken.

In the evolution equation of the matrix $\underline{\underline{u}}$ appearing in the ansatz, the indices α and β now play symmetrical roles and we obtain

$$\begin{array}{ll}
{\rm d}u_{\alpha\alpha} = -\Omega_\alpha {\rm d}t\, u_{\alpha c} + \gamma_\alpha {\rm d}t(1-u_{\alpha\alpha}) & {\rm d}u_{\alpha\beta} = -\frac{{\rm d}t}{2}[(\gamma_\alpha+\gamma_\beta)u_{\alpha\beta} + \Omega_\beta u_{\alpha c} + \Omega_\alpha u_{\beta c}] \\
{\rm d}u_{\beta\beta} = -\Omega_\beta {\rm d}t\, u_{\beta c} + \gamma_\beta {\rm d}t(1-u_{\beta\beta}) & {\rm d}u_{\alpha c} = -\frac{{\rm d}t}{2}[(\gamma_\alpha+\kappa)u_{\alpha c} + \Omega_\alpha u_{cc}] \\
{\rm d}u_{cc} = \kappa {\rm d}t(1-u_{cc}) & {\rm d}u_{\beta c} = -\frac{{\rm d}t}{2}[(\gamma_\beta+\kappa)u_{\beta c} + \Omega_\beta u_{cc}]
\end{array} \tag{5.65}$$

whose solution for the initial condition $\underline{\underline{u}}(0) = \mathbb{1}$ is written

$$u_{\alpha\alpha}(t) = 1 + \frac{\Omega_\alpha^2}{\gamma_\alpha(\kappa+\gamma_\alpha)}\left(1-{\rm e}^{-\gamma_\alpha t}\right) - \frac{2\Omega_\alpha^2}{\kappa^2-\gamma_\alpha^2}\left({\rm e}^{-\gamma_\alpha t} - {\rm e}^{-(\kappa+\gamma_\alpha)t/2}\right) \tag{5.66}$$

$$\begin{aligned}
u_{\alpha\beta}(t) =& \frac{\Omega_\alpha\Omega_\beta}{\gamma_\alpha+\gamma_\beta}\left(\frac{1}{\kappa+\gamma_\alpha}+\frac{1}{\kappa+\gamma_\beta}\right)\left(1-{\rm e}^{-(\gamma_\alpha+\gamma_\beta)t/2}\right) \\
&+ \frac{\Omega_\alpha\Omega_\beta}{(\kappa-\gamma_\beta)(\kappa+\gamma_\alpha)}\left({\rm e}^{-(\kappa+\gamma_\alpha)t/2} - {\rm e}^{-(\gamma_\alpha+\gamma_\beta)t/2}\right) \\
&+ \frac{\Omega_\alpha\Omega_\beta}{(\kappa-\gamma_\alpha)(\kappa+\gamma_\beta)}\left({\rm e}^{-(\kappa+\gamma_\beta)t/2} - {\rm e}^{-(\gamma_\alpha+\gamma_\beta)t/2}\right)
\end{aligned} \tag{5.67}$$

$$u_{\alpha c}(t) = -\frac{\Omega_\alpha}{\kappa+\gamma_\alpha}\left(1-{\rm e}^{-(\kappa+\gamma_\alpha)t/2}\right) \tag{5.68}$$

$$u_{\beta\beta}(t) = 1 + \frac{\Omega_\beta^2}{\gamma_\beta(\kappa+\gamma_\beta)}\left(1-{\rm e}^{-\gamma_\beta t}\right) - \frac{2\Omega_\beta^2}{\kappa^2-\gamma_\beta^2}\left({\rm e}^{-\gamma_\beta t} - {\rm e}^{-(\kappa+\gamma_\beta)t/2}\right) \tag{5.69}$$

$$u_{\beta c}(t) = -\frac{\Omega_\beta}{\kappa+\gamma_\beta}\left(1-{\rm e}^{-(\kappa+\gamma_\beta)t/2}\right) \tag{5.70}$$

$$u_{cc}(t) = 1\,. \tag{5.71}$$

The vector of mean coordinates $\bar{\mathbf{q}}$ appearing in the ansatz (5.26) obeys the stochastic equation

$${\rm d}\bar{\mathbf{q}} = \frac{1}{2}\begin{pmatrix} -\gamma_\alpha & 0 & 0 \\ 0 & -\gamma_\beta & 0 \\ \Omega_\alpha & \Omega_\beta & -\kappa \end{pmatrix} {\rm d}t\, \bar{\mathbf{q}} + \frac{1}{2}[\mathbb{1} - \underline{\underline{c}}(t)] \begin{pmatrix} \gamma_\alpha^{1/2}{\rm d}\zeta_\alpha(t) \\ \gamma_\beta^{1/2}{\rm d}\zeta_\beta(t) \\ -\kappa^{1/2}{\rm d}\zeta_c(t) \end{pmatrix}. \tag{5.72}$$

The unconditional mean $\langle P_a^2 \rangle$ always being 1/4, the mean and variance of P_a conditional on the integrated homodyne signal remain given by equations (5.38) and (5.39), by generalising expressions (5.46)-(5.48) of the variances and covariance of random variables $\bar{P}_a(t)$ and $\sigma(t)$ to the case of three independent stochastic processes $\mathrm{d}\zeta_\alpha(t')$, $\mathrm{d}\zeta_\beta(t')$ and $\mathrm{d}\zeta_c(t')$ as follows:

$$\langle \sigma(t)\bar{P}_a(t)\rangle_{\mathrm{stoch}} = \int_0^t \mathrm{d}t' \sum_{\nu\in\{\alpha,\beta,c\}} p_\nu(t,t')\sigma_\nu(t,t') \tag{5.73}$$

$$\langle \sigma^2(t)\rangle_{\mathrm{stoch}} = \int_0^t \mathrm{d}t' \sum_{\nu\in\{\alpha,\beta,c\}} \sigma_\nu^2(t,t') \tag{5.74}$$

$$\langle \bar{P}_a^2(t)\rangle_{\mathrm{stoch}} = \int_0^t \mathrm{d}t' \sum_{\nu\in\{\alpha,\beta,c\}} p_\nu^2(t,t') \tag{5.75}$$

with the compact expressions of the corresponding amplitudes

$$p_\nu(t,t') = (-1)^{\delta_{\nu c}} \frac{\sqrt{\gamma_\nu}}{2\Omega} \left\{ \Omega_\beta \mathrm{e}^{-\gamma_\alpha(t-t')/2}[\delta_{\alpha\nu} - c_{\alpha\nu}(t')] - \Omega_\alpha \mathrm{e}^{-\gamma_\beta(t-t')/2}[\delta_{\beta\nu} - c_{\beta\nu}(t')] \right\} \tag{5.76}$$

$$\sigma_\nu(t,t') = \frac{\delta_{\nu c}}{2t} + (-1)^{\delta_{\nu c}} \frac{\sqrt{\kappa\gamma_\nu}}{2t} \left\{ [\delta_{c\nu} - c_{c\nu}(t')] f_\kappa(t-t') \right. \tag{5.77}$$

$$\left. + \sum_{\mu\in\{\alpha,\beta\}} \frac{\Omega_\mu}{\kappa - \gamma_\mu} [\delta_{\mu\nu} - c_{\mu\nu}(t')][f_{\gamma_\mu}(t-t') - f_\kappa(t-t')] \right\}.$$

The index ν runs over the three values α, β, c and $\gamma_c = \kappa$ is posited. The function δ is the Kronecker function, and the function f_λ is the same as in equations (5.42)-(5.45).

The general solution we have just outlined has the five rates $\gamma_\alpha, \Gamma_{\mathrm{ex}} = \Omega_\alpha^2/\kappa, \gamma_{\mathrm{f}}$ on the one hand, γ_β, κ on the other. The experimentally relevant regime is the one where the last two are "infinitely" larger than the first three and contribute only through unobservable transient regimes. Mathematically, this limit is reached by making γ_{f} tend towards zero at fixed $\kappa, \gamma_{\mathrm{m}}, \gamma_0$ and Ω and at fixed $\tau = \Gamma_{\mathrm{ex}} t > 0$. Then the first three rates tend jointly to zero, i.e. in finite and non-zero limit rates $\Gamma_{\mathrm{ex}}/\gamma_{\mathrm{f}} \to \Omega^2\gamma_{\mathrm{m}}/[\kappa(\gamma_0+\gamma_{\mathrm{m}})^2]$ and $\gamma_\alpha/\gamma_{\mathrm{f}} \to 2\gamma_0/(\gamma_0+\gamma_{\mathrm{m}})$, the γ_β rate reduces to $\gamma \equiv 2(\gamma_0+\gamma_{\mathrm{m}})$ and the Faraday coupling Ω_β to Ω. All exponential transients disappear in the (5.66)-(5.70) matrix elements of $\underline{\underline{u}}$ except those relaxing at the

γ_α rate. The amplitudes (5.76) and (5.77) on the stochastic processes reduce to

$$\frac{p_\alpha(t,t')}{\sqrt{\Gamma_{\rm ex}}} = \frac{u(\tau')-1}{2u(\tau')}\sqrt{\epsilon}\,\mathrm{e}^{-\epsilon(\tau-\tau')/2} \tag{5.78}$$

$$\frac{p_\beta(t,t')}{\sqrt{\Gamma_{\rm ex}}} = \frac{\sqrt{\rho}}{(1+\rho)u(\tau')}\mathrm{e}^{-\epsilon(\tau-\tau')/2} \tag{5.79}$$

$$\frac{p_c(t,t')}{\sqrt{\Gamma_{\rm ex}}} = \frac{(1-\rho)}{2(1+\rho)u(\tau')}\mathrm{e}^{-\epsilon(\tau-\tau')/2} \tag{5.80}$$

$$\frac{\sigma_\alpha(t,t')}{\Gamma_{\rm ex}} = \frac{u(\tau')-1}{\tau\,u(\tau')}\sqrt{\epsilon}\,\frac{1-\mathrm{e}^{-\epsilon(\tau-\tau')/2}}{\epsilon} \tag{5.81}$$

$$\frac{\sigma_\beta(t,t')}{\Gamma_{\rm ex}} = \frac{\sqrt{\rho}}{(1+\rho)\tau}\left[\frac{2}{u(\tau')}\frac{1-\mathrm{e}^{-\epsilon(\tau-\tau')/2}}{\epsilon}+\rho+\frac{\gamma}{\kappa}(\rho-1)\right] \tag{5.82}$$

$$\frac{\sigma_c(t,t')}{\Gamma_{\rm ex}} = \frac{1}{\tau}\left[\frac{1}{2}+\frac{1-\rho}{1+\rho}\frac{1}{u(\tau')}\frac{1-\mathrm{e}^{-\epsilon(\tau-\tau')/2}}{\epsilon}+\frac{\rho}{1+\rho}\left(1+\frac{2\gamma}{\kappa}\right)\right] \tag{5.83}$$

where $\epsilon = \gamma_\alpha/\Gamma_{\rm ex}$ as in section 5.4, the function $u(\tau)$ is given by equation (5.58) and the notation $\rho = \Omega^2\kappa/[\gamma(\kappa+\gamma)^2]$ generalises that in note 10. Relations (5.38) and (5.39) remain valid, with the new expressions for the variance and covariance

$$\boxed{\frac{\langle\sigma^2\rangle_{\rm stoch}}{\Gamma_{\rm ex}} = \frac{\epsilon\tau-2(1-\mathrm{e}^{-\epsilon\tau/2})}{\epsilon^2\tau^2}+\frac{\Gamma_{\rm ex}}{4\tau\Gamma_{\rm sq}^{\rm gen}} \qquad \text{and} \qquad \frac{\langle\sigma\bar{P}_a\rangle_{\rm stoch}}{\sqrt{\Gamma_{\rm ex}}} = \frac{1-\mathrm{e}^{-\epsilon\tau/2}}{2\epsilon\tau}} \tag{5.84}$$

and the generalized squeezing rate

$$\boxed{\Gamma_{\rm sq}^{\rm gen} = \left[\frac{1}{\Gamma_{\rm ex}}+\frac{2(\gamma_0+\gamma_{\rm m})}{\gamma_{\rm f}\gamma_{\rm m}}\right]^{-1}} \tag{5.85}$$

reproducing the variance and covariance (5.61) and (5.62) of the one-mode model with decoherence when $\Gamma_{\rm ex}/\gamma_{\rm f}\to 0$ and the spin squeezing rate (5.51) of the three-mode model without decoherence when $\gamma_0\to 0$. The new results can be simplified in the useful low-decoherence limit $\gamma_\alpha/\Gamma_{\rm ex}\to 0$ by an expansion to order one in ϵ, which allows the results (5.63) on the conditional mean and variance to be generalised to a non-infinitesimal value of $\Gamma_{\rm ex}/\gamma_{\rm f}$ as follows:

$$m(t) = \frac{\Gamma_{\rm sq}^{\rm gen}t}{1+\Gamma_{\rm sq}^{\rm gen}t}-\frac{\gamma_\alpha}{\Gamma_{\rm sq}^{\rm gen}}\frac{(3+\Gamma_{\rm sq}^{\rm gen}t)(\Gamma_{\rm sq}^{\rm gen}t)^2}{12(1+\Gamma_{\rm sq}^{\rm gen}t)^2}+O[(\gamma_\alpha t)^2] \tag{5.86}$$

$$\mathcal{V}(t) = \frac{1}{4(1+\Gamma_{\rm sq}^{\rm gen}t)}+\frac{\gamma_\alpha}{\Gamma_{\rm sq}^{\rm gen}}\frac{(\Gamma_{\rm sq}^{\rm gen}t+3/2)(\Gamma_{\rm sq}^{\rm gen}t)^2}{12(1+\Gamma_{\rm sq}^{\rm gen}t)^2}+O[(\gamma_\alpha t)^2]. \tag{5.87}$$

This generalisation is simply a matter of replacing τ by $\Gamma_{\rm sq}^{\rm gen}t$ and ϵ by $\gamma_\alpha/\Gamma_{\rm sq}^{\rm gen}$ in the second members of (5.63). [14] The optimal squeezing on P_a is then obtained after a time $t_{\rm opt}\sim(3/\Gamma_{\rm sq}^{\rm gen}\gamma_\alpha)^{1/2}$ and corresponds to a conditional variance

$$\mathrm{Var}^{\rm opt}_{\sigma=\mathcal{S}}(P_a)\sim(\gamma_\alpha/12\Gamma_{\rm sq}^{\rm gen})^{1/2}. \tag{5.88}$$

[14] It is in fact valid at all orders in ϵ since the proposed replacement does not change $\epsilon\tau$ (still equal to $\gamma_\alpha t$) and moves from equations (5.61) and (5.62) to equation (5.84).

The optimal metrological gain is deduced from this by equation (3.26)

$$\boxed{\xi^2_{\mathrm{opt},\sigma=\mathcal{S}} \sim \frac{2}{\eta}\sqrt{\frac{\gamma_\alpha}{3}}\left[\frac{1}{\Gamma_{\mathrm{ex}}}+\frac{2(\gamma_0+\gamma_{\mathrm{m}})}{\gamma_{\mathrm{f}}\gamma_{\mathrm{m}}}\right]^{-1/2}.} \tag{5.89}$$

5.5 On the parameters of an experimental realisation

In this section we make some estimates of the model parameters for the prospect of an experimental realisation of the scheme. In the theoretical treatment throughout this chapter we have assumed the magnetic field to be zero, the effects of a small steering field will be discussed at the end of this section.

Recall of the proposed experimental scheme An overview of the set-up is shown in Figure 1.1. This setup consists of a helium-3 vapour cell at room temperature and a pressure of a few mbar placed inside an asymmetric optical cavity, ensuring that the photons leave the cavity predominantly through the output mirror. The experimental process can be schematically separated into four steps:
- A continuous discharge maintains a small fraction of the atoms in a metastable state while the majority of the ensemble remains in the ground-state (of purely nuclear spin).
- The collective atomic spins of the metastable and ground-state population are oriented in the Ox direction by optical pumping. Metastability exchange collisions then couple the ground-state and metastable spins so that quantum correlations are continuously transferred from one to the other.
- The input light is linearly polarized in the Ox direction; it passes through the cavity in the Oz direction and approaches the $2^3S_1 - 2^3P_0$ transition at C_8 at 1083 nm. For a large detuning and in the weak saturation limit, the 2^3P_0 excited state can be eliminated adiabatically, giving rise to the Faraday interaction Hamiltonian (3.2) [14]. During its propagation in the gas, the Oy polarised cavity field mode, initially empty, populates by the Faraday effect under the action of the quantum fluctuations of the spin of the Oz metastables.
- At the exit of the cavity, this Oy-polarised mode is measured continuously. This measurement combined with the exchange collisions provides a quantum nondemolition measurement of the nuclear spin.
We have considered two different quantum nondemolition measurements: by photon counting 1.1b or by a homodyne measurement 1.1c.

In this section, it is the case of homodyne detection that will be considered. Recall that in this work, we have assumed that the spatial inhomogeneities of the cavity mode are averaged during the motion of the atoms, which effectively couples the light homogeneously to all the atoms in the cell. Indeed, the squeezing time scale $1/\Gamma_{\mathrm{sq}}$ is long compared to the time scale $1/\gamma_0^{\mathrm{wall}}$ for atomic motion between the cell walls, $\gamma_0^{\mathrm{wall}}/\Gamma_{\mathrm{sq}} \sim 10^4$. The atomic motion therefore averages the spatial variations of the cavity mode, which ensures the validity of a description by collective interactions.

5.5.1 Numerical estimates of parameters and variables.

In this section we discuss the values of the model parameters that an experiment based on the homodyne scheme could take. The objective of a squeezed spin state can be achieved, a state which also demonstrates a metrological gain over a fully polarised state in the standard quantum limit for use in magnetometry for example. We will take the opportunity to discuss

the dependence of the parameters and results on nuclear polarisation (necessarily partial in our case). This will lead us to mention a possible alternative scheme, which was not studied during this thesis, but which represents a possible direction towards which the project can evolve.

Cell and cavity We consider a cylindrical cell of 20 mm length and 5 mm diameter, filled with $N_{\text{cell}} = 2.5 \times 10^{16}$ atoms of ^{3}He at a pressure of $p = 2$ Torr. The cell is at room temperature. It is placed inside an optical cavity to amplify the atom-light interaction [57]. For a finess of $\mathcal{F} = 50$ and a cavity length of 3 cm, we obtain $\kappa = 2\pi\, 1.0 \times 10^8$ Hz as the cavity output rate. The cavity is laser driven on the Ox axis polarisation so that 5 mW of the light exits the cavity in this polarisation, and we take the light to be $\Delta = 2\pi\, 2.0$ GHz detuned from the C_8 transition. In the steady state, we find that 6.5×10^5 s^{-1} photons Oy polarized leave the cavity (3.39). [15]

Atoms and light The discharge in the gas keeps $n_{\text{cell}} = 1.25 \times 10^{11}$ atoms stationary in the metastable state, in a rate $\frac{n_{\text{cell}}}{N_{\text{cell}}} = 5 \times 10^{-6}$. For a polarisation of $\eta = 0.4$, this gives an effective number of atoms (3.17) in the ground state of $N = 1.0{\times}10^{16}$ and $n = 1.3{\times}10^{10}$ in the metastable state. For the coupling between the light and the metastable population (3.25), we thus obtain $\Omega = 2\pi\, 4.15 \times 10^6$ Hz. From the metastability exchange rate coefficient (see table II p.19 of reference [1]), the effective metastability exchange rates $\gamma_{\text{m}} = 5.2 \times 10^6$ s^{-1} and $\gamma_{\text{f}} = 6.9$ s^{-1} are determined via (3.21). From the diffusion coefficient of the metastable atoms [58], we estimate that the metastable relaxation rate due to collisions with the wall is $\gamma_0^{\text{wall}} = 2.6 \times 10^4$ s^{-1} [59].[16]

Squeezing rate, decoherence rate and fundamental limit to the scheme The nuclear spin squeezing rate is evaluated from equation (5.85), the result of the analysis of the three-mode model with decoherence: $\boxed{\Gamma_{\text{sq}} = 1.0\ \text{s}^{-1}}$. We established at the very end of section 5.2 that the continuous homodyne scheme has an intrinsic limit to the final nuclear spin variance that can be obtained. According to (5.88), the highest squeezing that can be obtained would be $\boxed{-6.71\ \text{dB}}$. We can also calculate the metrological gain that this state allows if it is used within a magnetometer via equation (5.89): $\boxed{\xi^2 = 0.53}$. Here we can see the strong constraint imposed by the only partial polarisation of the atoms, since in the case of full polarisation the metrological gain would be $\eta\xi^2 = 0.21$.

Choice of nuclear polarization As a reminder, we are constrained to $\eta \neq 1$ as soon as we take the $F = 1/2$ component (hence the $\vec{K}$ spin) of the metastable spin as an intermediate in the scheme. Indeed, if we completely polarize the metastable population, then all the atoms are in the $|F = 3/2, M_F = +3/2\rangle$ state of the $F = 3/2$ multiplicity and none in a state of the $F = 1/2$ multiplicity inducing a zero $\vec{K}$ spin. In our case, we have to make a choice about the polarisation that will determine the theoretical and optimal results that the scheme can obtain. In figure 5.3 we show, as a function of the nuclear polarisation η, (a) the

[15] Recall that $\langle X_c^2\rangle(t) - 1/4 = \langle c^\dagger c\rangle(t)$ in the case of an empty initial state.

[16] Well above the non-resonant photon scattering rate in the metastable state, averaged over the cell, which we estimate at $\gamma_0^{\text{scat}} \approx 2.4 \times 10^3$ s^{-1}. Recall that the decoherence rate in the three-mode theory of section 5.4 is defined with a factor of 2: $\gamma_0 = \gamma_0^{\text{wall}}/2$.

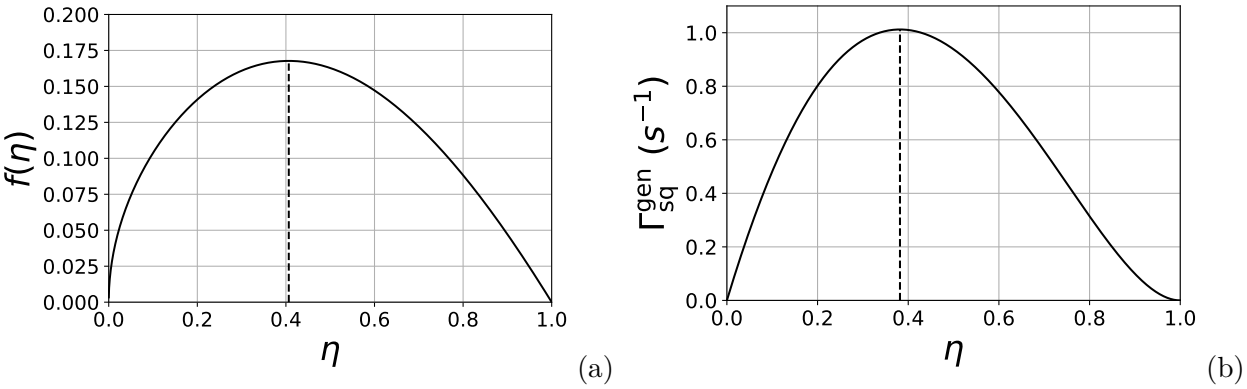

Figure 5.3: Dependence of the typical coupling and rate of the system on the nuclear polarisation η. The parameters are those of the section 5.5.1. The vertical dashed lines indicate the maxima. (a) Nuclear polarisation dependence of the Faraday pulsation $\Omega_\alpha = \chi\sqrt{n_{ph}n_{cell}}\sqrt{\frac{n_{\text{cell}}}{N_{\text{cell}}}}f(\eta)$. Similar to figure 3.1b, it differs by using the results of the three-mode model in the presence of decoherence in the metastable presented in section 5.4, equations (5.54). The maximum $f(\eta) = 0.168$ is found at $\eta = 0.406$. (b) Generalized squeezing ratio (5.85) as a function of polarization. The minimum $\Gamma_{\text{sq}}^{\text{gen}} = 1.01\ \text{s}^{-1}$ is found at $\eta = 0.382$.

dependence on this variable of the Faraday pulsation Ω_α for the hybridised nuclear bosonic mode,[17] and (b) the generalised nuclear spin squeezing rate. Note that the maximum of the effective coupling corresponds to that of the squeezing rate, both maxima being around a nuclear polarisation $\eta \simeq 0.4$. While in figure 5.4, we show in (a) the optimal nuclear spin squeezing with respect to the standard quantum limit in dB, and in (b) the metrological gain of the nuclear spin state for use as a magnetometer as defined by reference [25]. Comparing Figure 5.3(a) and 5.4(b), it can be seen that the maximum of the effective coupling (and hence the squeezing rate) does not correspond to the minima of squeezing and metrological gain, contrary to what one might expect.[18] This is because the standard quantum limit is proportional to the size of the spin, and hence the polarisation. Thus, there is a trade-off between the squeezing rate Γ_{sq} on the one hand and the spin squeezing or metrological gain on the other. The figures show that one can choose a polarisation of 0.4 to obtain a squeezing rate of around $\Gamma_{\text{sq}}^{\text{gen}} \simeq 1\ \text{s}^{-1}$ and an optimum metrological gain of $\xi^2 \simeq 0.5$ (this is what we have just presented) or one can prefer to maximise the optimum metrological gain with a polarisation of 0.8 to obtain a gain of $\xi^2 \simeq 0.3$ but slow down the squeezing with a rate of $\Gamma_{\text{sq}}^{\text{gen}} \simeq 0.3\ \text{s}^{-1}$.

[17] Unlike figure 3.1b, we take here the factor $f_\alpha(\eta)$ as it appears in the three-mode model with decoherence, constructed from equation (5.54)

[18] Since increasing the effective coupling Ω ensures that the spin is squeezed more strongly and more quickly. Indeed, the Faraday pulsation Ω_α depends linearly on Ω (5.54), the excitation rate in the nuclear mode Γ_{ex} depends quadratically on this pulsation (4.13), the squeezing rate of the nuclear spin Γ_{sq} depends linearly on this excitation rate (5.85) and finally, the optimal conditional variance depends on the squeezing rate at a power $-1/2$ (5.88).

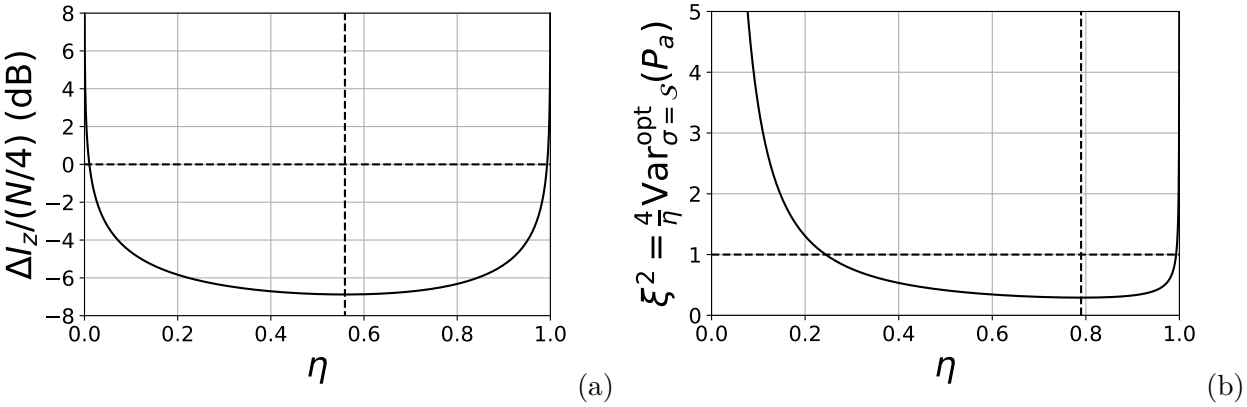

(a) (b)

Figure 5.4: Dependence of the metrological gain and the optimal spin squeezing on the nuclear polarisation η. The parameters are those of the section 5.5.1. The vertical dashed lines indicate the minima. The horizontal dashed lines indicate the standard quantum limit of a fully polarised state. (a) Optimal spin squeezing (5.88) with respect to the standard quantum limit of a fully polarised nuclear spin state. The minimum $\mathrm{Var}^{rmopt}_{sigma=athcalS}(P_a)/(N/4) = -6.880$ dB is found at $\eta = 0.559$. (b) Metrological gain ξ^2 for using the minimum variance state (5.88) as a magnetometer [25]. The minimum $\xi^2 = 0.291$ is found at $\eta = 0.790$.

Some words for an alternative to the scheme studied In order to take advantage of full polarisation, one idea would be to couple the light to the $F = 3/2$ multiplicity, and thus to the $\vec{J}$ spin. This possibility would have the distinct advantage that any additional degree of polarisation leads to a stronger and faster squeezing. But this solution also brings its own difficulties: as soon as the light couples with $\vec{J}$, it is no longer possible to discard the influence of the alignment tensor in the dynamics as we have done. The structure of the equations is then fundamentally different from the one studied in this section. However, there is an alternative way to proceed from this idea. It consists in choosing the cavity detuning so as to recover a Faraday-type Hamiltonian $H = \chi S_z J_z$ on spin $\vec{J}$, while keeping the components of the tensor $\vec{\vec{Q}}$ and the spin $\vec{K}$ subdominant, so that their fluctuations can be eliminated or neglected and the three-spin model of chapter 3 can be recovered.

5.5.2 Notes on the magnetic field in a cavity

In this section we return to the question of the magnetic field, imposed or residual, in a cavity, which has been neglected until now.

A residual magnetic field If during the squeezing phase there is a small static parasitic magnetic field (in addition to the director field) in the yOz plane, of angle ϕ with Oy, this field rotates at the $-\omega_{\mathrm{L}}^{(x)}$ pulsation in the rotating frame of reference; in the stochastic equation of the (5.7) one-mode model for homodyne detection, this adds a Hermitian Hamiltonian contribution $H_\alpha = \sqrt{N}\hbar\omega_L^{(y)}(\Omega_\beta/\Omega)[\cos(\phi - \omega_L^{(x)}t)X_\alpha + \sin(\phi - \omega_L^{(x)}t)P_\alpha]$ where $\omega_L^{(y)} \ll \omega_L^{(x)}$ is the Larmor pulsation of the nuclear spin in the parasitic field and Ω_β/Ω is given by the (4.5) equation The term in P_α is absorbed in a phase change of the ansatz (5.8). The term in X_α does not change the parameter u of the ansatz (5.8) and thus

the variance of P_α in a realisation but adds a deterministic oscillating part to $\bar{P}_\alpha$, namely $(\sqrt{N}\omega_L^{(y)}/2\omega_L^{(x)})(\Omega_\beta/\Omega)[\sin(\phi-\omega_L^{(x)}t)-\sin\phi]$ and, according to (5.14), a deterministic part $\sqrt{\Gamma_{\rm ex}}(\Omega_\beta/\Omega)(\sqrt{N}\omega_L^{(y)}/2\omega_L^{(x)})\{[\cos(\phi-\omega_L^{(x)}t)-\cos\phi]/(\omega_L^{(x)}t)-\sin\phi\}$ to the integrated signal $\sigma(t)$. The term in $\sin\phi$ in the signal can be cancelled out by playing on the initial time "$t=0$", of the squeezing phase; the other contributions cancel out for a duration t of the experiment which is an integer multiple of $2\pi/\omega_L^{(x)}$.

An imposed magnetic field In the experiment, it is intended to impose a directional field according to Ox of the order of μT in order to avoid "wild" precession of the mean spin around a residual magnetic field of unknown direction. For the polarisations and squeezing levels estimated in section 5.5.1, we estimate that the Larmor precession in a small guiding field of 10^{-7} G for $t=10$ s, approximately the total duration of the experiment, can be neglected. We consider the effect of a magnetic field B over a time t to be negligible if the precession of the noise ellipse from a squeezed state 10 dB degrades the squeezed variance by less than 10% (this corresponds to an angle of 1.8 degrees). Since the Larmor frequency in the ground state is 3.24 kHz/G, we obtain the condition $B[\mathrm{G}]\times t[s]\leq 1.5\times 10^{-6}$. Although the Larmor frequency in the metastable state is much larger, 1.87 MHz/G, the precession in this state is negligible for magnetic fields up to ~ 10 mG since the rotation in the zOy plane only occurs during the short $1/\gamma_{\rm m}$ time between two metastability exchange collisions, which corresponds to an angle of order 1 degree. From a theoretical point of view, however, we can incorporate this guiding field into the analysis by placing ourselves in the frame of reference rotating around Ox at the corresponding Larmor pulsation $\omega_L^{(x)}$ of the nuclear spin to eliminate this guiding field[19] ; in principle, the cavity must also be rotated at the angular velocity $\omega_L^{(x)}$ in order for it to be stationary in the rotating frame of reference ; if the cavity remains stationary in the laboratory reference frame, the Faraday coupling can be established and a measurement of the field leaving the cavity can be made not continuously but stroboscopically (each time the direction to be spin squeezed merges with the optical axis) [57].

On the other hand, if one wants to use the spin squeezed state to measure a magnetic field, one turns off the discharge and the steering field and arranges for the field to be measured $\vec{B}_{\rm mes}$ to be oriented along Oy. The collective nuclear spin then precesses in the xOz plane by an angle that needs to be measured to trace back to $B_{\rm mes}$, and the initial squeezing direction Oz is just the one needed to reduce the angular pointing uncertainty on the spin. Another strategy is to start from an ordinary, unsqueezed polarised state of the nuclear spin and to carry out, with the discharge on but the steering field off, the continuous measurement of the light field coming out of the cavity *in the presence* of $B_{\rm mes}\vec{u}_y$; in the single-mode model with homodyne detection of section 5.2, one then falls back on the magnetometry proposals of references [60, 61].

[19] The discrepancy between the metastable and fundamental Larmor momenta should be compensated for, for example, by means of a fictitious magnetic field created by light displacement, but this precaution seems superfluous because the metastable Larmor pulsation remains small in front of the effective metastability exchange rate $\gamma_{\rm m}$

5.6 Conclusion of Part I

This part presented a proposed experiment to prepare a quantum state (nuclear spin-squeezed state) in a helium-3 gas in its ground electronic state at room temperature. Such a state would be obtained by placing a cell of helium-3 in an optical cavity and making a continuous measurement on the outgoing mode of the cavity, after the light has interacted with the nuclear spins via a metastable electronic state. Theoretical analysis shows that significant nuclear spin squeezing is achievable under laboratory conditions and for characteristic times of the order of a second. In particular, the physical parameters of the gas (temperature and pressure) are similar to the conditions for simple optical pumping in helium-3, with the additional constraint that the cell must be placed inside a centimetric optical cavity.

Our study opens the way to the realisation of very long-lived (several hours) squeezed states in a system already well known and used in metrology.

Bibliography

[1] B. Saam T. R. Gentile P. J. Nacher and T. G. Walker. "Optically polarized He 3". en. In: *Reviews of Modern Physics* 89 (Dec. 2017), p. 045004. ISSN: 0034-6861, 1539-0756. DOI: 10.1103/RevModPhys.89.045004.

[2] Werner Heil. "Helium Magnetometers". en. In: *High Sensitivity Magnetometers*. Ed. by Asaf Grosz, Michael J. Haji-Sheikh, and Subhas C. Mukhopadhyay. Smart Sensors, Measurement and Instrumentation. Cham, 2017, pp. 493–521. ISBN: 978-3-319-34070-8. DOI: 10.1007/978-3-319-34070-8_16.

[3] John Kitching, Svenja Knappe, and Elizabeth A. Donley. "Atomic Sensors – A Review". In: *IEEE Sensors Journal* 11 (Sept. 2011), pp. 1749–1758. ISSN: 1558-1748. DOI: 10.1109/JSEN.2011.2157679.

[4] J R MacFall et al. "Human lung air spaces: potential for MR imaging with hyperpolarized He-3." In: *Radiology* 200 (Aug. 1996), pp. 553–558. ISSN: 0033-8419. DOI: 10.1148/radiology.200.2.8685356.

[5] Marcus J. Couch et al. "Hyperpolarized and inert gas MRI: the future". eng. In: *Molecular Imaging and Biology* 17 (Apr. 2015), pp. 149–162. ISSN: 1860-2002. DOI: 10.1007/s11307-014-0788-2.

[6] G. Vasilakis et al. "Limits on New Long Range Nuclear Spin-Dependent Forces Set with a $\mathbf{K}\mathrm{\text{\ensuremath{-}}}^{3}\mathrm{He}$ Comagnetometer". In: *Physical Review Letters* 103 (Dec. 2009), p. 261801. DOI: 10.1103/PhysRevLett.103.261801.

[7] Werner Heil et al. "Spin clocks: Probing fundamental symmetries in nature". In: *Annalen der Physik* 525 (2013), pp. 539–549. ISSN: 1521-3889. DOI: 10.1002/andp.201300048.

[8] M. Batz, P.-J. Nacher, and G. Tastevin. "Fundamentals of metastability exchange optical pumping in helium". en. In: *Journal of Physics: Conference Series* 294 (June 2011), p. 012002. ISSN: 1742-6596. DOI: 10.1088/1742-6596/294/1/012002.

[9] A. Dantan et al. "Long-Lived Quantum Memory with Nuclear Atomic Spins". In: *Physical Review Letters* 95 (Sept. 2005), p. 123002. DOI: 10.1103/PhysRevLett.95.123002.

[10] G. Reinaudi et al. "Squeezing and entangling nuclear spins in helium 3". In: *Journal of Modern Optics* 54 (Mar. 2007), pp. 675–695. ISSN: 0950-0340. DOI: 10.1080/09500340600677005.

[11] Or Katz et al. “Long-Lived Entanglement Generation of Nuclear Spins Using Coherent Light”. In: *Physical Review Letters* 124 (Jan. 2020), p. 043602. DOI: 10.1103/PhysRevLett.124.043602.

[12] Luca Pezzè et al. “Quantum metrology with nonclassical states of atomic ensembles”. In: *Reviews of Modern Physics* 90 (Sept. 2018), p. 035005. DOI: 10.1103/RevModPhys.90.035005.

[13] Félix Bussières et al. “Prospective applications of optical quantum memories”. In: *Journal of Modern Optics* 60 (Oct. 2013), pp. 1519–1537. ISSN: 0950-0340. DOI: 10.1080/09500340.2013.856482.

[14] Klemens Hammerer, Anders S. Sørensen, and Eugene S. Polzik. “Quantum interface between light and atomic ensembles”. In: *Reviews of Modern Physics* 82 (Apr. 2010), pp. 1041–1093. DOI: 10.1103/RevModPhys.82.1041.

[15] G. Vasilakis et al. “Generation of a squeezed state of an oscillator by stroboscopic back-action-evading measurement”. en. In: *Nature Physics* 11 (May 2015), pp. 389–392. ISSN: 1745-2481. DOI: 10.1038/nphys3280.

[16] Or Katz, Roy Shaham, and Ofer Firstenberg. “Quantum Interface for Noble-Gas Spins Based on Spin-Exchange Collisions”. In: *PRX Quantum* 3 (Jan. 2022), p. 010305. DOI: 10.1103/PRXQuantum.3.010305.

[17] C. Gemmel et al. “Ultra-sensitive magnetometry based on free precession of nuclear spins”. en. In: *The European Physical Journal D* 57 (Apr. 2010), pp. 303–320. ISSN: 1434-6079. DOI: 10.1140/epjd/e2010-00044-5.

[18] G. C. Phillips et al. “Demonstration of a Polarized ${\mathrm{He}}^{3}$ Target for Nuclear Reactions”. In: *Physical Review Letters* 9 (Dec. 1962), pp. 502–504. DOI: 10.1103/PhysRevLett.9.502.

[19] M. A. Bouchiat, T. R. Carver, and C. M. Varnum. “Nuclear Polarization in He 3 Gas Induced by Optical Pumping and Dipolar Exchange”. en. In: *Physical Review Letters* 5 (Oct. 1960), pp. 373–375. ISSN: 0031-9007. DOI: 10.1103/PhysRevLett.5.373.

[20] F. D. Colegrove and P. A. Franken. “Optical Pumping of Helium in the $^{3}S_{1}$ Metastable State”. In: *Physical Review* 119 (July 1960), pp. 680–690. DOI: 10.1103/PhysRev.119.680.

[21] G. K. Walters, F. D. Colegrove, and L. D. Schearer. “Nuclear Polarization of ${\mathrm{He}}^{3}$ Gas by Metastability Exchange with Optically Pumped Metastable ${\mathrm{He}}^{3}$ Atoms”. In: *Physical Review Letters* 8 (June 1962), pp. 439–442. DOI: 10.1103/PhysRevLett.8.439.

[22] F. D. Colegrove, L. D. Schearer, and G. K. Walters. “Polarization of ${\mathrm{He}}^{3}$ Gas by Optical Pumping”. In: *Physical Review* 132 (Dec. 1963), pp. 2561–2572. DOI: 10.1103/PhysRev.132.2561.

[23] S. S. Hodgman et al. “Metastable Helium: A New Determination of the Longest Atomic Excited-State Lifetime”. In: *Physical Review Letters* 103 (July 2009), p. 053002. DOI: 10.1103/PhysRevLett.103.053002.

[24] J. Dupont-Roc, M. Leduc, and F. Laloë. "Contribution à l'étude du pompage optique par échange de métastabilité dans 3He. - Première Partie". fr. In: *Journal de Physique* 34 (Nov. 1973), pp. 961–976. ISSN: 0302-0738, 2777-3396. DOI: 10.1051/jphys:019730034011-12096100.

[25] D. J. Wineland et al. "Squeezed atomic states and projection noise in spectroscopy". In: *Physical Review A* 50 (July 1994), pp. 67–88. DOI: 10.1103/PhysRevA.50.67.

[26] J. Cviklinski et al. "Conditional squeezing of an atomic alignment". In: *Phys. Rev. A* 76 (3 2007), p. 033830. DOI: 10.1103/PhysRevA.76.033830.

[27] Jacques Dupont-Roc. "Etude de quelques effets liés au pompage optique en champ faible". fr. thèse. Université Pierre et Marie Curie - Paris VI, Mar. 1972.

[28] Vladimir B. Braginskiĭ, Yu I Vorontsov, and V D Krivchenkov. "Unperturbed measurements of the n-quantum state of an harmonic oscillator". en. In: *Journal of Experimental and Theoretical Physics* 41 (May 1975), p. 28.

[29] Vladimir B. Braginskiĭ and Yurii I. Vorontsov. "Quantum-mechanical limitations in macroscopic experiments and modern experimental technique". en. In: *Soviet Physics Uspekhi* 17 (May 1975), p. 644. ISSN: 0038-5670. DOI: 10.1070/PU1975v017n05ABEH004362.

[30] Vladimir B. Braginskiĭ, Yurii I. Vorontsov, and F. Ya Khalili. "Quantum singularities of a ponderomotive meter of electromagnetic energy". English. In: *Journal of Experimental and Theoretical Physics* 46 (Oct. 1977), p. 705.

[31] Abbott B. P. et al. and LIGO Scientific Collaboration and Virgo Collaboration. "Observation of Gravitational Waves from a Binary Black Hole Merger". en. In: *Physical Review Letters* 116 (Feb. 2016), p. 061102. ISSN: 0031-9007, 1079-7114. DOI: 10.1103/PhysRevLett.116.061102.

[32] E. E. Muschlitz. "Metastable Atoms and Molecules". In: *Science* 159 (1968), pp. 599–604. DOI: 10.1126/science.159.3815.599. eprint: https://www.science.org/doi/pdf/10.1126/science.159.3815.599.

[33] V. Lefevre-Seguin and M. Leduc. "Metastability-exchange and depolarising collisions in xenon and krypton". en. In: *Journal of Physics B: Atomic and Molecular Physics* 10 (Aug. 1977), pp. 2157–2164. ISSN: 0022-3700. DOI: 10.1088/0022-3700/10/11/016.

[34] L. D. Schearer. "Depolarization Cross Sections for the Metastable Noble Gases by Optical Pumping". In: *Physical Review* 188 (Dec. 1969), pp. 505–506. DOI: 10.1103/PhysRev.188.505.

[35] T. Xia et al. "Polarization and hyperfine transitions of metastable $^{129}\mathrm{Xe}$ in discharge cells". In: *Physical Review A* 81 (Mar. 2010), p. 033419. DOI: 10.1103/PhysRevA.81.033419.

[36] Tetsuo Hadeishi and Chung-Heng Liu. "Nuclear Alignment of the $^{1}S_{0}$ Ground State of $^{131}\mathrm{Xe}$ by Electron Pumping and Metastability-Exchange Collisions". In: *Physical Review Letters* 19 (July 1967), pp. 211–213. DOI: 10.1103/PhysRevLett.19.211.

[37] Fei Luo, Clayton F. Giese, and W. Ronald Gentry. "Direct measurement of the size of the helium dimer". In: *The Journal of Chemical Physics* 104 (Jan. 1996), pp. 1151–1154. ISSN: 0021-9606. DOI: 10.1063/1.470771.

[38] D Vrinceanu and H R Sadeghpour. "Spin polarization transfer in ground and metastable helium atom collisions". en. In: *New Journal of Physics* 12 (June 2010), p. 065039. ISSN: 1367-2630. DOI: 10.1088/1367-2630/12/6/065039.

[39] B. J. Garrison, W. H. Miller, and H. F. Schaefer. "Penning and associative ionization of triplet metastable helium atoms". In: *The Journal of Chemical Physics* 59 (Sept. 1973), pp. 3193–3198. ISSN: 0021-9606. DOI: 10.1063/1.1680460.

[40] A. Kuzmich et al. "Quantum nondemolition measurements of collective atomic spin". In: *Phys. Rev. A* 60 (3 1999), pp. 2346–2350. DOI: 10.1103/PhysRevA.60.2346.

[41] Ben Q. Baragiola, Bradley A. Chase, and JM Geremia. "Collective uncertainty in partially polarized and partially decohered spin-$\frac{1}{2}$ systems". In: *Physical Review A* 81 (Mar. 2010), p. 032104. DOI: 10.1103/PhysRevA.81.032104.

[42] Yvan Castin, Jean Dalibard, and Klaus Mo/lmer. "A wave function approach to dissipative processes". In: *AIP Conference Proceedings* 275 (June 1993), pp. 143–156. ISSN: 0094-243X. DOI: 10.1063/1.43795.

[43] Klaus Mølmer, Yvan Castin, and Jean Dalibard. "Monte Carlo wave-function method in quantum optics". en. In: *Journal of the Optical Society of America B* 10 (Mar. 1993), p. 524. ISSN: 0740-3224, 1520-8540. DOI: 10.1364/JOSAB.10.000524.

[44] G. Lindblad. "On the generators of quantum dynamical semigroups". en. In: *Communications in Mathematical Physics* 48 (June 1976), pp. 119–130. ISSN: 1432-0916. DOI: 10.1007/BF01608499.

[45] Florentin Reiter and Anders S. Sørensen. "Effective operator formalism for open quantum systems". In: *Physical Review A* 85 (Mar. 2012), p. 032111. DOI: 10.1103/PhysRevA.85.032111.

[46] Yvan Castin and Klaus Mølmer. "Monte Carlo Wave-Function Analysis of 3D Optical Molasses". In: *Physical Review Letters* 74 (May 1995), pp. 3772–3775. DOI: 10.1103/PhysRevLett.74.3772.

[47] H. M. Wiseman and G. J. Milburn. "Quantum theory of field-quadrature measurements". In: *Physical Review A* 47 (Jan. 1993), pp. 642–662. DOI: 10.1103/PhysRevA.47.642.

[48] Yun Li, Y. Castin, and A. Sinatra. "Optimum Spin Squeezing in Bose-Einstein Condensates with Particle Losses". In: *Physical Review Letters* 100 (May 2008), p. 210401. DOI: 10.1103/PhysRevLett.100.210401.

[49] Stefano Zippilli et al. "Scheme for decoherence control in microwave cavities". In: *Physical Review A* 67 (May 2003), p. 052101. DOI: 10.1103/PhysRevA.67.052101.

[50] L. K. Thomsen, S. Mancini, and H. M. Wiseman. "Continuous quantum nondemolition feedback and unconditional atomic spin squeezing". en. In: *Journal of Physics B: Atomic, Molecular and Optical Physics* 35 (Nov. 2002), pp. 4937–4952. ISSN: 0953-4075. DOI: 10.1088/0953-4075/35/23/316.

[51] Lars Bojer Madsen and Klaus Mølmer. "Spin squeezing and precision probing with light and samples of atoms in the Gaussian description". In: *Physical Review A* 70 (Nov. 2004), p. 052324. DOI: 10.1103/PhysRevA.70.052324.

[52] Nicolas Gisin. "Stochastic quantum dynamics and relativity". en. In: *Helvetica Physica Acta* 62 (May 1989), p. 363. DOI: 10.5169/SEALS-116034.

[53] N Gisin and I C Percival. "The quantum-state diffusion model applied to open systems". en. In: *Journal of Physics A: Mathematical and General* 25 (Nov. 1992), pp. 5677–5691. ISSN: 0305-4470, 1361-6447. DOI: 10.1088/0305-4470/25/21/023.

[54] N. Gisin. "Quantum Measurements and Stochastic Processes". In: *Physical Review Letters* 52 (May 1984), pp. 1657–1660. DOI: 10.1103/PhysRevLett.52.1657.

[55] John K. Stockton et al. "Robust quantum parameter estimation: Coherent magnetometry with feedback". In: *Physical Review A* 69 (Mar. 2004), p. 032109. DOI: 10.1103/PhysRevA.69.032109.

[56] Haruka Tanji-Suzuki et al. "Chapter 4 - Interaction between Atomic Ensembles and Optical Resonators: Classical Description". en. In: *Advances In Atomic, Molecular, and Optical Physics*. Ed. by E. Arimondo, P. R. Berman, and C. C. Lin. Vol. 60. Advances in Atomic, Molecular, and Optical Physics. Jan. 2011, pp. 201–237. DOI: 10.1016/B978-0-12-385508-4.00004-8.

[57] G. Vasilakis et al. "Generation of a squeezed state of an oscillator by stroboscopic back-action-evading measurement". en. In: *Nature Physics* 11 (May 2015), pp. 389–392. ISSN: 1745-2481. DOI: 10.1038/nphys3280.

[58] W. A. Fitzsimmons, N. F. Lane, and G. K. Walters. "Diffusion of He(2^3S_1) in Helium Gas; $2^3S_1 - 1^1S_0$ Interaction Potentials at Long Range". In: *Physical Review* 174 (Oct. 1968), pp. 193–200. DOI: 10.1103/PhysRev.174.193.

[59] W. Franzen. "Spin Relaxation of Optically Aligned Rubidium Vapor". In: *Physical Review* 115 (Aug. 1959), pp. 850–856. DOI: 10.1103/PhysRev.115.850.

[60] JM Geremia et al. "Quantum Kalman Filtering and the Heisenberg Limit in Atomic Magnetometry". In: *Physical Review Letters* 91 (Dec. 2003), p. 250801. DOI: 10.1103/PhysRevLett.91.250801.

[61] Klaus Mølmer and Lars Bojer Madsen. "Estimation of a classical parameter with Gaussian probes: Magnetometry with collective atomic spins". In: *Physical Review A* 70 (Nov. 2004), p. 052102. DOI: 10.1103/PhysRevA.70.052102.

Part II

Phonon damping in a 2D superfluid boson gas

Introduction

Superfluidity is a fascinating phenomenon because it is one of the macroscopic manifestations of the quantum properties of matter. It is characterised by different properties depending on the system considered, including zero viscosity, the best known and the one which gave it its name, and superconductivity. In boson gases in dimension $d = 3$, superfluidity is a consequence of Bose-Einstein condensation, a collective state of a bosonic system where one mode of the field acquires a macroscopic population. In contrast, in the $d = 1$ and 2 cases, Bose-Einstein condensation is forbidden at non-zero temperature by the Mermin-Wagner theorem [1], which states the absence of long-range order at the thermodynamic limit. Intuitively, the quantum fluctuations of an N-body system in reduced dimensionality are always strong enough to destroy the coherence at finite distance. Remarkably, the superfluidity phenomenon survives in 2D at non-zero temperature and appears via an infinite-order transition, the so-called Berezenskii-Kosterlitz-Thouless (BKT) transition [2, 3], first observed in 1978 in a liquid helium-4 film [4].

In the condensed matter framework, the study of sound propagation and its attenuation provides important information on the thermodynamic properties and low-energy excitations of the system that are directly related to the transport properties [5, 6]. Moreover, in a degenerate gas, the intrinsic coherence time of a condensate is directly related to the interactions between phonons [7]. Furthermore, sound propagation in a superfluid has acquired a wider field of application when it has been linked to astrophysical problems [8], in particular via the concept of "analogue gravity" [9], such as Hawking radiation on the event horizon of a black hole [10] or the modelling of neutron stars [11].

Historically, the first condensation and superfluidity experiments were conducted in liquid helium-4. Liquid helium-4 is a strongly interacting system where the condensed fraction is therefore low (around 10 %), which makes its theoretical modelling difficult. This is why the obtaining of a Bose-Einstein condensate in a dilute atomic vapour in 1995,[20] rewarded by a Nobel Prize in Physics in 2001, was a small revolution in this field [12].

Today, cold dilute gases, which are weakly or strongly interacting systems, constitute a very favourable terrain for the study of superfluidity and Bose-Einstein condensation. Indeed, the dilute character of the system allows to easily enter the weak interaction regime and thus to obtain very large condensed fractions. Moreover, these are systems where the essential parameters are under the control of the experimentalists. By means of Feshbach resonances, it is indeed possible to control the strength of the interactions between the particles, while the external potential can be modulated at will (we even know how to make flat-bottom potential boxes [13]).

In this part, we are interested in the case of a cold superfluid boson gas in which the phonons are in the weak collisional regime. A given phonon of any wave vector $\vec{q}$ is in such a regime when its eigenpulsation $\omega_{\vec{q}} \sim cq$ with c the speed of sound in the fluid, is large compared to the thermal damping rate Γ^{th}, $\omega_{\vec{q}} \gg \Gamma^{\text{th}}$. In other words, the wavelength of the mode is much smaller than the mean free path of a thermal phonon in the medium. The opposite regime, where the mode oscillates more slowly than the thermalization rate of the system, is called "hydrodynamic". The study of sound in two-dimensional superfluid gases has received renewed interest thanks to experiments on cold atomic gases in potential boxes,

[20] The researchers were able to obtain a nearly pure condensate in a rubidium 87 gas cooled to 170 nK in a magnetic trap.

with bosons [14, 15] or fermions [16], see recent theoretical work in the bosonic case [17, 18].

We present a classical field numerical simulation of a system governed by the quantum hydrodynamics Hamiltonian developed by Landau and Khalatnikov in 1949 [19]. In particular, the evolution of the time correlation function of the phonons $\langle b_{\vec{q}}(t) b^{\dagger}_{\vec{q}}(0)\rangle$ in a box at thermal equilibrium is studied. In two dimensions, as in three, considering the $\vec{q}$ mode as a small system coupled to the reservoir formed by the rest of the gas, in the Born-Markov approximation, predicts an exponential decay of this correlation function with a rate $\Gamma_q/2$ where Γ_q is the damping rate computed by the Fermi golden rule of an initial overpopulation in the $\vec{q}$ mode. In the $d = 3$ case, we show that this prediction is accurate [20] in the limit of a reduced temperature $\epsilon = k_B T/mc^2 \to 0$ with m the mass of a boson. In the $d = 2$ case, on the other hand, and as we show, this condition is a priori no longer sufficient but only necessary. In particular, we show that the definition of a valid regime for the Fermi golden rule requires the introduction of a second "small parameter" u^{-1} proportional to the scaled effective coupling constant $\tilde{g} = \frac{1}{\rho\xi^2}$ (introduced in papers [14, 15]) with ρ the average boson density and $\xi = \hbar/mc$ the relaxation length.

In our simulations, we indeed find a systematic deviation from the exponential rate law $\Gamma_q/2$ even at low reduced temperature. Thanks to the diagrammatic theory of N-body Green's functions (within a range of validity that we specify), we are able to propose a prediction for this second-order deviation in the interaction between phonons at all orders in ϵ and at the leading order in $1/u$. Our simulations agree very well with this prediction. We thus highlight significant deviations from the exponential decay predicted by Fermi's golden rule, contrary to what happens in the three-dimensional case. These deviations seem to us to be accessible to experimental verification; as such, we have chosen the parameters of a series of runs of the simulation program close to the conditions of the experiment described in reference [15].

This part is structured as follows: in chapter 1 we present the general framework of our study, namely Landau-Khalatnikov quantum hydrodynamics, and we calculate the phonon damping rate by Fermi's golden rule. In Chapter 2 we present the computer program in detail, with a discussion of the various approximations and numerical methods we have used. Chapter 3 discusses the diagrammatic theory of N-body Green's functions. From this we extract the u^{-1} parameter as a small additional parameter to the $d = 2$ theory and obtain an integral expression for the time correlation function. Finally, in chapter 4 we present the results of the numerical simulations we have performed. They are compared with Fermi's golden rule and the diagrammatic theory.

Chapter 1

Theoretical framework : Quantum hydrodynamics

Foreword

In 1949, Landau and Khalatnikov [19], in the context of the calculation of the viscosity of superfluid helium, propose an effective low-energy theory allowing access to the behaviour of the fluid at non-zero temperature in an exact manner even in the strong interaction regime but on a spatial scale that could be described as "mesoscopic" since the model is a "coarse-grained" description of the fluid so as to average out the microscopic properties of the fluid while describing its collective long-wave excitations. The only element to be provided to the theory is the equation of state of the fluid at zero temperature. A comparison between this effective theory and microscopic approaches to phonon damping in the 3D case was made in [21]. This chapter introduces this model, its validity regime and the Hamiltonian that is the subject of the numerical simulations. This will lead us to explain the observable of the system on which we will work in the following chapters. In the last section, we will apply Fermi's golden rule in order to obtain a first prediction on the damping rates of collective excitations in the gas.

1.1 Hydrodynamic Hamiltonian

The quantum hydrodynamic model is a description of the "coarse-grained" fluid [22]. To formalise this starting point we consider a discretisation of the box containing the fluid by a square unit cell of length l chosen in such a way that the density and velocity of the fluid inside a unit cell are well defined and quasi-homogeneous. This requires a length l that is very small compared to the typical wavelength of the collective thermal excitations of the fluid $\frac{2\pi}{q_{\text{th}}}$ but much larger than the average distance between particles $\rho^{-1/2}$, i.e.

$$\rho^{-1/2} \ll l \ll q_{\text{th}}^{-1} \tag{1.1}$$

with ρ the average density of bosons at thermodynamic equilibrium at temperature T and $q_{\text{th}} = \frac{k_B T}{\hbar c}$ with c the speed of sound in the fluid. If this condition is satisfied, two canonically conjugate Hermitian operators are introduced: a local particle density field $\hat{\rho}(\vec{r})$ and a local

phase field $\hat{\phi}(\vec{r})$,[1]

$$[\hat{\rho}(\vec{r}), \hat{\phi}(\vec{r}')] = \mathrm{i}\frac{\delta_{\vec{r},\vec{r}'}}{l^2} \tag{1.2}$$

with $\vec{r}$ and $\vec{r}'$ as two points of the lattice. The velocity field is defined from a discrete gradient on this lattice $\vec{v}(\vec{r}) = \frac{\hbar}{m}\nabla\hat{\phi}(\vec{r})$ with m the mass of a particle. The dynamics of these fields is described by the hydrodynamic Hamiltonian

$$\hat{H}_{\text{hydro}} = l^2 \sum_{\vec{r}} \frac{\hbar^2}{2m}(\nabla\hat{\phi}) \cdot \hat{\rho}(\nabla\hat{\phi}) + e_0(\hat{\rho}). \tag{1.3}$$

The term e_0 denotes the energy density in the ground state, related to the chemical potential at zero temperature by the relation $\mu = \frac{\mathrm{d}e_0}{\mathrm{d}\rho}$.[2]

The next step is to linearise the Hamiltonian (1.3) around the homogeneous steady state at thermodynamic equilibrium

$$\hat{\rho}(\vec{r}) = \hat{\rho}_0 + \delta\hat{\rho}(\vec{r}) \tag{1.4}$$

$$\hat{\phi}(\vec{r}) = \hat{\phi}_0 + \delta\hat{\phi}(\vec{r}) \tag{1.5}$$

where we have introduced the spatial averages $\hat{\rho}_0$ and $\hat{\phi}_0$ of the operators $\hat{\rho}(\vec{r})$ and $\hat{\phi}(\vec{r})$; we simply have $\hat{\rho}_0 = \hat{N}/L^d$ where $\hat{N}$ is the total number of particles operator; as it is a conserved quantity, we replace in the following $\hat{\rho}_0$ by its quantum average ρ in the system state. The fluctuation operators $\delta\hat{\rho}(\vec{r})$ and $\delta\hat{\phi}(\vec{r})$ have non-zero Fourier components only on non-zero wave vectors and carry the collective excitations of the fluid. By introducing these developments into the hydrodynamic Hamiltonian and separating the contributions of different orders into the fluctuation operators, we obtain the following decomposition

$$\hat{H}^{(0)}_{\text{hydro}} = l^2 \sum_{\vec{r}} e_{0,0}(\rho) = e_{0,0}(\rho)L^2 \tag{1.6}$$

$$\hat{H}^{(1)}_{\text{hydro}} = l^2 \sum_{\vec{r}} \mu(\rho)\delta\hat{\rho}(\vec{r}) = 0 \tag{1.7}$$

$$\hat{H}^{(2)}_{\text{hydro}} = l^2 \sum_{\vec{r}} \frac{\hbar^2}{2m}\rho(\nabla\delta\hat{\phi})^2(\vec{r}) + \frac{1}{2}\frac{\mathrm{d}\mu(\rho)}{\mathrm{d}\rho}(\delta\hat{\rho})^2(\vec{r}) \tag{1.8}$$

$$\hat{H}^{(3)}_{\text{hydro}} = l^2 \sum_{\vec{r}} \frac{\hbar^2}{2m}\nabla\delta\hat{\phi} \cdot \delta\hat{\rho}\nabla\delta\hat{\phi}(\vec{r}) + \frac{1}{6}\frac{\mathrm{d}^2\mu(\rho)}{\mathrm{d}\rho^2}(\delta\hat{\rho})^3(\vec{r}). \tag{1.9}$$

We note that $\hat{H}^{(0)}_{\text{hydro}}$ is a constant (with L^2 the volume of the box) which can therefore be ignored. In the end, it is the quadratic Hamiltonian $\hat{H}^{(2)}_{\text{hydro}}$ that makes the first contribution to field dynamics. Since this Hamiltonian is easy to diagonalize and $\hat{H}^{(3)}_{\text{hydro}}$ is of higher order, it is useful to think of the system as a perturbed Hamiltonian $\hat{H}_0 + \hat{V}$ with $\hat{H}^{(2)}_{\text{hydro}}$ in the

[1] The possibility of introducing the phase operator $\hat{\phi}(\vec{r})$ at site $\vec{r}$ results from the high occupancy condition on the site $\rho l^d \gg 1$.

[2] In principle, a bare energy density $e_{0,0}$ should be introduced, which then needs to be renormalized by the zero-point energy of the modes to obtain the true energy density in the ground state and remove the dependence on the unit cell pitch. This procedure is described in reference [22].

role of the well-known and simple Hamiltonian and $\hat{H}^{(3)}_{\rm hydro}$ in the role of the perturbation. Indeed, one can put the $\hat{H}^{(2)}_{\rm hydro}$ Hamiltonian into the normal form

$$\hat{H}^{(2)}_{\rm hydro} = \sum_{\vec{q}} \varepsilon_k \hat{b}^\dagger_{\vec{q}} \hat{b}_{\vec{q}} \tag{1.10}$$

by means of a Bogolioubov transformation on the fluctuations of the fields

$$\delta\hat{\rho}(\vec{r}) = \sqrt{\frac{\rho}{L^2}} \sum_{\vec{q}\in\mathcal{D}^*} \sqrt{\frac{\hbar q}{2mc}} \left(\hat{b}_{\vec{q}} + \hat{b}^\dagger_{-\vec{q}}\right) \mathrm{e}^{\mathrm{i}\vec{q}\,\cdot\,\vec{r}} \tag{1.11}$$

$$\delta\hat{\phi}(\vec{r}) = \frac{-\mathrm{i}}{\sqrt{\rho L^2}} \sum_{\vec{q}\in\mathcal{D}^*} \sqrt{\frac{mc}{2\hbar q}} \left(\hat{b}_{\vec{q}} - \hat{b}^\dagger_{-\vec{q}}\right) \mathrm{e}^{\mathrm{i}\vec{q}\,\cdot\,\vec{r}} \tag{1.12}$$

with $\mathcal{D}$ the first Brillouin zone of the lattice and $\mathcal{D}^*$ this same zone deprived of $\vec{q}=\vec{0}$. We recognise the creation $\hat{b}^\dagger_{\vec{q}}$ and annihilation $\hat{b}_{\vec{q}}$ operators of a quantum in the mode $\vec{q}$ which obey the bosonic switching rules $[\hat{b}_{\vec{q}};\hat{b}^\dagger_{\vec{k}}] = \delta_{\vec{q},\vec{k}}$. The resulting phonon excitation spectrum is purely linear $\varepsilon_q \equiv \hbar\omega_q = \hbar cq$ where the speed of sound is given by $\rho\frac{\mathrm{d}\mu}{\mathrm{d}\rho} = mc^2$ which is none other than the usual thermodynamic relation, thus justifying the name "phonons" for these quanta.

However, in order to be able to describe all the physics of the problem, in particular to know which interaction processes between phonons conserve energy and can lead to the damping of sound, we are led to introduce "by hand", as Landau and Khalatnikov did, a curvature γ which represents the first correction to the linear phonon spectrum :

$$\varepsilon_q \underset{q\to 0}{=} \hbar cq \left(1 + \frac{\gamma}{8}\left(\frac{\hbar q}{mc}\right)^2 + \dots\right) \tag{1.13}$$

This curvature can be introduced in a systematic way by adding to the hydrodynamic Hamiltonian the gradient corrections [23].

Having said this, we can insert the expressions of the fields as a function of the eigenmodes into (1.9) to obtain

$$\begin{aligned}\hat{H}^{(3)}_{\rm hydro} = \frac{mc^2}{\sqrt{\rho L^2}} \sum_{\vec{k}_1;\vec{k}_2;\vec{k}_3} \sqrt{\frac{\hbar^3 k_1 k_2 k_3}{8m^3c^3}} \left(3\Lambda + u_{\vec{k}_1;\vec{k}_2} + u_{\vec{k}_1;\vec{k}_3} + u_{\vec{k}_2;\vec{k}_3}\right) \\ \times \left[\frac{1}{2}\delta_{\vec{k}_1+\vec{k}_2;\vec{k}_3}\left(\hat{b}^\dagger_{\vec{k}_1}\hat{b}^\dagger_{\vec{k}_2}\hat{b}_{\vec{k}_3} + \text{h.c.}\right) + \frac{1}{6}\delta_{\vec{k}_1+\vec{k}_2+\vec{k}_3;\vec{0}}\left(\hat{b}^\dagger_{\vec{k}_1}\hat{b}^\dagger_{\vec{k}_2}\hat{b}^\dagger_{\vec{k}_3} + \text{h.c.}\right)\right]\end{aligned} \tag{1.14}$$

with $u_{\vec{k}_1;\vec{k}_2} = \frac{\vec{k}_1\,\cdot\,\vec{k}_2}{k_1k_2}$ the cosine of the angle between $\vec{k}_1$ and $\vec{k}_2$ and $\Lambda = \frac{\rho}{3}\frac{\mathrm{d}^2\mu}{\mathrm{d}\rho^2}\left(\frac{\mathrm{d}\mu}{\mathrm{d}\rho}\right)^{-1}$ a thermodynamic parameter. This last expression of $\hat{H}^{(3)}_{\rm hydro}$ in terms of the phonon eigenmodes of $\hat{H}^{(2)}_{\rm hydro}$ is particularly interesting in that it makes explicit the interaction processes between phonons. Indeed, in the sum over the wave vectors, the term proportional to $\hat{b}^\dagger_{\vec{k}_1}\hat{b}^\dagger_{\vec{k}_2}\hat{b}_{\vec{k}_3}$ for example represents the annihilation of a phonon $\vec{k}_3$ and the creation of two phonons of wave vectors $\vec{k}_1$ and $\vec{k}_2$ with the constraint of conservation of the momentum $\vec{k}_3 = \vec{k}_1 + \vec{k}_2$. This

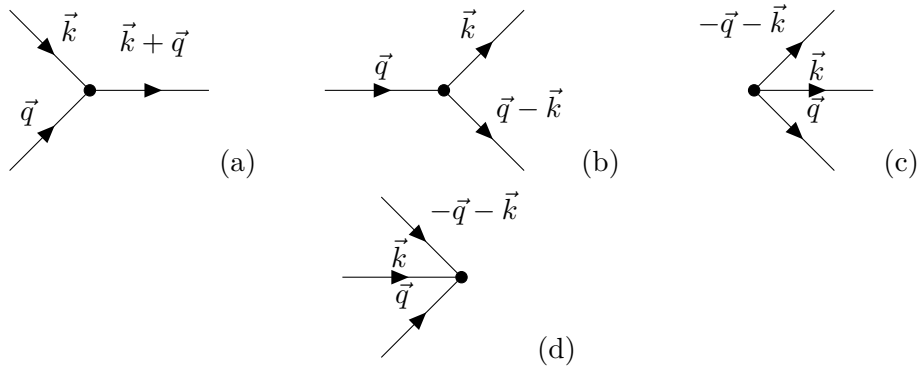

Figure 1.1: Diagrams of the interaction processes associated with the cubic Hamiltonian $\hat{H}^{(3)}_{\text{hydro}}$ given by (1.14). (a) Landau process associated with the term $\hat{b}^\dagger_{\vec{k}_3}\hat{b}_{\vec{k}_2}\hat{b}_{\vec{k}_1}$. (b) Beliaev process associated with the term $\hat{b}^\dagger_{\vec{k}_1}\hat{b}^\dagger_{\vec{k}_2}\hat{b}_{\vec{k}_3}$. (c) and (d) non-resonant processes associated with the terms $\hat{b}^\dagger_{\vec{k}_1}\hat{b}^\dagger_{\vec{k}_2}\hat{b}^\dagger_{\vec{k}_3}$ and $\hat{b}_{\vec{k}_3}\hat{b}_{\vec{k}_2}\hat{b}_{\vec{k}_1}$ respectively.

term is then interpreted as the disintegration of one phonon into two others. It is called the Beliaev process and we represent it as an interaction diagram in figure 1.1b. We also show the processes associated with the other terms in the sum. Namely, the Landau process associated with $\hat{b}^\dagger_{\vec{k}_3}\hat{b}_{\vec{k}_2}\hat{b}_{\vec{k}_1}$ where two phonons $\vec{k}_1$ and $\vec{k}_2$ merge into a single wave vector $\vec{k}_3$, shown in (a), and the non-resonant processes $\hat{b}^\dagger_{\vec{k}_1}\hat{b}^\dagger_{\vec{k}_2}\hat{b}^\dagger_{\vec{k}_3}$ and $\hat{b}_{\vec{k}_3}\hat{b}_{\vec{k}_2}\hat{b}_{\vec{k}_1}$, shown in (c) and (d) respectively, where three phonons are created from the vacuum or annihilate.

Expression of the Hamiltonian as a function of $\hat{\psi}_{\vec{r}}$ Let us introduce the boson field operator, expressed in modulo-phase viewpoint

$$\hat{\psi}_{\vec{r}} = \sqrt{\hat{\rho}(\vec{r})}\mathrm{e}^{\mathrm{i}\hat{\phi}(\vec{r})} \tag{1.15}$$

and the fluctuation operator of this field $\hat{\psi}_{\vec{r}} = \sqrt{\rho} + \delta\hat{\psi}_{\vec{r}}$ for the choice $\hat{\phi}_0 = 0$. We then have

$$\delta\hat{\psi}_{\vec{r}} = \sqrt{\rho}\left(\frac{\delta\hat{\rho}}{2\rho} + \mathrm{i}\delta\hat{\phi}\right). \tag{1.16}$$

By noting $\mathrm{Re}\,\delta\hat{\psi}_{\vec{r}} = \frac{\delta\hat{\psi}_{\vec{r}} + \delta\hat{\psi}^\dagger_{\vec{r}}}{2}$ and $\mathrm{Im}\,\delta\hat{\psi}_{\vec{r}} = \frac{\delta\hat{\psi}_{\vec{r}} - \delta\hat{\psi}^\dagger_{\vec{r}}}{2\mathrm{i}}$ we can express the fluctuations of the fields as $\delta\hat{\rho} = 2\sqrt{\rho}\,\mathrm{Re}\,\delta\hat{\psi}_{\vec{r}}$ and $\delta\hat{\phi} = \frac{1}{\sqrt{\rho}}\mathrm{Im}\,\delta\hat{\psi}_{\vec{r}}$ and insert these formulas into the expression (1.9) of the third order Hamiltonian

$$\hat{H}^{(3)}_{\text{hydro}} = \frac{l^2}{\sqrt{\rho}}\sum_{\vec{r}}\frac{\hbar^2}{m}\nabla\left(\mathrm{Im}\,\delta\hat{\psi}_{\vec{r}}\right)\left(\mathrm{Re}\,\delta\hat{\psi}_{\vec{r}}\nabla\,\mathrm{Im}\,\delta\hat{\psi}_{\vec{r}}\right) + 4mc^2\Lambda\left(\delta\hat{\psi}_{\vec{r}}\right)^3. \tag{1.17}$$

To conclude this section, let us introduce the $\hat{a}_{\vec{q}}$ operators into the reciprocal space defined by the discrete Fourier transform of $\delta\hat{\psi}_{\vec{r}}$

$$\delta\hat{\psi}_{\vec{r}} = \frac{1}{\sqrt{L^2}}\sum_{\vec{q}\in\mathcal{D}^*}\hat{a}_{\vec{q}}\,\mathrm{e}^{\mathrm{i}\vec{q}\,\cdot\,\vec{r}}. \tag{1.18}$$

These $\hat{a}_{\vec{q}}$ operators do not coincide with the $\hat{b}_{\vec{q}}$ phononic modes, but one can switch from one to the other by simple linear combination [3]

$$\hat{a}_{\vec{q}} = u_{\vec{q}}\hat{b}_{\vec{q}} + v_{\vec{q}}\hat{b}^\dagger_{-\vec{q}} \quad \text{with} \quad u_{\vec{q}} + v_{\vec{q}} = \sqrt{\frac{\hbar q}{2mc}} \quad \text{and} \quad u_{\vec{q}} - v_{\vec{q}} = \sqrt{\frac{2mc}{\hbar q}}. \tag{1.19}$$

Monitored observable Before concluding this section, we introduce the target observable that the simulations in Chapter 2 and the theory of N-body Green's functions in Chapter 3 study and analyse. It is the time correlation function of the mode $\vec{q}$ at thermodynamic equilibrium

$$\langle \hat{b}_{\vec{q}}(t)\hat{b}^\dagger_{\vec{q}}(0)\rangle. \tag{1.20}$$

At the initial instant this quantity is expressed as a function of the average $n_{\vec{q}} = \langle \hat{b}^\dagger_{\vec{q}}(t)\hat{b}_{\vec{q}}(t)\rangle$ occupancy number of the mode $\vec{q}$, i.e. $\langle \hat{b}_{\vec{q}}(0)\hat{b}^\dagger_{\vec{q}}(0)\rangle = 1+n_{\vec{q}}$. A priori, this correlation function tends towards 0 at long times. More precisely, in the pilot equation method, well known in quantum optics, which treats the mode $\vec{q}$ as a small system coupled to the reservoir formed by the other modes in the Born-Markov approximation, it is shown that this correlation function decreases exponentially with a rate $\Gamma_q/2$ where Γ_q is the damping rate predicted by Fermi's golden rule and calculated in section 1.3 [24, 25].

1.2 Unitless scaling of quantities

In the remainder of this part, we will use scaled quantities without unit. Thus, we introduce the reduced temperature $\epsilon = \frac{k_B T}{mc^2}$ which must be $\ll 1$ in the regime of validity of quantum hydrodynamics. As we shall see, in the $d = 3$ case, this small parameter controls the validity of Fermi's golden rule. In the $d = 2$ case, on the other hand, ϵ must share its realm with a second small physical parameter. Moreover, we have written our simulations only in terms of scaled quantities, which offers some comfort in writing the program and interpreting the output data since the dynamics now depend only on a limited number of input parameters that reflect ratios of physical quantities in the system (as we will see in Chapter 2 devoted to the program description).

The scaled version of a quantity x will always be denoted $\bar{x}$. In most cases, scaling is done by means of the temperature T. All energies are thus scaled by $k_B T$, times by $\frac{\hbar}{k_B T}$, distances by $\frac{\hbar c}{k_B T}$. For example, we note $\hat{H}^{(2)}_{\text{hydro}} = k_B T \bar{H}^{(2)}$ and $\hat{H}^{(3)}_{\text{hydro}} = k_B T \bar{H}^{(3)}$. We also introduce the relaxation length $\xi = \frac{\hbar}{mc}$ by which we express the reduced density $\rho\xi^2$. The rest of this section consists of rewriting the relations and quantities discussed so far in their dimensionless version.

[3] To find these expressions, simply express $\delta\hat{\psi}_{\vec{r}}$ in terms of $\hat{b}_{\vec{q}}$ via equations (1.16) and (1.11)-(1.12) and compare to the Fourier decomposition (1.18) wave vector by wave vector.

Local fluctuation operators for density and phase

$$\delta\bar{\rho}(\vec{r}) = \sqrt{\frac{\rho\xi^2}{2\epsilon\bar{L}^2}} \sum_{\vec{q}\in\mathcal{D}^*} \sqrt{\bar{q}} \left(\hat{b}_{\vec{q}}(t) + \hat{b}^\dagger_{-\vec{q}}(t)\right) \mathrm{e}^{\mathrm{i}\vec{q}\,\cdot\,\vec{r}} \tag{1.21}$$

$$\delta\bar{\phi}(\vec{r}) = \frac{-\mathrm{i}}{\sqrt{2\rho\xi^2}} \frac{\epsilon}{\bar{L}^2} \sum_{\vec{q}\in\mathcal{D}^*} \sqrt{\frac{1}{\bar{q}}} \left(\hat{b}_{\vec{q}}(t) - \hat{b}^\dagger_{-\vec{q}}(t)\right) \mathrm{e}^{\mathrm{i}\vec{q}\,\cdot\,\vec{r}} \tag{1.22}$$

and the phonon spectrum

$$\bar{\varepsilon}_q = \bar{q}\left(1 + \frac{\gamma}{8}\epsilon^2\bar{q}^2\right). \tag{1.23}$$

Hydrodynamic Hamiltonians of order 2 and 3 The second order Hamiltonian as a function of phonon operators $\hat{b}_{\vec{q}}$

$$\bar{H}^{(2)} = \sum_{\vec{k}} \bar{\varepsilon}_k \hat{b}^\dagger_{\vec{k}} \hat{b}_{\vec{k}}, \tag{1.24}$$

third order Hamiltonian as a function of phonon operators

$$\bar{H}^{(3)} = \sqrt{\frac{1}{\bar{L}^2}\frac{\epsilon^3}{8\rho\xi^2}} \sum_{\vec{k}_1;\vec{k}_2;\vec{k}_3\in\mathcal{D}^*} \sqrt{\bar{k}_1\bar{k}_2\bar{k}_3} \left(3\Lambda + u_{\vec{k}_1;\vec{k}_2} + u_{\vec{k}_1;\vec{k}_3} + u_{\vec{k}_2;\vec{k}_3}\right) \tag{1.25}$$
$$\times \left[\frac{1}{2}\delta_{\vec{k}_1+\vec{k}_2;\vec{k}_3}\left(b^\dagger_{\vec{k}_1} b^\dagger_{\vec{k}_2} b_{\vec{k}_3} + \mathrm{h.c.}\right) + \frac{1}{6}\delta_{\vec{k}_1+\vec{k}_2+\vec{k}_3;\vec{0}}\left(b^\dagger_{\vec{k}_1} b^\dagger_{\vec{k}_2} b^\dagger_{\vec{k}_3} + \mathrm{h.c.}\right)\right]$$

and third order Hamiltonian as a function of bosonic field fluctuation operators $\hat{\psi}_{\vec{r}}$

$$\bar{H}^{(3)} = \frac{\epsilon^2}{\sqrt{\rho\xi^2}}\bar{l}^2 \sum_{\vec{r}} \mathrm{Re}\,\delta\bar{\psi}_{\vec{r}} \nabla \left(\mathrm{Im}\,\delta\bar{\psi}_{\vec{r}}\right)^2 + 4\Lambda \left(\mathrm{Re}\,\delta\bar{\psi}_{\vec{r}}\right)^3. \tag{1.26}$$

1.3 Landau-Beliaev damping rate via Fermi's golden rule

The calculation of the damping rate via Fermi's golden rule that we will present in this section 1.3 is not an original result and can be found for example in reference [26]. However, we will present it in detail because it provides a first point of comparison for simulations and because we will use similar notations and arguments in the case of the theory of Green's functions in chapter 3.

Let us consider the situation of a mode $\vec{q}$ out of thermodynamic equilibrium and ask ourselves what is the evolution equation of its average occupancy number $n_{\vec{q}} = \langle \hat{b}^\dagger_{\vec{q}}(t)\hat{b}_{\vec{q}}(t)\rangle$? As we are in the standard case of an Hamiltonian H_0 that is known to be weakly perturbed by an Hamiltonian V with a more complex structure[4] [27] , Fermi's golden rule allows us to answer the question.

[4] Which is better known as "Fermi's golden rule" although it was actually Dirac who did most of the work in 1927 [27]. Only Fermi quoted the equation as the "golden rule n°2" in his book *Nuclear Physics* in 1950. This expression entered the common vocabulary of physics. It is a measure of the immensity of the contributions of these two figures to modern physics that this qui-pro-quo does not in any way affect the intellectual legacy of either of them.

To write the equation for the evolution of the mean population of the non-equilibrium mode $\vec{q}$ according to Fermi's golden rule, we simply list the processes that populate or depopulate the mode $\vec{q}$. Then, these contributions must be summed up with a "+" for those that populate and a "−" for those that depopulate, with the square norm of the matrix element of the perturbation Hamiltonian between the initial and final states of the process as a factor, the occupation numbers of the modes involved before and after the interaction (they intervene through the bosonic amplification factors) and finally the Dirac and Kronecker distributions of conservation of energy and momentum during the process :

$$\begin{aligned}
\frac{\mathrm{d}}{\mathrm{d}t}n_{\vec{q}} = &-\frac{1}{2}\frac{2\pi}{\hbar}\sum_{\vec{k}_1,\vec{k}_2\in\mathcal{D}^*}\left|\langle\vec{k}_1,\vec{k}_2|\hat{H}^{(3)}_{\text{hydro}}|\vec{q}\rangle\right|^2(1+\bar{n}_{k_1})(1+\bar{n}_{k_2})n_{\vec{q}}\delta_{\vec{q},\vec{k}_1+\vec{k}_2}\delta(\varepsilon_{k_1}+\varepsilon_{k_2}-\varepsilon_q) \\
&+\frac{2\pi}{\hbar}\sum_{\vec{k}_1,\vec{k}_2\in\mathcal{D}^*}\left|\langle\vec{q},\vec{k}_2|\hat{H}^{(3)}_{\text{hydro}}|\vec{k}_1\rangle\right|^2(1+n_{\vec{q}})(1+\bar{n}_{k_2})\bar{n}_{k_1}\delta_{\vec{k}_2+\vec{q},\vec{k}_1}\delta(\varepsilon_{k_2}+\varepsilon_q-\varepsilon_{k_1}) \\
&-\frac{2\pi}{\hbar}\sum_{\vec{k}_1,\vec{k}_2\in\mathcal{D}^*}\left|\langle\vec{k}_1|\hat{H}^{(3)}_{\text{hydro}}|\vec{q},\vec{k}_2\rangle\right|^2(1+\bar{n}_{k_1})\bar{n}_{k_2}n_{\vec{q}}\delta_{\vec{q}+\vec{k}_2,\vec{k}_1}\delta(\varepsilon_{k_1}-\varepsilon_{k_2}-\varepsilon_q) \\
&+\frac{1}{2}\frac{2\pi}{\hbar}\sum_{\vec{k}_1,\vec{k}_2\in\mathcal{D}^*}\left|\langle\vec{q}|\hat{H}^{(3)}_{\text{hydro}}|\vec{k}_1,\vec{k}_2\rangle\right|^2(1+n_{\vec{q}})\bar{n}_{k_2}\bar{n}_{k_1}\delta_{\vec{q},\vec{k}_2+\vec{k}_1}\delta(\varepsilon_q-\varepsilon_{k_1}-\varepsilon_{k_2}) \\
&-\frac{1}{2}\frac{2\pi}{\hbar}\sum_{\vec{k}_1,\vec{k}_2\in\mathcal{D}^*}\left|\langle 0|\hat{H}^{(3)}_{\text{hydro}}|\vec{q},\vec{k}_1,\vec{k}_2\rangle\right|^2\bar{n}_{k_1}\bar{n}_{k_2}n_{\vec{q}}\delta_{\vec{q}+\vec{k}_2+\vec{k}_1,\vec{0}}\delta(0-\varepsilon_{k_1}-\varepsilon_{k_2}-\varepsilon_q) \\
&+\frac{1}{2}\frac{2\pi}{\hbar}\sum_{\vec{k}_1,\vec{k}_2\in\mathcal{D}^*}\left|\langle\vec{q},\vec{k}_1,\vec{k}_2|\hat{H}^{(3)}_{\text{hydro}}|0\rangle\right|^2(1+n_{\vec{q}})(1+\bar{n}_{k_2})(1+\bar{n}_{k_1})\delta_{\vec{0},\vec{q}+\vec{k}_2+\vec{k}_1}\delta(\varepsilon_q+\varepsilon_{k_1}+\varepsilon_{k_2}-0)
\end{aligned} \tag{1.27}$$

with $\bar{n}_k$ the thermal occupation number of the $\vec{k}$ mode (which depends only on its norm) and $|0\rangle$ the phonon vacuum. The first sum corresponds to the case where a Beliaev process depopulates the mode $\vec{q}$ from the $|\vec{q}:n_{\vec{q}};\vec{k}_1:\bar{n}_{k_1};\vec{k}_2:\bar{n}_{k_2}\rangle$ state to the $|\vec{q}:n_{\vec{q}}-1;\vec{k}_1:\bar{n}_{k_1}+1;\vec{k}_2:\bar{n}_{k_2}+1\rangle$ state. The factor $1/2$ in front of the sum is a counting factor; indeed, the state vectors obtained by exchanging $\vec{k}_1$ and $\vec{k}_2$ describe the same physical situation that needs to be counted only once. It is sufficient to apply this same logic for each of the processes, moving the supernumerary $\vec{q}$ phonon into the initial or final state and tuning the sign before the sum accordingly. The expression we have just written is very heavy but two observations will simplify it. The first is that the last two sums, related to non-resonant processes, are zero. [5] The second observation is that lines 1 and 4 on the one hand, and 2 and 3 on the other, involve the same matrix element as well as the same Dirac and Kronecker of conservation of energy and momentum (this is a manifestation of the principle of microreversibility). We can therefore re-express the evolution equation (1.27) as the sum of two terms, one associated with the direct and inverse Beliaev processes, the other with the direct and inverse Landau processes:

$$\frac{\mathrm{d}}{\mathrm{d}t}n_{\vec{q}} = \left.\frac{\mathrm{d}n_{\vec{q}}}{\mathrm{d}t}\right|_{\text{Bel}} + \left.\frac{\mathrm{d}n_{\vec{q}}}{\mathrm{d}t}\right|_{\text{Lan}} \tag{1.28}$$

[5] Note that all phonons and sums of phonons involved in a term must lie in the first Brillouin zone deprived of the null vector $\mathcal{D}^*$. Thus, the wave vectors $\vec{k}_1$, $\vec{k}_2$, $\vec{q}$ but also $\vec{k}_1+\vec{k}_2$ in the first line of (1.27), $\vec{k}_2+\vec{q}$ in the second, etc., are concerned.

with

$$\left.\frac{\mathrm{d}n_{\vec{q}}}{\mathrm{d}t}\right|_{\mathrm{Bel}} = -\frac{1}{2}\frac{2\pi}{\hbar}\sum_{\vec{k}_1,\vec{k}_2\in\mathcal{D}^*}\left|\langle\vec{k}_1;\vec{k}_2|\hat{H}^{(3)}_{\mathrm{hydro}}|\vec{q}\rangle\right|^2\left[(1+\bar{n}_{k_1})(1+\bar{n}_{k_2})n_{\vec{q}}-(1+n_{\vec{q}})\bar{n}_{k_2}\bar{n}_{k_1}\right] \tag{1.29}$$
$$\times\,\delta_{\vec{q};\vec{k}_1+\vec{k}_2}\delta(\varepsilon_{k_1}+\varepsilon_{k_2}-\varepsilon_q)$$

$$\left.\frac{\mathrm{d}n_{\vec{q}}}{\mathrm{d}t}\right|_{\mathrm{Lan}} = -\frac{2\pi}{\hbar}\sum_{\vec{k}_1,\vec{k}_2\in\mathcal{D}^*}\left|\langle\vec{k}_1|\hat{H}^{(3)}_{\mathrm{hydro}}|\vec{q};\vec{k}_2\rangle\right|^2\left[(1+\bar{n}_{k_1})\bar{n}_{k_2}n_{\vec{q}}-(1+n_{\vec{q}})(1+\bar{n}_{k_2})\bar{n}_{k_1}\right] \tag{1.30}$$
$$\times\,\delta_{\vec{q}+\vec{k}_2;\vec{k}_1}\delta(\varepsilon_{k_1}-\varepsilon_{k_2}-\varepsilon_q).$$

Let us now consider a regime of small perturbation of the mode $\vec{q}$ around the thermodynamic equilibrium state $n_{\vec{q}} = \bar{n}_q + \delta n_{\vec{q}}$. It is easy to verify that the evolution equation (1.28) is identically zero for $n_{\vec{q}} = \bar{n}_{\vec{q}}$. Indeed, for a gas of bosons, the thermodynamic equilibrium obeys the Bose-Einstein distribution law $\bar{n}_k = \frac{1}{\exp(\beta\varepsilon_k)-1}$ with $\beta = \frac{1}{k_B T}$ rewritten as $1+\bar{n}_k = \exp(\beta\varepsilon_k)\bar{n}_k$. Using this relation in the expressions in square brackets in (1.29) and (1.30), we find that they cancel out given the Dirac of conservation of energy. At first order in the mode $\vec{q}$ perturbation, we then have

$$\frac{\mathrm{d}}{\mathrm{d}t}\delta n_{\vec{q}} = -\Gamma_{\vec{q}}\delta n_{\vec{q}} \tag{1.31}$$

with

$$\Gamma_{\vec{q}} = \Gamma^{\mathrm{Bel}}_{\vec{q}} + \Gamma^{\mathrm{Lan}}_{\vec{q}} \tag{1.32}$$

and

$$\Gamma^{\mathrm{Bel}}_{\vec{q}} = \frac{\pi}{\hbar}\sum_{\vec{k}\in\mathcal{D}^*}\left|\langle\vec{k};\vec{q}-\vec{k}|\hat{H}^{(3)}_{\mathrm{hydro}}|\vec{q}\rangle\right|^2\left(1+\bar{n}_k+\bar{n}_{|\vec{q}-\vec{k}|}\right)\delta(\varepsilon_k+\varepsilon_{|\vec{q}-\vec{k}|}-\varepsilon_q) \tag{1.33}$$

$$\Gamma^{\mathrm{Lan}}_{\vec{q}} = \frac{2\pi}{\hbar}\sum_{\vec{k}\in\mathcal{D}^*}\left|\langle\vec{k}+\vec{q}|\hat{H}^{(3)}_{\mathrm{hydro}}|\vec{q};\vec{k}\rangle\right|^2\left(\bar{n}_k-\bar{n}_{|\vec{q}+\vec{k}|}\right)\delta(\varepsilon_{|\vec{q}+\vec{k}|}-\varepsilon_k-\varepsilon_q) \tag{1.34}$$

where we have used the Kronecker of conservation of momentum. These quantities $\Gamma_{\vec{q}}$, $\Gamma^{\mathrm{Bel}}_{\vec{q}}$ and $\Gamma^{\mathrm{Lan}}_{\vec{q}}$ can therefore be interpreted as damping rates of the perturbation or as thermalization rates of the mode. In the remainder of this section, we unroll the calculation to obtain the rate $\Gamma_{\vec{q}}$ in the limit of a reduced temperature small before 1, i.e. $\epsilon \ll 1$. We will proceed process by process, the calculations for Beliaev and Landau being almost identical. The plan of the calculation is the following : we pass to the thermodynamic limit in order to consider the expressions of $\Gamma^{\mathrm{Bel}}_{\vec{q}}$ and $\Gamma^{\mathrm{Lan}}_{\vec{q}}$ as integrals on the variable $\vec{k}$. In polar coordinates of axis $\vec{q}$, they are double integrals, one on the norm k, the other on the angle θ between $\vec{k}$ and $\vec{q}$. We then move to the classical field approximation, which modifies the distribution law and thus the population factor in the integrals, but also introduces a cut η on the norm of the wave vectors $\vec{k}$ and $\vec{q}\mp\vec{k}$. We then place ourselves in the $\epsilon\to 0$ limit and express the Dirac of energy conservation in terms of the θ variable at leading order in ϵ. We obtain solutions θ_0 which we reintroduce into the now simple integral which we can integrate directly.

1.3.1 Expressions of the scaled rates as integrals over the momenta

Furthermore, we will do all the rest of the calculation in the scaled variables introduced in section 1.2 of this chapter. From the expression (1.25) of $\bar{H}^{(3)}$, let us express the matrix elements (scaled, therefore) involved in (1.33) and (1.34)

$$\langle \vec{k}; \vec{q}-\vec{k}|\bar{H}^{(3)}|\vec{q}\rangle = 2\sqrt{\frac{1}{\bar{L}^2}\frac{\epsilon^3}{2^5\rho\xi^2}}\sqrt{\bar{q}\bar{k}|\vec{q}-\vec{k}|}\left(3\Lambda + u_{\vec{q},\vec{k}} + u_{\vec{k},\vec{q}-\vec{k}} + u_{\vec{q},\vec{q}-\vec{k}}\right) \tag{1.35}$$

$$\langle \vec{k}+\vec{q}|\bar{H}^{(3)}|\vec{q}; \vec{k}\rangle = 2\sqrt{\frac{1}{\bar{L}^2}\frac{\epsilon^3}{2^5\rho\xi^2}}\sqrt{\bar{q}\bar{k}|\vec{q}+\vec{k}|}\left(3\Lambda + u_{\vec{q},\vec{k}} + u_{\vec{k},\vec{q}+\vec{k}} + u_{\vec{q},\vec{q}+\vec{k}}\right). \tag{1.36}$$

To perform the crossing to the thermodynamic limit, we simply make the transformation $\sum_{\vec{k}\in\mathcal{D}^*} \to \bar{L}^2 \int \frac{\mathrm{d}^2\vec{k}}{(2\pi)^2}$ and insert the matrix elements :

$$\bar{\Gamma}_q^{\mathrm{Bel}} = \frac{\epsilon^3\pi}{2^3\rho\xi^2}\int \frac{\mathrm{d}^2\vec{k}}{(2\pi)^2}\bar{q}\bar{k}|\vec{q}-\vec{k}|\left(3\Lambda + u_{\vec{q},\vec{k}} + u_{\vec{k},\vec{q}-\vec{k}} + u_{\vec{q},\vec{q}-\vec{k}}\right)^2\left(1+\bar{n}_k+\bar{n}_{|\vec{q}-\vec{k}|}\right)\delta(\bar{\varepsilon}_k + \bar{\varepsilon}_{|\vec{q}-\vec{k}|} - \bar{\varepsilon}_q) \tag{1.37}$$

$$\bar{\Gamma}_q^{\mathrm{Lan}} = \frac{\epsilon^3\pi}{2^2\rho\xi^2}\int \frac{\mathrm{d}^2\vec{k}}{(2\pi)^2}\bar{q}\bar{k}|\vec{q}+\vec{k}|\left(3\Lambda + u_{\vec{q},\vec{k}} + u_{\vec{k},\vec{q}+\vec{k}} + u_{\vec{q},\vec{q}+\vec{k}}\right)^2\left(\bar{n}_k-\bar{n}_{|\vec{q}+\vec{k}|}\right)\delta(\bar{\varepsilon}_{|\vec{q}+\vec{k}|} - \bar{\varepsilon}_k - \bar{\varepsilon}_q). \tag{1.38}$$

We introduce θ the angle between $\vec{q}$ and $\vec{k}$. Then, by definition, we can write $u_{\vec{q},\vec{k}} = \cos\theta$ and

$$u_{\vec{q},\vec{k}} + u_{\vec{q},\vec{q}-\vec{k}} + u_{\vec{k},\vec{q}-\vec{k}} = \cos\theta + \frac{\bar{q}-\bar{k}}{|\vec{q}-\vec{k}|}(1+\cos\theta) \tag{1.39}$$

$$u_{\vec{q},\vec{k}} + u_{\vec{q},\vec{q}+\vec{k}} + u_{\vec{k},\vec{q}+\vec{k}} = \cos\theta + \frac{\bar{q}+\bar{k}}{|\vec{q}+\vec{k}|}(1+\cos\theta). \tag{1.40}$$

Thus

$$\bar{\Gamma}_q^{\mathrm{Bel}} = \frac{\epsilon^3}{2^5\pi\rho\xi^2}\int_0^{+\infty}\mathrm{d}\bar{k}\int_{-\pi}^{+\pi}\mathrm{d}\theta\,\bar{q}\bar{k}^2|\vec{q}-\vec{k}|\left(3\Lambda+\cos\theta+\frac{\bar{q}-\bar{k}}{|\vec{q}-\vec{k}|}(1+\cos\theta)\right)^2 \times\left(1+\bar{n}_k+\bar{n}_{|\vec{q}-\vec{k}|}\right)\delta(\bar{\varepsilon}_k+\bar{\varepsilon}_{|\vec{q}-\vec{k}|}-\bar{\varepsilon}_q) \tag{1.41}$$

$$\bar{\Gamma}_q^{\mathrm{Lan}} = \frac{\epsilon^3}{2^4\pi\rho\xi^2}\int_0^{+\infty}\mathrm{d}\bar{k}\int_{-\pi}^{+\pi}\mathrm{d}\theta\,\bar{q}\bar{k}^2|\vec{q}+\vec{k}|\left(3\Lambda+\cos\theta+\frac{\bar{q}+\bar{k}}{|\vec{q}+\vec{k}|}(1+\cos\theta)\right)^2 \times\left(\bar{n}_k-\bar{n}_{|\vec{q}+\vec{k}|}\right)\delta(\bar{\varepsilon}_{|\vec{q}+\vec{k}|}-\bar{\varepsilon}_k-\bar{\varepsilon}_q). \tag{1.42}$$

1.3.2 Classical field solution

Although it is possible to finish the calculation directly for the quantum field, we present in detail here only the classical field version since it is in this approximation that the computer

program of the simulations was written, which allows a direct comparison. The classical field approximation consists of considering only the highly populated modes, such as $n_{\vec{q}} \geq 1$, and ignoring the sparsely populated ones for which the Bose and Boltzmann distributions are radically different. We must therefore introduce a cut-off in the momentum space, here noted η, to which all (scaled) wave numbers that appear must be smaller. In this approximation, the model can no longer be compared quantitatively with experiments because all derived quantities will depend on this non-physical parameter η which we choose at will.

For our two integrals, going to the classical field limit imposes three modifications. The first is to remove from the population factors the term $+1$ which represents the contribution of quantum fluctuations, ignored in this approximation. The second is to consider for the thermal occupancy number of a mode the equipartition formula of classical statistical physics $\bar{n}_q = \frac{k_B T}{\varepsilon_q} = \frac{1}{\bar{\varepsilon}_q}$. The last one is to consider the "ultraviolet" cut-off η on each phonon involved in the process. Of course, we choose the mode $\vec{q}$ such that it is allowed, i.e. $\bar{q} \leq \eta$. For the two other phonons of each process, we insert in the corresponding integral as many times as necessary a Heaviside function $\Theta(x)$, null for $x < 0$ and equal to 1 otherwise. That is to say, by parity, integrals on $\theta > 0$,

$$\bar{\Gamma}_q^{\mathrm{Bel}} = \frac{\epsilon^3}{16\pi\rho\xi^2} \int_0^{+\infty} \mathrm{d}\bar{k} \int_0^{+\pi} \mathrm{d}\theta \bar{q}\bar{k}^2 \overline{|\vec{q}-\vec{k}|} \left(3\Lambda + \cos\theta + \frac{\bar{q}-\bar{k}}{\overline{|\vec{q}-\vec{k}|}}(1+\cos\theta) \right)^2 \times \left(\frac{1}{\bar{\varepsilon}_k} + \frac{1}{\bar{\varepsilon}_{|\vec{q}-\vec{k}|}} \right) \delta(\bar{\varepsilon}_k + \bar{\varepsilon}_{|\vec{q}-\vec{k}|} - \bar{\varepsilon}_q) \Theta(\eta - \bar{k}) \Theta(\eta - \overline{|\vec{q}-\vec{k}|}) \tag{1.43}$$

$$\bar{\Gamma}_q^{\mathrm{Lan}} = \frac{\epsilon^3}{8\pi\rho\xi^2} \int_0^{+\infty} \mathrm{d}\bar{k} \int_0^{+\pi} \mathrm{d}\theta \bar{q}\bar{k}^2 \overline{|\vec{q}+\vec{k}|} \left(3\Lambda + \cos\theta + \frac{\bar{q}+\bar{k}}{\overline{|\vec{q}+\vec{k}|}}(1+\cos\theta) \right)^2 \times \left(\frac{1}{\bar{\varepsilon}_k} - \frac{1}{\bar{\varepsilon}_{|\vec{q}+\vec{k}|}} \right) \delta(\bar{\varepsilon}_{|\vec{q}+\vec{k}|} - \bar{\varepsilon}_k - \bar{\varepsilon}_q) \Theta(\eta - \bar{k}) \Theta(\eta - \overline{|\vec{q}+\vec{k}|}). \tag{1.44}$$

1.3.3 Development to the leading order in ϵ

We will go to the limit of an $\epsilon \ll 1$, a choice motivated by the validity regime of quantum hydrodynamics. However, we could have solved these (1.43) and (1.44) integrals numerically, which we did by calculating numerically the eigenenergy function, of which these integrals are only the value at a particular point, in order to obtain a diagrammatic prediction of the Green's functions at all orders in ϵ, as we shall see in chapter 3. Our resolution to the leading order in ϵ relies on the fact that for a sufficiently small reduced temperature, the angle θ_0 that satisfies energy conservation is itself small.

The energy conservation relations in each of the Diracs are expressed in terms of θ as follows:

$$\bar{\varepsilon}_k + \bar{\varepsilon}_{|\vec{q}-\vec{k}|} - \bar{\varepsilon}_q = \bar{k} - \bar{q} + \frac{\gamma}{8}\epsilon^2(\bar{k}^3 - \bar{q}^3) + (\bar{k}^2 + \bar{q}^2 - 2\bar{k}\bar{q}\cos\theta)^{1/2} + \frac{\gamma}{8}\epsilon^2(\bar{k}^2 + \bar{q}^2 - 2\bar{k}\bar{q}\cos\theta)^{3/2} \tag{1.45}$$

$$\bar{\varepsilon}_{|\vec{q}+\vec{k}|} - \bar{\varepsilon}_q - \bar{\varepsilon}_k = (\bar{q}^2 + \bar{k}^2 + 2\bar{q}\bar{k}\cos\theta)^{1/2} + \frac{\gamma}{8}\epsilon^2(\bar{q}^2 + \bar{k}^2 + 2\bar{q}\bar{k}\cos\theta)^{3/2} - \bar{q} - \frac{\gamma}{8}\epsilon^2\bar{q}^3 - \bar{k} - \frac{\gamma}{8}\epsilon^2\bar{k}^3. \tag{1.46}$$

Let θ_0 be the positive solution in the variable θ of the equation $\bar{\varepsilon}_k + \bar{\varepsilon}_{|\vec{q}-\vec{k}|} - \bar{\varepsilon}_q = 0$ or $\bar{\varepsilon}_{|\vec{q}+\vec{k}|} - \bar{\varepsilon}_k - \bar{\varepsilon}_q = 0$ with $\bar{k}$ and $\bar{q}$ fixed. We are convinced that in the limit $\epsilon \to 0$, the solution of these equations is $\theta_0 = 0$ (for Beliaev, however, a real solution exists only for $\bar{k} \leq \bar{q}$). Therefore, by continuity, we can assume that for a sufficiently small ϵ we have $\theta_0 \ll 1$. Let us take the expressions of the Dirac arguments (1.45) and (1.46) and expand them to the small angles (and to the dominant order in ϵ) :

$$\bar{\varepsilon}_k + \bar{\varepsilon}_{|\vec{q}-\vec{k}|} - \bar{\varepsilon}_q = \bar{k} - \bar{q} + |\bar{k} - \bar{q}| + \frac{\gamma}{8}\epsilon^2 \left(\bar{k}^3 - \bar{q}^3 + |\bar{k} - \bar{q}|^3\right) + \frac{\bar{k}\bar{q}}{|\bar{k} - \bar{q}|}\frac{\theta^2}{2} + O(\theta^4) \tag{1.47}$$

$$\bar{k} > \bar{q} \quad : \quad \bar{\varepsilon}_k + \bar{\varepsilon}_{|k-q|} - \bar{\varepsilon}_q = 2(\bar{k} - \bar{q}) + \frac{\bar{k}\bar{q}}{\bar{k} - \bar{q}}\frac{\theta^2}{2} + O(\theta^4) \tag{1.48}$$

$$\longrightarrow \quad \text{no solution in } \theta.$$

$$\bar{k} \leq \bar{q} \quad : \quad \bar{\varepsilon}_k + \bar{\varepsilon}_{|k-q|} - \bar{\varepsilon}_q = \frac{3\gamma}{8}\epsilon^2 \bar{q}\bar{k}\left(\bar{q} - \bar{k}\right) + \frac{\bar{k}\bar{q}}{\bar{q} - \bar{k}}\frac{\theta^2}{2} + O(\theta^4) \tag{1.49}$$

$$\longrightarrow \quad \theta_0^2 \simeq \frac{3\gamma}{4}\epsilon^2 \left(\bar{q} - \bar{k}\right)^2. \tag{1.50}$$

$$\bar{\varepsilon}_{|\vec{q}+\vec{k}|} - \bar{\varepsilon}_q - \bar{\varepsilon}_k = \frac{3\gamma}{8}\bar{q}\bar{k}(\bar{q} + \bar{k})\epsilon^2 - \frac{\bar{q}\bar{k}}{2(\bar{q} + \bar{k})}\theta^2 + O(\theta^4) \tag{1.51}$$

$$\longrightarrow \quad \theta_0^2 \simeq \frac{3\gamma}{4}\epsilon^2 \left(\bar{q} + \bar{k}\right)^2. \tag{1.52}$$

It is these θ_0 solutions that we must now insert into the integral to take account of the Dirac of conservation of energy. Let us note here that the energy denominators are of order 2 in ϵ (when a solution exists), this observation will be of great importance in chapter 3 when higher order diagrams are discussed.

1.3.4 Integration

Let us first recall the formula $\delta(f(x)) = \sum_{x^*} \frac{\delta(x-x^*)}{|f'(x^*)|}$ for the Dirac of any differentiable function f , with f' its derivative and $\{x^*\}$ its roots. Thus, for the angular integration of the Dirac of conservation of energy, we need the derivatives with respect to θ of the equations (1.45) and (1.46) evaluated at the solutions θ_0, i.e., at the leading order in ϵ,

$$\left|\frac{\mathrm{d}}{\mathrm{d}\theta}(\bar{\varepsilon}_k + \bar{\varepsilon}_{|\vec{q}-\vec{k}|} - \bar{\varepsilon}_q)(\theta_0)\right| \simeq \frac{\sqrt{3\gamma}}{2}\bar{k}\bar{q}\epsilon \tag{1.53}$$

$$\left|\frac{\mathrm{d}}{\mathrm{d}\theta}(\bar{\varepsilon}_{|\vec{q}+\vec{k}|} - \bar{\varepsilon}_q - \bar{\varepsilon}_k)\right| \simeq \frac{\sqrt{3\gamma}}{2}\bar{k}\bar{q}\epsilon. \tag{1.54}$$

All that remains is to gather all its ingredients to calculate the integral according to θ,

$$\bar{\Gamma}_q^{\mathrm{Bel}} = \frac{\epsilon^2}{2^3\sqrt{3\gamma}\pi\rho\xi^2}\int_0^{\bar{q}} \mathrm{d}\bar{k}\,\bar{k}(\bar{q} - \bar{k})\,(3\Lambda + 3)^2 \left(\frac{1}{\bar{k}} + \frac{1}{\bar{q} - \bar{k}}\right)\Theta(\eta - \bar{k})\Theta(\eta - (\bar{q} - \bar{k})) \tag{1.55}$$

$$\bar{\Gamma}_q^{\mathrm{Lan}} = \frac{\epsilon^2}{2^2\sqrt{3\gamma}\pi\rho\xi^2}\int_0^{+\infty} \mathrm{d}\bar{k}\,\bar{k}(\bar{q} + \bar{k})\,(3\Lambda + 3)^2 \left(\frac{1}{\bar{k}} - \frac{1}{\bar{q} + \bar{k}}\right)\Theta(\eta - \bar{k})\Theta(\eta - (\bar{q} + \bar{k})). \tag{1.56}$$

The integration in Beliaev is restricted to $\bar{k} \leq \bar{q}$ because there is no solution above $\bar{q}$ as we have seen. Note that $\eta - \bar{q} \geq 0$ and $\eta - (\bar{q} - \bar{k}) \geq 0$ for $\bar{k} \in [0; \bar{q}]$ so the Heaviside functions in Beliaev have no effect on the integration. In Landau on the other hand, the second Heaviside function imposes $[0; \eta - \bar{q}]$ as the integration interval. This being said, the integrals can simply be carried out and give:

$$\bar{\Gamma}_q^{\text{Bel}} = \frac{9\,(1+\Lambda)^2\,\epsilon^2}{2^3\sqrt{3\gamma}\pi\rho\xi^2}\bar{q}^2 \tag{1.57}$$

$$\bar{\Gamma}_q^{\text{Lan}} = \frac{9\,(1+\Lambda)^2\,\epsilon^2}{2^2\sqrt{3\gamma}\pi\rho\xi^2}\bar{q}(\eta - \bar{q}). \tag{1.58}$$

Hence the damping rate of phonon of momentum $\vec{q}$, calculated according to the Fermi-Dirac golden rule and for the classical field, is written

$$\boxed{\bar{\Gamma}_q^{\text{class}} = \frac{9}{4}\frac{(1+\Lambda)^2}{\sqrt{3\gamma}\pi}\frac{\epsilon^2}{\rho\xi^2}\bar{q}\left(\eta - \frac{\bar{q}}{2}\right).} \tag{1.59}$$

Note that it depends quadratically on $\bar{q}$ and that it is of order 2 in ϵ.

Returning to the quantum case For the sake of completeness, let us return to the quantum case. Once we have passed the limit $\epsilon \to 0$, we are led to write

$$\bar{\Gamma}_q^{\text{quant}} = \frac{9}{8}\frac{(1+\Lambda)^2}{\sqrt{3\gamma}\pi}\frac{\epsilon^2}{\rho\xi^2}\left(I_B + 2I_L\right) \tag{1.60}$$

with I_B and I_L two integrals from the Beliaev and Landau case respectively

$$I_B = \int_0^{\bar{q}} \mathrm{d}\bar{k}\,\bar{k}(\bar{q} - \bar{k})(1 + \bar{n}_k + \bar{n}_{q-k}) \tag{1.61}$$

$$I_L = \int_0^{+\infty} \mathrm{d}\bar{k}\,\bar{k}(\bar{q} + \bar{k})(\bar{n}_k - \bar{n}_{q+k}) \tag{1.62}$$

with this time $\bar{n}_k = 1/(\mathrm{e}^{\bar{k}} - 1)$. It turns out that it is possible to express these integrals separately using Bose functions $g_\alpha(z) = \sum_{n=1}^{\infty}\frac{z^n}{n^\alpha}$ but that these functions compensate each other when the integrals are added together! So we have $I_B + 2I_L = \frac{\bar{q}^3}{6} + 4\bar{q}\zeta(2)$ with $\zeta(2) = \frac{\pi^2}{6}$ the value of the Riemann zeta function $\zeta(s)$ in $s = 2$, and

$$\boxed{\bar{\Gamma}_q^{\text{quant}} = \frac{9}{8}\frac{(1+\Lambda)^2}{\sqrt{3\gamma}\pi}\frac{\epsilon^2}{\rho\xi^2}\bar{q}\left(\frac{2\pi^2}{3} + \frac{\bar{q}^2}{6}\right).} \tag{1.63}$$

Let's compare our result with the paper by M.-C. Chung and A.B. Bhattacherjee (2009) [26]. The authors present calculations of phonon damping in weakly interacting boson gases in the $d = 2$ and $d = 3$ case. In 2D and in the low temperature limit $k_BT/mc^2 \to 0$, they find the boundary behaviours (see equations (30) and (22) of [26] written in our notations taking into account a factor of 2 in the definition of the rates)

$$\Gamma_q \underset{\bar{q}\to 0}{\sim} \frac{\sqrt{3}\pi}{4\rho}\left(\frac{k_BT}{\hbar c}\right)^2 cq \tag{1.64}$$

$$\Gamma_q \underset{\bar{q}\to \infty}{\sim} \frac{\sqrt{3}}{16\pi\rho}cq^3. \tag{1.65}$$

The behaviour at small q being dominated by Landau and that at high q by Beliaev. In the weak interaction limit, one should take $\gamma = 1$ (as in the Bogolioubov spectrum) and $\Lambda = 0$ (as in the mean field equation of state $\mu = \rho g$); these results are then in perfect agreement with ours (1.63).

On the other hand, the recent study [17] predicts well, in the $q \to 0$ limit, a linear damping rate in q but with a coefficient $\propto T$ at low temperature, in disagreement with (1.64) and with the reference [26]. Indeed, the method used, based on the Hartree-Fock approximation, does not take into account the linear part of the excitation spectrum in the description of the thermal state, see equation (11) of this reference, which becomes unrealistic when $k_B T \ll mc^2$ where the thermodynamics is dominated by phonons (a similar study was done in reference [18]).

Chapter 2

The numerical simulation

Foreword

In this chapter, we present the program for the numerical simulation. That is to say, its structure, its parameters and the modelling choices that governed its writing, as well as the numerical methods that we used. We leave the exploitation of the data from the program executions, the physical discussion of the chosen parameters as well as the figures verifying the respect of the good physical properties of the system to chapter 4, which presents all our results. The program is written in Fortran.[1]

The object whose evolution the computer program determines is the classical field $\delta\psi_{\vec{r}} = \sqrt{\rho}(\frac{\delta\rho}{2\rho} + i\delta\phi)$ which describes the fluctuations of a bosonic field $\psi_{\vec{r}} = \sqrt{\rho(\vec{r})}e^{i\phi(\vec{r})}$ around the homogeneous case $\psi_0 = \sqrt{\rho}$ of the thermodynamic equilibrium. This field lives in a two-dimensional quantization box with periodic boundary conditions. In practice, one can therefore express the $\psi_{\vec{r}}$ field through the $a_{\vec{q}}$ coefficients of its plane wave development or its $b_{\vec{q}}$ coefficients on the phonon modes (see equations (1.11), (1.12) and (1.19)). So it is represented in the computer by an array of complex numbers with two entries.[2] Each element of these arrays represents either the value of the field at a given position in the box (for ψ) or the value of the field for a given wave vector (for $a_{\vec{q}}$ and $b_{\vec{q}}$). To have a finite number of coefficients $a_{\vec{q}}$ we have to make an approximation : we have to discretize the space. The program is written in such a way as to be centred on the array $b_{\vec{q}}$ which is taken as the object of the program, the other arrays only intervening as calculation intermediaries in the functions which carry out the evolution. The core of the program thus consists in taking as input an array $b_{\vec{q}}$, a Hamiltonian and a time step and in giving as output an array $b'_{\vec{q}}$, an estimate of the field evolved by the Hamiltonian. In other words, we want to integrate the time functions $b_{\vec{q}}(t)$ of evolution governed by the system of differential equations (2.2) between an initial 0 and final $\bar{t}_{\max}$ time. To define such an evolution, we need a number of

[1] It is a powerful and very accomplished language, particularly adapted to scientific and numerical calculations, which is why it is still one of the most used languages for high performance computing and supercomputers, in spite of its venerable age. Its crucial advantage lies in its high computational performance for arithmetic on very large arrays. Furthermore, its longevity and continued presence in the scientific world has led to the emergence of highly optimised computing libraries, some of which have been tested and debugged for decades. In this project, for example, it is a well-known fast Fourier transform program written by Daisuke Takahashi [28] that we have intensively used for the temporal evolution of the system as we will see.

[2] Numbers numerically represented by two floats in double precision.

parameters that fix the characteristics of the box, the fluid in it and the Hamiltonian, i.e. the interactions that take place in it. Since we cannot integrate the system of differential equations of $b_{\vec{q}}$ analytically, it is necessary to introduce a number of approximations in the numerical treatment of these equations. At regular intervals during the integration, we store on disk the values of the $b_{\vec{q}}$ for a number of modes. It is from these saved values that we can extract an estimate of the $\langle b_{\vec{q}}(t) b^*_{\vec{q}}(0)\rangle$ observable. In our simulations, the $\langle \ldots \rangle$ is averaged over a sufficient number of independent trajectories that are representative of a thermodynamic equilibrium state.

This chapter is divided into two main sections. The first section introduces the program by presenting the main lines of the simulation, such as the issue of discretization, the estimation of ensemble averages $\langle \ldots \rangle$ before concluding by summarizing the numerical input parameters of the program. The second section presents the implementation of the Hamiltonian evolution of the field. It begins with a discussion of the initialization of the system before describing the algorithm that realizes a time step in practice by describing the various numerical methods and approximations that we had to use to integrate the differential equations quickly but accurately.

2.1 Program structure

2.1.1 Space discretization: network size and step

Let us note L_x and L_y the two lengths that fix the size of the two-dimensional box. As mentioned in the foreword, we need to consider a finite set of possible positions in the box in order to model the problem numerically. Thus, we discretise the space into its two directions with a unit cell of length l_x and l_y respectively. We will then represent any field in this rectangular box as a two-entry array of $n_x n_y$ elements with $n_x = L_x/l_x$ and $n_y = L_y/l_y$, the number of points in each direction. For the sake of brevity, the results for $L_x = L_y$ and $n_x = n_y$ are given (we have performed some calculations for $L_x \neq L_y$ without observing much change in the results). Furthermore, we consider a box with periodic boundary conditions according to Ox and Oy. This discretization imposes a cut in the reciprocal space and amounts to limiting the wave vectors to the first Brillouin zone

$$k_\alpha \in \left[-\frac{\pi}{l_\alpha}, \frac{\pi}{l_\alpha}\right[\quad \text{with} \quad \alpha = x, y. \tag{2.1}$$

2.1.2 Umklapp process

The treatment of real space by means of a discrete grating has a bad consequence in the reciprocal space of the momenta : the appearance of so-called Umklapp processes. Consider two wave vectors, say $\vec{k}_1$ and $\vec{k}_2$, of the first Brillouin zone just defined. It is quite possible that the sum wave vector (one can imagine the coalescence of two phonons into a third) is outside the first Brillouin zone. Taking into account the periodicity of space, one could translate this sum vector as equivalent to a vector of the first zone. But this equivalence implies a loss of momentum conservation (only the quasi-momentum is conserved)! In crystals and solids in general, these processes are called "Umklapp" and are quite physical and play an important role in the thermodynamic and propagation properties; they correspond to oscillations of smaller wavelength than the fundamental unit cell, the effective wave can

then be associated to a wave vector of the first Brillouin zone. In our case, the underlying numerical "crystal" is completely artificial and should not play any role in the field dynamics. It is therefore crucial to never allow an Umklapp process when calculating phonon interactions. For this purpose, we define a numerical lattice twice as large as the physical Brillouin zone lattice. That is, all arrays will have $n_x n_y$ elements with $n_x = 2n_x^{\mathrm{FBZ}}$, $n_y = 2n_y^{\mathrm{FBZ}}$. The first Brillouin zone is then the inner rectangle of this array with dimensions $n_x^{\mathrm{FBZ}}, n_y^{\mathrm{FBZ}}$. In the following, only the wave vectors of the first Brillouin zone are considered as physical, the others only exist to manage the Umklapp processes numerically. In fact, thanks to the doubling of the network, each time we have to sum two wave vectors of the first Brillouin zone, the Umklapp processes will involve points of the non-physical numerical zone, on which we will be able to set to 0 the value of the field at each time step. This aspect, which is called "filtering of Umklapp processes", will be clarified in section two when we detail the algorithm for the evolution of the array. Finally, it should be noted that the origin of the reciprocal array, the null wave vector $\vec{0}$, is one of the unphysical modes that we will have to filter out as it is a phonon forbidden mode.

In practice, it is these numbers of physical modes $n_x^{\mathrm{FBZ}}, n_y^{\mathrm{FBZ}}$ per direction that are used as input parameters to the program.

2.1.3 The ultraviolet cutoff

Our program works in the classical field approximation which replaces the bosonic operator $\hat{b}_{\vec{q}}$ by a complex variable. Numerically, we must therefore manipulate an array of two-dimensional complex numbers of numerical size $n_x n_y$. This transformation into a classical field requires the introduction of a cut-off in the momentum space to avoid the catastrophe of the blackbody radiation. We will therefore retain as physical only the wave vectors $\vec{q}$ such as $q \leq q_{\max}$ corresponding to the energy cut-off $\hbar c q_{\max} = \eta k_B T$ with η a positive real number, which is an input parameter of the program. For this classical treatment to be physically consistent, it is necessary for the cut-off to be high enough to retain the populated modes but low enough to ignore the modes governed by quantum fluctuations, i.e. modes whose average population at thermodynamic equilibrium is very small compared to 1. This is why we have always taken $\eta = 1$ in our simulations. Note that considering the scaled quantities, we have $\bar{q}_{\max} = \eta$.

2.1.4 Estimation of an ensemble average

As we mentioned in the introduction, the evolution we will apply to the system is Hamiltonian. This implies that the evolution is deterministic. However, running the program once would not allow us to recover the complete information about the evolution of the observable simply because we are interested in the evolution in the macroscopic state of thermodynamic equilibrium. To obtain this overall evolution, we must start from a microscopic state taken from the probability law of the thermodynamic equilibrium and make the system evolve. By repeating these two steps and averaging the trajectories obtained, we must converge to the ensemble averages of the thermodynamic equilibrium. Thus the number of trajectories to be performed is also an input parameter which we note n_{traj} but which is always 3200 in the results of this thesis.

2.1.5 Summary of input parameters

The program is written entirely in terms of the scaled quantities introduced in chapter 1. To define the system, the reduced temperature $\epsilon = \frac{k_B T}{mc^2}$, the density of the gas at equilibrium (scaled by the relaxation length) $\rho\xi^2$, the thermodynamic parameter Λ and the curvature of the phonon spectrum γ must be given. These physical parameters determine the interactions between phonons in the gas as well as all the thermodynamic variables. Then, an ultraviolet cut-off η and a number of physical modes per direction n_x^{FBZ} must be provided which fix the size of the system by the relations $n_x = 2n_x^{\mathrm{FBZ}}$, $\bar{l}_x = \pi/(2\eta)$ and $\Delta\bar{k}_x = 2\eta/n_x^{\mathrm{FBZ}}$ (scaled form of $\Delta k_x = 2\pi/L_x$) with $\Delta\bar{k}_x$ the reciprocal lattice length in the direction x and thus $\bar{L}_x = n_x\bar{l}_x$ (similarly for the direction y). Finally, we need to define a time integration step, $\Delta\bar{t}$, an integration time $\bar{t}_{\max}$ and the number of trajectories n_{traj} to be performed and averaged. We list these parameters in the following table.

Physical input parameters	Description	Used value in our simulations
ϵ	reduced temperature of the gas	1/2 or 1/3
γ	Curature of the phonon spectrum	1
$\rho\xi^2$	Scaled equilibrium density of the gas	10 or 1.5625
Λ	Thermodynamic parameter	0
Numerical input parameters		
η	Ultraviolet cut-off on momentum	1
$n_x^{\mathrm{FBZ}} \times n_y^{\mathrm{FBZ}}$	Number of physical modes (FBZ)	32×32, 64×64, 128×128
$\Delta\bar{t}$	Time step for the temporal integration	1/8 or 0.0195
$\bar{t}_{\max}$	Integration time	10^3 or 10^4
n_{traj}	Number of independant trajectories	3200
Derived parameteres		
$n_x = 2n_x^{\mathrm{FBZ}}$ and n_y	Size of the numerical arrays	64, 128, 256
$\bar{l}_x = \pi/(2\eta)$ and $\bar{l}_y$	Unit cell length in position space	$\pi/2$
$\Delta\bar{k}_x = 2\eta/n_x^{\mathrm{FBZ}}$ and $\Delta\bar{k}_y$	Unit cell length in momentum space	1/16, 1/32, 1/64

2.2 Implementation of Hamiltonian evolution

This section is devoted to the description of the time evolution algorithm. However, we will first describe the method of drawing the initial state of the system sampling the thermal equilibrium for the full Hamiltonian. As there is no obvious direct way to do this in the presence of phonon interactions, an indirect method is used which involves time evolution. In the following, we deal with the differential equations to be solved with the approximations that allow us to integrate them on a time step $\Delta\bar{t}$.

2.2.1 Initialization of the field

As we explained in the previous section, at each new trajectory, we have to initialize the $b_{\vec{k}}$ array with a state taken from the probability law of the thermodynamic equilibrium of $\bar{H}$, i.e. with the law $\mathcal{N}\mathrm{e}^{-\beta\bar{H}[b_{\vec{k}}]}$ where $\mathcal{N}$ is a normalization constant. But the presence of $\bar{H}^{(3)}$ in this law does not allow us to obtain a simple function for this law. Therefore we use an indirect method : since $\bar{H}^{(3)}$ is small compared to $\bar{H}^{(2)}$ at thermodynamic equilibrium, see section 4.2 of chapter 3, we can initially derive a state of thermodynamic equilibrium for $\bar{H}^{(2)}$, let us call this state $\{b^{(2)}_{\vec{k}}(0)\}$, which is a good approximation. To derive a thermal state of the full Hamiltonian, we can evolve $\{b^{(2)}_{\vec{k}}(0)\}$ for some time according to the ergodic evolution generated by $\bar{H}$ so as to thermalise the state $\{b^{(2)}_{\vec{k}}(0)\}$. In the series of executions, we have chosen a thermalization time of the order of one thousandth of the total evolution time, i.e. between 300 and $1200\hbar/k_BT$, which is equivalent to a number of time steps of the order of 10^3. Let us specify that we initialise the non-physical modes with a zero value.

In practice: we must draw, for each physical mode $\vec{q}$, a complex number $b_{\vec{q}}$ with the law $\frac{\beta\varepsilon_q}{\pi}\mathrm{e}^{-\beta\varepsilon_k b^*_{\vec{q}}b_{\vec{q}}}$. Obviously, this law does not depend on the phase of $b_{\vec{q}}$, so we can start by drawing a phase in the interval $[0;2\pi[$ with a uniform law. As for the modulus at equilibrium, it follows the exponential law [3] $P(n_{\vec{q}}) = \beta\varepsilon_q\mathrm{e}^{-\beta\varepsilon_q n_{\vec{q}}}$. This law can be sampled by drawing a real number $u \in [0;1]$ with a uniform law, the value $\frac{-1}{\beta\varepsilon_q}\log(1-u)$ then samples the previous exponential law. [4]

To summarise, initially, for the non-physical modes, the value is initialized to 0, for the others:

- We draw u and v two real numbers in the interval $[0;1]$ according to a uniform distribution.
- The value of the amplitude in mode $\vec{q}$ is initialised by $b_{\vec{q}} = \mathrm{e}^{2i\pi v}\sqrt{\frac{k_BT}{\varepsilon_q}}\sqrt{-\log(1-u)}$.
- This state is made to evolve for a certain time t_{therm} by the complete Hamiltonian of the system.

[3] We note $b_{\vec{q}} = x_{\vec{q}} + iy_{\vec{q}}$ and $n_{\vec{q}} = b^*_{\vec{q}}b_{\vec{q}} = x^2_{\vec{q}} + y^2_{\vec{q}}$ with $x_{\vec{q}}, y_{\vec{q}}, n_{\vec{q}} \in \mathbb{R}$ and consider any function $f : \mathbb{R} \to \mathbb{R}$. We can express the mean value of $f(n_{\vec{q}})$ with $b_{\vec{q}}$ drawn in the thermodynamic state of $\bar{H}^{(2)}$ by $\langle f(n_{\vec{q}})\rangle = \int \mathrm{d}x_{\vec{q}}\mathrm{d}y_{\vec{q}}\frac{\beta\varepsilon_q}{\pi}f(n_{\vec{q}})\mathrm{e}^{-\beta\varepsilon_q(x^2_{\vec{q}}+y^2_{\vec{q}})} = 2\beta\varepsilon_q\int\mathrm{d}\rho\rho f(\rho^2)\mathrm{e}^{-\beta\varepsilon_q\rho^2}$ or $\rho = \sqrt{x^2_{\vec{q}}+y^2_{\vec{q}}}$. We can re-express it as an integral over n, $\langle f(n_{\vec{q}})\rangle = \int_0^\infty \mathrm{d}n\beta\varepsilon_q f(n)\mathrm{e}^{-\beta\varepsilon_q n}$, which gives the law of n.

[4] To sample a law $P(x)$, we must indeed solve for $\int_0^x \mathrm{d}x'P(x') = u$ where u is drawn uniformly in $[0,1]$. For our case, we have $\beta\varepsilon_q\int_0^{n_{\vec{q}}}\mathrm{d}x\mathrm{e}^{-\beta\varepsilon_q x} = u \Rightarrow \frac{\beta\varepsilon_q}{\beta\varepsilon_q}(1-\mathrm{e}^{-\beta\varepsilon_q n_{\vec{q}}}) = u$ which inverts into $n_{\vec{q}} = \frac{-1}{\beta\varepsilon_q}\log(1-u)$.

2.2.2 Evolution on a time step

Let us come to the Hamiltonian evolution. As a reminder, the evolution of the $b_{\vec{q}}$ array is deterministic and governed by the Hamiltonian $\bar{H} = \bar{H}^{(2)} + \bar{H}^{(3)}$, separated into two contributions described by equations (1.24) and (1.26) respectively. A naive method of evolving the $b_{\vec{q}}$ array by a time step $\Delta\bar{t}$ would be to simply integrate the equations over $b_{\vec{q}}$, i.e. to calculate expressions of the form

$$i\hbar\frac{\mathrm{d}}{\mathrm{d}t}b_{\vec{q}} = \frac{1}{l_x l_y}\partial_{b^*_{\vec{q}}}\bar{H} = \varepsilon_q b_{\vec{q}} + \sum_{\vec{k}}(\ldots)b_{\vec{k}}b_{\vec{q}-\vec{k}} + \ldots \tag{2.2}$$

with the sum over $\vec{k}$ such as $\vec{k} \in \mathrm{FBZ}$ and $\vec{q}-\vec{k} \in \mathrm{FBZ}$. The coefficient $(\ldots)$ depends on $\vec{q}$ and $\vec{k}$ but, of course, not on $b_{\vec{q}}$, $b_{\vec{k}}$ or $b_{\vec{q}-\vec{k}}$. It is then sufficient to update the array of $b_{\vec{q}}$ with an Euler scheme: $b_{\vec{q}}(t+\Delta\bar{t}) = b_{\vec{q}}(t) + \Delta\bar{t}\left(\frac{\mathrm{d}}{\mathrm{d}t}b_{\vec{q}}(t)\right)$. But this naive scheme requires a number of operations in $\mathcal{N}^2$ to update the whole array per time step with $\mathcal{N} = n_x^{\mathrm{FBZ}} n_y^{\mathrm{FBZ}}$ the number of physical modes in the simulation. This quadratic dependence on the number of modes would not allow exploration of sufficiently large box sizes.

2.2.2.1 The integration method: splitting the full Hamiltonian

Therefore we considered another method, which could be called "by splitting the Hamiltonian", which takes advantage of the respective properties of $\bar{H}^{(2)}$ and $\bar{H}^{(3)}$ in addition to the quasi-linear complexity of the discrete fast Fourier transform algorithms in the number of points. It suffices to note that $\bar{H}^{(2)}$ is local in direct momentum space, since it depends on a sum over $\vec{k}$ of $b_{\vec{k}}$, see equation (1.24), but that $\bar{H}^{(3)}$ is local in direct space since it can be expressed over a sum over the positions of $\psi_{\vec{r}}$, see equation (1.26). Thus, we could first do an evolution according to $\bar{H}^{(2)}$ with a time step of $\Delta\bar{t}/2$, then an evolution according to $\bar{H}^{(3)}$ with a time step of $\Delta\bar{t}$ and finally an evolution according to $\bar{H}^{(2)}$ with a time step of $\Delta\bar{t}/2$. Each of these operations has a linear complexity in the number of modes. We do have to do a Fourier transform to move the array from direct space to reciprocal space and back again but, as we have said, the fast Fourier transform algorithm is of quasi-linear complexity[5] in the number of modes. This method therefore produces an evolution with a computation time growing linearly with the number of modes and not quadratically as in the naive method!

This cleavage constitutes an approximation of the evolution operator since it consists in replacing the $\mathrm{e}^{-i\bar{H}\Delta\bar{t}}$ operator by the $\mathrm{e}^{-i\bar{H}^{(2)}\Delta\bar{t}/2}\mathrm{e}^{-i\bar{H}^{(3)}\Delta\bar{t}}\mathrm{e}^{-i\bar{H}^{(2)}\Delta\bar{t}/2}$ operator. We can show that this approximation has an error proportional to $\Delta\bar{t}^3$. We start from the evolution operator which can be split within the exponential as

$$U \equiv \mathrm{e}^{-i\bar{H}\Delta\bar{t}} = \mathrm{e}^{-i\bar{H}^{(2)}\Delta\bar{t}/2 - i(\bar{H}^{(3)}+\bar{H}^{(2)}/2)\Delta\bar{t}}. \tag{2.3}$$

[5] More precisely of $\mathcal{N}\log\mathcal{N}$.

Then using the Zassenhaus[6] formula twice, once on the left, once on the right, we can write

$$\begin{aligned} U =& \mathrm{e}^{-i\bar{H}^{(2)}\Delta\bar{t}/2}\mathrm{e}^{-i\bar{H}^{(3)}\Delta\bar{t}}\mathrm{e}^{-i\bar{H}^{(2)}\Delta\bar{t}/2} \\ &\times \mathrm{e}^{-\frac{1}{4}[\bar{H}^{(2)},\bar{H}^{(3)}](\Delta\bar{t})^2}\exp\left\{-\frac{(-i\Delta\bar{t})^3}{12}\left[\bar{H}^{(2)}+\bar{H}^{(3)},\left[\bar{H}^{(2)},\bar{H}^{(3)}\right]\right]\right\}\dots \\ &\times \mathrm{e}^{\frac{1}{4}[\bar{H}^{(2)},\bar{H}^{(3)}](\Delta\bar{t})^2}\exp\left\{\frac{(-i\Delta\bar{t})^3}{12}\left[\bar{H}^{(2)}+2\bar{H}^{(3)},\left[\bar{H}^{(2)},\bar{H}^{(3)}\right]\right]\right\}\dots \end{aligned} \tag{2.4}$$

Note that each exponential of the development by the Zassenhaus formula is of a well defined order of $\Delta\bar{t}$ in our case. In particular, all hidden terms in $\dots$ are of order $(\Delta\bar{t})^4$ or higher. Let us now restrict the evolution operator to terms of order 3 in $\Delta\bar{t}$. In the previous equation, this amounts to removing the $\dots$ from the equation. But not only that, because it should be noted that the terms of the last four exponentials in the equation are of order 2 or 3 in $\Delta\bar{t}$. This implies that any commutation between two of these terms is of order 4 or 5 in $\Delta\bar{t}$. So at order 3 in $\Delta\bar{t}$, $\dots$ disappears and we can combine the last four exponentials into one. We then see that these second-order terms cancel each other out and we finally obtain

$$U \simeq \mathrm{e}^{-i\bar{H}^{(2)}\Delta\bar{t}/2}\mathrm{e}^{-i\bar{H}^{(3)}\Delta\bar{t}}\mathrm{e}^{-i\bar{H}^{(2)}\Delta\bar{t}/2}\exp\left\{-i\frac{(\Delta\bar{t})^3}{6}\left[\bar{H}^{(2)}+\frac{3}{2}\bar{H}^{(3)},\left[\bar{H}^{(2)},\bar{H}^{(3)}\right]\right]\right\}. \tag{2.5}$$

Our "split evolution" thus corresponds to a third-order approximation in $\Delta\bar{t}$. The disappearance by symmetry of the second-order term in $\Delta\bar{t}$ confirms the quality of our time integration scheme.

2.2.2.2 The steps of the integration on a time step

Now that we have exposed the method of integration by cleavage, we can ask ourselves the question of the concrete evolution of the numerical arrays. We must therefore consider the differential equations as defined by the Hamiltonian field theory

$$i\frac{\mathrm{d}}{\mathrm{d}\bar{t}}b_{\vec{q}} = \partial_{b^*_{\vec{q}}}\bar{H}^{(2)}(\vec{q}) \tag{2.6}$$

$$i\hbar\frac{\mathrm{d}}{\mathrm{d}\bar{t}}\bar{\psi}_{\vec{r}} = \frac{1}{l_x l_y}\partial_{\bar{\psi}^*_{\vec{r}}}\bar{H}^{(3)} \tag{2.7}$$

where the $\bar{\psi}_{\vec{r}}$ field is of Fourier coefficients $a_{\vec{q}}$, a linear combination of the $b_{\vec{q}}$ as we saw in chapter 1.

Evolution according to $\bar{H}^{(2)}$ From the expression (1.24) of the second order Hamiltonian in terms of $b_{\vec{q}}$, it comes :

$$i\frac{\mathrm{d}}{\mathrm{d}\bar{t}}b_{\vec{q}}(\bar{t}) = \partial_{b^*_{\vec{q}}}\bar{H}^{(2)}(\vec{q}) = -i\bar{\varepsilon}_q b_{\vec{q}}(\bar{t}) \tag{2.8}$$

$$b_{\vec{q}} \to \mathrm{e}^{-i\bar{\varepsilon}_q\Delta\bar{t}/2}b_{\vec{q}}. \tag{2.9}$$

Equation (2.9) represents the transformation that is actually operated on the numerical vector, note the 1/2 factor on the time step. Note that this transformation is exact and therefore does not involve any error due to the non-infinitesimal value of $\Delta\bar{t}$.

[6] $\mathrm{e}^{X+Y} = \mathrm{e}^X\mathrm{e}^Y\mathrm{e}^{-\frac{1}{2}[X,Y]}\mathrm{e}^{\frac{1}{6}[X+2Y,[X,Y]]}\dots$ for any two square matrices X and Y.

Evolution according to $\bar{H}^{(3)}$ The next step in the evolution algorithm is to transform the $b_{\vec{q}}$ array into the $a_{\vec{q}}$ array by linear combination (1.19) before applying a Fourier transform to obtain the $\psi_{\vec{r}}$ array. To carry out the evolution of this array, we consider the evolution equation defined by $i\hbar\frac{\mathrm{d}}{\mathrm{d}\bar{t}}\psi_{\vec{r}} = \partial_{\psi^*_{\vec{r}}}\bar{H}^{(3)}$. This gives us the evolution equation

$$\frac{\mathrm{d}\bar{\psi}_{\vec{r}}}{\mathrm{d}\bar{t}} = -i\rho\xi^2\left[\frac{\epsilon^2}{2}\left(\nabla \operatorname{Im}\psi_{\vec{r}}\right)^2 - i\epsilon^2\nabla\left(\operatorname{Re}(\psi_{\vec{r}})\nabla[\operatorname{Im}\psi_{\vec{r}}]\right) + 6\Lambda(\operatorname{Re}\psi_{\vec{r}})^2\right]. \tag{2.10}$$

In subsection 2.2.3, we derive this expression explicitly from the third-order Hamiltonian in viewpoint $\vec{r}$. In general, the computation of a gradient on a lattice is not local in position but is a local operation in momentum; to preserve the locality of the integration on $\bar{H}^{(3)}$ and to avoid multiplying the Fourier transforms, we present in this same subsection 2.2.3 the approximate form of the gradient that we use in the program. This is a very good approximation and has been checked for error by comparison with the exact gradient.

Filtering of Umklapp processes In expression (2.10), note that the array $\bar{\psi}_{\vec{r}}$ is squared. From a numerical point of view, this means that once we switch back to the momentum representation, all the numerical modes, including those described as non-physical at the beginning of this chapter, will a priori be of non-zero amplitude because the quadratic terms in $\bar{\psi}_{\vec{r}}$ mix all the modes. Indeed, we can write $\bar{\psi}_{\vec{r}} = \frac{1}{\sqrt{\bar{L}_x\bar{L}_y}}\sum_{\vec{k}} a_{\vec{k}}\mathrm{e}^{i\vec{k}\,\cdot\,\vec{r}}$ by definition of the Fourier transform and therefore $\bar{\psi}^2_{\vec{r}} = \frac{1}{\bar{L}_x\bar{L}_y}\sum_{\vec{k}_1;\vec{k}_2} a_{\vec{k}_1}a_{\vec{k}_2}\mathrm{e}^{i(\vec{k}_1+\vec{k}_2)\,\cdot\,\vec{r}}$. Numerically, some non-physical modes will be populated since the sum $\vec{k}_1+\vec{k}_2$ can represent a wave vector whose momentum is greater than η or the null vector $\vec{0}$ or a wave vector outside the first Brillouin zone. These are the so-called Umklapp processes that we discussed in section 2.1.2 earlier in this chapter. To prevent these terms from interfering with the time integration, we need to remove them whenever they appear. In the practice of the programme, this means setting the field strength on the non-physical modes of the $b_{\vec{q}}$ array to 0 each time a non-linear operation on $\bar{\psi}_{\vec{r}}$ is performed.

Naive time integration method: Euler To implement an evolution, a time integration method must be decided upon, as one cannot explicitly integrate the expression (2.10). In the case of an Euler method, the evolution during $\Delta\bar{t}$ is done by $\bar{\psi}_{\vec{r}}(t+\Delta\bar{t}) \simeq \bar{\psi}_{\vec{r}}(t) + \Delta\bar{t}\frac{\mathrm{d}\bar{\psi}_{\vec{r}}}{\mathrm{d}\bar{t}}$. Once the time derivative has been calculated and this transformation of the array has been carried out, we can apply the inverse Fourier transform to obtain $a_{\vec{q}}$ again and then $b_{\vec{q}}$. We can then filter the Umklapp processes by putting the non-physical modes in this array at 0 and then carry out a second time the evolution according to $\bar{H}^{(2)}$ exactly as in the first step (2.9). [7] The error committed on a time step has two sources : the approximation of the Euler method which depends on $\Delta\bar{t}$ and the approximation when calculating the (2.10) derivative, i.e. our gradient approximation (see section 2.2.3). Finally, during this time step $\Delta\bar{t}$, we had to do two 2D Fourier transforms.

[7] Since the relationship between $a_{\vec{q}}$ and $b_{\vec{q}}$ is a linear transformation, the filtering of Umklapp processes can be done on either one, or even in the numerical linear transfomation from one to the other by positing $u_{\vec{k}} = v_{\vec{k}} = 0$ for any non-physical mode $\vec{k}$.

Time integration method: Runge Kutta of order 4 The Euler method is known to be unsatisfactory for time integration. It is indeed an unstable scheme for conservative evolution since it consists of approximating a curve by its tangent at the known initial point and its error over one step grows as $\Delta\bar{t}^2$ while its total accumulated error is of order $\Delta\bar{t}$. For this type of physical system, this scheme is characterised by the linear divergence in time of the total energy of the system, whose slope is controlled by $\Delta\bar{t}$. [8] Conversely, schemes of the Runge-Kutta form are very popular because of their ease of implementation on the one hand, but also because of their accuracy and the stability of the evolution they allow on the other. In this case, we have chosen the Runge-Kutta method of order 4, which allows us to obtain very good results for the conservation of total energy (as we illustrate in section 4.2) while keeping the computation time reasonable. In this method, we need to calculate the derivative four times according to equation (2.10) at different points that depend on each other.[9] To avoid Umklapp processes, we will therefore need to make three returns to the $b_{\vec{q}}$ array, one after each calculation of the derivative, in order to filter out unphysical modes. Each return requires two Fourier transforms, one to return to $a_{\vec{q}}/b_{\vec{q}}$, then another to return to $\bar{\psi}_{\vec{r}}$ after the filter. This corresponds to 6 additional Fourier transforms to the total integration scheme compared to the Euler method, bringing the total number of Fourier transforms to 8. [10]

Summary Let us summarize the numerical steps in our scheme to realize the evolution during a step $\Delta\bar{t}$ from the array $b_{\vec{q}}(\bar{t})$:

- Application of $\bar{H}^{(2)}$: $b_{\vec{q}} \to b'_{\vec{q}} = b_{\vec{q}}(t)\exp(-i\bar{\varepsilon}_q\Delta\bar{t}/2)$
- Obtaining $a_{\vec{q}} = u_{\vec{q}}b_{\vec{q}} + v_{\vec{q}}b^*_{-\vec{q}}$
- Fourier transform of $a_{\vec{q}}$: $\bar{\psi}_{\vec{r}} = \frac{1}{\sqrt{\bar{L}_x\bar{L}_y}}\sum_{\vec{k}} a_{\vec{k}}\mathrm{e}^{i\vec{k}\,\cdot\,\vec{r}}$
- Runge-Kutta method of order 4 from $\bar{\psi}_{\vec{r}}$, for a step of integration $\Delta\bar{t}$ and as an expression of the derivative the equation (2.10). Performing the method excluding Umklapp processes involves 4 Fourier transforms.
- Inverse Fourier transform to obtain $a_{\vec{q}}$ then $b_{\vec{q}}$ and filter the Umklapp processes.
- Application of $\bar{H}^{(2)}$ a second time: $b_{\vec{q}} \to b'_{\vec{q}} = b_{\vec{q}}(t)\exp(-i\bar{\varepsilon}_q\Delta\bar{t}/2)$

[8] Indeed, let us take a differential equation $i\dot{\alpha} = \omega\alpha$ and thus $\alpha(\mathrm{d}t) = \alpha(0)\mathrm{e}^{-i\omega\mathrm{d}t}$ exactly. Euler's method is to take $\alpha(\mathrm{d}t) \simeq (1 - i\omega\mathrm{d}t)\alpha(0)$ and therefore $\alpha(n\mathrm{d}t) \simeq (1 - i\omega\mathrm{d}t)^n\alpha(0)$. The problem then is that $|1 - i\omega\mathrm{d}t| > 1$ so the scheme is unstable! We can explain this property by the formula $(1 - i\omega\mathrm{d}t)^n = \mathrm{e}^{n\log(1-i\omega\mathrm{d}t)} = \mathrm{e}^{n[-i\omega\mathrm{d}t + \frac{(\omega\mathrm{d}t)^2}{2} + \cdots]} = \mathrm{e}^{-i\omega t}\mathrm{e}^{\omega t\frac{\mathrm{d}t}{2}}$ with $t = n\mathrm{d}t$.

[9] If we have a function $y(t)$ whose derivative $f(t, y(t))$ is known and can be calculated, a known value of y at a given time y_n and a step of integration h, the Runge Kutta method of integration of order 4 to find a value y_{n+1} to t_{n+1} from y_n to t_n consists in evolving according to the expression $y_{n+1} = y_n + h\frac{k_1+2k_2+2k_3+k_4}{6}$ with $k_1 = f(t_n, y_n)$, $k_2 = f(t_n + h/2, y_n + hk_1/2)$, $k_3 = f(t_n + h/2, y_n + hk_2/2)$, $k_4 = f(t_n + h, y_n + hk_3)$.

[10] If we had chosen the Runge Kutta method of order 2, we would have had to do an additional filtering operation, so 4 Fourier transforms in total.

2.2.3 The gradient operator on a discrete lattice

In this subsection we obtain the evolution equation of the classical field $\bar{\psi}_{\vec{r}}$ of the (dimensionless) Hamiltonian $\bar{H}^{(3)}$ of equation (1.26). We can write:

$$i\frac{\mathrm{d}}{\mathrm{d}\bar{t}}\bar{\psi}_{\vec{r}} = \frac{1}{l_x l_y}\partial_{\bar{\psi}^*_{\vec{r}}}\bar{H}^{(3)}. \tag{2.11}$$

Let us place ourselves in the 1D case to simplify the rest of the development. In this case, the gradient of a complex-valued field $\psi^*(x)$ defined on a discrete lattice of steps l_x can be written

$$\partial_x\psi(x) = \sum_{m\in\mathbb{Z}} c_m\psi(x+ml_x) \tag{2.12}$$

with c_m real coefficients obeying the constraint $c_{-m} = -c_m$. That is, a gradient is a certain antisymmetric linear combination of the values taken by the field on the grid in a certain direction. We can write our Hamiltonian in terms of these coefficients:

$$\bar{H}^{(3)} = \frac{l_x l_y}{\sqrt{\rho\xi^2}}\sum_y\left[\epsilon^2\,\mathrm{Re}\,\psi(y)\left(\sum_{m\in\mathbb{Z}} c_m\frac{\psi(y+ml_x)-\psi^*(y+ml_x)}{2i}\right)^2 + 4\Lambda\left(\mathrm{Re}\,\psi(y)\right)^3\right] \tag{2.13}$$

$$= \frac{l_x l_y}{\sqrt{\rho\xi^2}}\sum_y\left[-\frac{\epsilon^2}{4}\,\mathrm{Re}\,\psi(y)\sum_{m,n\in\mathbb{Z}} c_m c_n\left(\psi(y+ml_x)-\psi^*(y+ml_x)\right)\left(\psi(y+nl_x)-\psi^*(y+nl_x)\right)\right. \tag{2.14}$$

$$\left.+4\Lambda\left(\mathrm{Re}\,\psi(y)\right)^3\right].$$

We can now perform the partial derivation with respect to $\psi^*(x)$

$$\partial_{\psi^*(x)}\bar{H}^{(3)} = \frac{l_x l_y}{\sqrt{\rho\xi^2}}\sum_y\left[6\Lambda\left(\mathrm{Re}\,\psi(x)\right)^2\delta_{x,y} + \frac{\epsilon^2}{2}\sum_{m,n\in\mathbb{Z}} c_m c_n\delta_{x,y+ml_x}\,\mathrm{Re}\,\psi(y)(\psi(y+nl_x)-\psi^*(y+nl_x))\right. \tag{2.15}$$

$$\left.-\frac{\epsilon^2}{8}\delta_{x,y}\sum_{m,n\in\mathbb{Z}} c_m c_n\left(\psi(y+ml_x)-\psi^*(y+nl_x)\right)\left(\psi(y+nl_x)-\psi^*(y+nl_x)\right)\right].$$

In the second member, we recognize in the third contribution (the double sum), a squared gradient. Furthermore, we can sum over y and take into account the Kronecker deltas in each contribution.

$$\partial_{\psi^*(x)}\bar{H}^{(3)} = \frac{l_x l_y}{\sqrt{\rho\xi^2}}\left[6\Lambda\left(\mathrm{Re}\,\psi(x)\right)^2 + \frac{\epsilon^2}{2}\left(\partial_x\,\mathrm{Im}\,\psi(x)\right)^2\right. \tag{2.16}$$

$$\left.+\frac{\epsilon^2}{2}\sum_{m,n\in\mathbb{Z}} c_m c_n\,\mathrm{Re}\,\psi(x-ml_x)\left(\psi(x-ml_x+nl_x)-\psi^*(x-ml_x+nl_x)\right)\right].$$

In the second member, we recognise in the sum over n the expression of the gradient :

$$\partial_{\psi^*(x)}\bar{H}^{(3)} = \frac{l_x l_y}{\sqrt{\rho\xi^2}}\left[6\Lambda\left(\operatorname{Re}\psi(x)\right)^2 + \frac{\epsilon^2}{2}\left(\partial_x \operatorname{Im}\psi(x)\right)^2 + \frac{\epsilon^2}{2}\sum_{m\in\mathbb{Z}} c_m \operatorname{Re}\psi(x-ml_x)\partial_x\left(\psi(x-mdx)-\psi^*(x-mdx)\right)\right]. \tag{2.17}$$

Finally we can make the change of dummy variable $m \longrightarrow -m'$ and then find the expression of the gradient using $c_{-m'} = -c_{m'}$. This leaves

$$\partial_{\psi^*(x)}\bar{H}^{(3)} = \frac{l_x l_y}{\sqrt{\rho\xi^2}}\left[6\Lambda\left(\operatorname{Re}\psi(x)\right)^2 + \frac{\epsilon^2}{2}\left(\partial_x \operatorname{Im}\psi(x)\right)^2 - i\epsilon^2\partial_x \operatorname{Re}\psi(x)\partial_x\left(\operatorname{Im}\psi(x)\right)\right]. \tag{2.18}$$

We return to the evolution of $\bar{\psi}_{\vec{r}}$ and the general case of the d dimensional lattice:

$$i\frac{\mathrm{d}}{\mathrm{d}t}\bar{\psi}_{\vec{r}} = \frac{1}{\sqrt{\rho\xi^2}}\left[6\Lambda\left(\operatorname{Re}\bar{\psi}_{\vec{r}}\right)^2 + \frac{\epsilon^2}{2}\left(\nabla \operatorname{Im}\bar{\psi}_{\vec{r}}\right)^2 - i\epsilon^2\nabla\left(\operatorname{Re}\bar{\psi}_{\vec{r}}\nabla \operatorname{Im}\bar{\psi}_{\vec{r}}\right)\right]. \tag{2.19}$$

Numerical computation of the gradient As we have just written, the expression of the differential equation on $\bar{\psi}_{\vec{r}}$ relies on the computation of discrete gradients of functions of $\bar{\psi}_{\vec{r}}$. The generic expression of the discrete gradient as we have written it (2.12) is not local in position and therefore implies that its numerical computation is quadratic in the number of modes since for each point of the lattice, one has to sum over the terms in each direction. Naive numerical summation would surely slow down the program and kill the linear complexity that we had gained by "splitting" the total evolution operator.

We then have two possibilities to preserve this linearity : the first is to compute these gradients in the momentum space because the operation is local there. Indeed $\partial_x\psi(x) = \partial_x \sum_{k_x} a_x \mathrm{e}^{-ixk_x} = \sum_{k_x} -ik_x a_{k_x}\mathrm{e}^{-ixk_x}$. This possibility, which has the advantage of being exact, adds as many Fourier transform pairs as there are gradients for a time step. For our Runge-Kutta type scheme of order 4, this amounts to adding 16 Fourier transforms. It is therefore a rather heavy choice. The second possibility, and the one we have chosen, is simply to approximate the gradient by a finite difference, i.e. to restrict the generic formula (2.12) to only a few non-zero coefficients on the neighbouring points. We have chosen as truncation the formula

$$\partial_x\psi(x) \simeq \frac{4}{3}\left(A - \frac{1}{4}B\right) \tag{2.20}$$
$$\text{with} \quad A = \frac{\psi(x+l_x)-\psi(x-l_x)}{2l_x} \quad \text{and} \quad B = \frac{\psi(x+2l_x)-\psi(x-2l_x)}{4l_x}.$$

It is possible to convince oneself that this expression is a good approximation of the gradient by considering the test function $\psi(x) = \mathrm{e}^{ikx}$. Its exact derivative is $\partial_x\psi(x) = ik\mathrm{e}^{ikx}$ whereas our approximation gives

$$\partial_x\psi(x) \simeq ik\mathrm{e}^{ikx}\frac{4}{3}\left(\frac{\sin(kl_x)}{kl_x} - \frac{1}{4}\frac{\sin(2kl_x)}{2kl_x}\right). \tag{2.21}$$

Assuming $u = kl_x$ is small enough, we can expand the sines with $\frac{\sin u}{u} = 1 - \frac{u^2}{6} + O(u^4)$. This gives, for the factor in the previous equation

$$F = \frac{4}{3}\left(\frac{\sin(kl_x)}{kl_x} - \frac{1}{4}\frac{\sin(2kl_x)}{2kl_x}\right) = \frac{4}{3}\left(1 - \frac{(kl_x)^2}{6} - \frac{1}{4}\left(1 - \frac{4(kl_x)^2}{6}\right) + O(u^4)\right) = 1 + O(u^4) \tag{2.22}$$

where the $O(u^4)$ is non-zero, which makes our truncation a fourth order approximation of the spatial derivative. But is kl_x small enough? Is it legitimate to limit ourselves to a Taylor expansion to the second order? On this point, we are helped by the fact that $k \leq \frac{\pi}{2l_x}$ for any k physical wave vector of the network. Admittedly, $\frac{\pi}{2l_x} l_x \simeq 1.57$ is not small a priori but the factor F is strictly decreasing with a very flat centre on the interval $[0; \frac{\pi}{2}]$ and $F(\frac{\pi}{2}) = \frac{8}{3\pi} \simeq 0.85$. This is why we have taken the liberty of using this approximation in the numerical integration, an approximation which is quite reasonable and which speeds up the calculation.

These approximations will be confirmed in chapter 4 where, before presenting the final results of our simulations, we will show the figures of conservation of energy as well as the achievement of thermodynamic equilibrium.

Chapter 3

Analysis by N-body Green's functions

Foreword

In quantum physics, the N-body problem for a system at thermodynamic equilibrium can be studied by means of the formalism of Green's functions, averages of the $\psi(\vec{r}_2, t_2)\psi^\dagger(\vec{r}_1, t_1)$ operator in the equilibrium state with $\psi_{\vec{r}}(t)$ the field operator creating a particle at position $\vec{r}$ at the instant t in the Heisenberg picture [29]. This function is interesting because it is possible to extract from the singularities of its Fourier transform information on the dynamic properties of the system, on its excited states as well as on its responses to an external perturbation. We will also see how Fermi's golden rule described in chapter 1 is retreive in the Green's function approach as a poorly controlled approximation and how this approach allows to go beyond it by systematically taking into account all the diagrams of the same order in the perturbation.

First, in sections 3.1 and 3.2, this chapter focuses on defining the different functions and quantities involved in the method, which we relate to our observable before constructing the diagrammatic series we use later. In a second step, sections 3.3 and 3.4 present the new results we have obtained. The specificity of the $d = 2$ case compared to the $d = 3$ case in the $\epsilon = k_B T/mc^2 \to 0$ reduced low temperature limit is explored, leading to a discussion of the applicability of Fermi's golden rule in two-dimensional boson gases.

3.1 Expression of the signal in terms of the self-energy function Σ

The study by Green's functions of our phonon damping problem has been mainly carried out by Yvan Castin. In this section, we present the main ingredients, in order to arrive at the integral formulation (3.13) which we have calculated numerically at all orders in ϵ for comparison with our simulations.

Using the teachings of A. Fetter and J. Walecka presented in their book *Quantum Theory of Many-Particle Systems* [29], in particular in their section 31 p.292 and their equations

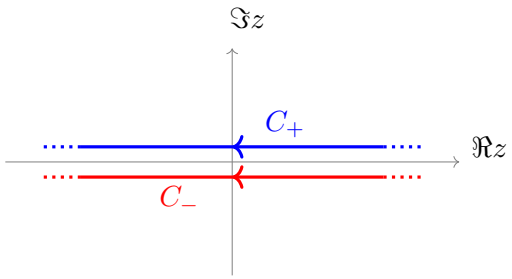

Figure 3.1: Path integrals C_+ and C_- in the complex plane of the z variable.

(31.23) and (31.24), we can express our signal for $t \geq 0$ as

$$\langle \hat{b}_{\vec{q}}(t)\hat{b}^\dagger_{\vec{q}}(0)\rangle = \int_{-\infty}^{+\infty} \frac{\mathrm{d}\omega}{-2\mathrm{i}\pi} \mathrm{e}^{-\mathrm{i}\omega t} \left(\frac{\mathcal{G}(\vec{q},\omega+\mathrm{i}0^+)}{1-\mathrm{e}^{-\beta\hbar\omega}} + \frac{\mathcal{G}(\vec{q},\omega-\mathrm{i}0^+)}{1-\mathrm{e}^{\beta\hbar\omega}} \right) \tag{3.1}$$

$$= \int_{-\infty}^{+\infty} \frac{\mathrm{d}\omega}{-2\mathrm{i}\pi} \mathrm{e}^{-\mathrm{i}\omega t} \left(\mathcal{G}(\vec{q},\omega+\mathrm{i}0^+) + \frac{\mathcal{G}(\vec{q},\omega+\mathrm{i}0^+) - \mathcal{G}(\vec{q},\omega-\mathrm{i}0^+)}{\mathrm{e}^{\beta\hbar\omega}-1} \right) \tag{3.2}$$

where the Green's function $\mathcal{G}(\vec{q},\omega)$, analytic in the complex plane deprived of the real axis (on which it has a cut-off line), is defined in terms of the self-energy function Σ by

$$\mathcal{G}(\vec{q},z) \equiv \frac{1}{z-\varepsilon_q-\Sigma(\vec{q},z)} \qquad \forall z \in \mathbb{C}\setminus\mathbb{R}. \tag{3.3}$$

To develop an intuition of the expression (3.1), let us give a simplified form in the weak coupling limit where the integral on ω is dominated by a neighbourhood of $\varepsilon_q/\hbar$. We can then replace $\mathrm{e}^{\pm\beta\hbar\omega}$ by $\mathrm{e}^{\pm\beta\varepsilon_q}$ in the denominators of the integrand. Let us also restrict ourselves to the case $t > 0$ which allows us to reduce to a curvilinear integral in the complex plane [1]

$$\langle \hat{b}_{\vec{q}}(t)\hat{b}^\dagger_{\vec{q}}(0)\rangle \simeq (1+\bar{n}_q) \int_{C_+} \frac{\mathrm{d}z}{2\mathrm{i}\pi} \mathrm{e}^{-\mathrm{i}zt/\hbar} \mathcal{G}(\vec{q},z) \tag{3.4}$$

where C_+ denotes a straight line parallel to the real axis in the upper half-plane, directed towards $-\infty$, as in Figure 3.1. Σ can be extended analytically, so $\mathcal{G}$ from the upper to the lower half-plane through their cut-off line; the extended Green's function $\mathcal{G}_\downarrow(\vec{q},z)$ usually admits one or more poles z_0, defined by $z_0 = \varepsilon_q + \Sigma_\downarrow(\vec{q},z_0)$, and which play a role in the dynamics of the observable. Indeed, by closing the path C_+ by a semicircle in the lower half-plane, with a radius that is made to tend to infinity, we create a closed integration path allowing us to apply the residue theorem. From then on, each pole makes an exponentially decreasing contribution to the mean $\langle \hat{b}_{\vec{q}}(t)\hat{b}^\dagger_{\vec{q}}(0)\rangle$. The application of the residue theorem, however, requires moving and then bypassing the $\mathcal{G}(\vec{q},z)$ cut-off line, see Figure 3.2, with the bypassing yaw making a contribution to the correlation function tending towards 0 algebraically (power law) at long times.

[1] The contribution of the path C_- defined in figure 3.1 is zero in this case as can be shown by closing the contour in the lower half-plane on a large semicircle and using the analyticity of $\mathcal{G}$ in this half-plane.

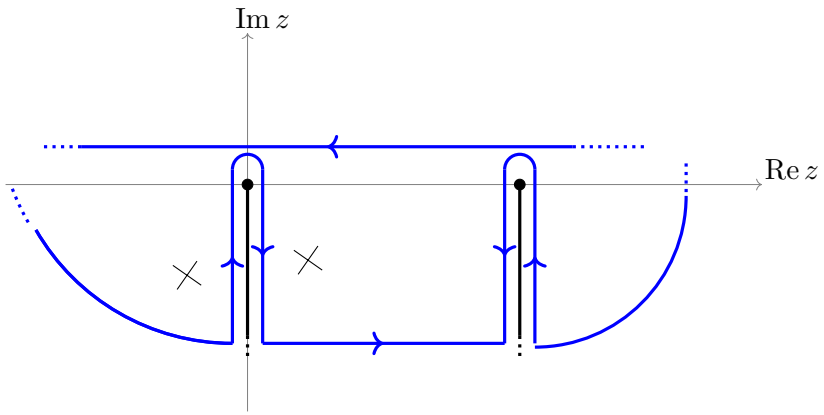

Figure 3.2: Path integral in the complex plane allowing the residue theorem to be applied on the simplified form (3.4) of the signal. The black dots are the connection points and the black lines starting from them are the displaced cut-off lines. The black crosses represent the poles of the function $\mathcal{G}_{\downarrow}$.

3.2 Perturbative development of the self-energy function

Following the Fetter-Walecka, a perturbative development of the self-energy function into powers of the cubic phonon-phonon interaction can be performed in the form of Feynman diagrams:

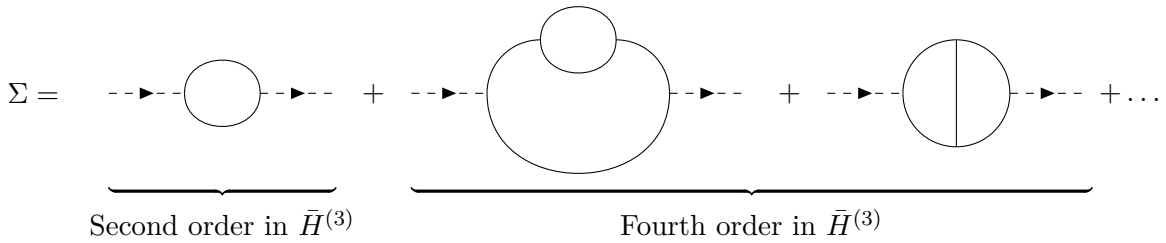

(3.5)

where we represent the diagrams of orders 2 (the first term) and 4 (the next two) in $H^{(3)}$. The dashed lines represent the $\tilde{\mathcal{G}}_0(\vec{q},\omega)$ factors that always frame Σ in the development of Green's function in imaginary time $\mathcal{G}(\vec{q},\mathrm{i}\omega)$. Each vertex of each graph corresponds to an action of $H^{(3)}$ so is always the meeting point of three lines and contributes by a factor equal to the corresponding matrix element of $H^{(3)}$.[2] The next step is to orient each line of a given diagram, to assign to each line two quantities (the impulse and the Matsubara frequency of the mode) conserved at the nodes. Finally, the contributions on all possible orientations of the internal lines, on all independent wave vectors and internal Matsubara frequencies must be summed.

[2]Note a departure from the instructions in the manual : we omit the interaction lines (represented by wavy lines in [29]) as they are not useful in our case. This is because the matrix element calculations in Fetter and Walecka are done between unsymmetrized states and therefore have to distinguish between direct and exchange terms, whereas the phonon states we consider are automatically symmetrized.

3.2.1 Expressions of the self-energy functions of order 2

If we focus on order 2, this gives the sum of diagrams

$\Sigma^{(2)} =$ 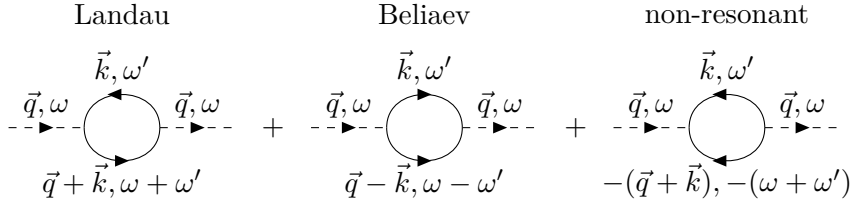

(3.6)

where we can easily recognise, from left to right in (3.6), the Landau, Beliaev and non-resonant processes that we had already introduced as diagrams in chapter 1 (figure 1.1). The rules for constructing function Σ from the diagrams, the so-called "Feynman rules", are given in the Fetter-Walecka. For example, for the Beliaev diagram, this gives:

$$\Sigma^{(2)}_{\text{Bel}}(\vec{q},\mathrm{i}\omega) = \frac{1}{-\beta\hbar^2}\int\frac{\mathrm{d}^d\vec{k}}{(2\pi)^d}\sum_{\omega'\in\frac{2\pi}{\beta\hbar}\mathbb{Z}}\frac{\frac{1}{2}\left|\langle\vec{k},\vec{q}-\vec{k}|\hat{\mathcal{H}}^{(3)}|\vec{q}\rangle\right|^2}{[\mathrm{i}\omega'-\varepsilon_k/\hbar][\mathrm{i}(\omega-\omega')-\varepsilon_{\vec{q}-\vec{k}}/\hbar]} \tag{3.7}$$

where $\hat{\mathcal{H}}^{(3)}$ is the density Hamiltonian. To sum over ω', we decompose the factor $\frac{1}{(z'-a)(b-z')} = \frac{1}{b-a}(\frac{1}{z'-a}+\frac{1}{b-z'})$ where $z'=i\omega'$ into simple elements and use the Fetter-Walecka result p.249 $\lim_{\eta\to0}\sum_{\omega'\in\frac{2\pi}{\beta\hbar}\mathbb{Z}}\frac{\mathrm{e}^{\mathrm{i}\eta\omega'}}{\mathrm{i}\omega'-x} = \frac{-\beta\hbar}{\mathrm{e}^{\beta\hbar x}-1}$ for any non-zero real x. Note the factor $1/2$ in the numerator of (3.7) which avoids double counting: the diagram is indeed invariant by rotation by an angle π around the horizontal axis. This factor $1/2$ appears in $\Sigma^{(2)}_{\text{non-res}}$ for the same reason but not in $\Sigma^{(2)}_{\text{Lan}}$.

As the method is reproduced for the Landau and non-resonant processes, we extend analytically to $\mathbb{C}\setminus\mathbb{R}$ by replacing the discrete variable $\mathrm{i}\hbar\omega$ by the continuous variable z and obtain

$$\Sigma^{(2)}_{\text{Bel}}(\vec{q},z) = \int\frac{\mathrm{d}^d\vec{k}}{(2\pi)^d}\frac{\frac{1}{2}\left|\langle\vec{k},\vec{q}-\vec{k}|\hat{\mathcal{H}}^{(3)}|\vec{q}\rangle\right|^2}{z-(\varepsilon_k-\varepsilon_{\vec{q}-\vec{k}})}\left(1+\bar{n}_{\vec{k}}+\bar{n}_{\vec{q}-\vec{k}}\right) \tag{3.8}$$

$$\Sigma^{(2)}_{\text{Lan}}(\vec{q},z) = \int\frac{\mathrm{d}^d\vec{k}}{(2\pi)^d}\frac{\left|\langle\vec{q}+\vec{k}|\hat{\mathcal{H}}^{(3)}|\vec{k},\vec{q}\rangle\right|^2}{z+\varepsilon_k-\varepsilon_{\vec{q}+\vec{k}}}\left(\bar{n}_{\vec{k}}-\bar{n}_{\vec{q}+\vec{k}}\right) \tag{3.9}$$

$$\Sigma^{(2)}_{\text{non-res}}(\vec{q},z) = -\int\frac{\mathrm{d}^d\vec{k}}{(2\pi)^d}\frac{\frac{1}{2}\left|\langle\vec{0}|\hat{\mathcal{H}}^{(3)}|\vec{k},\vec{q},-(\vec{q}+\vec{k})\rangle\right|^2}{z+\varepsilon_k+\varepsilon_{-(\vec{q}+\vec{k})}}\left(1+\bar{n}_{-(\vec{q}+\vec{k})}+\bar{n}_{\vec{k}}\right). \tag{3.10}$$

3.2.2 Expression of the signal for the classical field

Before studying further the properties of this self-energy function in the $d=2$ case, let us return to the (3.1) expression of the signal as an integral of Green's function and adapt it to the case of the classical field approximation. In this case, we replace Bose's law $\frac{1}{\mathrm{e}^{\beta\hbar\omega}-1}$ with the classical physics equipartition law $\frac{1}{\beta\hbar\omega}$, which gives

$$\langle\hat{b}_{\vec{q}}(t)\hat{b}^\dagger_{\vec{q}}(0)\rangle^{\text{class}} = \int_{-\infty}^{+\infty}\frac{\mathrm{d}\omega}{-2\mathrm{i}\pi}\frac{\mathrm{e}^{-\mathrm{i}\omega t}}{\beta\hbar\omega}\left(\mathcal{G}(\vec{q},\omega+\mathrm{i}0^+)-\mathcal{G}(\vec{q},\omega-\mathrm{i}0^+)\right). \tag{3.11}$$

Since Σ admits a cut-off line on the real axis, causing a discontinuity in its imaginary part but not in its real part, we can write

$$\Sigma(\vec{q},\omega\pm \mathrm{i}0^+) = \Sigma_R(\vec{q},\omega) \pm \mathrm{i}\Sigma_I(\vec{q},\omega) \tag{3.12}$$

where functions Σ_R and Σ_I are real-valued. By introducing these expressions into the signal, we obtain

$$\langle \hat{b}_{\vec{q}}(t)\hat{b}^\dagger_{\vec{q}}(0)\rangle^{\text{class}} = \int_{-\infty}^{+\infty} \frac{\mathrm{d}\omega}{\pi} \frac{\mathrm{e}^{-\mathrm{i}\omega t}}{\beta\hbar\omega} \frac{-\Sigma_I(\vec{q},\omega)}{\left[\hbar\omega-\varepsilon_q-\Sigma_R(\vec{q},\omega)\right]^2+\left[\Sigma_I(\vec{q},\omega)\right]^2}. \tag{3.13}$$

3.2.3 Principle of a numerical calculation

Note that it is always possible to rewrite our self-energy functions as integrals over a real variable of a density of state over an energy denominator. Indeed, we can write the schematic expression

$$\Sigma(\vec{q},z) = \int \frac{\mathrm{d}^d\vec{k}}{(2\pi)^d} \frac{\dots}{z-\Delta\varepsilon} = \int \frac{\mathrm{d}^d\vec{k}}{(2\pi)^d} \int_{-\infty}^{+\infty} \mathrm{d}\varepsilon \delta(\Delta\varepsilon-\varepsilon) \frac{\dots}{z-\varepsilon} = \int_{-\infty}^{+\infty} \frac{\mathrm{d}\varepsilon}{z-\varepsilon} \int \frac{\mathrm{d}^d\vec{k}}{(2\pi)^d} \delta(\Delta\varepsilon-\varepsilon)(\dots)$$

from which we can define a density of states $\rho(\vec{q},\varepsilon) = \int \frac{\mathrm{d}^d\vec{k}}{(2\pi)^d}\delta(\Delta\varepsilon-\varepsilon)(\dots)$ and thus $\Sigma(\vec{q},z) = \int_{-\infty}^{+\infty} \frac{\mathrm{d}\varepsilon}{z-\varepsilon}\rho(\vec{q},\varepsilon)$. For our three second-order processes in $\hat{H}^{(3)}$, the densities of states can be written as

$$\rho_{\text{Bel}}(\vec{q},\varepsilon) = \int \frac{\mathrm{d}^d\vec{k}}{(2\pi)^d}\delta(\varepsilon_k-\varepsilon_{\vec{q}-\vec{k}}-\varepsilon)\frac{1}{2}\left|\langle\vec{k},\vec{q}-\vec{k}|\hat{H}^{(3)}|\vec{q}\rangle\right|^2\left(1+\bar{n}_{\vec{k}}+\bar{n}_{\vec{q}-\vec{k}}\right) \tag{3.14}$$

$$\rho_{\text{Lan}}(\vec{q},\varepsilon) = \int \frac{\mathrm{d}^d\vec{k}}{(2\pi)^d}\delta(\varepsilon_{\vec{q}+\vec{k}}-\varepsilon_k-\varepsilon)\left|\langle\vec{q}+\vec{k}|\hat{H}^{(3)}|\vec{k},\vec{q}\rangle\right|^2\left(\bar{n}_{\vec{k}}-\bar{n}_{\vec{q}+\vec{k}}\right) i \tag{3.15}$$

$$\rho_{\text{non-res}}(\vec{q},\varepsilon) = -\int \frac{\mathrm{d}^d\vec{k}}{(2\pi)^d}\delta(\varepsilon_k+\varepsilon_{\vec{q}+\vec{k}}+\varepsilon))\frac{1}{2}\left|\langle\vec{0}|\hat{H}^{(3)}|\vec{k},\vec{q},-(\vec{q}+\vec{k})\rangle\right|^2\left(1+\bar{n}_{\vec{q}+\vec{k}}+\bar{n}_{\vec{k}}\right). \tag{3.16}$$

We recognise here a generalised form of the (1.33)-(1.34) integrals for the Beliaev-Landau damping rates according to Fermi's golden rule calculated in chapter 1. One can indeed write $\Gamma^{\text{proc}}_{\vec{q}} = \rho_{\text{proc}}(\vec{q},\varepsilon_q)$. A numerical calculation can then follow the same strategy as that taken on that occasion: one integrates the energy conserving Dirac on the variable θ, angle between $\vec{q}$ and $\vec{k}$, and reinserts the roots θ_0 into the matrix element and the occupation numbers to finally integrate explicitly on the wave number k. Care must be taken to ensure that the energy conserving angles θ_0 do not introduce any zero momentum phonons or phonons with a wave number greater than the ultraviolet cut-off η (whether $\vec{k}$, $\vec{q}+\vec{k}$ or $\vec{q}-\vec{k}$). Finally, let us note that the non-resonant processes contribute this time to the final result, of course on Σ_R but even on Σ_I if ε is quite negative, although this contribution is negligible in practice compared to those of the Beliaev and Landau processes. Finally, we show that

$$\Sigma_I(\vec{q},\omega) = -\pi\rho(\vec{q},\hbar\omega), \tag{3.17}$$

$$\Sigma_R(\vec{q},\omega) = -\int_{-\infty}^{+\infty}\mathrm{d}\varepsilon\frac{\rho(\vec{q},\hbar\omega+\varepsilon)-\rho(\vec{q},\hbar\omega-\varepsilon)}{2\varepsilon} \tag{3.18}$$

in particular by expressing the integrand of Σ_R in terms of the Cauchy principal value and that of Σ_I in terms of the Dirac distribution:

$$\Sigma(\vec{q},\hbar\omega+\mathrm{i}0^+)=\int_{-\infty}^{+\infty}\mathrm{d}\varepsilon\,\rho(\vec{q},\varepsilon)\left(\mathrm{v.p.}\frac{1}{\hbar\omega-\varepsilon}-\mathrm{i}\pi\delta(\hbar\omega-\varepsilon)\right). \tag{3.19}$$

3.3 Specificity of the 2D case

In order to clarify the specificity of the $d=2$ case, we propose in this section an analysis of the behaviour of Σ in the $\epsilon\to 0$ limit at fixed $\rho\xi^2$ and $\bar{q}$. The objective is to determine the applicability of the Fermi golden rule in this limit. As such, a comparison will be made with the $d=3$ case where it can be applied. The argument is based on the consideration of the dominant order in ϵ of Σ on the one hand, and that of the scale of variation of Σ in $z-\varepsilon_q\equiv\zeta$ on the other hand. The two corresponding power laws have already been discussed and even expressed in chapter 1. In fact, in the expressions of Σ_{proc} (3.8)-(3.10), it can be seen that it is the "energy defect" term of form $\frac{1}{\zeta-\Delta\varepsilon}$, which determines the variation of Σ in ζ. However, these energy defects have already been calculated to the leading order in ϵ. We can read on equations (1.49) and (1.51) that these defects are of order ϵ^3 (reasoning on the scaled quantities), consequence of the dependence in ϵ of the angle θ_0 [see equations (1.50) and (1.52)].

Similarly, we can read from the expression of $\bar{\Gamma}_q$ (1.59) the order ϵ^3 for the dominant order of Σ. This is because, as with the integral of the damping rates, the squared matrix element contributes a factor of ϵ^3 while the squared energy defect contributes a factor of ϵ^{-1} to the leading order. $\bar{\Sigma}$ is therefore of order 2 in ϵ and Σ of order 3 in ϵ.

The two power laws involved are therefore identical, which will have important consequences for the behaviour of the signal for small values of ϵ. In the case $d=3$ a contrario, the scale of variation in ζ of Σ remains of order ϵ^3 but the clean energy function is of order ϵ^5, the damping rate varying as T^5 [30].

Consequences for the accuracy of the pole approximation Let us introduce a scaling of Σ, ζ and t in the limit $\epsilon\to 0$

$$\Sigma(\vec{q},z)\equiv\epsilon^{\nu}\sigma(\vec{q},\frac{z-\varepsilon_q}{\epsilon^{\mu}}=\frac{\zeta}{\epsilon^{\mu}}) \quad ; \quad \frac{t}{\hbar}\equiv\epsilon^{-\nu}\underline{t} \quad ; \quad \zeta\equiv\epsilon^{\nu}\underline{\zeta} \tag{3.20}$$

and write the signal (3.4) in terms of these scaled variables

$$\frac{\langle\hat{b}_{\vec{q}}(t)\hat{b}^{\dagger}_{\vec{q}}(0)\rangle}{\bar{n}_q}\mathrm{e}^{\varepsilon_q t/\hbar}\underset{\epsilon\to 0}{\simeq}\int_{C_+}\frac{\mathrm{d}\underline{\zeta}}{2\mathrm{i}\pi}\frac{\mathrm{e}^{-\mathrm{i}\underline{\zeta}\underline{t}}}{\underline{\zeta}-\sigma(\vec{q},\underline{\zeta}\epsilon^{\nu-\mu})}. \tag{3.21}$$

The result is clear: for the case $d=3$ where $\nu=5$ and $\mu=3$, there is $\epsilon^{\nu-\mu}=\epsilon^2\to 0$ so the pole approximation replacing the function Σ in the denominator of (3.21) by the constant $\sigma(\vec{q},0)$ is accurate in the limit $\epsilon\to 0$. On the other hand, in the case $d=2$, there is $\nu=\mu=3$ hence $\epsilon^{\nu-\mu}=1$, which implies that this limit is not sufficient to make the pole approximation and therefore Fermi's golden rule exact!

3.4 Diagrammatic theory at the dominant order in ϵ

Now that we have established the specificity of the $d = 2$ case with respect to the $\epsilon \to 0$ limit, it would be useful to obtain a "small parameter" of the model that would characterize the strength of the interactions and by means of which we could obtain a condition of validity of the Fermi golden rule. We start by scaling the variables again by

$$\tilde{t} \equiv \epsilon^2 \frac{3\gamma}{8} \bar{q} \bar{t} \quad ; \quad \bar{z} - \bar{\varepsilon}_q \equiv \epsilon^2 \frac{3\gamma}{8} \tilde{\zeta} \quad ; \quad \bar{\Sigma}^{(2)} \equiv \epsilon^2 \frac{3\gamma}{8} \tilde{\Sigma}^{(2)}. \tag{3.22}$$

The scaled Beliaev and Landau self-energy functions at order 2 in $\bar{H}^{(3)}$ are then written in the $\epsilon \to 0$ limit in the upper half-plane:

$$\tilde{\Sigma}^{(2)}_{\text{Bel}}(\bar{q}, \tilde{\zeta}) = \frac{1}{\mathrm{i}u} \int_0^{\bar{q}/2} \frac{\mathrm{d}\bar{k}}{\bar{q}} \frac{\left(\bar{k}(\bar{q} - \bar{k})\right)^{3/2} (1 + \bar{n}_k + \bar{n}_{q-k})}{\left(\bar{k}(\bar{q} - \bar{k}) + \tilde{\zeta}\right)^{1/2}} \tag{3.23}$$

$$\tilde{\Sigma}^{(2)}_{\text{Lan}}(\bar{q}, \tilde{\zeta}) = \frac{1}{\mathrm{i}u} \int_0^{+\infty} \frac{\mathrm{d}\bar{k}}{\bar{q}} \frac{\left(\bar{k}(\bar{q} + \bar{k})\right)^{3/2} (\bar{n}_k - \bar{n}_{q+k})}{\left(\bar{k}(\bar{q} + \bar{k}) - \tilde{\zeta}\right)^{1/2}} \tag{3.24}$$

$$\text{with} \quad \boxed{u = \frac{\pi \rho \xi^2 \gamma^{3/2}}{\sqrt{3}(1 + \Lambda)^2}}. \tag{3.25}$$

Thus, at order 2 in ϵ, the physics of the system depends only on the physical parameter u ! In particular, these relations suggest that Fermi's golden rule can be successfully applied when $u \gg 1$. [3] However, the order of magnitude in ϵ and u of the higher order self-energy functions must be checked

3.4.1 Studying the higher orders of the self-energy function

To study these higher orders, we use a method of "power counting" the terms in the integrals contributing to Σ in order to evaluate the leading order in ϵ and u without having to explicitly calculate these integrals. In particular, this method relies on the following argument : we assume that for all diagrams at all orders in $\bar{H}^{(3)}$, the angles that satisfy the Dirac of conservation of energy are small and of order ϵ and therefore the energy denominators are also small and of order ϵ^3. This is what we had indeed seen at order 2 in the expressions (3.8) and (3.9). This assumption is not so strong because of the quasi-linearity of our phonon spectrum. If it were exactly linear (a true $\varepsilon = ck$ phonon spectrum), only collinear phonons could have interacted on the energy layer, i.e. $\theta_0 = 0$ would have been the only possible solution for energy conservation. [4] Therefore, by continuity, a small curvature must lead to a small angle.

As an example, consider a fourth-order diagram in $\bar{H}^{(3)}$ shown in Figure 3.3. To begin with, any matrix element can be represented schematically (see equation (1.14)) by

[3] The characteristic time scale of the golden rule corresponds to $\tilde{t} \sim u$ so $\tilde{\zeta} \sim 1/u$ in frequency space so that in the $u \to +\infty$ limit, $\tilde{\Sigma}^{(2)}(\bar{q}, \tilde{\zeta})$ can be approximated by $\tilde{\Sigma}^{(2)}(\bar{q}, \mathrm{i}0^+)$ in the signal integrand, giving back the pole approximation and thus Fermi's golden rule for damping.

[4] This is why one cannot be satisfied with this spectrum, which restricts collisions in a way that differs from experimental reality.

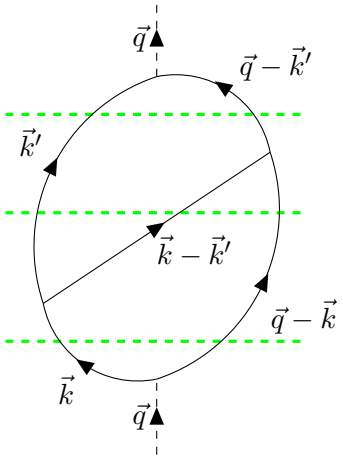

Figure 3.3: One of the fourth-order in $\bar{H}^{(3)}$ diagrams with an intermediate phonon coupling the two branches of the loop. We have noted the momentum of each phonon, taking into account the conservation of the momentum at each node, which leaves two internal wave vectors to integrate on. The green dashed lines represent the energy denominators ΔE. The matrix elements of the cubic interaction $\bar{H}^{(3)}$ will be divided by the energy of each intermediate state as many times as there are independent intermediate states (ΔE contains the sum of the energies of the phonons intersected by a given green dash).

$\langle f|\mathcal{H}^{(3)}|i\rangle \propto \sqrt{\frac{\hbar k_1}{mc}\frac{\hbar k_2}{mc}\frac{\hbar k_3}{mc}}\frac{mc^2}{\sqrt{\rho}} \propto \frac{\epsilon^{3/2}mc^2}{\sqrt{\rho}}$ because each wave number is of order $k_BT/\hbar c$. Thus, we can write (counting 4 matrix elements of $H^{(3)}$ on the diagram)

$$\Sigma^{(4)} \propto \int \mathrm{d}^2\vec{k} \int \mathrm{d}^2\vec{k}' \left(\frac{\epsilon^{3/2}mc^2}{\sqrt{\rho}}\right)^4 \frac{1}{\Delta E \Delta E \Delta E} \tag{3.26}$$

where ΔE represents a different energy denominator each time. There are three of them because, as can be seen in figure 3.3, for each possible diagram at this order (i.e. for all possible orientations of the inner lines of the diagram), there are three intermediate states (there was only one at order 2). We switch to polar coordinates of axis $\vec{q}$ in the momentum space and take into account that the angular width is $\approx \epsilon$ and $\Delta E \approx k_BT\epsilon^2$. So

$$\Sigma^{(4)} \propto \int \mathrm{d}k\mathrm{d}k'\, kk' \int \mathrm{d}\theta\mathrm{d}\theta' \left(\frac{\epsilon^{3/2}mc^2}{\sqrt{\rho}}\right)^4 \frac{1}{\Delta E \Delta E \Delta E} \tag{3.27}$$

$$\propto \left(\left(\frac{k_BT}{\hbar c}\right)^2\right)^2 (\epsilon)^2 \left(\frac{\epsilon^{3/2}mc^2}{\sqrt{\rho}}\right)^4 \left(\frac{1}{k_BT\epsilon^2}\right)^3. \tag{3.28}$$

In conclusion,

$$\Sigma^{(4)} \propto k_BT \left(\frac{\epsilon}{\rho\xi^2}\right)^2 \quad \text{where} \quad \boxed{\bar{\Sigma}^{(4)} \propto \frac{\epsilon^2}{(\rho\xi^2)^2}.} \tag{3.29}$$

With the same arguments, let us consider adding a higher order. From the point of view of the diagram, we must add two nodes $H^{(3)}$ that is to say two matrix elements, an intermediate

phonon thus an integration $\int \mathrm{d}k\, k \int \theta$, two intermediate states thus two energy denominators. Thus we add a factor of order

$$\int \mathrm{d}k\, k \int \theta \langle f|H^{(3)}|i\rangle \frac{1}{\Delta E \Delta E \Delta E} \propto \left(\frac{k_B T}{\hbar c}\right)^2 \epsilon \left(\frac{\epsilon^{3/2} m c^2}{\sqrt{\rho}}\right)^2 \left(\frac{1}{k_B T \epsilon^2}\right)^2 = \frac{1}{\rho \xi^2} \tag{3.30}$$

According to this method of counting powers associated with the hypothesis of the small denominators of energy for the small angles, the diagrams of higher order are all of dominant order ϵ^2 but of increasingly higher order in $1/u$:

$$\boxed{\bar{\Sigma}^{(2n)} \propto \frac{\epsilon^2}{(\rho \xi^2)^n} \quad \forall n \in \mathbb{N}^*} \tag{3.31}$$

which thus appears like a small unexpected parameter in the diagrammatic series.

Chapter 4

Results and comparison

Foreword

In this chapter we discuss the results from two runs of the simulation that differ in their interaction regime. Although both runs remain in the weakly collisional regime for all modes of the simulation, they differ in the value of the parameter $u = \frac{\pi\gamma^{3/2}}{\sqrt{3}(1+\Lambda)^2}\rho\xi^2$ that we introduced in the previous chapter and that characterises the strength of the interactions in the two-dimensional boson gas. Among the physical parameters of the two series, several are identical: the phonon curvature $\gamma = 1$, the thermodynamic parameter $\Lambda = 0$, the ultraviolet cut-off $\eta = 1$ and the reduced temperature $\epsilon = 1/2$. They therefore differ only in the value of the scaled density $\rho\xi^2$. We have $\rho\xi^2 = 10$ for series 1 and $\rho\xi^2 = 1.5625$ for series 2. We also present results from simulations identical to series 1 except for the value of the reduced temperature $\epsilon = 1/3$, which we call series 1 bis. Before presenting the results of the simulations, we check that the sets of parameters agree with the constraints of validity of the quantum hydrodynamics theory before addressing the question of the interaction regime defined by these physical parameters. Then we present some data extracted from the simulations that assure us of the physical consistency of our numerical integration before illustrating in the section that follows the behaviour of the temporal autocorrelation of a mode $\langle b_{\vec{q}}(t)b^*_{\vec{q}}(0)\rangle$ which is compared to the prediction of the Fermi golden rule. Finally, in the last section of this chapter, this part and this thesis, we study in detail the discrepancy between our simulations and the pole approximation as well as the different predictions on this discrepancy from the diagrammatic method of the N-body Green's functions. This discussion allows us to conclude on the validity and viability of our simulations and our theory.

4.1 Series validity and interaction regime

As mentioned in section 1.1 of chapter 1, quantum hydrodynamics, a low-energy mesoscopic theory, is subject to restrictions on the parameters of the system that guarantee the consistency of its description. The constraints boil down to (i) $\frac{\rho}{q_{\text{th}}^2} = \frac{\rho\xi^2}{\epsilon^2} \gg 1$ which ensures the relevance of the coarse-grained description of (1.1) hydrodynamics and (ii) $k_BT \ll mc^2 \Rightarrow \epsilon \ll 1$ which ensures that the temperature is low enough to populate only the phonon part of the excitation spectrum. Another useful quantity to judge the suitability of our description is the number of particles in a unit cell of our lattice. For our "coarse-grained" description

to be relevant, this number must be large in front of 1, so $\rho \mathrm{d}x\mathrm{d}y = \rho\xi^2 \left(\frac{\pi}{\eta\epsilon}\right)^2 \gg 1$.[1] We summarise our series and the value of these constraints in the following table :

Serie	$\rho\xi^2$	ϵ	u	$\rho \mathrm{d}x\mathrm{d}y$	$\frac{\rho\xi^2}{\epsilon^2}$	$\Gamma^{\mathrm{th}}/\omega_{\vec{q}}^{\mathrm{min}}$
1	10	1/2	18.14	394.8	40	$2.2 \cdot 10^{-2}$
1 bis	10	1/3	18.14	888.3	90	0.11
2	1.5625	1/2	2.83	61.7	6.25	0.96

For our three series, the constraint $\frac{\rho\xi^2}{\epsilon^2} \gg 1$ seems to be well realised. If the value $\epsilon = 1/2$ may seem a bit large to satisfy the constraint $\epsilon \ll 1$, which would imply that the collective excitations are not quite phononic, one should not forget that the curvature of the spectrum is of the form $\frac{\gamma}{8}\epsilon^2 \simeq 0,031$ in the simulation, which remains small. It can therefore be seen that what clearly differentiates the two series is the value of the parameter $u = \frac{\pi\gamma^{3/2}}{\sqrt{3}(1+\Lambda)^2}\rho\xi^2$ which we introduced in chapter 3 [see (3.25)] and which is none other than the inverse of the small parameter of the diagrammatic development. It is 18.14 for series 1 and 2.83 for series 2. Therefore, the Fermi golden rule should be closer to series 1 than to series 2.

Collisional regime of the simulations With these parameters, are we, for a given mode, rather in the hydrodynamic or weakly collisional regime? We can answer this question by comparing the pulsation of the mode with the damping of a typical thermal mode. For example, we can consider the fundamental excitation mode of each grid, with a scaled pulsation of $\bar{\omega}_{\vec{q}}^{\mathrm{min}} = 2\eta/n_x^{\mathrm{FBZ}}$, and the damping rate of the maximum energy mode with an average population of 1, which we find from the simulation data (see section 4.3). The hydrodynamic regime then corresponds to the limit $\Gamma^{\mathrm{th}}/\omega_{\vec{q}}^{\mathrm{min}} \gg 1$, while the low collisional regime refers to the inverse limit $\Gamma^{\mathrm{th}}/\omega_{\vec{q}}^{\mathrm{min}} \ll 1$. According to the last column of the previous table, which gives the value of this ratio, the three series 1, 1 bis and 2 are in the low collisional regime for all modes, even for the largest size 128×128. [2]

4.2 Conservation of energy checks

Constraints on the parameter values imposed by the model approximations are not the only ones we need to pay attention to in order to be sure that our simulations are a good account of the physical phenomena. The numerical methods we use to calculate the evolution in practice must also be accurate enough. In this section we check the stability properties of the time integration method, which is approached threefold (see chapter 2): firstly in the integration done via the fourth-order Runge Kutta method on $\bar{H}^{(3)}$, secondly by the four-point formula used for the calculation of the gradient, and thirdly by splitting the Hamiltonian into $\bar{H}^{(2)}$ and $\bar{H}^{(3)}$.

[1] Note, however, that this quantity depends on the ultraviolet cutoff which weakens its physical interpretation and thus its importance as a validity condition.

[2] This indicates that the limited size of the box prevents us from observing low-energy modes that could be found in the hydrodynamic regime. In this case, this regime seems within reach in view of series 2, since doubling or quadrupling the number of modes would bring a fraction of the lowest energy modes into this regime. For the moment, we have not been able to explore this regime in depth, we put at the end of this chapter, as a conclusion, a first glance from a third series of runs trying to catch a glimpse of these small modes in the hydrodynamic regime in the case $\rho\xi^2 = 1.5625$.

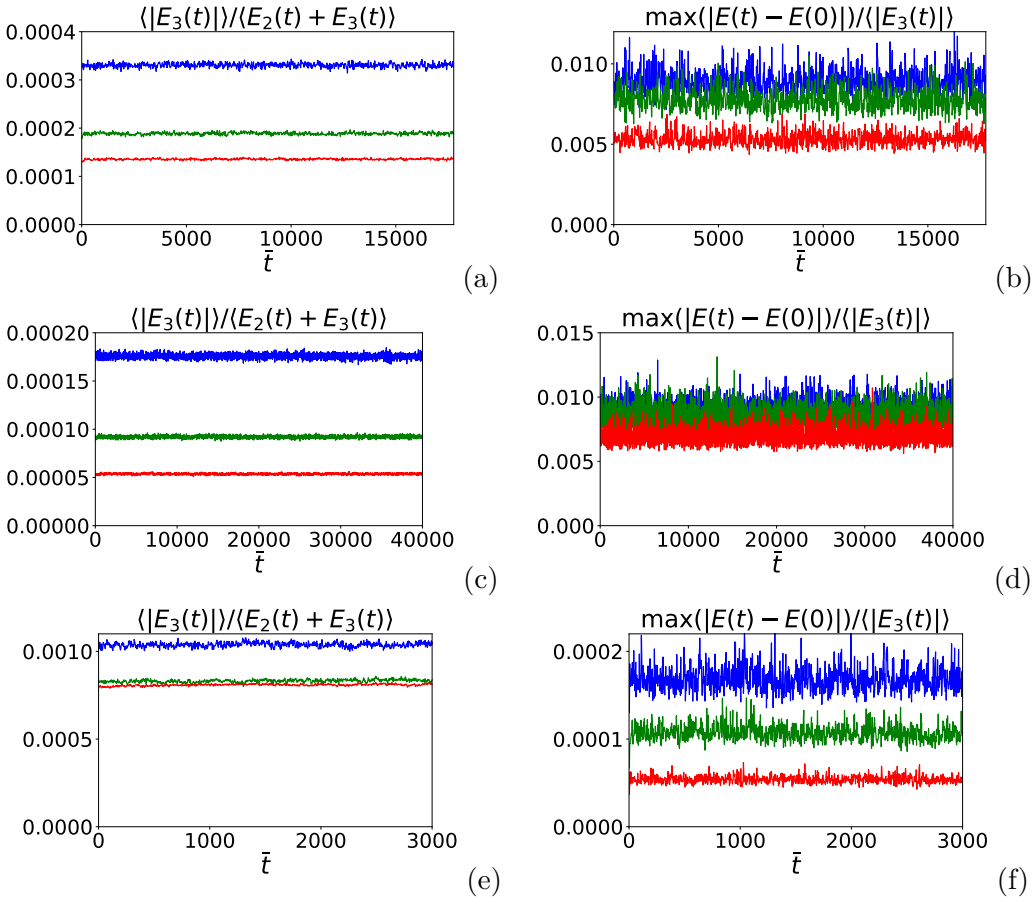

Figure 4.1: We represent two average quantities related to the energy of the gas and its conservation during integration. Each colour corresponds to a different system size: blue for 32×32 physical modes, green for 64×64 and red for 128×128. Each point that makes up the curves is the ensemble average over the 3200 realisations at instant $\bar{t}$. On the left, we represent the ratio of the average of the absolute value of the interaction energy, i.e. the absolute value of $\bar{H}^{(3)}$, to the total energy, the average of $\bar{H} = \bar{H}^{(2)} + \bar{H}^{(3)}$ over time. On the right, is shown the ratio of the maximum value among the 3200 realisations of the quantity $|E_{\text{tot}}(\bar{t}) - E_{\text{tot}}(0)|$ with $E_{\text{tot}}(\bar{t})$ the value of $\bar{H}$ for a given realisation at a given time to the average of the absolute value of $\bar{t}$ at this instant. (a) and (b) correspond to series 1, (c) and (d) to series 1 bis, (e) and (f) to series 2.

In figure 4.1 we show two types of quantities related to the energy of the gas and its conservation over time in the simulations. These averages are always taken over the realisations, the sub-figures in the left column represent the ratio of the average of the absolute value of the Hamiltonian $\bar{H}^{(3)}$ at an instant $\bar{t}$, to the average of the total Hamiltonian $\bar{H}^{(2)} + \bar{H}^{(3)}$ at this same instant. As for the sub-figures in the right-hand column, they represent the ratio of the maximum deviation (in absolute value) among all realisations between the total energy at time $\bar{t}$ and at time 0, to the average of the absolute value of the interaction energy at time $\bar{t}$. As we can see, the simulations are satisfactorily accurate. The constancy of the ratio between the interaction energy and the total energy of the sub-figures on the left confirms that the system has thermalized, i.e. reached a state of equilibrium. The sub-figures on the right give us information on two topics. Firstly, we can see that the Runge-Kutta time integration method of order 4 is quite satisfactory since the total energy fluctuates very little and is stable over time. Furthermore, by comparing the sub-figures on the left, we can see that the total energy is conserved in relative value to within 10^{-6} for series 1 and 1 bis and 10^{-7} for series 2 without apparent divergence. The second piece of information from the figures on the right is that the fluctuation of the total energy is always a very small fraction of the interaction energy, at worst $\simeq 1\%$ for series 1 and 1 bis and at best $\simeq 0.005\%$ in the subseries 128×128 of series 2. Having such a small ratio is important as all the effects we want to observe in these simulations result from the interaction Hamiltonian, so it is important that its effect on the system is larger than the numerical errors and uncertainties. The fact that the ensemble mean of $\bar{H}^{(3)}$ is always much larger than the maximum deviation from energy conservation confirms that this constraint is satisfied.

Finally, we can point out that the ratio of the energies of the left sub-figures is a physical variable of the system. As such, it should not depend on the size of the numerical box if it has reached the thermodynamic limit. In the figures, we can see that there is a certain dependence on the size while agreeing on the order of magnitude, but also that the larger subsets are much closer to the thermodynamic limit. This is why the following figures focus on these subseries. We will return to the question of reaching the thermodynamic limit in the last section when we find that the dynamics depend little on the size of the system by showing that modes with different momenta but the same wavenumber have close dynamics.

4.3 Fermi-Dirac golden rule versus simulation

In the approximation underlying the Fermi-Dirac golden rule, the evolution of the observable $\langle \hat{b}_{\vec{q}}(t)\hat{b}^{\dagger}_{\vec{q}}(0)\rangle$ or its classical field version is purely exponential with a scaled damping rate $\frac{\bar{\Gamma}_q}{2}$ with $\bar{\Gamma}_q$ given in equation (1.59). In figure 4.2, we represent, on the left, the evolution over time of this observable $\langle b_{\vec{q}}(\bar{t})b^{*}_{\vec{q}}(0)\rangle$ normalised by the population $\bar{n}_q$ of the thermodynamic equilibrium for the first 16 modes on each half-axis of the lattice for the subseries 128×128 of each series and on the right, a numerical estimate of the damping rate of this observable for these same modes and this same subseries 128×128 (from top to bottom: series 1, then 1 bis then 2). By mode on a half-axis, we mean modes of wave vector of the form $(\pm\frac{2l}{n_x^{\mathrm{FBZ}}}, 0)$ or $(0, \pm\frac{2l}{n_y^{\mathrm{FBZ}}}, 0)$ with $l \in [\![1; n_{x/y}^{\mathrm{FBZ}}/2]\!]$. For a given l, the 4 vectors on each of the half-axes play symmetrical roles for a square array. The observables of these 4 modes must therefore behave in the same way because they are subject to strictly the same evolutionary equations. We have therefore averaged the signals of these 4 modes to obtain the overall

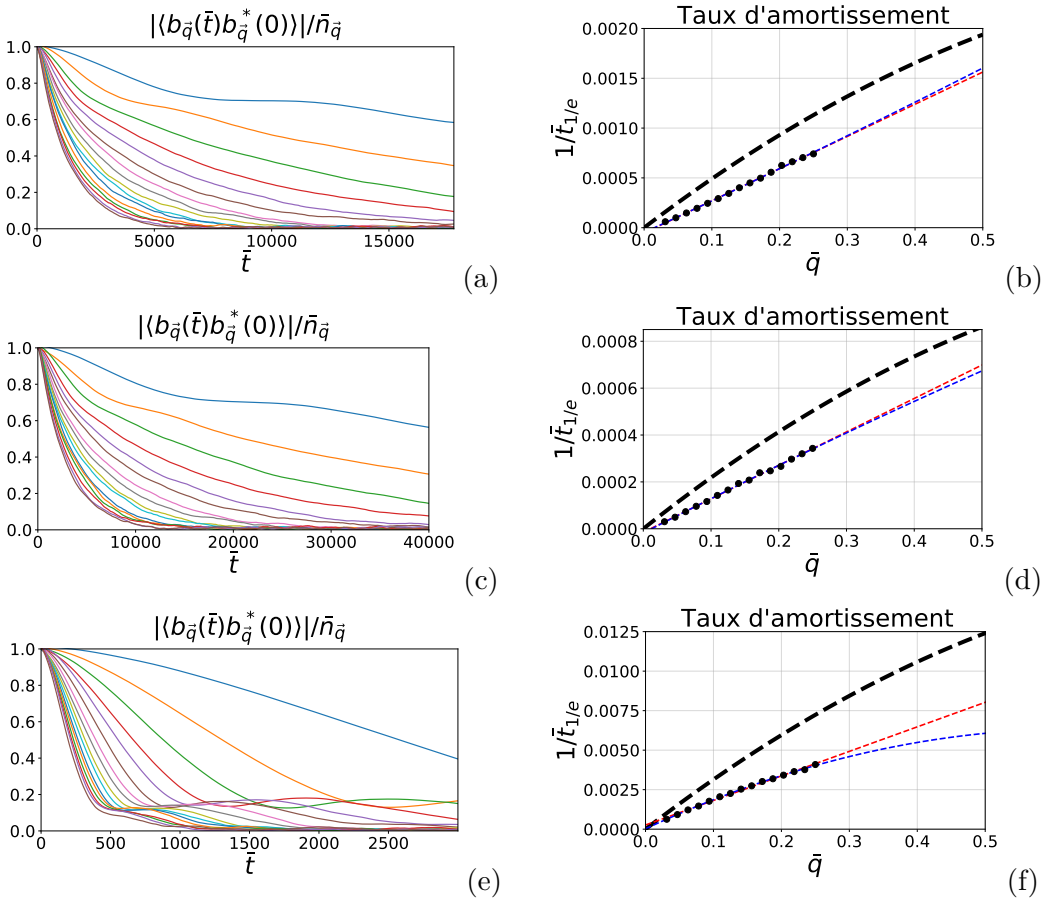

Figure 4.2: In the left-hand column, we show the absolute value of our target observable in the 128×128 subseries for each series, reduced to the thermodynamic equilibrium population, with which it coincides at the initial time, for the first 16 modes per half-axis, i.e. whose wave vector is of the form $(\pm\frac{2n}{n_x^{\mathrm{FBZ}}},0)$ or $(0,\pm\frac{2n}{n_y^{\mathrm{FBZ}}})$ with n integer between 1 and 16. We have averaged the signals of the four modes of equal n since they are equivalent in the square quantization box. In the right-hand column, we plot the damping rates as a function of $\bar{q}$. The black dots are taken from the curves in the left-hand column, each point is taken as the inverse of the time at which the amplitude of the signal has decreased by a factor of 1/e. The red dashed line corresponds to an affine fit in $\bar{q}$ while the blue corresponds to a quadratic fit. Finally, the black dashed line is the Landau-Beliaev damping rate (divided by two) as calculated by the Fermi-Dirac golden rule (1.59). Figures (a) and (b) are from series 1, (c) and (d) from 1 bis and (e) and (f) from 2.

averages of the observable with a statistical uncertainty reduced by a factor of 2. Note that the temporal correlation function we represent is strictly equal to the average population of the thermodynamic equilibrium at the initial time. This is why all these curves must start at 1, which is the case on the figures. We also notice very well the not quite exponential damping at short and long times, as our theory predicts [3], with these "bounces" that we can see in the correlation function. This is a consequence of the richer structure of the self-energy function, which has a cut-off line from a branch point in addition to a pole in its analytical extension. Since the damping is not quite exponential, it is difficult to extract a damping rate by fitting. Instead, to obtain an estimate of a rate, we determined the time $\bar{t}_{1/e}$ after which our temporal autocorrelation observable has decayed by a factor $1/e \simeq 0.368$. If the Fermi-Dirac golden rule were correct, then we would have a perfect match between these rates $\frac{\bar{\Gamma}_q}{2} = 1/\bar{t}_{1/e}$. It is therefore the inverse of this time that we represent in the figures in the right-hand column (black dots), rates determined directly from the curves of the figures in the left-hand column. [4] In the black dashed line, we plot the rate (divided by two) from the Fermi-Dirac golden rule (1.59). The red and blue dashed lines correspond to affine and quadratic fits of the black points. It is the slope obtained by the affine fit that we used to estimate the Γ^{th} thermalization rate, i.e. that of the $\bar{q} = 1$ modes.

It can be seen that the modes decay more slowly than the golden rule prediction. Nevertheless, the obvious linearity of the decay rates at $1/e$ to low $\bar{q}$ does not contradict this and supports the idea that these simulations are indeed in the weak collision regime and not in the hydrodynamic regime.

4.4 Comparison between Green's functions theory and numerical simulations

In this last section we present the results of our simulations for the deviation between the reduced signal and the pole approximation. In particular, the figures in this section all represent the quantity

$$\frac{\langle b_{\vec{q}}(\bar{t}) b^*_{\vec{q}}(0)\rangle}{\bar{n}_q} \mathrm{e}^{\mathrm{i}\bar{\varepsilon}_q \bar{t}} - \mathrm{e}^{-\mathrm{i}\Sigma(\bar{q},\bar{\varepsilon}_q+\mathrm{i}0^+)\bar{t}} \tag{4.1}$$

for values $\bar{q}$ equal to $1/4$ and $5/16$. In equation (4.1), the self-energy function $\Sigma(\bar{q},\bar{\omega})$ is calculated to order 2 in $\bar{H}^{(3)}$. Forming this quantity is equivalent to subtracting from the curves in the left-hand column of Figure 4.2 the prediction of the $\mathrm{e}^{-\mathrm{i}\Sigma(\bar{q},\bar{\varepsilon}_q+\mathrm{i}0^+)\bar{t}}$ pole approximation that is obtained numerically by performing integrations (3.17) and (3.18) and then retaining the 0th-order $\bar{\omega} = \bar{\varepsilon}_q + \mathrm{i}0^+$ pole approximation. Recall also that $\bar{n}_q = 1/\bar{\varepsilon}_q$ according to the equipartition law of classical physics. As Σ is calculated to order 2 in $\bar{H}^{(3)}$, the imaginary part gives back (within a factor of 2) the damping rate of Fermi's golden rule; on the other hand, the real part describes a shift in the eigenpulsation of the modes due to their interactions, which escapes the golden rule and contributes to the phase of the signal. We compare these results with the predictions of the diagrammatic Green's functions

[3] Let us note however that the non-exponential departure is not specific to the two-dimensional case. Indeed, Fermi's golden rule which predicts a purely exponential damping is never valid at short times, whatever the order in ϵ and the dimensionality of the system.

[4] Only 15 points are counted because the fundamental mode has not damped sufficiently to be assigned a time $\bar{t}_{1/e}$.

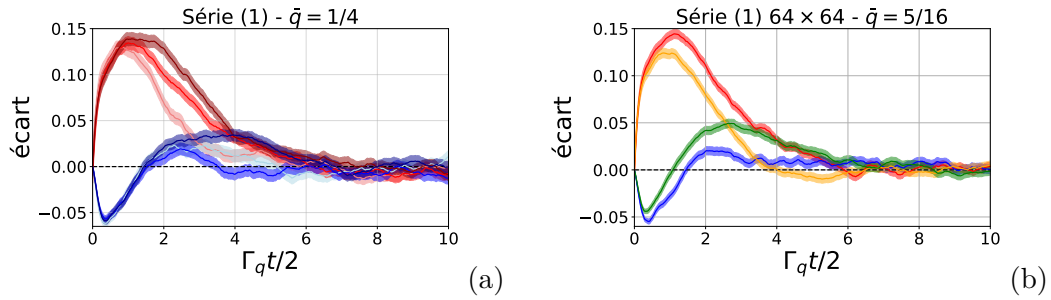

Figure 4.3: Series 1: deviations from the pole approximation of the autocorrelation function as in the equation (4.1) for different lattice sizes and different wavenumbers in the lattice. Red is associated with the real part of the signal, blue with its imaginary part. The colored area corresponds to the statistical uncertainty on the mean given by the usual formula (standard deviation)/$\sqrt{n_{\text{traj}} n_{\text{mode}}}$ with n_{mode} the number of mode of the same wavenumber on the axis. Time is in units of $2/\bar{\Gamma}_q$, Fermi's golden rule prediction for the classical field (1.59). (a) The signal for the three subseries of different sizes for the modes with $\bar{q} = 1/4$ on the semi-axes of the lattice. Each color gradient is associated with a lattice size gradient (the lightest corresponds to the smallest lattice and the darkest to the largest). (b) The signal of modes of momentum $\bar{q} = 5/16$ for the sub-series of size 64×64, we compare the signal of the modes on the axis (red and blue) and on the off-axis modes (orange and green) defined in note 5.

method with a calculation of the self-energy function, at all $\bar{\omega}$ pulsations, at order 2 and at all orders in ϵ.

As a reminder, the power counting argument discussed in Section 3.3 of Chapter 3 suggests that in the two-dimensional case, the pole approximation is not sufficient to predict phonon damping, even at low temperatures. For Fermi's golden rule to be applicable, a second parameter, $1/u$, must be small. Our simulations attempt to confirm or refute this fact by time integration at all orders in $\bar{H}^{(3)}$ and ϵ. We present the different results per series. The colour and shape code is identical in all the following figures: the red colour is associated with the real part of the signal and the blue colour with the imaginary part. The solid lines represent the results of the simulations. The dashed lines are associated with a diagrammatic prediction at all orders in ϵ while the dotted lines are associated with the prediction at order 2. The darker the colour, the larger the system size.

4.4.1 Series 1

Let us start by considering series 1, which is characterised by the parameters $\rho\xi^2 = 10$ and $\epsilon = 1/2$. Figure 4.3a shows the deviation (4.1) for the phononic modes with momentum $\bar{q} = 1/4$ for systems with sizes. For a perfect achievement of the thermodynamic limit, these three subseries should give strictly the same results since the considered correlation function should not depend on the extensive variables of the system anymore. We see on this figure that the three subseries agree well even if we remark that the real part has not completely converged except at short times. Notice the structure of this signal: an abrupt increase in the deviation from the pole approximation before an oscillating convergence towards it at long

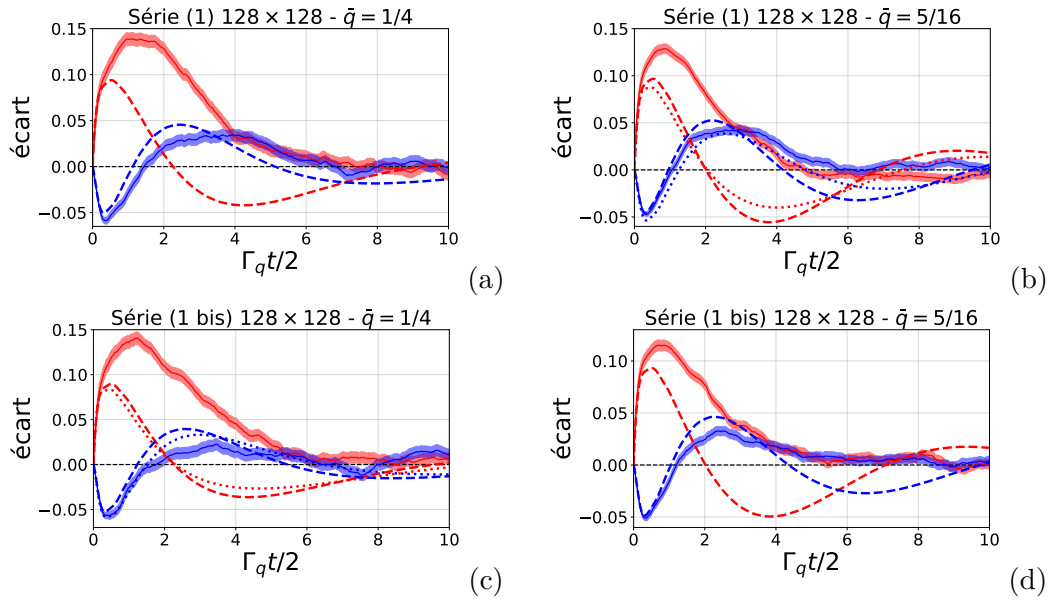

Figure 4.4: In series 1, for simulations in the lattice with 128×128 physical modes, the deviation from the pole approximation of the temporal correlation function (4.1) for two distinct modes of the lattice. Shapes and colors of the curves identical to the figure 4.3, see its description as well as the text for details. By numerical integration of the equations (3.17) and (3.18) of chapter 3, we obtain a prediction at all orders in ϵ (dashed) and at order 2 in ϵ (dotted). (a) The signal for the phononic modes of momentum $\bar{q} = 1/4$. (b) The signal for modes of momentum $\bar{q} = 5/16$ and which are outside the axes of the lattice. Figures (c) and (d) are the equivalent of (a) and (b) for series 1 bis.

times. This structure will be seen again in all future figures as well as in the diagrammatic predictions. In sub-figure (b) we compare on-axis and off-axis modes [5] of same momentum $\bar{q} = 5/16$ in the intermediate sub-series of size 64×64. Again, any difference in the dynamics of these two modes can only be an effect of the finite size of the system. The conclusion we draw is the same as for sub-figure (a), the dynamics are broadly similar even though the modes have not perfectly converged with each other. It should be noted that, by nature, thermodynamic convergence for this gap is difficult to achieve since we are trying to extract and highlight a subdominant term in the dynamics.

In Figure 4.4 we focus on the largest subset, closest a priori to the thermodynamic limit, and compare the signal with the predictions of the diagrammatic Green's functions methods obtained by numerical integration of equations (3.17) and (3.18) in Chapter 3. Sub-figure

[5] By off-axis modes, we mean the 8 modes with coordinates $(\pm 3n_x^{\mathrm{FBZ}}/2, 4n_x^{\mathrm{FBZ}}/2)$ and $(\pm 4n_x^{\mathrm{FBZ}}/2, 3n_x^{\mathrm{FBZ}}/2)$ in the numerical wave vector lattice. The scaled wavenumber of these modes is indeed equal to $\bar{q} = 5/16$. This mode was chosen precisely for the "Pythagorean triplet" $5^2 = 3^2 + 4^2$ which matches an on-axis mode with the off-axis modes of the same wavenumber. For reasons of disk memory economy, we record only the 16 smallest modes on each axis for each series, which is why we do not have the $\bar{q} = 5/16$ on-axis mode for the larger 128×128 grid because this mode is of coordinates $(\pm 20, 0)$ and $(0, \pm 20)$ on the numerical array. Finally, note that the signal of these Pythagorean modes has been averaged over the 8 modes of the same wave number on the grid (and not only 4 as for the modes on the axes).

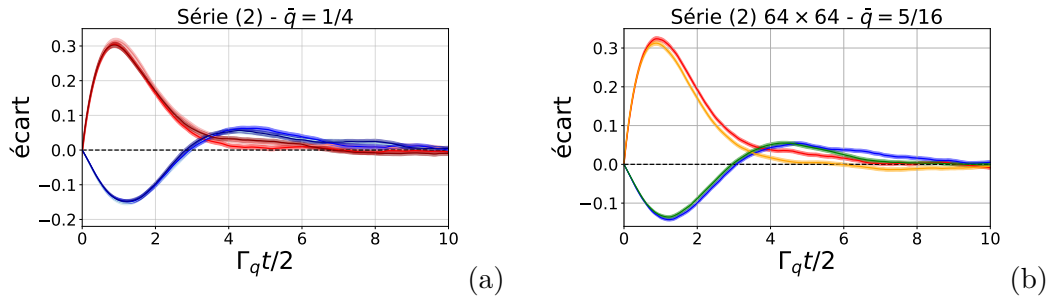

Figure 4.5: In series 2, several gaps from the approximation of the pole of the autocorrelation function as in (4.1) compared according to the size of the lattice on the one hand and the position of the mode in the lattice on the other. Shapes and colors of the curves identical to the figure 4.3, see its description as well as the text for details. (a) The signal for the three subseries of different sizes for the modes $\bar{q} = 1/4$ on the lattice axes. (b) The signal of the modes of wavenumber $\bar{q} = 5/16$ for the sub-series of size 64×64, we compare the signal of the modes on the axis (red and blue) and off-axis modes (orange and green).

(a) still is for the $\bar{q} = 1/4$ modes and sub-figure (b) for the (off-axis) modes with $\bar{q} = 5/16$. A very good qualitative and quantitative agreement between the Green's functions predictions (dashed and dotted lines) and the simulations (solid lines) can be seen, but it is at very short times that the best agreement between the different curves is obtained. In addition, we present results for a variant of series 1 with a lower reduced temperature $\epsilon = 1/3$. This is the series that we introduced earlier as 1 bis and that we illustrate in sub-figures (c) and (d). Comparison with subfigures (a) and (b) of series 1 shows that the two variants are very similar, at most we note without surprise that the prediction of the diagrammatic method at order 2 in ϵ agrees less well with that at all orders in series 1 than in series 1 bis. The change $\epsilon = 1/2 \to \epsilon = 1/3$ may not seem impressive but it should be remembered that the curvature of the spectrum for the scaled wave vector $\bar{q}$ is in ϵ^2 as are most of the physical properties we study such as damping rates. This change introduces a factor 2.25 on the value of ϵ^2, which is not negligible. As suggested by the table in section 4.1 which summarises the parameters, series 1 and 1 bis, although of different parameters and regime, are both deep in the low collisional regime and indeed there is little difference in our simulations. One should remember the lessons of chapter 3 : at order 2 in ϵ, u is the only physical parameter (besides ϵ) of the system. Series 2 explores the effect of a change in this parameter on the phonon dynamics.

4.4.2 Series 2

Series 2 corresponds to a regime of much stronger interactions than series 1, since its parameter u is much smaller (from $u \simeq 18$ we move to $u \simeq 3$). We have already pointed out that the first modes of the numerical grid are close to the hydrodynamic regime as $\Gamma^{\text{th}}/\omega_{\vec{q}}^{\text{min}} \simeq 1$. We plot in Figure 4.5 the deviation (4.1) of the autocorrelation function from the pole approximation for each of the subseries of different sizes, as we did earlier for series 1. First, we notice that the simulations converged much better with the size of the system: in subfigure (a) the curves for the $\bar{q} = 1/4$ modes for different sizes of the simulations show almost

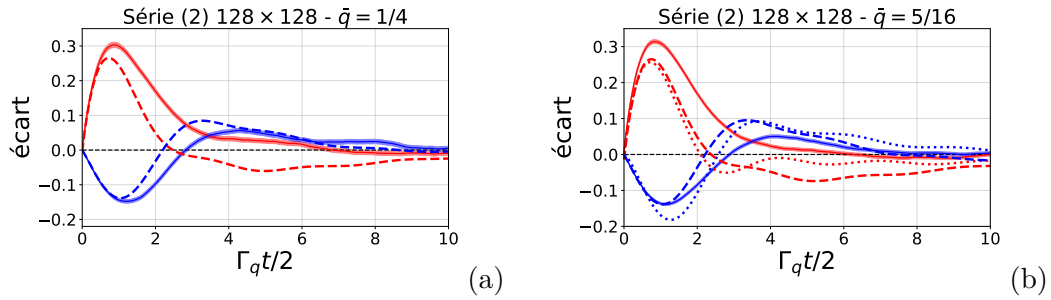

Figure 4.6: In series 2, for simulations on the lattice with 128×128 physical modes, the deviation from the pole approximation of the autocorrelation function as in (4.1) for two distinct lattice modes. Shapes and colors of the curves as in the figure 4.3, see its legend as well as the text for more details. By numerical integration of the equations (3.17) and (3.18) from chapter 3, we obtain a prediction at all orders in ϵ (dashed) or at order 2 in ϵ (dotted). (a) The signal for the phononic modes on the axes and of wavenumber $\bar{q} = 1/4$. (b) The off-axis modes signal with wavenumber $\bar{q} = 5/16$.

indistinguishable curves; the same is true in sub-figure (b) which compares the $\bar{q} = 5/16$ mode on-axis and off-axis in the 64×64 size simulations. In contrast to series 1, therefore, the thermodynamic limit is clearly reached.

Figure 4.6 focuses on the 128×128 subseries and compares the simulations with the diagrammatic predictions. The predictions at all orders in ϵ (dashed lines) agree very well with the simulations while those at order 2 diverge (dotted lines). This good agreement was not a foregone conclusion. Indeed, as we learned in chapter 3, the diagrams that the Green's functions prediction ignores, even if we restrict ourselves to the order ϵ^2, differ by their order in $1/u$. By decreasing u, we have thus increased the contribution of these subdominant diagrams, which should worsen the error that the diagrammatic method makes at order 2 in $\bar{H}^{(3)}$. However, the agreement remains just as good.

The diagrammatic theory by Green's functions that we have successfully tested in our simulations for different parameter regimes can be adapted to the quantum case and thus compared with real measurements from experiments. We believe we have thus established the ability of our numerical scheme to describe these two-dimensional superfluids. It is a very versatile computer program from which we can explore other parameter regimes. For example, increasing the size of the system would allow us to probe the transition to the hydrodynamic regime. Another direction directly accessible without having to adapt the program would be to explore the concave $\gamma < 0$ case where it is now the fourth-order diagrams in $\bar{H}^{(3)}$ that characterise the dissipative dynamics, the second-order diagrams having a purely real contribution to the eigenenergy function in the pole approximation.

4.5 Conclusion of the second part

We have performed simulations based on Landau and Khalatnikov quantum hydrodynamics to study phonon damping in a two-dimensional boson gas in the superfluid and low temperature regime. The simulations showed a significant deviation from the exponential decay

predicted by Fermi's golden rule even at low temperatures. This is a surprising behaviour and different from the three-dimensional case where the Fermi golden rule becomes exact in the limit where the temperature tends to zero. In Chapter 3, we used the diagrammatic method of N body Green's functions to study the phonon dynamics of the system. By this method, we obtain a prediction at order 2 in the $H^{(3)}$ interaction Hamiltonian (cubic in the phonon creation and annihilation operators) which qualitatively confirms the deviation from Fermi's golden rule visible in the simulations, conducted at all orders in $H^{(3)}$. Furthermore, the diagrammatic method informs us that, in two dimensions, the Fermi golden rule does not become exact in the very low temperature limit and suggests the existence of a second "small parameter" necessary for its validity.

The characterisation of this discrepancy is a new result, to our knowledge, and is in a regime close to recent experimental observations in two-dimensional gases of cold atoms [14, 15, 16].

Bibliography

[1] N. D. Mermin and H. Wagner. "Absence of Ferromagnetism or Antiferromagnetism in One- or Two-Dimensional Isotropic Heisenberg Models". In: *Physical Review Letters* 17 (Nov. 1966), pp. 1133–1136. DOI: 10.1103/PhysRevLett.17.1133.

[2] V L Berezinskii. "Destruction of Long-Range Order in One Dimensional and Two Dimensional Systems possessing a Continuous Symmetry Group. II. Quantum Systems". en. In: *Soviet Physics JETP* 34 (Sept. 1971), p. 7.

[3] J. M. Kosterlitz and D. J. Thouless. "Ordering, metastability and phase transitions in two-dimensional systems". en. In: *Journal of Physics C: Solid State Physics* 6 (Apr. 1973), pp. 1181–1203. ISSN: 0022-3719. DOI: 10.1088/0022-3719/6/7/010.

[4] D. J. Bishop and J. D. Reppy. "Study of the superfluid transition in two-dimensional 4 He films". In: *Phys. Rev. Lett.* 40 (1978), p. 1727.

[5] I.M. Khalatnikov et D.M. Chernikova. "Relaxation Phenomena in Superfluid Helium". In: *ZhETF* 49 (June 1966), p. 1957.

[6] Charles D. H. Williams et Adrian F. G. Wyatt Damian H. S. Smith Ruslan V. Vovk. "Pressure dependence of phonon interactions in liquid 4 He". In: *Phys. Rev. B* 72 (Aug. 2005), p. 054506.

[7] et E. Witkowska A. Sinatra Y. Castin. "Coherence time of a Bose-Einstein condensate". In: *Phys. Rev. A* 80 (Sept. 2009), p. 033614.

[8] G. E. Volovik. "Superfluid analogies of cosmological phenomena". en. In: *Physics Reports* 351 (Sept. 2001), pp. 195–348. ISSN: 0370-1573. DOI: 10.1016/S0370-1573(00)00139-3.

[9] Carlos Barceló, Stefano Liberati, and Matt Visser. "Analogue Gravity". en. In: *Living Reviews in Relativity* 14 (May 2011), p. 3. ISSN: 1433-8351. DOI: 10.12942/lrr-2011-3.

[10] L. J. Garay et al. "Sonic Analog of Gravitational Black Holes in Bose-Einstein Condensates". In: *Physical Review Letters* 85 (Nov. 2000), pp. 4643–4647. DOI: 10.1103/PhysRevLett.85.4643.

[11] Pieter van Wyk et al. "Superfluid Fermi atomic gas as a quantum simulator for the study of the neutron-star equation of state in the low-density region". In: *Phys. Rev. A* 97 (1 2018), p. 013601. DOI: 10.1103/PhysRevA.97.013601.

[12] M. H. Anderson et al. "Observation of Bose-Einstein Condensation in a Dilute Atomic Vapor". In: *Science* 269 (1995), pp. 198–201. DOI: 10.1126/science.269.5221.198. eprint: https://www.science.org/doi/pdf/10.1126/science.269.5221.198.

[13] Alexander L. Gaunt et al. "Bose-Einstein Condensation of Atoms in a Uniform Potential". In: *Phys. Rev. Lett.* 110 (20 2013), p. 200406. DOI: 10.1103/PhysRevLett.110.200406.

[14] J. L. Ville et al. "Sound Propagation in a Uniform Superfluid Two-Dimensional Bose Gas". In: *Physical Review Letters* 121 (Oct. 2018), p. 145301. DOI: 10.1103/PhysRevLett.121.145301.

[15] Panagiotis Christodoulou et al. "Observation of first and second sound in a BKT superfluid". In: *Nature* 594 (June 2021), pp. 191–194. ISSN: 1476-4687. DOI: 10.1038/s41586-021-03537-9.

[16] Markus Bohlen et al. "Sound Propagation and Quantum-Limited Damping in a Two-Dimensional Fermi Gas". In: *Phys. Rev. Lett.* 124 (24 2020), p. 240403. DOI: 10.1103/PhysRevLett.124.240403.

[17] A. Cappellaro, F. Toigo, and L. Salasnich. "Collisionless dynamics in two-dimensional bosonic gases". In: *Physical Review A* 98 (Oct. 2018), p. 043605. DOI: 10.1103/PhysRevA.98.043605.

[18] Miki Ota et al. "Collisionless Sound in a Uniform Two-Dimensional Bose Gas". In: *Physical Review Letters* 121.14 (Oct. 2018), p. 145302. DOI: 10.1103/PhysRevLett.121.145302.

[19] L.D. Landau and I.M. Khalatnikov. "The theory of the viscosity of Helium II: II. Calculation of the viscosity coefficient". In: *Journal of Experimental and Theoretical Physics* 19 (1949), p. 709.

[20] P. O. Fedichev and G. V. Shlyapnikov. "Finite-temperature perturbation theory for a spatially inhomogeneous Bose-condensed gas". In: *Physical Review A* 58 (Oct. 1998), pp. 3146–3158. DOI: 10.1103/PhysRevA.58.3146.

[21] H. Kurkjian, Y. Castin, and A. Sinatra. "Three-Phonon and Four-Phonon Interaction Processes in a Pair-Condensed Fermi Gas". In: *Annalen der Physik* 529 (2017), p. 1600352. ISSN: 1521-3889. DOI: 10.1002/andp.201600352.

[22] Hadrien Kurkjian, Yvan Castin, and Alice Sinatra. "Brouillage thermique d'un gaz cohérent de fermions". fr. In: *Comptes Rendus Physique*. Quantum microwaves / Micro-ondes quantiques 17 (Aug. 2016), pp. 789–801. ISSN: 1631-0705. DOI: 10.1016/j.crhy.2016.02.005.

[23] D.T. Son and M. Wingate. "General coordinate invariance and conformal invariance in nonrelativistic physics: Unitary Fermi gas." In: *Ann. Physics* 321 (2006), 197–224.

[24] C. Cohen-Tannoudji, J. Dupont-Roc, and G. Grynberg. *Processus d'interaction entre photons et atomes.* 1988.

[25] A. Sinatra, Y. Castin, and E. Witkowska. "Nondiffusive phase spreading of a Bose-Einstein condensate at finite temperature". In: *Phys. Rev. A* 75 (Mar. 2007), p. 033616.

[26] Ming-Chiang Chung and Aranya B. Bhattacherjee. "Damping in 2D and 3D dilute Bose gases". en. In: *New Journal of Physics* 11 (Dec. 2009), p. 123012. ISSN: 1367-2630. DOI: 10.1088/1367-2630/11/12/123012.

[27] Paul Adrien Maurice Dirac. "The quantum theory of the emission and absorption of radiation". In: *Proceedings of the Royal Society of London. Series A, Containing Papers of a Mathematical and Physical Character* 114 (Mar. 1927), pp. 243–265. DOI: 10.1098/rspa.1927.0039.

[28] Daisuke T. *FFTE: A Fast Fourier Transform Package*. 2020. URL: http://www.ffte.jp/.

[29] Fetter A. L. et Walecka D. J. *Quantum Theory of Many-Particle Systems*. 1971.

[30] H. Kurkjian, Y. Castin, and A. Sinatra. "Three-Phonon and Four-Phonon Interaction Processes in a Pair-Condensed Fermi Gas". In: *Annalen der Physik* 529 (2017), p. 1600352. ISSN: 1521-3889. DOI: 10.1002/andp.201600352.

Résumé

Dans une première partie, nous étudions la possibilité d'obtenir des états comprimés de spin nucléaire dans un gaz d'hélium 3 à température ambiante en cellule par mesure quantique non destructive en continu. Comme les atomes dans l'état fondamental interagissent très peu avec l'environnement, nous les couplons à une faible fraction d'atomes dans l'état métastable par des collisions d'échange de métastabilité, ces derniers pouvant interagir avec un champ électromagnétique en cavité. Nous avons considéré deux configurations dans lesquelles on mesure un nombre de photons ou une quadrature du champ en sortie de la cavité. Nous prédisons qu'une compression significative du spin nucléaire de très longue durée de vie pourrait être ainsi obtenue avec des valeurs des paramètres à la portée d'une expérience.

Dans une seconde partie, nous étudions, à température non nulle, l'amortissement des modes de phonons dans un superfluide bidimensionnel d'atomes froids bosoniques ou d'hélium 4 liquide. À cette fin, nous utilisons un hamiltonien effectif de basse énergie, celui de l'hydrodynamique quantique de Landau et Khalatnikov qui vaut même dans le régime d'interactions fortes pour peu que l'on connaisse l'équation d'état du système dans son état fondamental. Par des simulations de champ classique très précises, à notre connaissance jamais effectuées pour ce type d'hamiltonien, nous mettons en évidence des écarts significatifs à la décroissance exponentielle prédite par la règle d'or de Fermi, contrairement à ce qui se passe dans le cas tridimensionnel. Ces résultats sont confirmés par la méthode diagrammatique des fonctions de Green à N corps (dans son domaine de validité que nous précisons) et nous semblent accessibles à une vérification expérimentale.

Mots-clés Métrologie quantique, compression de spin, spin nucléaire, hélium 3, mesure quantique non destructive en continu, fonction d'onde Monte-Carlo.
Condensat de Bose-Einstein bidimensionnel, superfluide, amortissement des phonons, hydrodynamique quantique, processus Landau-Beliaev, fonction de Green à N corps.

Abstract

In a first part, we study the possibility of obtaining nuclear spin squeezing in a room temperature helium-3 gas in a cell by continuous quantum non-demolition measurement. As atoms in the ground state interact very little with the environment, we couple them to a small fraction of atoms in the metastable state by metastability exchange collisions, the latter being able to interact with an electromagnetic field in an optical cavity. We have considered two configurations in which either a photon number or a quadrature of the field at the cavity output is measured. We predict that a significant very long-lived squeezing of the nuclear spin could be obtained in this way with experimentally feasible parameter values.

In a second part, we study, at non-zero temperature, the damping of phonon modes in a two-dimensional superfluid of cold bosonic atoms or liquid helium-4. For this purpose, we use an effective low-energy Hamiltonian, the Landau-Khalatnikov quantum hydrodynamics Hamiltonian, which holds even in the strong interaction regime as long as the equation of state of the system in its ground state is known. By means of very precise classical field simulations, to our knowledge never carried out for this type of Hamiltonian, we highlight significant deviations from the exponential decay predicted by Fermi's golden rule, contrary to what happens in the three-dimensional case. These results are confirmed by the diagrammatic method of many-body Green's functions (in its domain of validity that we specify) and seem accessible to experimental verification.

Keywords Quantum metrology, spin squeezing, nuclear spin, helium 3, continuous quantum non-destructive measurement, Monte-Carlo wave functions.
Bose-Einstein condensate in 2D, superfluid, phonons damping, quantum hydrodynamic, Landau-Beliaev process, many-body Green functions.